UNIVERSITY OF CALIFORNIA, SAN DIEGO

Geophysical and geological studies of margin evolution: impacts of sea level fluctuations, tectonic deformation, and climate

Doctor of Philosophy

in

Earth Sciences

by

Shannon Angelina Klotsko

Committee in charge:

Professor Neal W. Driscoll, Chair
Professor Christopher D. Charles
Professor Jeffery S. Gee
Professor Falko Kuester
Professor David T. Sandwell

2017

The Dissertation of Shannon Angelina Klotsko is approved, and it is acceptable in quality and form for publication on microfilm and electronically:

_____

_____

_____

_____

_____

Chair

University of California, San Diego

2017

Dedication

To my parents,
Mama Gale and Papa Klot

Epigraph

"Could the waters of the Atlantic be drawn off, so as to expose to view this great sea-gash, which separates continents, and extends from the Arctic to the Antarctic, it would present a scene the most rugged, grand, and imposing. The very ribs of the solid earth, with the foundations of the sea, would be brought to light and we should have presented to us at one view, the empty cradle of the ocean." - M. F. Maury 1855

Table of Contents

List of Figures

List of Tables

ACKNOWLEDGEMENTS

First and foremost, I would like to thank my advisor, Neal Driscoll, for all of the inspiration and education he has given me over the years. He has provided a wide range of research opportunities during my time as a graduate student and I am incredibly thankful that he has pushed me to learn all aspects of research, from data collection through paper writing. I know I would not be the same scientist that I am today without all of his help.

I would like to thank everyone that I have been to sea with during my graduate studies. Without you all, long days on the Point Loma and long nights on large ships would have been a lot less fun, to say the least. But with all the effort we put in, we were able to collect great data and make amazing memories.

I would like to thank Lloyd Keigwin for his support and collaboration with the Arctic project. He has taught me a lot about paleoceanography and was always there on his scooter when I needed a break from sampling sediment cores at WHOI. I would like to thank Graham Kent for his collaboration in San Onofre and his help figuring out how to plot the Block Island Sound data. Without him, Chapter 3 would have taken a lot longer.

Jenna Hill deserves special recognition for setting me on the path I am today. Without me wandering into her office to ask if she needed someone to work for her over the summer as an undergrad, I have no idea where I would have ended up. She taught me the joys of seafloor mapping, unix, and data visualization, sparking my interest in a completely new area of marine science. Even after I moved on to graduate school, she has been there to help me whenever I need it. I know my career would not be the same without her.

I would like to thank all of the lab mates I have had over the years, but especially those that have been with me the longest: Jillian Maloney, James Holmes, Valerie

Sahakian and Emily Wei. They have been an amazing support system and have helped make the Driscoll lab the best lab at Scripps.

Finally, I would like to thank my amazing family and friends for their support over the years. My dad is probably the reason I have had such a strong interest in the ocean—almost every vacation we took when I was younger was focused on places that he could go surfing at, which gave me a lot of time on the beach. My mother has instilled in me the drive to attain my goals and has shown me that even if you are from a small town, you can get out and see the world. My sister, Natalie, has never been afraid to put me in my place when necessary, but also knows exactly how to lift me up when I need the encouragement. To the amazing friends I have met at Scripps and in San Diego, you have made this adventure the time of a life. I especially want to thank Michael Bean, who I was lucky enough to meet in San Diego. He has been an unwavering support system throughout our time together, and has always been there when I needed to be reminded that not everyone is a scientist.

Chapter 2, in full, is a reprint of the material as it appears in: Klotsko, S., Driscoll, N., Kent, G., & Brothers, D., 2015. Continental shelf morphology and stratigraphy offshore San Onofre, California: The interplay between rates of eustatic change and sediment supply. Marine Geology, 369, 116-126. The dissertation author was the primary researcher and author, and the co-authors listed in this publication directed and supervised the research.

Chapter 3 has been submitted for publication in: Klotsko, S. and Driscoll, N., Submitted. Geomorphological and stratigraphic evidence for rapid glacial lake draining in Block Island Sound, RI, Quaternary Research. The dissertation author was the primary researcher and author, and the co-author listed in this publication directed and supervised the research.

Chapter 4 is being prepared for submission in: L.D. Keigwin, S. Klotsko, N. Zhao,

B. Reily, L.Giosan, and N. W. Driscoll, In Prep. Deglacial Floods in the Beaufort Sea. The dissertation author was the involved in acquisition, processing, and interpretation of part of the data that forms the basis of this chapter. The dissertation author is secondary author on this publication.

Chapter 5 is being prepared for publication in: Klotsko, S., Driscoll, N., and Keigwin, L., In Prep, Geologic and geophysical constraints on deglacial sediment dispersal along the Beaufort Margin, Arctic Ocean. The dissertation author was the primary researcher and author, and the co-authors listed in this publication directed and supervised the research.

Vita

2008-2011	Undergraduate Research Assistant Burroughs & Chapin Center for Marine and Wetland Studies Coastal Carolina University
2011	Bachelor of Science, Marine Science Minors, Mathematics and Coastal Geology Coastal Carolina Univsersity
2013	Master of Science, Earth Sciences Scripps Institution of Oceanography University of California, San Diego
2017	Doctor of Philosophy, Earth Sciences Scripps Institution of Oceanography University of California, San Diego

Publications

Klotsko, S., Driscoll, N., Kent, G., & Brothers, D., 2015. Continental shelf morphology and stratigraphy offshore San Onofre, California: The interplay between rates of eustatic change and sediment supply. Marine Geology, 369, 116-126.

Abstract of the Dissertation

Geophysical and geological studies of margin evolution: impacts of sea level fluctuations, tectonic deformation, and climate

by

Shannon Angelina Klotsko

Doctor of Philosophy in Earth Sciences

University of California, San Diego, 2017

Professor Neal W. Driscoll, Chair

Understanding modern process that shape continental margins has both scientific and societal relevance. By studying modern marine deposits, where the stratigraphy can be imaged at unprecedented scales and accurately dated with radiocarbon techniques, we can assess the link between the forcing factors and the consequent deposit. Toward this goal, this thesis presents geological and geophysical data that provide new insights into how different forcing mechanisms (e.g., sea level fluctuations, tectonic deformation, climate variability, glacial lake drainage) shaped continental margins. Three different

margins were examined: San Onofre, CA, Block Island Sound, RI, and the Beaufort Margin, Arctic Ocean. In San Onofre, CHIRP data on the shelf imaged multiple transgressive deposits that gave insights into their controlling processes. Although numerous faults dissect the area, there is no evidence of recent activity or deformation on the fault systems offshore San Onofre. Instead, the rate of sea level rise, sediment supply, and preexisting morphology were found to be the controlling factors in sediment dispersal. Compressional features were imaged along the Cristianitos fault that runs from onshore to offshore in the study area. This suggests that the fault is actually a strike-slip fault with a down-to-the-northwest dip-slip component, versus a simple normal fault as purported.

In Block Island Sound, CHIRP data, scanned 3.5 kHz seismic profiles, and bathymetry data provide important insights into the morphologic evolution of the sound and the draining manner of glacial lakes that formerly occupied Block Island Sound and neighboring Long Island Sound. Architecture of sediment units imaged in the seismic data and erosive features imaged by bathymetry data suggest a rapid draining of the glacial lakes. Only partial infill of erosive features in Block Island Sound suggests a rapid transgression and/or a lack of modern sediment deposition.

Along the Beaufort Margin, seismic data and sediment cores were used to constrain the deglacial history of the area. Oxygen isotopes document a large input of freshwater that entered the Arctic via the Mackenzie River. Timing of this event correlates with the onset of the Younger Dryas cold period, suggesting that this flood may have triggered the attendant climate cool period. This study reveals that the slope west of the Mackenzie River has higher rates of Holocene sedimentation, suggesting it is influenced more by Barrow Canyon and continental runoff. The slope east of the Mackenzie River has a much stronger record of Mackenzie input, including a rapid depositional event. Ice rafted debris from the Amundsen Gulf is observed throughout most of the margin, but is

more prevalent in the eastern Beaufort.

1

Introduction

1.1 MARGIN PROCESSES AND SEQUENCE STRATIGRAPHY

Understanding continental margin evolution is a fundamental problem in Earth science and has both scientific importance, as well as societal relevance. Margins are essential environments to study, as they are the gateway that all terrigenous material must pass through to the deep ocean. Margin architecture is driven by three main processes: tectonic evolution, sea level fluctuations, and climate (Posamentier and Allen, 1993). Tectonic processes involve the uplift and subsidence of margins through active faulting and folding, changing the amount of accommodation available for sediment deposition. Eustatic sea level fluctuations are driven by many factors, including glacial cycles and meltwater pulses (Fairbanks, 1989). Climate variability can have substantial effects, such as changes in the rate of sediment supply due to drier or wetter conditions. The main goal of this dissertation is to study how these processes have interacted in the past to shape continental margin architecture. If we can link process and product, we are better able to interpret the sedimentary record, which may provide insight into future margin evolution.

Sediments are the tape recorders of the Earth, and to interpret these records we use sequence stratigraphy. Sequence stratigraphy allows us to use depositional sequences and stratal geometry to place the geologic record into a chronostratigraphic framework (Vail 1987; Van Wagoner et al., 1990; Christie-Blick and Driscoll; 1995). The deposition and preservation of sedimentary sequences are largely controlled by the rate of sediment supply and the rate of accommodation change. As tectonics, sea level fluctuations, and climate are the main factors controlling accommodation and the rate of sediment supply, we can use sequence stratigraphy to determine which factors are dominant and subordinate in controlling sediment deposition. This allows us to investigate the role of these processes in shaping margin architecture.

The time period focused on in this dissertation is from the Last Glacial Maximum to present (LGM, ~20 ka). Surficial stratigraphic layers deposited during this period can

be imaged at high resolution and the layers can be accurately dated using radiocarbon. To examine margin morphology and stratigraphy, we use a suite of methods to image the seafloor and layers below it. Seismic reflection data images the subsurface layers allowing us to study how the area has evolved through time. CHIRP (compressed high intensity radar pulse) is a high-resolution system that images layers at sub-decimeter vertical scales and penetrates beneath the seafloor to depths of ~50 m. This is ideal for studying fine scale variation in shallow stratigraphy and this technology is employed in all of my research. Other seismic systems are of lower resolution, but penetrate farther beneath the seafloor. These systems are often referred to by their acoustic source (e.g., mini sparker or boomer) and are used in this dissertation (Chapters 2 and 3) for a nested seismic approach. Having seismic reflection data that resolve different scales allows us to interpret the shallow stratigraphy in more detail, but also study the influence of deeper structures. Seafloor morphology is imaged at high resolution using multibeam bathymetric systems. These data image features that provide insight into across- and along-margin variability and formation processes. When high-resolution multibeam is not available, other publicly available bathymetric data with varying resolutions are used. For groundtruthing and examination of paleoceanographic data, sediment cores were examined in Chapters 4 and 5.

1.2 THESIS OVERVIEW

This thesis examines the role of tectonics, sea level fluctuations, and climate on continental margin architecture since the LGM. By focusing on three distinct study areas that represent highly different environments we are able to understand the different processes that shape continental margins. Chapter 2 focuses on San Onofre in southern California, a tectonically active region dissected by multiple fault systems. One of the overarching goals of this study was to understand the role the fault systems played

in sediment dispersal on the shelf. The major faults in this region are the Newport-Inglewood/Rose Canyon (NI/RC) fault, which runs along the outer shelf edge, and the Cristianitos Fault, which crosses the shelf from onshore to offshore. The NI/RC Fault has ruptured to the north of the study area multiple times in the 1900s (Freeman et al., 1992) and has ruptured to the south of the study area at least three times in the past 8.1 ky (Lindvall and Rockwell, 1995). The Cristianitos Fault has not ruptured in the past ~80 ky (Shlemon, 1992), but it could be as long as ~500 ka (McNey, 1979) based on different measurements. CHIRP data imaged the sediment deposits that overlay the transgressive surface; the boundary that separates subaerially exposed sediments below from marine deposits above. This surface forms as sea level transgresses the land with wave energy eroding topographic highs and infilling topographic lows. The data indicate that the major proceses controlling transgressive deposit dispersal are the rate of sea level rise and sediment supply, with effects form preexisting morphology. There is not evidence that the NI/RC has ruptures in this area since the transgression, providing a minimum estimate for most recent earthquake event at ~10-18 ka. CHIRP data from the Cristianitos Fault indicates that is a strike-slip fault with a compressional component.

Chapter 3 focuses on Block Island Sound in Rhode Island. This sound is located just east of Long Island Sound. The southern reaches of the Laurentide ice sheet extended over this area until ~23-24 ka, and then retreated, leaving behind a series of moraines (Stone and Borns, 1986; Dyke and Prest, 1987; Uchupi et al., 2001). These moraines served as earthen dams that created glacial meltwater lakes, glacial lake Block Island Sound in present day Block Island Sound and glacial Lake Connecticut in present day Long Island Sound. Two alternative hypotheses have been proposed to characterize the draining of the glacial lakes. In one model (Lewis and Stone, 1991), the lakes drained gradually, together. The rate of draining of glacial Lake Connecticut was controlled by erosion of the spillway between the two lakes. In the alternative model (Uchupi et al.,

2001), the lakes drained in a quick, catastrophic manner, with Lake Block Island Sound draining first and Lake Connecticut draining about 500 years later through Block Island Sound. The method of draining also has implications for how the observed seafloor morphology and subbottom stratigraphy formed. New seismic data provides important new constraints to test between these alternative hypotheses and indicates that the catastrophic draining scenario is the more likely of the two.

Chapters 4 and 5 focus on the Beaufort Margin in the Arctic Ocean. The goal of this work was to examine the effects of the deglaciation on the margin and determine if evidence exists to support a northern route for glacial Lake Agassiz drainage at the onset of the Younger Dryas cold period. The Younger Dryas was a return to glacial like conditions in northern Europe ~12.8 ka. It has been suggested that the cause of the Younger Dryas was a massive freshwater input into the North Atlantic, which slowed down North Atlantic Deepwater formation (Broecker et al., 1989). This would cause a slow down in the global thermohaline circulation, bringing less heat to Europe. Glacial Lake Agassiz was the major meltwater lake that formed from the Laurentide ice sheet. The waters from this lake took many pathways to the ocean through time (Teller et al., 2005), but there has never been a consensus as to the pathway of meltwaters at the onset of the Younger Dryas. Evidence was found onshore by Murton et al. (2010) that suggested the route was north into the Arctic Ocean via the Mackenzie River. Our study documents many depositional events, reflecting the processes that affect the Beaufort margin. One of these events indicated a major freshwater input into the Arctic via the Mackenzie River and timing correlates with the onset of the Younger Dryas. Other depositional sequences document along- and across-margin transport. Ice rafted debris layers in sediment cores along the continental slope record the retreat of the ice stream in Amundsen Gulf. Thick Holocene sediment layers found west of the Mackenzie River, reflect the large continental input and discharge down Barrow Canyon. Sediment cores

and seismic profiles help constrain the sedimentation patterns for the Beaufort Margin and relative influences from each source.

REFERENCES

Broecker, W. S., Kennett, J. P., Flower, B. P., Teller, J. T., Trumbore, S., Bonani, G., & Wolfli, W., 1989. The routing of meltwater from the Laurentide ice-sheet during the Younger Dryas cold episode. Nature 341: 318-321.

Christie-Blick, N., Driscoll, N.W., 1995. Sequence stratigraphy. Annual Review of Earth and Planetary Sciences 23, 451–478.

Dyke, A.S., Prest, V.K., 1987. Late Wisconsinan and Holocene History of the Laurentide Ice Sheet. Géographie physique et Quaternaire 41, 237-263.

Fairbanks, R.G., 1989: A 17,000 year glacio-eustatic sea level record: Influence of glacial melting rates on the Younger Dryas event and deep- ocean circulation. Paleoceanography, 342, 637–642.

Freeman, S. Thomas, Heath, Edward G., Guptill, Paul D., Waggoner, John T. 1992. Seismic hazard assessment, Newport-Inglewood fault zone. Association of Engineering Geologists, Southern California Section, Special Publication No. 4, p. 211-231.

Lewis, R. S., & Stone, J. R., 1991. Late Quaternary stratigraphy and depositional history of the Long Island Sound basin: Connecticut and New York. Journal of Coastal Research, 1-23.

Lindvall, S. and Rockwell, T.K., 1995. Holocene activity of the Rose Canyon fault, San Diego, California: Journal of Geophysical Research, v. 100, no. B12, p. 24121-24132.

McNey, J.L., 1979. General Geology, San Onofre Area, in: Geologic Guide of San Onofre Nuclear Generating Station and Adjacent Regions of Southern California, Fife, D.L., Editor. A-71-A-85.

Murton, J. B., Bateman, M. D., Dallimore, S. R., Teller, J. T., & Yang, Z., 2010. Identification of Younger Dryas outburst flood path from Lake Agassiz to the Arctic Ocean. Nature, 464(7289), 740-743.

Posamentier, H.W., Allen, G.P., 1993. Variability of the sequence stratigraphic model: effects of local basin factors. Sedimentary Geology 86, 91–109.

Shlemon, R. J., 1992. The Cristianitos fault and quaternary geology, San Onofre State Beach, California. The regressive Pleistocene shoreline in southern California: South Coast Geological Society Annual Field Trip Guidebook, 20, 9-12.

Stone, B.D., and Borns, Harold W., 1986. Pleistocene glacial and interglacial stratigraphy of New England, Long Island, and adjacent Georges Bank and Gulf of Maine. Quaternary Science Reviews 5, 39-52.

Teller, J. T., Boyd, M., Yang, Z., Kor, P. S., & Fard, A. M., 2005. Alternative routing of Lake Agassiz overflow during the Younger Dryas: new dates, paleotopography, and a re-evaluation. Quaternary Science Reviews, 24 (16), 1890-1905.

Uchupi, E., Driscoll, N., Ballard, R. D., & Bolmer, S. T., 2001. Drainage of late Wisconsin glacial lakes and the morphology and late quaternary stratigraphy of the New Jersey–southern New England continental shelf and slope. Marine Geology 172, 117-145.

Vail, P.R., Mitchum Jr., R.M., Todd, R.G., Widmier, J.M., Thompson III, S., Sangree, J.B., Bubb, J.N., Hatlelid, W.G., 1977. Seismic stratigraphy and global changes of sea-level. In: Payton, C.E. (Ed.), Seismic Stratigraphy—Applications to Hydrocarbon Exploration. American Association of Petroleum Geologists Memoir, vol. 26, pp. 49–212.

Van Wagoner, J.C., Mitchum, R.M., Campion, K.M., Rahmanian, V.D., 1990. Siliciclastic sequence stratigraphy in well logs, cores, and outcrops. American Association of Petroleum Geologists Methods in Exploration Series 7 (55 pp).

2

Continental shelf morphology and stratigraphy offshore San Onofre, California: The interplay between rates of eustatic change and sediment supply

Marine Geology 369 (2015) 116–126

Contents lists available at ScienceDirect

Marine Geology

journal homepage: www.elsevier.com/locate/margeo

Continental shelf morphology and stratigraphy offshore San Onofre, California: The interplay between rates of eustatic change and sediment supply

Shannon Klotsko [a,*], Neal Driscoll [a], Graham Kent [b], Daniel Brothers [c]

[a] Scripps Institution of Oceanography, UC San Diego, 9500 Gilman Drive, La Jolla, CA 92093, United States
[b] Nevada Seismological Laboratory, University of Nevada, Reno, Laxalt Mineral Engineering Building, Room 322, Reno, NV 89557, United States
[c] U.S. Geological Survey, 400 Natural Bridges Drive, Santa Cruz, CA 95060, United States

ARTICLE INFO

Article history:
Received 31 January 2015
Received in revised form 18 July 2015
Accepted 1 August 2015
Available online 5 August 2015

Keywords:
San Onofre
Continental margin processes
Cristianitos Fault
CHIRP seismic
Transgressive deposits
Sediment controls

ABSTRACT

New high-resolution CHIRP seismic data acquired offshore San Onofre, southern California reveal that shelf sediment distribution and thickness are primarily controlled by eustatic sea level rise and sediment supply. Throughout the majority of the study region, a prominent abrasion platform and associated shoreline cutoff are observed in the subsurface from ~72 to 53 m below present sea level. These erosional features appear to have formed between Melt Water Pulse 1A and Melt Water Pulse 1B, when the rate of sea-level rise was lower. There are three distinct sedimentary units mapped above a regional angular unconformity interpreted to be the Holocene transgressive surface in the seismic data. Unit I, the deepest unit, is interpreted as a lag deposit that infills a topographic low associated with an abrasion platform. Unit I thins seaward by downlap and pinches out landward against the shoreline cutoff. Unit II is a mid-shelf lag deposit formed from shallower eroded material and thins seaward by downlap and landward by onlap. The youngest, Unit III, is interpreted to represent modern sediment deposition. Faults in the study area do not appear to offset the transgressive surface. The Newport Inglewood/Rose Canyon fault system is active in other regions to the south (e.g., La Jolla) where it offsets the transgressive surface and creates seafloor relief. Several shoals observed along the transgressive surface could record minor deformation due to fault activity in the study area. Nevertheless, our preferred interpretation is that the shoals are regions more resistant to erosion during marine transgression. The Cristianitos fault zone also causes a shoaling of the transgressive surface. This may be from resistant antecedent topography due to an early phase of compression on the fault. The Cristianitos fault zone was previously defined as a down-to-the-north normal fault, but the folding and faulting architecture imaged in the CHIRP data are more consistent with a strike-slip fault with a down-to-the-northwest dip-slip component. A third area of shoaling is observed off of San Mateo and San Onofre creeks. This shoaling has a constructional component and could be a relict delta or beach structure.

1. Introduction

Transgressive deposits have been studied along continental margins worldwide and form during a relative sea level rise when rapid increases in accommodation outpace sediment supply (Vail et al., 1977; Van Wagoner et al., 1990; Posamentier and Allen, 1993; Christie-Blick and Driscoll, 1995; Jin and Chough, 1998; Posamentier, 2002; Amorosi et al., 2009; Lantzsch et al., 2009; Nordfjord et al., 2009; Schwab et al., 2014). These deposits are important reservoir rocks for hydrocarbons because they are well sorted and have high permeability (Snedden and Dalrymple, 1999; Posamentier, 2002; Cattaneo and Steel, 2003). Changes in the rate of sea level rise and sediment supply during the transgression imparts both along and across margin variability in the stacking patterns and facies distribution of transgressive deposits (Swift, 1968; Posamentier and Allen, 1993; Cattaneo and Steel, 2003; Catuneanu et al., 2009). Understanding this along and across margin variability of transgressive deposits; however, remains limited because of data quality and density (Nordfjord et al., 2009). A notable exception is the transgressive deposits along the trailing New Jersey/New York margin (e.g., Rampino and Sanders, 1981; Milliman et al., 1990; Greenlee et al., 1992; Miller et al., 1998; Goff et al., 1999, 2004; Nordfjord et al., 2009; Goff and Duncan, 2012; Schwab et al., 2014).

Continental shelves have been exposed to wave-based erosion for the last 2.7 my as sea level has fluctuated up and down ~125 m on a 100–125 ky glacial–interglacial cycle (Petit et al., 1999; Lisiecki and Raymo, 2005). Fluctuations in the rate of eustatic sea level rise since

* Corresponding author.
E-mail address: sklotsko@ucsd.edu (S. Klotsko).

http://dx.doi.org/10.1016/j.margeo.2015.08.003
0025-3227/

the Last Glacial Maximum (LGM; ~21 kya) are well documented (Fairbanks, 1989; Bard et al., 1990; Fairbanks, 1990, 1992; Shackleton, 2000; Peltier and Fairbanks, 2006), with the most rapid rises associated with Melt Water Pulse 1A and Melt Water Pulse 1B (MWP 1A and 1B). During these melt water pulses, rates of eustatic sea level rise topped out at ~40 mm/ky (Hogarth et al., 2012). In between these periods of rapid rise are times of slower sea level rise or even stillstands. These changes in rates of sea level cause different morphologic expressions along and across the margin during the transgression. For example, during slow rises in sea level, there is a greater period of time for wave-base erosion at certain water depths forming abrasion platforms (i.e., terraces). These terraces create localized lows across the shelf that can subsequently be infilled by coarse-grained transgressive lag deposits resulting in thickness and grain size variability (Hart and Plint, 1993; Cattaneo and Steel, 2003). Near sediment dispersal systems, localized prograding packages may develop during these periods of slow sea level rise within the overall backstepping architecture of the transgressive deposit (Posamentier and Allen, 1993; Cattaneo and Steel, 2003). This temporary situation where sediment supply outpaces the relative sea level rise is referred to as a stepped transgressive surface (Swift et al., 1991; Cattaneo and Steel, 2003).

Here we present a high resolution CHIRP survey, together with reprocessed multi-channel seismic data (MCS) from San Onofre, southern California where we define the along and across-margin variability in transgressive deposits in response to changes in the rate of sea level rise and sediment supply. The data also reveal the importance of pre-existing physiography associated with relict tectonic deformation in controlling sediment dispersal and thickness variations of the transgressive deposits (e.g., Posamentier and Allen, 1993; Cattaneo and Steel, 2003). Finally, we present new constraints on local faults (e.g., Newport Inglewood/Rose Canyon and Cristianitos Faults) in high resolution, leading to new conclusions about their deformational style and timing of the most recent earthquake along the faults, which has important implications for geohazard assessment. For example, the deformation and folding style of the Cristianitos Fault, which crosses through the survey area, reveal there is compression across the fault; the fault style and geometry are more consistent with a strike slip fault with a dip-slip component than purely a normal fault as previously proposed (Shlemon, 1992). In summary, high-resolution seismic imaging on continental margins can reveal the across and along margin variability of the transgressive deposit and provide important constraints on the dominant processes through time.

2. Regional setting

2.1. Study area and geologic background

San Onofre is located in seismically active southern California between San Clemente and Oceanside, north of San Diego (Fig. 1A and B). This region offshore is known as the Inner California Continental Borderlands (ICB), a highly deformed portion of the margin (Ehlig, 1977; Crouch, 1979; Legg, 1991; Crouch and Suppe, 1993; Magistrale, 1993; Nicholson et al., 1994; Bohannon and Geist, 1998; Meade and Hagar, 2005; Ryan et al., 2009, 2012). The section of the borderlands that encompasses San Onofre, from Dana Point to Carlsbad Canyon (Fig. 1A), is also characterized by a wider continental shelf than the surrounding area. Onshore, the sea cliffs are composed of four major geologic units at beach level (Fig. 1C). Exposed in the northern part of the region (Fig. 1C) and buried to the south is the San Onofre Breccia, which formed from early to middle Miocene. This is composed of bolder-sized clasts in a finer-grained matrix. Clasts are commonly blue schist, green schist, and quartz schist (Ehlig, 1977). The Monterey Formation (Fm) is exposed in the cliff at beach level south of the Cristianitos Fault (Fig. 1C). This is a deep marine deposit, formed from middle to late Miocene (Ehlig, 1977). The lithology of the formation ranges laterally along the coast from bedded siltstone and clayey siltstone, to interbedded siltstone and biotite-rich sandstone (Ehlig, 1977). The bedded sections of the formation were likely deposited by pelagic sedimentation in an anoxic environment, consistent with the lack of observed bioturbation. At beach level, the cliffs north of the Cristianitos fault zone are composed of the San Mateo Fm, a massive, coarse-grained arkosic sandstone deposited in the late Miocene/early Pliocene (Ehlig, 1977). It is of marine origin and is likely backfill of a channel extending offshore from San Mateo and San Onofre creeks. Toward the southern end of the survey region, the cliffs transition to a coarse-grained arkosic sandstone, which has been previously designated as sandy Monterey Fm (Ehlig, 1977; Kennedy, 2001). Based on grain size evidence and new observations, Sorenson et al. (2009, unpublished UCSD senior thesis) concluded that the grain size distribution is more consistent with the San Mateo Formation. Evidence for a previously undocumented fault with down to the southeast slip would allow for the transition back to San Mateo Formation from Monterey Formation. North of San Mateo and San Onofre creeks, the Capistrano Fm is exposed at beach level in the Capistrano Embayment (Fig. 1C). The Capistrano Fm formed from late Miocene to Early Pliocene and is composed of bedded siltstone, mudstone, and sandstone (Ehlig, 1977), with cemented conglomerate sandstone in marine channels (Kennedy and Tan, 2005). The large clasts are made up of volcanic, metamorphic and sedimentary rocks. Overlying these formations is a reddish-brown Quaternary alluvium deposit. Cut into these deposits is a set of marine terraces. Pebble and cobble gravel lag cover lower terraces, while the upper terraces have more beach sand (Ehlig, 1977). The terraces are thought to have formed during the Pleistocene from eustatic sea level variations and have since been uplifted by tectonic processes (Ehlig, 1977).

2.2. Major faults

The major fault that crosses through the San Onofre region is the Cristianitos (Fig. 1C), a north–northeast trending fault that extends offshore (Ehlig, 1977), coinciding with widest part of the shelf here. The fault is exposed at the coast, where it separates the San Mateo and Monterey formations. There, its strike is 32° northeast and the dip is 58° northwest (Ehlig, 1977). A possible splay of the Cristianitos Fault was identified by Sorenson et al. (2009) ~2.5 km south of where the main fault trace is exposed in the cliff (Fig. 1C). Based on microfossil ages from the Monterey and Capistrano formations, the Cristianitos Fault formed ~10 Ma (Ehlig, 1979). The minimum age of the last rupture has been placed at 125 ka (Marine Isotope Stage 5e; MIS5e) from exposed marine terraces (Shlemon, 1992), but it could be as young as the MIS5a terrace (~80 ka). Paleoseismic trench analysis yields older estimates for the most recent event (MRE) of ~500 ka (McNey, 1979). The Cristianitos Fault has previously been defined as a normal fault (Ehlig, 1977, 1979; Shlemon, 1992), but here, we present evidence suggesting its geometry and deformational style are more consistent with a strike-slip fault with a down-to-the-northwest component.

The major fault along the continental shelf in this region is the Newport Inglewood/Rose Canyon Fault (NI/RC; Fig. 1C), the junction of the Newport Inglewood Fault to the north and the Rose Canyon Fault to the south. It is a right-lateral strike-slip fault that trends northwest–southeast in the survey area along the shelf edge; along some portions of the margin the NI/RC fault delineates the shelf break and in other regions it is within the shelf (Ryan et al., 2009). The Newport Inglewood Fault has been active since at least the Miocene (Freeman et al., 1992). It ruptured multiple times in the 1900s, including a magnitude 6.3 (M_w), highly destructive earthquake in Long Beach. The slip rate for the Newport Inglewood Fault is estimated to be 0.5 mm/yr (Freeman et al., 1992). The Rose Canyon Fault, which formed in the late Pliocene (Ehlig, 1980; Grant et al., 1997), has ruptured at least three times in the past 8.1 ka based on paleoseismic excavations (Lindvall and Rockwell, 1995). The youngest rupture could have occurred as recent as the past few hundred years

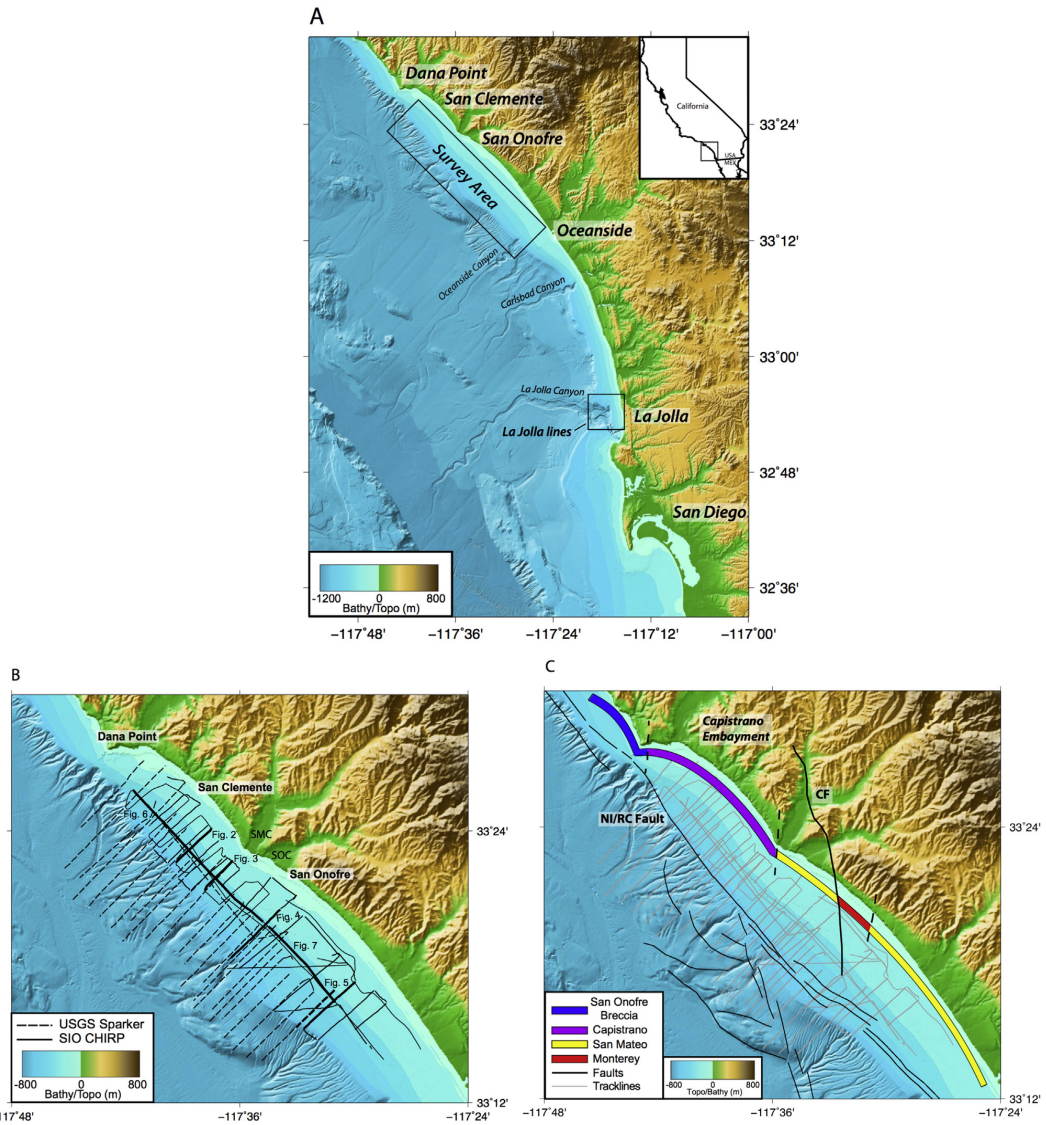

Fig. 1. (A) Regional map of southern California showing the study region from Dana Point to La Jolla Cove. (Inset of California showing map location.) Bathymetry is modified from Dartnell et al. (2015). Large box shows the main study area offshore San Onofre and the small box shows the location of CHIRP lines from La Jolla shown in Fig. 10. (B) Location map for 2008, 2009, and 2013 SIO CHIRP surveys along with USGS mini sparker survey (Sliter et al., 2010). CHIRP tracklines are shown in solid black lines and USGS sparker tracklines are shown in black dashed lines. Seismic lines shown in this paper are bold with labeled figure number. SMC = San Mateo Creek and SOC = San Onofre Creek. (C) Cliff geology and fault map for survey area. Faults are shown in black. Offshore faults are from the USGS fault database and the Cristianitos Fault is based on this study (offshore) and Ehlig (1977; onshore). Geologic formations exposed in the sea cliffs at beach level are shown (Ehlig, 1977; Sorenson et al., 2009; Rentz, 2010). NI/RC = Newport Inglewood/Rose Canyon Fault; CF = Cristianitos Fault.

(Rockwell, 2010). Estimates for the Rose Canyon fault slip rate are between 1 and 2 mm/yr (Lindvall and Rockwell, 1995).

3. Methods

In 2008, 2009, and 2013 CHIRP seismic data were acquired on the continental shelf offshore of San Onofre, CA (Fig. 1) using the Scripps Institution of Oceanography EdgeTech X-Star CHIRP subbottom reflection sonar with sub-meter vertical resolution. The CHIRP system was towed 1–2 m below the surface. Profile spacing ranges from ~0.5 to 2 km. The profiles were acquired using an acoustic source with either a 50 ms, 1–6 kHz or a 30 ms 1–15 kHz swept frequency acoustic source, which allowed for sub-seafloor penetration up to 50 m. All data were recorded in jsf format with real-time GPS navigation recorded with each shot for location accuracy. The data were converted to SEG-Y format and further processed using SIOSEIS (Henkart, 2003) and then imported into IHS Kingdom Suite software package (kingdom.ihs.com) for interpretation. USGS single-channel mini sparker data (Sliter et al., 2010) were reprocessed and imported into Kingdom Suite to increase data density as well as provide deeper seismic imaging. Kingdom Suite was

used to calculate depth to determined surfaces, and layer thicknesses. Generic Mapping Tools (GMT; gmt.soest.hawaii.edu/) were used to apply a continuous curvature surface algorithm and interior tension of 0.35 to convert data points to interpolated grid surfaces. Depth values were calculated using a nominal velocity of 1500 m/s to convert from two way travel time (TWTT); both depth and TWTT are shown on the seismic profiles (Figs. 2–7).

4. Results

4.1. Regional unconformity

A high amplitude subsurface reflector is observed throughout the survey area; it separates truncated horizons and dipping reflectors below from more flat-lying acoustically transparent units above (Fig. 2). This regional unconformity is generally the highest amplitude sub-seafloor reflector; however, it does exhibit lateral amplitude variability. This regional unconformity predominantly shoals from west to east across the study area, ranging from ~75 m to 10 m depth below modern sea level. Abrupt changes in depth and dip along the regional unconformity are observed (Figs. 3 and 4). In particular, there is a marked change in dip at about 53 m below the sea surface from ~0.8° to ~1.77° (Figs. 2 and 3). Furthermore, the regional unconformity exhibits local shoaling across- and along-shelf (e.g., Figs. 5, 6, and 7). Areas of shoaling along the erosion surface in the CHIRP data often appear to correlate spatially with regions of faulting or folding beneath the regional unconformity observed in the mini sparker data (Figs. 5 and 7).

Beneath the regional unconformity the character of the truncated reflectors changes across the shelf and several folds (i.e., antiforms and synforms) are observed. Small fault traces are identified by offsets of the truncated reflectors (Figs. 2 and 3); however, no offsets above the regional unconformity are observed. In addition, below the regional unconformity there are several features that have channel like characteristics (i.e., sediment infill, truncation; Fig. 2). On the southwestern end of most of the dip lines, there is a sequence of subparallel high amplitude reflectors with variable dip in water depths ranging from ~70 m to 115 m that are truncated by the regional unconformity (e.g., Figs. 2 and 3). The gradient of the features appears to steepen toward the west, approaching the shelf edge.

4.2. Acoustic units

There are three well-defined sedimentary units above the regional angular unconformity (Figs. 2 and 3). The basal unit, Unit I, lies directly above the regional unconformity. It infills a structural low seaward of a change in the slope of the regional unconformity at ~53 m below current sea level (Figs. 2 and 3). This unit predominantly occurs in water depths ranging from ~40 to 75 m and onlaps landward and downlaps seaward. In the region of onlap, the reflector amplitude is high and systematically diminishes offshore, where it becomes acoustically blotchy and discontinuous (Fig. 3). The isopach map for Unit I (Fig. 8A) shows the thickness depocenter is offshore San Mateo and San Onofre creeks (~12 m thick) in water depths >40 m. Throughout the rest of the survey area, the thickness of Unit I is less than ~5 m. A marked increase in thickness occurs along the mid-shelf (~40–60 m present water depth) where the slope of the regional unconformity increases (Fig. 3).

In addition to onlapping the regional unconformity across the margin (Fig. 2), Unit I exhibits lateral onlap onto a shoal in the regional unconformity (Fig. 6). A different acoustic character in Unit I is observed on either side of the local shoal. A mounded structure is observed above the regional unconformity in this region, which has a high acoustic reflectivity and relief (purple package in Fig. 6). Despite the fact that Unit I characteristically infills structural lows and diminishes relief, this mounded structure is included in the isopach map for Unit I (Fig. 8A) because it appears to be a laterally time-equivalent facies and it is overlain by Unit II (Fig. 6). South of the mound structure (Fig. 7), Unit I exhibits lateral onlap onto another local shoal on the regional unconformity (Fig. 7). In contrast to the northern shoal (Fig. 6), the reflectors beneath the regional unconformity in this region are folded and faulted (Fig. 7).

Unit II overlies Unit I, or the regional unconformity where Unit I is absent (Figs. 2–5). In the seismic data, it has a lenticular shape and is observed in water depths ranging between ~20 and 70 m, pinching out by either onlap landward or downlap seaward. The top of the unit

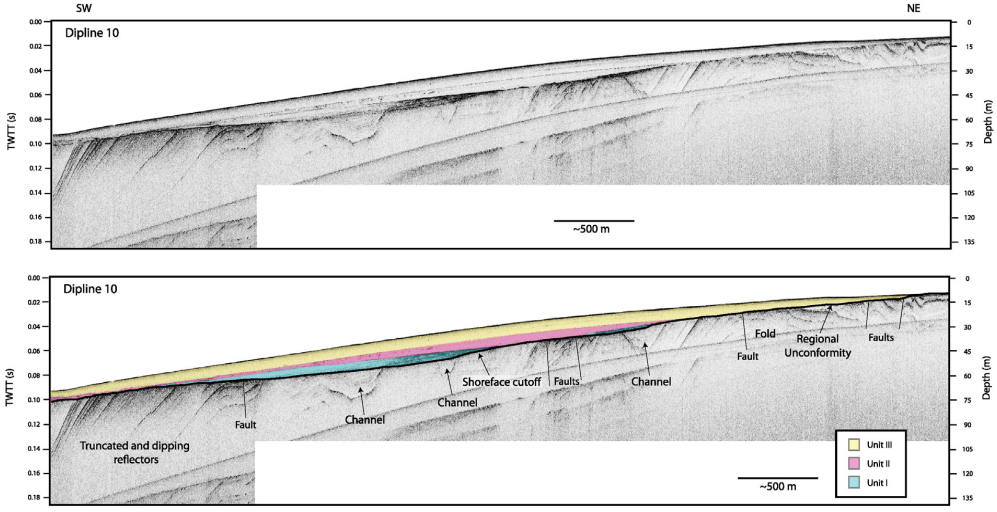

Fig. 2. CHIRP dipline 10 with uninterpreted (Top) and interpreted (Bottom) versions. Unit I is shown in cyan, Unit II is shown in pink, and Unit III is shown in yellow. Several folds and faults are observed beneath the transgressive surface, but do not appear to offset it. Unit I is observed at midshelf depths and thins by onlap landward and downlap seaward. Unit II is shifted landward with respect to Unit I. Both Units I and II are overlain by Unit III. (For interpretation of the references to color in this figure legend, the reader is referred to the web version of this article.)

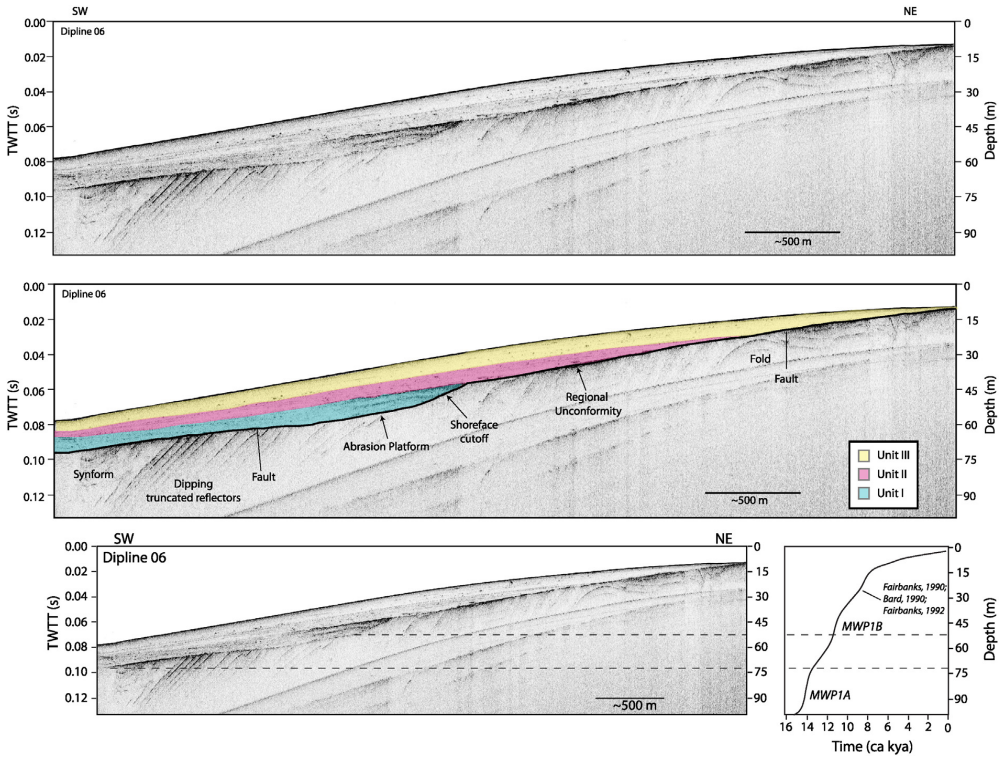

Fig. 3. CHIRP dipline 06 with uninterpreted (top) and interpreted (middle) versions. Along the southwestern portion of the profile, there is pronounced truncation beneath the transgressive surface. Moving toward the northeast along the abrasion platform is a marked change in relief, which is interpreted as a shoreface cutoff. The stacking patterns of Units I, II, and III exhibit a similar pattern as observed in CHIRP dipline 10. The bottom CHIRP profile is shown with the LGM sea level curve based on Fairbanks (1990), Bard et al. (1990), and Fairbanks (1992). The decrease in the rate of sea-level rise following MWP 1A correlates with the deeper portion of the abrasion platform; the upper depth limit correlates to the increase in sea-level rise associated with MWP 1B. The more rapid rise at MWP 1B also allows the shoreline cutoff to be preserved as wave-base erosion moved landward. Dashed lines show the decreased rate of sea level rise between MWP 1A and MWP 1B and associated depth corridor on the shelf.

is delineated by a faint acoustic reflector, which can be traced throughout most of the study region (Figs. 3, 4, and 7). This unit contains some internal reflectors, which are discontinuous and variable in amplitude (Figs. 2 and 3). An isopach map of Unit II (Fig. 8B) shows that the thickest deposits (~12 m thick) are along the center of the survey offshore the San Mateo and San Onofre creeks similar to the depocenter for Unit I. Nevertheless, the depocenter for Unit II is located eastward (~15–45 m water depth) with respect to the depocenter for Unit I (Fig. 8A and B).

Unit III is the uppermost unit and blankets most of the study area. It is mostly acoustically transparent, but includes some discontinuous, low amplitude, reflectors. Unit III thins landward and is absent toward the east where the regional unconformity is exposed at the seabed (e.g., Figs. 2 and 4). The isopach map for Unit III (Fig. 8C) shows its broad regional extent, which systematically thickens offshore reaching a maximum thickness of ~10 m near the mid-shelf (~30–40 m water depth), where it then thins seaward (Fig. 8C).

5. Discussion

5.1. Transgressive surface

The regional unconformity observed throughout the data is interpreted to be the transgressive surface formed by wave-base erosion as sea level rose following the LGM (Posamentier and Allen, 1993; Le Dantec et al., 2010; Hogarth et al., 2012). This boundary is defined by truncation and onlap; by inference it separates deposits exposed subaerially during the LGM below from marine deposits above. Channels are observed beneath the transgressive surface, and are interpreted to have formed during the last glacial maximum by fluvial incision and downcutting. As previously mentioned, the transgressive surface shows a change in dip at ~53 m below sea level from ~0.8° to ~1.77°. This change in dip is interpreted to be the boundary between the wave-cut abrasion platform and the shoreline cutoff (Figs. 3 and 9; e.g., Posamentier and Allen, 1993; Muhs et al., 1994). The deepest abrasion platform is observed at water depths of 72–53 m (Figs. 2 and 3). Based on water depth and no tectonic uplift, this abrasion platform appears to be cut during the slowdown in sea level rise between MWP 1A and MWP 1B (Fig. 3; Bard et al., 1990, 1996; Fairbanks, 1990, 1992). The rate of sea level rise is up to ~40 mm/yr for MWP 1A and MWP 1B and diminishes to ~8 mm/yr during the intervening decrease in sea level rise (Hogarth et al., 2012). This slow down allowed for a longer period of wave-base erosion creating a pronounced shoreline cutoff observed along the shelf in our study area (Fig. 3). In our conceptual model, Unit I was deposited after MWP 1B as the abrasion platform moved landward (Fig. 9B). The eroded sediment is then advected landward and seaward, with the coarse transgressive lag infilling the relief on the transgressive surface (Unit I; e.g., Hogarth et al., 2012). Such an interpretation is consistent with the high amplitude reflectors that onlap the shoreline cutoff (Figs. 2 and 3). The top

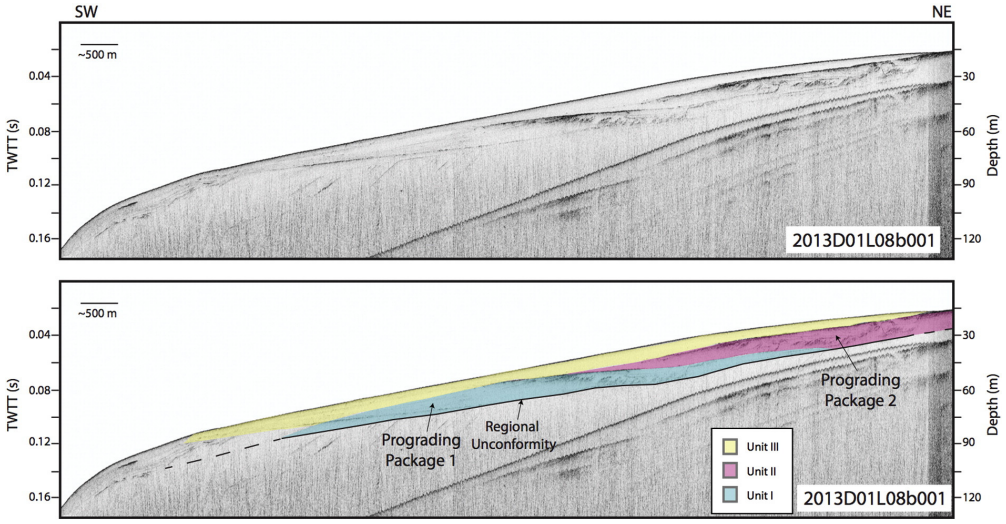

Fig. 4. 2013 dipline D01L08b001 with uninterpreted (top) and interpreted (bottom) versions. The transgressive surface is shown in black, and is dashed where uncertain. Prograding package 1 is shown in cyan and is associated with Unit I. Prograding package 2 is shown in pink and is associated with Unit II. Near San Mateo and San Onofre creeks the sediment supply after MWP 1B outpaces the eustatic rise and the unit progrades. Likewise package 2 progrades after ~8 ka, when sediment supply outpaces new accommodation. (For interpretation of the references to color in this figure legend, the reader is referred to the web version of this article.)

of the infilling lag deposit (Unit I) has a similar dip to the shallower abrasion platform (Figs. 3 and 9B), with deposition occurring below wave base. The isopach maps show the important control on shelf sediment thickness by the shoreline cutoff (Fig. 8). The depocenter for Unit I occurs just to the west of the shoreline cutoff (Fig. 8A), with the depocenter for Unit II occurring just east of this (Fig. 8B). These

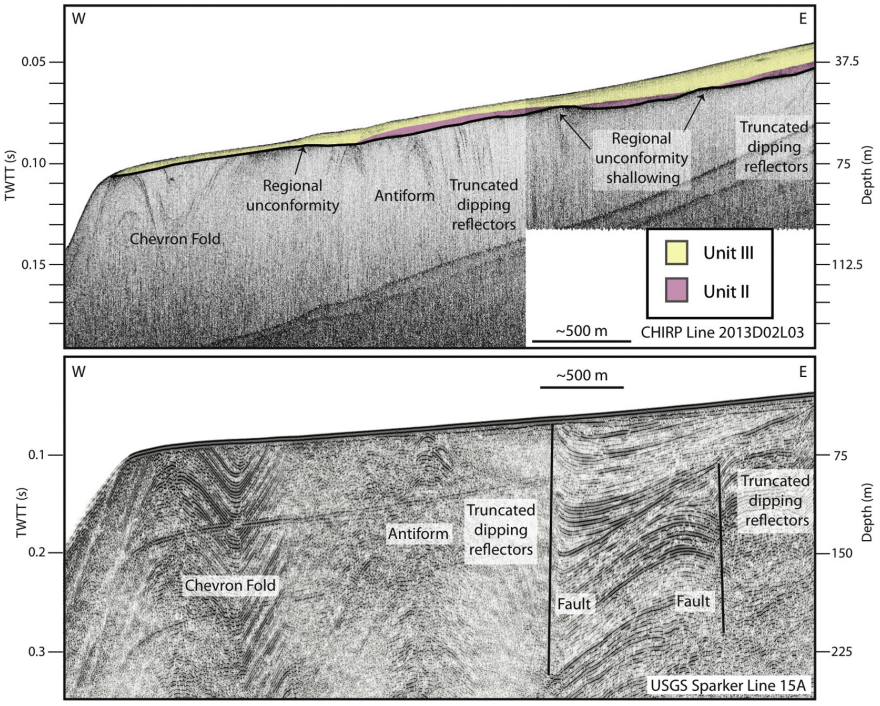

Fig. 5. Comparison of 2013 SIO CHIRP line D02L03 (top) and USGS mini sparker line 15A (bottom). On the CHIRP profile, Unit II is shown in pink, and Unit III is shown in yellow. Faults observed in the sparker data correspond with regions of shoaling along the transgressive surface imaged in the CHIRP data. (For interpretation of the references to color in this figure legend, the reader is referred to the web version of this article.)

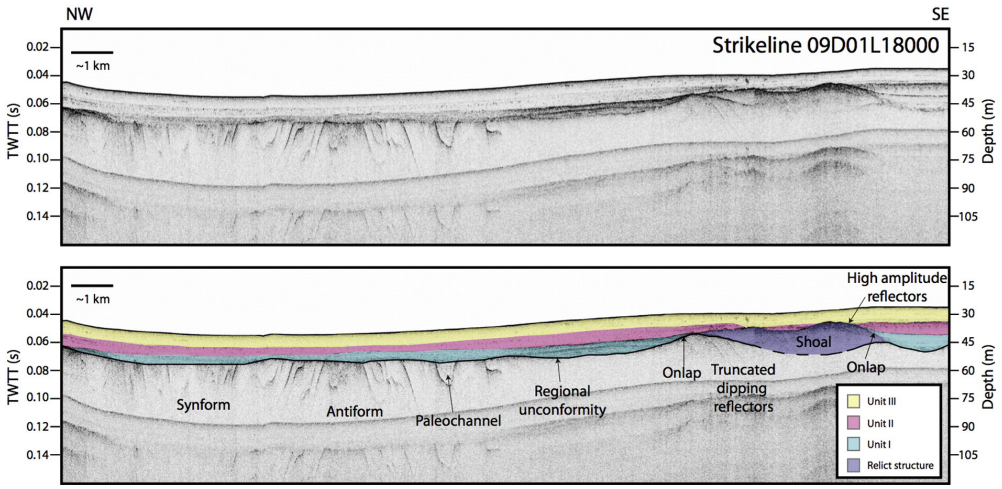

Fig. 6. CHIRP strikeline 18 with uninterpreted (top) and interpreted (bottom) versions. Shown in purple is an interpreted relict beach or delta structure, sediment was likely sourced from the San Mateo and San Onofre creeks. (For interpretation of the references to color in this figure legend, the reader is referred to the web version of this article.)

depocenters occur off of San Mateo and San Onofre Creeks where the sediments were actually able to outpace the transgression and prograded out (Fig. 4).

In addition to the relief and control of across shelf sediment thickness by the submerged relict shoreline cutoff (Kern and Rockwell, 1992), there are along-strike shoals that also control shelf sediment dispersal and thickness (Figs. 6 and 7). The northern shoaling region occurs offshore San Mateo and San Onofre creeks. This shallowing region is composed of two close shoals in the transgressive surface with truncated dipping reflectors below (Fig. 6). In this region, it is unclear why there is differential relief along the transgressive surface, but topography resistant to erosion could be a potential cause. Above these shoals in the transgressive surface is a high amplitude constructional sediment unit that post-dates the formation of the transgressive surface as evidenced by the observed truncation of reflectors at the transgressive surface (purple package in Fig. 6). This sedimentary package creates relief and is interpreted as a relict beach or delta deposit formed from sediment supply from the San Onofre and San Mateo Creeks. Unit I is younger than this constructional sediment package based on the observed onlap of Unit I onto this feature (Fig. 6). A few kilometers northwest of the shoal, a tight zone of folding and deformation is observed beneath the transgressive surface (Fig. 6) and correlates with a facies change observed in the sea cliffs at beach level from San Mateo Formation (Fm) to the south and Capistrano Fm toward the north (Fig. 1C; Rentz, 2010). This zone of deformation projects onshore to the southern end of the Capistrano Embayment (Ehlig, 1979) and potentially correlates with a down-to-the-northwest strike-slip fault (Rentz, 2010). We interpret this deformation zone to be a northern splay of the Cristianitos Fault. The down-to-the-northwest Cristianitos Fault and the down-to-the-northwest splay explain the formations exposed in the sea cliffs being younger to the north. At Dana Point, the strike slip fault system reverses and is down-to-the-northeast, which

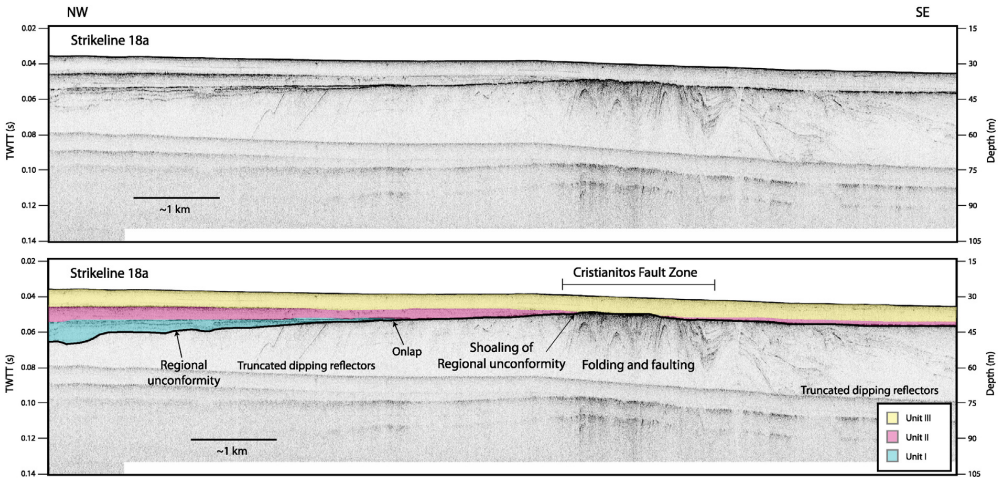

Fig. 7. CHIRP strikeline 18a with uninterpreted (top) and interpreted (bottom) versions. The Cristianitos fault zone corresponds to the region of folding and faulting observed beneath the transgressive surface.

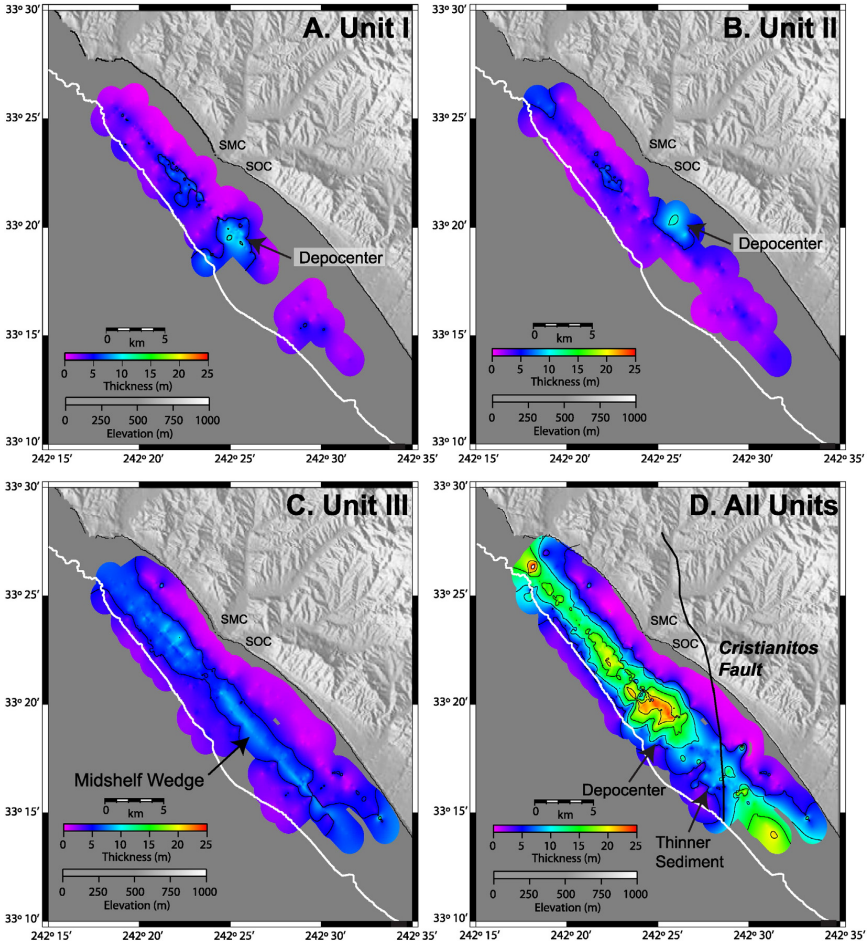

Fig. 8. Sediment thickness maps. (A) Unit I, (B) Unit II, (C) Unit III, (D) total sediment thickness from transgressive surface to seafloor. Maps show the 100 meter bathymetric contour in white. 5 meter contours of layer thickness are shown by thin black lines. SMC = San Mateo Creek and SOC = San Onofre Creek. Notable features are labeled.

juxtaposes the older San Onofre Breccia to the north against the younger Capistrano Fm (Fig. 1C).

Farther south, another region of folding and deformation is observed beneath the transgressive surface (Fig. 7), which correlates with a structural high on the transgressive surface. The trace of this deformation projects landward to the Cristianitos Fault, which is interpreted onshore to be a down-to-the-northwest normal fault as it separates older Monterey Fm to the south from younger San Mateo Fm (Fig. 1C; Ehlig, 1977, 1979; Shlemon, 1992). The identification of the Cristianitos Fault is also supported by the difference in seismic character on either side of the fault zone, which is analogous to the onshore deposits (Figs. 1C and 7). The San Mateo Fm is a blocky, homogenous sandstone, which may explain the lack of reflectors observed in the CHIRP profiles. South of the fault, the dipping reflectors appear to be caused by impedance contrasts in the Monterey Fm, a claystone with layers of indurated porcelanite. The folding and faulting observed beneath the transgressive surface, associated with the Cristianitos fault zone, is more consistent with a strike-slip fault with a down-to-the-northwest dip-slip component. Despite the observed deformation, there is no clear offset of the transgressive surface (Fig. 7). This shoal either records deformation (uplift) since the erosion of the transgressive surface or antecedent topography that was more resistant to wave-base erosion. Onshore a transgressive lag/abrasion platform, interpreted to be formed during either Marine Isotopic Stage (MIS) 5A (80 ka) or (MIS) 5E (125 ka), is not offset across the Cristianitos Fault (Shlemon, 1992). Therefore, our preferred hypothesis is that the shoal on the transgressive surface is resistant antecedent topography.

Other shoals along the transgressive surface correlate with the Newport Inglewood/Rose Canyon (NI/RC) fault (Figs. 1C and 5). Nested geophysical sparker and CHIRP profiles allow us to examine the deformation and stratigraphy across a variety of spatial and temporal scales. The two faults identified in the sparker data correlate with shoals observed in the CHIRP data. Moreover, there is no observed offset of the transgressive surface across the shoal. Note that the folds observed in the sparker data can be observed beneath the transgressive surface in the CHIRP data (Fig. 5). In this region, it is possible that recent NI/RC fault deformation has little to no vertical component of slip and thus would be difficult to image in the CHIRP data; however, at depth beneath the transgressive surface in the sparker data, a vertical component of slip with folding is observed across the NI/RC fault zone (Fig. 5).

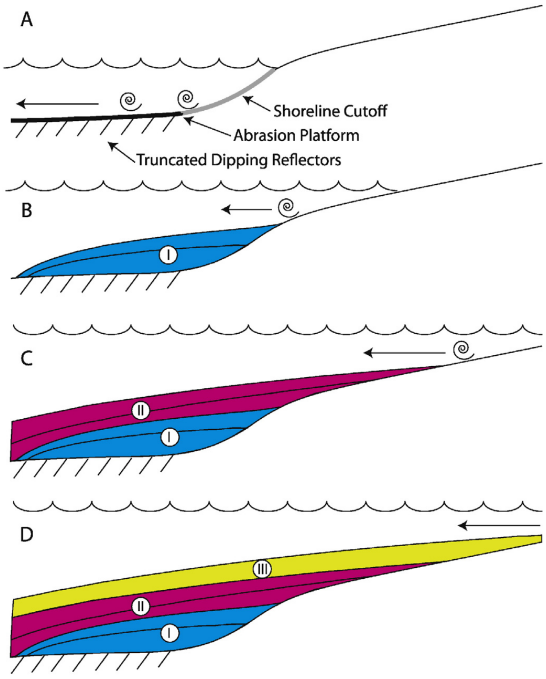

Fig. 9. Formation of a marine terrace. Swirls represent location of erosion of seafloor. (A) When the rate of sea-level rise diminishes, the corresponding depth corridor is exposed to a longer period of wave-base erosion and formation of the abrasion platform. The eroded sediment is transported both onshore and offshore. (B) As the rate of sea level rise increases, the depth corridor exposed to wave-base erosion migrates landward and the eroded material is transported landward and seaward. Coarse-grained sediment infills the relief associated with the previous abrasion platform and shoreline cutoff. This infilling lag deposit (Unit I) is shown in cyan. (C) With continued sea-level rise, the wave-base erosion continues to move landward with eroded material being transported landward and seaward. This midshelf lag deposit (Unit II) is shown in pink. (D) Sea level rises higher and the zone of erosion moves shoreward, with this material transported onshore and offshore. This modern sediment deposit (Unit III) is shown in yellow. (For interpretation of the references to color in this figure legend, the reader is referred to the web version of this article.)

Given the lack of deformation in the high-resolution CHIRP data above the transgressive surface, our preferred interpretation is that the most recent event pre-dates the formation of this surface.

Some deformation and uplift associated with the NI/RC fault (Fig. 5) could post-date the formation of the transgressive surface and be recorded by the onlap of Unit II. Nevertheless, this is not our preferred interpretation based on the following observations. First, the Cristianitos Fault exhibits very similar deformational pattern, creating a shoal on the transgressive surface, but onshore evidence suggests that there has been no slip younger than 125 ky (Shlemon, 1992), implying the fault is inactive. In addition to the south (Fig. 1A), where the Rose Canyon Fault appears active with measured Holocene slip in onshore trench data (Lindvall and Rockwell, 1995), the offshore CHIRP data north of the Rose canyon images deformation of the transgressive surface and seafloor (Fig. 10). Onshore paleoseismic data in La Jolla yield slip rates of 1–2 mm/yr (Lindvall and Rockwell, 1995), with the Most Recent Event (MRE) occurring in 1650 AD. The previous 5 events appear clustered and occurred between 9.3 and 5 ka (Lindvall and Rockwell, 1995). Farther north along the NI/RC fault, long-term slip rates are estimated at 0.5 mm/yr based on well data from Long Beach and Seal Beach oil fields (Freeman et al., 1992) and 0.34–0.55 mm/yr based on cone penetrometer testing (Grant et al., 1997). These slip rates are less than what has been determined from La Jolla trench sites (1–2 mm/yr; Lindvall and Rockwell, 1995). Unlike the shoaling of the transgressive surface across the Cristianitos Fault, there is no independent age information to determine between the two scenarios mentioned above (transgressive shoal records recent deformation versus antecedent resistant topography). Even though our preferred hypothesis is the shoaling of the transgressive surface in our study area is antecedent topography, we cannot rule out that the shoaling is due to more recent deformation on the NI/RC fault.

5.2. Sediment units

All unit interpretations were based on acoustic character and stratal geometry. Units I, II, and III are interpreted to be an infilling lag deposit, a midshelf lag deposit, and modern sediment, respectively. Unit I is bounded by the transgressive surface below and above by Unit II, where present, or Unit III (Figs. 2 and 3). The backstepping sequence of Units I and II is consistent with the landward migration of sediments associated with sea level rise. Similar uplifted wave-cut terraces are observed onshore in the region with mainly beach gravels, pebbles, and sand deposits (Ehlig, 1977; McNey, 1979; Shlemon, 1992), which record past relative sea level cycles. Likewise, dipping and truncated reflectors observed in the western part of the shelf are interpreted to be prograding units formed during older Pleistocene relative sea-level falls.

Unit II lies primarily between the infilling lag deposit (Unit I) and the modern sediment, but overlies the transgressive surface where Unit I is absent (Fig. 7). The depocenter for Unit II is located landward (shallower) than Unit I (Fig. 8). Even though Unit II is characterized by only a minor increase in acoustic reflectivity and more-gentle onlap, the material was likely sourced and transported seaward to its current location from a shallower abrasion surface (e.g., Figs. 3 and 9). No shoreline cutoff is observed along the landward edge of the abrasion platform. The lack of a shoreline cutoff suggests that the rate of sea-level rise post MWP 1B was more uniform with less abrupt changes in rate (i.e., no evidence for large changes in the rate of sea level rise following MWP 1B; Fairbanks, 1989, 1990; Bard et al., 1990; Fairbanks, 1992; Shackleton, 2000; Peltier and Fairbanks, 2006). Unit III is the result of modern sedimentation that overlies the other units. The unit is acoustically transparent suggesting it is well sorted and homogenous, typical of modern marine deposition on inner-California shelves (Le Dantec et al., 2010; Hogarth et al., 2012).

5.3. Controls on sediment thickness

In regions away from the San Mateo and San Onofre creeks, sediment dispersal is controlled predominantly by variations in the rate of sea level rise. Specific depth corridors along the shelf either experience more or less erosion and reworking if they correlate with slow rates of sea level rise or periods of rapid sea level rise, respectively. For example, the 53–72 m depth corridor corresponds to a diminished rate of sea level rise between MWP 1A and MWP 1B and experienced prolonged wave-base erosion with the formation of a shoreline cutoff (Fig. 3). Other shoals and changes in relief along the transgressive surface (e.g., Cristianitos Fault and NI/RC fault; Figs. 5 and 7) play an important role in controlling the distribution of Unit I and to a lesser extent Unit II (Figs. 5 and 7), which is captured in the isopach maps for these units (Fig. 8A and B). Sediment input from the San Mateo and San Onofre creeks also plays a role in sediment stacking patterns observed in Units I and II (Figs. 4, 6, and 8B). This local source of riverine sediment creates an area of increased supply and enhanced sediment thickness for Units I and II (Fig. 8A, B, and D). In this region, we also observe prograding packages along the margin following MWP 1B and the slowdown in sea level rise after ~8 kya (Fig. 4). Based on the observed stratal geometry and prograding packages, an increase in sediment supply occurs near the San Mateo and San Onofre creeks (Fig. 4). In summary, tectonic deformation along this portion of the southern California

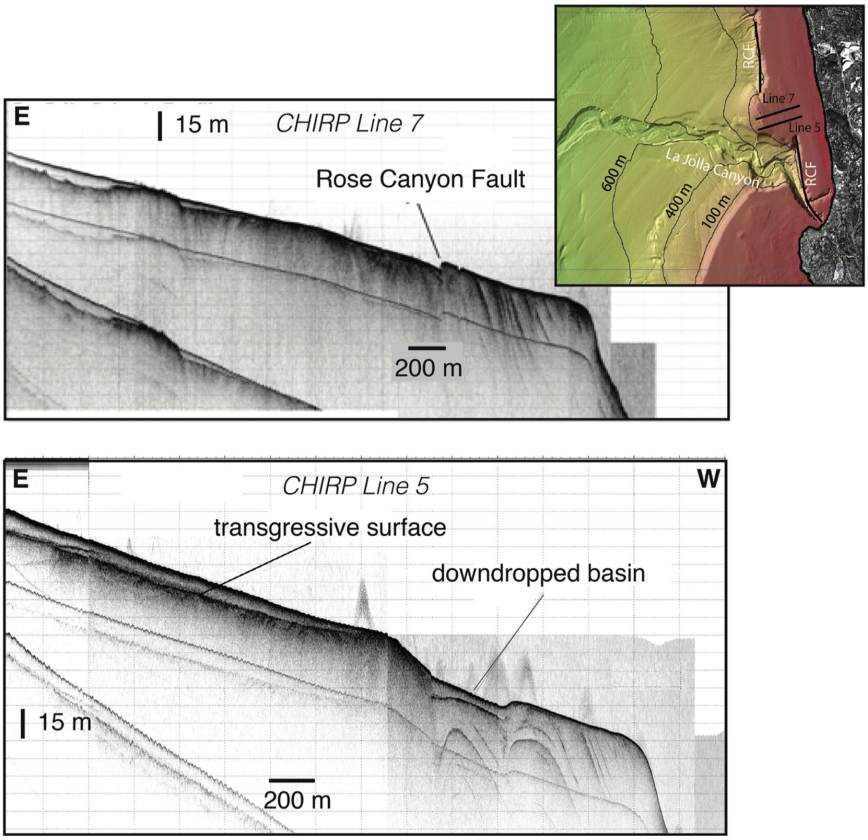

Fig. 10. CHIRP seismic profiles across the Torrey Pine pop-up structure (Hogarth et al., 2007). (Top) Line 7 crosses the Rose Canyon Fault and images a seafloor scarp with ~5 m of relief. (Bottom) Line 5 crosses the Rose Canyon Fault where it is expressed by two strands and creates a down-dropped block between the bounding fault stands. Note the offset of the transgressive surface and the increased sediment thickness across the down-dropped block. Inset shows location of the CHIRP data. RCF = Rose Canyon Fault. Site is also shown in Fig. 1A.

continental shelf plays a subordinate role to rates of eustastic change and sediment supply.

6. Conclusions

Analysis of new high-resolution CHIRP data and USGS mini sparker data has provided information about the factors controlling sediment distribution and facies variations within the transgressive sequence on the continental shelf offshore of San Onofre, CA. The shelf exhibits three depositional units that record the interplay between the rate of eustatic sea level rise and sediment supply. Unit I and Unit II are interpreted as lag deposits, coarser material that was eroded from an abrasion platform. Unit I fills in lows in the transgressive surface and younger Unit II transverses the midshelf. Unit III is acoustically transparent modern marine sedimentation. An observed change in dip of the transgressive surface at ~53 m (moving upslope) was carved by the slowdown in eustatic sea level rise between MWP 1A and MWP 1B. Unit I infills this along-shelf low, with its thickest deposits to the west. A shoaling of the transgressive surface is observed offshore of San Mateo and San Onofre creeks. Enhanced sediment supply from the San Mateo and San Onofre creeks created an extended beach or delta structure in this region (Fig. 6). Other areas of shoaling of the transgressive surface are associated with folding and faulting (Figs. 5 & 7). In regions where folding and faulting beneath the transgressive surface are observed, it is possible that the shoaling occurred after the formation of the transgressive surface, but more likely the shoals are erosion-resistant antecedent topography. The Cristianitos fault zone, where extensive compressional folding is observed, causes one of these shoals (Fig. 7). This leads to the conclusion that the Cristianitos Fault is not a simple normal fault, but is in fact, a strike-slip fault with a down-to-the-northwest component. In this region, local tectonics do not play a major role in sediment distribution, rather rates of eustatic sea level change and local sediment supply appear to be the governing factors. The abrasion platform formed during the still stand between MWP 1A and MWP 1B (Younger Dryas) places important age constraints on the activity for this segment of the NI/RC fault.

Acknowledgments

Support for SK was provided by the National Science Foundation's Graduate Research Fellowship (DGE-1144086). Support for data acquisition and processing was provided by Southern California Edison. Comments from two anonymous reviewers and J.E. Conrad greatly improved the manuscript.

References

Amorosi, A., Lucchi, M.R., Rossi, V., Sarti, G., 2009. Climate change signature of small-scale parasequences from Lateglacial–Holocene transgressive deposits of the Arno valley fill. Palaeogeogr. Palaeoclimatol. Palaeoecol. 273, 142–152.

Bard, E., Hamelin, B., Fairbanks, R.G., Zindler, A., 1990. Calibration of the ^{14}C timescale over the past 30,000 years using mass spectrometric U–Th ages from Barbados corals. Nature 345, 405–409.

Bard, E., Hamelin, B., Arnold, M., Montaggioni, L., Cabioch, G., Faure, G., Rougerie, F., 1996. Deglacial sea-level record from Tahiti corals and the timing of global meltwater discharge. Nature 382 (6588), 241–244.

Bohannon, R.G., Geist, E., 1998. Upper crustal structure and Neogene tectonic development of the California continental borderland. Geol. Soc. Am. Bull. 110 (6), 779–800.

Cattaneo, A., Steel, R.J., 2003. Transgressive deposits: a review of their variability. Earth-Sci. Rev. 62, 187–228.

Catuneanu, O., Abreu, V., Bhattacharya, J.P., Blum, M.D., Dalrymple, R.W., Eriksson, P.G., Winker, C., 2009. Towards the standardization of sequence stratigraphy. Earth Sci. Rev. 92, 1–33.

Christie-Blick, N., Driscoll, N.W., 1995. Sequence stratigraphy. Annu. Rev. Earth Planet. Sci. 23, 451–478.

Crouch, J.K., 1979. Neogene tectonic evolution of the western Transverse Ranges and the California Continental Borderland. Geol. Soc. Am. Bull. 90, 338–345.

Crouch, J.K., Suppe, J., 1993. Late Cenozoic tectonic evolution of the Los Angeles Basin and inner California borderland; a model for core complex-like crustal extension. Geol. Soc. Am. Bull. 105 (11), 1415–1434.

Dartnell, P., Driscoll, N.W., Brothers, D., Conrad, J.E., Kluesner, J., Kent, G., Andrews, B., 2015. Colored shaded-relief bathymetry, acoustic backscatter, and selected perspective views of the inner continental borderland. Geological Survey Scientific Investigations Map 3324, 3 sheets, Southern California, U.S. http://dx.doi.org/10.3133/sim3324.

Ehlig, P.L., 1977. Geologic report on the area adjacent to the San Onofre Nuclear Generating Station, Northwestern San Diego County, California. Neotectonics and Coastal Instability: Orange and Northern San Diego Counties, Californiapp. 113–132.

Ehlig, P.L., 1979. The Late Cenozoic evolution of the Capistrano embayment. In: Fife, D.L. (Ed.), Geologic Guide of San Onofre Nuclear Generating Station and Adjacent Regions of Southern California.

Ehlig, P., 1980. Rose Canyon Fault. Unpublished Report for Southern California Edison, January, 32 pp.

Fairbanks, R.G., 1989. A 17,000 year glacio-eustatic sea level record: Influence of glacial melting rates on the Younger Dryas event and deep-ocean circulation. Paleoceanography 342, 637–642.

Fairbanks, R.G., 1990. The age and origin of the "Younger Dryas climate event" in Greenland ice cores. Paleoceanography 5 (6), 937–948.

Fairbanks, R., 1992. Barbados sea level and Th/U ^{14}C calibration. IGBP PAGES/World Data Center for Paleoclimatology Data Contribution Series # 92-020. NOAA/NGDC Paleoclimatology Program, Boulder CO, USA.

Freeman, S. Thomas, Heath, Edward G., Guptill, Paul D., Waggoner, John T., 1992. Seismic hazard assessment, Newport–Inglewood fault zone. Association of Engineering Geologists, Southern California Section, Special Publication No. 4.

Goff, J.A., Duncan, C.S., 2012. Re-examination of sand ridges on the middle and outer New Jersey shelf based on combined analysis of multibeam bathymetry and backscatter, seafloor grab samples and chirp seismic data. In: Li, M.Z., Sherwood, C.R., Hill, P.R. (Eds.), Sediments, Morphology and Sedimentary Processes on Continental Shelves: Advances in Technologies, Research, and Applications. John Wiley and Sons, Ltd., Chichester, West Sussex, pp. 121–142.

Goff, J.A., Swift, D.J.P., Duncan, C.S., Mayer, L.A., Hughes-Clarke, J., 1999. High resolution swath sonar investigation of sand ridge, dune and ribbon morphology in the offshore environment of the New Jersey margin. Mar. Geol. 161, 309–339.

Goff, J.A., Kraft, B.J., Mayer, L.A., Schock, S.G., Sommerfield, C.K., Olson, H.C., Nordfjord, S., 2004. Seabed characterization on the New Jersey middle and outer shelf: correlatability and spatial variability of seafloor sediment properties. Mar. Geol. 209 (1), 147–172.

Grant, L.B., Waggoner, J.T., Rockwell, T.K., von Stein, C., 1997. Paleoseismicity of the north branch of the Newport–Inglewood fault zone in Huntington Beach, California, from cone penetrometer test data. Bull. Seismol. Soc. Am. 87 (2), 277–293.

Greenlee, S.M., Devlin, W.J., Miller, K.G., Mountain, G.S., Flemings, P.B., 1992. Integrated sequence stratigraphy of Neogene deposits, New Jersey continental shelf and slope: comparison with the Exxon model. Geol. Soc. Am. Bull. 104 (11), 1403–1411.

Hart, B.S., Plint, A.G., 1993. Tectonic influence on deposition and erosion in a ramp setting: upper cretaceous cardium formation, Alberta foreland basin. Am. Assoc. Pet. Geol. Bull. 77, 2092–2107.

Henkart, P., 2003. SIOSEIS, Software. Scripps Institution of Oceanography, La Jolla, CA (available at http://sioseis.ucsd.edu).

Hogarth, L.J., Babcock, J., Driscoll, N.W., Le Dantec, N., Haas, J.K., Inman, D.L., Masters, P.M., 2007. Long-term tectonic control on Holocene shelf sedimentation offshore La Jolla, California. Geology 35 (3), 275–278. http://dx.doi.org/10.1130/G23234A.1.

Hogarth, L.J., Driscoll, N.W., Babcock, J.M., Orange, D.L., 2012. Transgressive deposits along the actively deforming Eel River Margin, Northern California. Mar. Geol. 303, 99–114.

Jin, J.H., Chough, S.K., 1998. Partitioning of transgressive deposits in the southeastern Yellow Sea: a sequence stratigraphic interpretation. Mar. Geol. 149, 79–92.

Kennedy, M.P., 2001. Geologic map of the Las Pulgas Canyon 7.5-minute quadrangle, San Diego County, California: a digital database. California Geological Survey, Preliminary Geologic Maps, scale 1:24,000.

Kennedy, M.P., Tan, S.S., 2005. Geologic map of the Oceanside 30′ × 60′ Quadrangle. California: Regional Geologic Map Series, 1:100,000.

Kern, J.P., Rockwell, T.K., 1992. Chronology and deformation of Quaternary marine shorelines, San Diego County, California. In: Heath, E., Lewis, L. (Eds.), The Regressive Pleistocene Shoreline in Southern California: Santa Ana. California: South Coast Geological Society Annual Field Trip Guidebook 20, pp. 1–7.

Lantzsch, H., Hanebuth, T.J., Bender, V.B., Krastel, S., 2009. Sedimentary architecture of a low-accumulation shelf since the Late Pleistocene (NW Iberia). Mar. Geol. 259, 47–58.

Le Dantec, N., Hogarth, L.J., Driscoll, N.W., Babcock, J.M., Barnhardt, W.A., Schwab, W.C., 2010. Tectonic controls on nearshore sediment accumulation and submarine canyon morphology offshore La Jolla, southern California. Mar. Geol. 268, 115–128.

Legg, M.R., 1991. Developments in understanding the tectonic evolution of the California Borderlands. In: Osbourne, R.H. (Ed.)Society of Economic Paleontologists and Mineralogists Special Publication 46, pp. 291–312.

Lindvall, S., Rockwell, T.K., 1995. Holocene activity of the Rose Canyon fault, San Diego, California. J. Geophys. Res. 100 (B12), 24121–24132.

Lisiecki, L.E., Raymo, M.E., 2005. A Pliocene–Pleistocene stack of 57 globally distributed benthic δ^{18}O records. Paleoceanography 20. http://dx.doi.org/10.1029/2004PA001071.

Magistrale, H., 1993. Seismicity of the Rose Canyon fault zone near San Diego, California. Bull. Seismol. Soc. Am. 83 (6), 1971–1978.

McNey, J.L., 1979. General geology, San Onofre area. In: Fife, D.L. (Ed.), Geologic Guide of San Onofre Nuclear Generating Station and Adjacent Regions of Southern California.

Meade, B.J., Hagar, B.H., 2005. Block models of crustal motion in Southern California constrained by GPS measurements. J. Geophys. Res. 110 (B03403).

Miller, K.G., Mountain, G.S., Browning, J.V., Kominz, M., Sugarman, P.J., Christie-Blick, N., Wright, J.D., 1998. Cenozoic global sea level, sequences, and the New Jersey transect: results from coastal plain and continental slope drilling. Rev. Geophys. 36, 569–601.

Milliman, J.D., Jiezao, Z., Anchun, L., Ewing, J.I., 1990. Late Quaternary sedimentation on the outer and middle New Jersey continental shelf: results of to local deglaciation. J. Geol. 98, 966–976.

Muhs, D.R., Kennedy, G.L., Rockwell, T.K., 1994. Uranium-series ages of marine terrace corals from the Pacific coast of North America and implications for last-interglacial sea level history. Quat. Res. 42 (1), 72–87.

Nicholson, C., Sorlien, C.C., Atwater, T., Crowell, J.C., Luyendyk, B.P., 1994. Microplate capture, rotation of the western Transverse Ranges, and initiation of the San Andreas transform as a low-angle fault system. Geology 22 (6), 491–495.

Nordfjord, S., Goff, J.A., Austin, J.A., Duncan, L.S., 2009. Shallow stratigraphy and complex transgressive ravinement on the New Jersey middle and outer continental shelf. Mar. Geol. 266, 232–243.

Peltier, W.R., Fairbanks, R.G., 2006. Global glacial ice volume and last glacial maximum duration from an extended Barbados sea level record. Quat. Sci. Rev. 25, 3322–3337.

Petit, J.R., Jouzel, J., Raynaud, D., Barkov, N.I., Barnola, J.M., Basile, I., Stievenard, M., 1999. Climate and atmospheric history of the past 420,000 years from the Vostok ice core, Antarctica. Nature 399 (6735), 429–436.

Posamentier, H.W., 2002. Ancient shelf ridges — a potentially significant component of the transgressive system tract: case study from offshore northwest Java. AAPG Bull. 86, 75–106.

Posamentier, H.W., Allen, G.P., 1993. Variability of the sequence stratigraphic model: effects of local basin factors. Sediment. Geol. 86, 91–109.

Rampino, M.R., Sanders, J.E., 1981. Evolution of the barrier islands of southern Long Island, New York. Sedimentology 28, 37–47.

Rentz, P.T., 2010. The Influence of Tectonics, Sea Level, and Sediment Supply on Coastal Morphology in the Oceanside Littoral Cell, CA (UCSD Master's Thesis) .

Rockwell, T., 2010. The Rose Canyon fault zone in San Diego. Fifth International Conference on Recent Advances in Geotechnical Earthquake Engineering and Soil Dynamics.

Ryan, H.F., Legg, M.R., Conrad, J.E., Sliter, R.W., 2009. Recent faulting in the Gulf of Santa Catalina; San Diego to Dana Point. Spec. Pap. Geol. Soc. Am. 454, 291–315.

Ryan, H.F., Conrad, J.E., Paull, C.K., McGann, M., 2012. Slip rate on the San Diego Trough fault zone, inner California borderland, and the 1986 Oceanside earthquake swarm revisited. Bull. Seismol. Soc. Am. 102 (6), 2300–2312. http://dx.doi.org/10.1785/0120110317.

Schwab, W.C., Baldwin, W.E., Denny, J.F., Hapke, C.J., Gayes, P.T., List, J.H., Warner, J.C., 2014. Modification of the Quaternary stratigraphic framework of the inner-continental shelf by Holocene marine transgression: an example offshore of Fire Island, New York. Mar. Geol. 355, 346–360.

Shackleton, N.J., 2000. The 100,000-year ice-age cycle identified and found to lag temperature, carbon dioxide, and orbital eccentricity. Science 289, 1897–1902.

Shlemon, R.J., 1992. The Cristianitos fault and quaternary geology, San Onofre State Beach, California. The regressive Pleistocene shoreline in southern California. South Coast Geological Society Annual Field Trip Guidebook 20 pp. 9–12.

Sliter, Ray W., Ryan, Holly F., Triezenberg, Peter J., 2010. High-resolution seismic-reflection data offshore of Dana Point, southern California borderland. U.S. Geological Survey Open-file Report 2010-1111 (http://pubs.usgs.gov/of/2010/1111/).

Snedden, J.W., Dalrymple, R.W., 1999. Modern shelf sand ridges: from historical perspective to a unified hydrodynamic and evolutionary model. In: Bergman, K.M., Snedden, J.W. (Eds.), Isolated Shallow Marine Sand Bodies: Sequence Stratigraphic Analysis and Sedimentological Interpretation. SEPM Special Publication vol. 64, pp. 13–28.

Sorenson, J., Young, A., Driscoll, N., 2009. Tectonic Controls on Sea Cliff Geology of San Onofre State Beach. Unpublished UCSD Senior Thesis.

Swift, D.J.P., 1968. Coastal erosion and transgressive stratigraphy. J. Geol. 76, 444–456.

Swift, D.J.P., Phillips, S., Thorne, J.A., 1991. Sedimentation on continental margins: V. Parasequences. In: Swift, D.J.P., Oertel, G.F., Tillman, R.W., Thorne, J.A. (Eds.), Shelf Sand and Sandstone Bodies—Geometry, Facies and Sequence Stratigraphy. International Association of Sedimentologists Special Publication vol. 14, pp. 153–187.

Vail, P.R., Mitchum Jr., R.M., Todd, R.G., Widmier, J.M., Thompson III, S., Sangree, J.B., Bubb, J.N., Hatlelid, W.G., 1977. Seismic stratigraphy and global changes of sea-level. In: Payton, C.E. (Ed.), Seismic Stratigraphy—Applications to Hydrocarbon Exploration. American Association of Petroleum Geologists Memoir vol. 26, pp. 49–212.

Van Wagoner, J.C., Mitchum, R.M., Campion, K.M., Rahmanian, V.D., 1990. Siliciclastic sequence stratigraphy in well logs, cores, and outcrops. Am. Assoc. Pet. Geol. Methods Explor. Ser. 7 (55 pp.).

Chapter 2, in full, is a reprint of the material as it appears in: Klotsko, S., Driscoll, N., Kent, G., & Brothers, D., 2015. Continental shelf morphology and stratigraphy offshore San Onofre, California: The interplay between rates of eustatic change and sediment supply. Marine Geology, 369, 116-126. The dissertation author was the primary researcher and author, and the co-authors listed in this publication directed and supervised the research.

3

Geomorphological and stratigraphic evidence for rapid glacial lake draining in Block Island Sound, RI

3.1 ABSTRACT

Block Island Sound (BIS), Rhode Island was occupied by a glacial meltwater lake during the last deglaciation. New CHIRP seismic data, swath bathymetry, and scanned seismic profiles from BIS provide important insights and constraints on the morphologic evolution of a glaciated margin from the last glacial maximum to present. Interpretation of geophysical data revealed four well-defined sediment units: acoustic basement, glaciolacustrine varved sediments, a lag deposit, and Holocene sediment. The morphology and architecture of the sedimentary units suggest that Lake BIS drained quickly, followed by the catastrophic drainage of glacial Lake Connecticut (LC) through BIS ~500 years later (LC occupied present day Long Island Sound). The draining waters carved depressions (~100 m deep) on the BIS lakefloor and in the region between the lakes (The Race). The draining waters also carved southeast trending regional channels that have been partially filled in by reworked beach and bar deposits. Continued existence of the depressions and regional channels suggests a rapid transgression with limited sediment supply. Modern current-controlled deposits are patchy, thin, and only infill smaller channels. Our observations are consistent with evidence from other catastrophic glacial lake drainage in the northeastern and northwestern United States and Canada during the last deglaciation.

3.2 INTRODUCTION

High latitude continental margins in the Northern Hemisphere have been subjected to multiple glaciations (Svendsen et al., 2004; Sejdrup et al., 2005; Nørgaard-Pedersen et al., 2007) since the onset of the 100 ky glacial-interglacial cycle some time between 1.2 Ma and 600 kya (Ruddiman et al., 1989; Berger and Jansen, 1994; Lisiecki and Raymo, 2005). A diagnostic morphology develops along glaciated margins such as eskers (Clark and Walder, 1994; Brennand, 2000), drumlins (Smalley and Unwin,

1968; Shaw et al., 1989) and moraines (Borns, 1973; Ivy-Ochs et al., 2004; Brugger, 2007; Winkelmann et al., 2010). Meltwaters from the ice can become trapped behind terminal and recessional moraines creating glacial lakes. The lakes can drain gradually or in a rapid, catastrophic nature (Veillette, 1994). These glacial outburst floods, in the style of Jokulaups in Iceland, can release massive amounts of water with estimates up to 26 million cubic meters per second (Russell and Knudsen, 1998; Waitt, 1998). These floods cause substantial erosion, incising previous deposits, as evidenced by glacial Lake Missoula creating the Channeled Scablands of Washington State (Baker, 1973; Shaw et al., 1999). Sediments from this flood have been found far offshore in trenches and fracture zones in the form of massive turbidite deposits (Brunner et al., 1999; Normark and Reid, 2003; Zuffa et al., 2000).

During sea level transgression, morphology on the continental shelf is typically reworked by exposure to wave base erosion, which erodes highs and infills the lows (Cattaneo and Steel, 2003; Catuneanu et al., 2009). Along the New England/New Jersey margin, however, evidence of the previous glaciation (Wisconsin) is preserved (Schwab et al., 1997; Uchupi et al., 2001; Donnelly et al., 2005; Thieler et al. 2007). Block Island Valley and Hudson Shelf Valley are prominent across shelf drainage systems with adjacent sediment lobes. They were formed during the Wisconsin deglaciation, but their preservation during the transgression is poorly understood. To understand better the impacts of glaciation on landscape evolution, we must study former glaciated regions. This paper focuses on the formation and preservation of geomorphology and stratigraphy that developed at the southern reaches of the Laurentide ice sheet in Block Island Sound, RI from the Last Glacial Maximum to Present.

In the early 1980s, a seismic reflection survey was performed in Block Island Sound, RI (BIS) to define the sound's Quaternary geologic history (Needell and Lewis, 1984; Poppe et al., 2002; Fig. 1B). This survey revealed six major depressions in the

shelf between 60 and 100 meters in depth. Some of the depressions were more elongated with a southeast orientation, while others were more circular. The cause for all of these depressions was proposed to be modern tidal current scouring near constrictions (Lewis and Stone, 1991). In their theory, the glacial lakes that formally occupied Block Island Sound (glacial Lake Block Island Sound; Lake BIS) and Long Island Sound (glacial Lake Connecticut) gradually drained together without deep erosional downcutting or scouring (Lewis and Stone, 1991). Other work (Uchupi et al., 2001) suggests a rapid draining of the lakes, with Lake BIS draining first, then Lake Connecticut draining ~500 years later through BIS. The scours are located around the low of the moraine that separated the lakes, named "the Race" (Fig. 1B). In the catastrophic scenario, the fast-draining waters of Lake Connecticut would have carved out the depressions as they flowed across the subaerially exposed BIS. Here we present high-resolution subbottom and swath bathymetry data to test between these alternative models and provide new insights into margin evolution along glaciated regions.

3.3 REGIONAL SETTING

3.3.1 Deglaciation of Southern New England

Block Island Sound is located just northeast of Long Island Sound in southern New England (Fig. 1). During the most recent glacial period (Wisconsin), the southern lobe of the Laurentide Ice Sheet extended across southern New England mantling the inner continental shelf. The ice sheet reached its maximum extent ~23-24 kya, before retreating, leaving behind a series of terminal moraines (Stone and Borns, 1986; Dyke and Prest, 1987; Uchupi et al., 2001). Long Island, Cape Cod, and Block Island are subaerial remnants of these terminal moraines (Oldale and Ohara, 1980; Sirkin, 1982), composed mainly of glaciofluvial sands and gravels, and layers of diamicton (Colgan et al., 2003). As the ice retreated, other glacial deposits formed, including drumlin fields,

(Colgan et al., 2003), kames and eskers (Poppe et al., 2006), kettle hole lakes (Damman and French, 1987), and recessional moraines (Sirkin, 1982; Sirkin, 1991; Uchupi et al., 2001). As meltwaters drained from the Laurentide ice sheet, some was channeled through tunnels in the end moraines (Cutler et al., 2002), but in southern New England meltwater was predominantly dammed by both recessional and terminal moraines, creating an extensive glacial lake system. From about 17 kya to 15 kya most of the lakes drained across the then exposed shelf carving out valleys that have bathymetric expression, for example Hudson Shelf Valley and Block Island Valley (Fig. 2; Uchupi et al, 2001; Donnelly et al., 2005; Thieler et al., 2007). This was during the rapid ice recession in New England, based on lake varves (Ridge et al., 2012).

3.3.2 Geology of Block Island Sound

Block Island Sound has a complicated history, which in turn has created complex morphology and stratigraphy. The bedrock underlying the sound is comprised of pre-Mesozoic igneous and metamorphic rocks that dip towards the south (McMaster et al., 1968; Bertoni et al., 1977; Lewis and DiGiacomo-Cohen, 2000). The crystalline basement on Block Island is thought to be composed of gneisses, schists, and granitic intrusions, similar to the mainland (Woodworth et al., 1934). Throughout the sound, the basement rock has been cut into by an extensive Tertiary drainage system generally trending towards the south-southeast (McMaster et al., 1968; McMaster and Ashraf, 1973). The bedrock in BIS is, in some places, overlain by coastal plain strata (Needell and Lewis, 1984). This unit is composed of un- to semi-consolidated gravels, sands, silts, and clays (Lewis and DiGiacomo-Cohen, 2000), but is often found mixed in with glacial deposits on land. In seismic profiles from Needell and Lewis (1984), the difference between the coastal plain strata and the basement rock is often difficult to discern, with the main difference being the coastal plain strata sometimes has faint internal reflectors.

As such, they were combined together for a structure contour depth to surface map. These basal layers are commonly overlain by two glacial drift sheets, with one attributed to a late Wisconsin ice advance and the other to a previous ice advance (Sirkin, 1982; Needell and Lewis, 1984). The southern terminal moraine for the Laurentide ice sheet is the Ronkonkoma-Block Island-Nantucket moraine, deposited ~23-24 kya (Balco et al., 2002), which formed part of Long Island, Block Island, and Martha's Vineyard. The Harbor Hill-Roanoke Point-Charlestown recessional moraine deposited ~18-19 kya, and extended from northern Long Island, across Fisher's Island, connecting to the mainland (Balco et al., 2002). The moraines are mostly composed of boulders, layered sands and gravels, sediment flow materials, and till (Stone et al., 1998). The Harbor Hill-Roanoke Point-Charlestown recessional moraine created a boundary between Long Island Sound and Block Island Sound, separating glacial Lake Connecticut and glacial Lake Block Island Sound. The Lake BIS water surface is estimated to have been ~20 m below present sea level where there is a break in topography (Boothroyd et al., 1998). During the existence of glacial Lake BIS, laminated glaciolacustrine sediments were deposited (Needell and Lewis, 1984). These deposits are composed of layered silts and clays based on sediment cores (Bertoni et al., 1977). After the lake drained, BIS was subaerially exposed and eroded by flash floods and other continental waters (Uchupi et al., 2001). At the terminus of the ice sheet, Block Island Sound was isostatically depressed. Recent estimates by Oakley and Boothroyd (2012) suggest the depression was less than previously reported by coarse models and isolated data points (Andrews, 1973; Lewis and Stone, 1991; Stone et al., 2005) and was on the order of 35 m or less. As sea level rose, estuarine and marsh sediments were deposited, followed by beach and bar deposits. Reworking continues today by strong tidal currents (Lewis and DiGiacomo-Cohen, 2000) that reach up to 4 knots (Poppe et al., 2007; NOAA), as well as by storms and waves. The current seafloor sediment ranges from boulders and gravels to silty-sands depending

on the energy environment (Poppe et al., 2014a), with the finer sediments found in the deeper, outer parts of the Sound.

3.4 DATA ACQUISITION AND PROCESSING

In 1999, high-resolution CHIRP seismic data were acquired in Block Island Sound, RI. The survey was conducted using an EdgeTech X-Star CHIRP subbottom seismic reflection sonar with sub-meter vertical resolution. The CHIRP system was towed a few meters below the surface, under sail by Sea Education Association's S/V Westward. The profiles were acquired using a 1-6 kHz swept frequency acoustic source, which allowed for seafloor penetration up to 50 meters. All data were recorded in SEG-Y format with real-time GPS navigation recorded with each shot for location accuracy. The data were processed using SIOSEIS (Henkart, 2006) and then imported into the Kingdom software package (kingdom.ihs.com) for interpretation. A nominal value of 1500 m/s was applied to convert two way travel time to depth; both are shown on seismic profiles. Paper 3.5 kHz seismic records from the early 1990s acquired on the R/V Henlopen were converted to digital SEG-Y using the Matlab code image2segy.m (Farran, 2008; http://gma.icm.csic.es/node/67) and also imported into Kingdom Suite. A detailed description of the conversion procedure is provided in the supplemental material. Additionally, an early 1980s USGS seismic reflection survey was examined for comparison to the newer datasets (Needell and Lewis, 1984; Poppe et al., 2002). Multiple high-resolution multibeam datasets were used to examine the seafloor morphology in Block Island Sound and the outer shelf and slope offshore of the study area (Gardner et al., 2006; Poppe et al., 2007; Poppe et al., 2014a Poppe et al., 2014b; Andrews et al., 2016).

3.5 RESULTS

3.5.1 Acoustic Units and Stratigraphy

There are four clearly defined acoustic units imaged throughout the surveyed area and will be described from oldest to youngest. The deepest unit is acoustic basement and based on core data and outcrops, is an undifferentiated mixture of bedrock, coastal plain strata, and glacial moraine deposits (Bertoni et al, 1977; Needell and Lewis, 1984; Fig. 3). The acoustic basement has a high amplitude acoustic character and is often internally acoustically transparent. Internal reflectors in the acoustic basement are typically artifacts in the data that are multiples and ghosts (Fig. 4). The acoustic basement exhibits much relief, over 40 m in the channels, and often has a rounded, mound-like morphology. The acoustic basement is often covered with sediment, but crops out at the seafloor in some regions (Figs. 3 and 4). The reflector character at the top of the acoustic basement varies laterally, ranging from a crisp, sharp reflector to a more blotchy acoustic character (Figs. 5 and 6). This observed variation in acoustic character does not correlate with relief on the acoustic basement.

The next unit, identified as glaciolacustrine sediments, often mantles the acoustic basement (Figs. 3 – 6). The glaciolacustrine sediments exhibit a well-laminated acoustic character that are predominately parallel and often mimic the shape of the underlying acoustic basement. Such sediment draping is indicative of low energy lacustrine environments where sediment is largely deposited from suspension. Nevertheless, some layers do exhibit minor thickness variations, with their thickness increasing toward the topographic lows (Fig. 5). The units that have thickness variations are usually acoustically transparent. Their thickness variations and acoustic character suggest these are gravity flows. In some regions where the acoustic basement is shallow and exposed at the seafloor, the glaciolacustrine sediments do not mimic the underlying acoustic basement; rather they onlap onto it (Fig. 3).

Throughout the study area there is geophysical evidence of gas; the gas is observed near the top of the glaciolacustrine unit and beneath the modern sediments. The gas exhibits a high amplitude blotchy acoustic character and the stratigraphy below the gas is typically not imaged because of acoustic wipe out by the gas (Figs. 4, 5, and 6). Some windows through the gas are imaged and reveal the underlying strata (Fig. 4). A regional angular unconformity separates the underlying glaciolacustrine unit from the overlying sediments. In some regions the angular unconformity outcrops at the seafloor (e.g., Figs. 6 and 9) in other areas it is mantled by a lag deposit (Fig. 3) or modern sediments (Fig. 5). Another erosional feature is observed at the top of the glaciolacustrine unit and has a v-shaped morphology (Figs. 7 and 8). These v-shaped paleochannels exhibit a variety of scales ranging form a few meters to over a kilometer in width (Figs. 3, 7, and 8). The smaller paleochannels observed in Line 32 (Fig. 8) have a high amplitude reflector that delineates the base of the channel and may be the result of gas charging along the boundary. Where the glaciolacustrine sediments crop out at the seafloor, the surface is smoother (Fig. 5); however, where sediments cover the unit, its boundary is rougher and exhibits a hummocky scalloped morphology (Figs. 5 and 7) with notches (Fig. 6). The thickness of the glaciolacustrine sediments exhibit marked variations as a result of differential erosion; in some regions only a thin veneer above the bedrock is observed (Fig. 5). In other regions, the thickness is greater than 50 m (Figs. 5 and 8). The cause for this differential erosion and attendant thickness variations of the glaciolacustrine unit will be discussed below.

The third unit is a lag deposit that fills in paleochannels and overlies the glaciolacustrine sediments (Figs. 3, 7, and 8). Where the lag deposit is observed, there are no clear reflectors separating the channel fill from the lag deposit observed above the transgressive surface. The transgressive surface has truncation below and separates subaerially exposed strata from marine deposits above (Klotsko et al., 2015). The lag

deposit has abundant internal reflectors, with some reflectors more organized and linear, while others are more chaotic in nature (Fig. 3). The thickness of the lag deposit exhibits much variability throughout the region (Fig. 7) and is largely formed on the interchannel highs (Figs. 10 and 11). Where it fills in channels, the lag deposit reaches thicknesses over 15 m, but thins out away from the localized depocenters (Fig. 3).

The upper unit (Yellow – Modern Sediment) has some internal acoustic reflectors, however, large areas are acoustically transparent (Figs. 5, 6, and 8). Prograding reflectors are observed to be migrating downslope, originating in shallow water and then pinching out downslope onto a high in the acoustic bedrock (Fig. 4). Sculpting of the sediment layer is also observed with moating along the steep erosional unconformity observed in the glaciolacustrine sediments (Fig. 5). Beneath the transparent modern deposits is an angular unconformity in the glaciolacustrine unit (Fig. 5). The Holocene sediment thickness ranges from less than 1 m to approximately 15 m thick (Fig. 5) with some areas having as much as 20 m (Fig. 6). Regions with thick modern sediment in the large depressions are often obscured by gas (Figs. 5 and 6) and make it difficult to assess the true thickness. In the shallow regions, symmetric and asymmetric bedforms are observed (Figs, 3, 6, 11).

3.5.2 Physiography

The CHIRP data acquired on the S/V Westward were focused on the large, circular depression in the seafloor, which is observed in bathymetry data from the region (Figs. 1). We refer to this feature as the “large depression”. The large depression is ~100 m deep with a steep eastern slope being approximately 18° (Fig. 4). The glaciolacustrine sediments crop out at the seafloor along the steep eastern side of the large depression (Fig. 10). There is an absence of modern sediment within the deepest part of the large depression toward the east (Fig. 10). Modern sediment is observed on the southwestern

side of the large depression, where the slope is more gradual and sediment is prograding downslope (Figs. 4, 5, and 6). An acoustic basement high blocks the prograding sediment from filling the eastern deepest-most portion of the large depression. Moating and current scour are observed in the upper unit along the northern portion of the large depression (Figs. 5 and 6).

The swath bathymetry images the complex morphology in BIS (Fig. 11). Different perspective look angles are shown to capture the relationships between the various physiographic features. Figure 11A shows a look angle to the north with the large depression centered in the image. There are two large erosional channels (green regions) imaged in the swath bathymetry and are separated by a shoal (yellow region) mantled with sediment waves. The large circular depression is located near the beginning of the northern erosional channel. Depressions associated with the Race are located along the left portion of the image (Fig. 11A). An enlargement of Figure 11A is shown in Figure 11B imaging the steep eastern wall and sand waves to the southwest. Figure 11C is looking toward the east, showing the two regional erosional channels with the large depression located along the northern channel. Block Island is observed in the distance (Fig. 11C). Looking west toward the Race reveals the scoured and eroded topography between Long Island Sound and Block Island Sound. An isolated depression is observed eastward of the northern erosional channel (Fig. 11D). The sediment waves imaged in the region are largely confined to the shoals (yellow color) and exhibit a variety of morphologies from linear to arcuate.

3.6 DISCUSSION

Block Island Sound's complicated, irregular morphology appears to have developed in multiple stages (Needell and Lewis, 1984). Several conceptual models have been proposed to explain the observed morphology and subbottom reflectors in

BIS (Bertoni et al., 1977; Needell and Lewis, 1984; Lewis and Stone, 1991; Uchupi et al., 2001; Poppe et al., 2014b; McMullen et al., 2015). The high resolution CHIRP and bathymetry data acquired in BIS provides important new constraints on the evolution of the region. We will first discuss the existing conceptual models for the evolution of BIS morphology and stratal geometry and outline how the new data have refined these models.

It is generally agreed upon that the regional erosional channels imaged in the bathymetry were caused by glacial lake draining and overprinting by fluvial and storm processes (Figs. 7, 8, and 12; Needell and Lewis, 1984; Lewis and Stone, 1991; Uchupi et al., 2001; McMullen, 2014; Poppe et al., 2014; McMullen, 2015). As the meltwaters drained across the exposed seafloor of BIS, they carved southeastward trending channels towards the entrance of Block Island Sound. The nature of glacial lake draining, however, is still debated. One model suggests that Lake Connecticut and Lake Block Island Sound drained gradually and occurred concomitantly because erosion of the spillway between the lakes was controlled by the rate of draining of Lake BIS (Lewis and Stone, 1991; Stone et al., 1998). In this model, complete draining and exposure occurred by 15.5 kya. In contrast, Uchupi et al. (2001) proposed a catastrophic draining of glacial Lake Block Island Sound by approximately 16 kya, followed by the catastrophic draining of glacial Lake Connecticut about 500 years later (~15.5 kya). In this model, the large depression and the depressions near the Race (Figs. 1A and 11) are the result of rapid draining and scouring. Conversely, in the gradual lake draining model, there is no mechanism during the lake drainings to erode the observed depressions, as the draining is hypothesized to be slower and with low energy. In this model, the erosion and formation of the depressions by the Race are attributed to modern tidal current erosion associated with the constriction caused by the Harbor Hill recessional moraine (Fig. 1; Bertoni et al., 1977; Needell and Lewis, 1984; Lewis and Stone, 1991). Another model to explain the observed

morphology is that fluvial erosion formed the large depression after the lakefloor became exposed, with modern tidal currents maintaining and further eroding the depressions (Poppe et al., 2006; McMullen et al., 2015).

We examine new and existing data to test between these alternative glacial lake drainage models. One of the new CHIRP profiles acquired across the large depression (Fig. 12) is spatially coincident with an existing uniboom MCS profile acquired by Needell and Lewis (1984). The high-resolution CHIRP data image the boundary between the modern sediment and the underlying glaciolacustrine deposit (Figs. 5 and 12). In the uniboom data, this boundary is not well imaged and as a result of the resolution, Needell and Lewis (1984) infer that the underlying material is bedrock (PZ). This stratal relationship provides important constraints on the timing of erosion as glaciolacustrine deposits are below the deepest part of the large depression and have been truncated. Gas obscures part of this unconformity, but it is clearly imaged both north and south of the gas (Fig. 12). In addition, the continuation of modern sediment on the edge of the large depression down into the depression is imaged in the new CHIRP data (Figs. 4 and 12). These sediments show signs of current scour and moating (Figs. 5 and 12). In Needell and Lewis (1984) the sediment fill in the large depression is interpreted to be fluvial and estuarine deposits because the connection to other sediment packages is not imaged due to a more regional survey grid. Based on stratal geometry observed in in this region, our preferred interpretation is that the glaciolacustrine sediments were truncated prior to the transgression. After the transgression, modern sediments formed and make up the prograding and infilling deposits in the large depression. Bottom photographs reveal the change in sediments between the eastern and western sides of the large depression (Fig. 13). The glaciolacustrine sediments are reddish-brown and gray silty-clay where they crop out on the steep eastern wall of the depression. On the more gentle western side of the large depression, where the prograding stratal packages are observed, the seafloor is

composed of fine sand and is heavily bioturbated (McMullen et al., 2015). Away from the large depression, paleochannels could be infilled by fluvial and estuarine deposits and capped by transgressive lag deposits with a high amplitude acoustic character (Figs. 7 and 8).

Varve chronology suggests that the glacial lakes persisted up to a few thousand years (Uchupi et al., 2001), and have a distinct acoustically laminated signature in the CHIRP data (e.g., Figs. 5 and 6). In our conceptual model, the adjacent continental shelf to Block Island Sound would be sediment starved when the glacial lakes existed; as the lakes would be an efficient sediment trap, consistent with the delta deposits observed along their northern margins (Lewis and Stone, 1991). Breaching of the moraines and draining of the lakes could result from several processes acting alone or in concert. Given the terminal moraine would have some degree of permeability, sapping may have prevented the lake waters from over-flowing the dam, but also may have contributed to the failure of the dam itself. Continued filling of the lakes from glacial meltwater also could have caused toping along low points of the terminal moraine (Uchupi et al., 2001). Storm surge and large waves also could cause dam breaching. Once breached, flow through the moraine would have caused increased erosion and downcutting with rapid lake draining that may be on the order of 100's of years. Another consequence of such an accumulation of water behind the terminal moraines is changing the pattern and magnitude of ground water flow. It has been postulated that ground water flowed south to the slope, a free surface despite the large distance, and may have caused slope failure and canyon erosion (Robb, 1984; Uchupi and Oldale, 1994; Uchupi et al., 2001).

Offshore high-resolution bathymetric data along the shelf and slope exhibit morphologic features that are more consistent with the proposed rapid lake draining model (Gardner et al., 2006; Andrews et al., 2016). Block Island Valley extends from the entrance of BIS across the shelf (Figs. 1 and 2) and slide scars and slump deposits

are observed down slope (e.g., the southern New England landslide complex; Fig. 2B). It is difficult to reconcile the observed morphology on the shelf and slope with a gradual lowering of the lake levels, as proposed by Lewis and Stone (1991). A glacial outburst flood is more likely to carve such a large feature on the shelf and deliver large amounts of sediment to the shelf edge and slope. Rapid deposition on the slope also could potentially be a cause for the observed slope failures (e.g., Driscoll et al., 2000).

Similar morphology is observed where other glacial outburst floods have been proposed (Uchupi et al., 2001; Donnelly et al., 2005; Thieler et al., 2007). Hudson Shelf Valley and Block Island Valley are the largest physiographic features on the U.S. mid-Atlantic continental shelf (Fig. 2; Thieler et al., 2007). Hudson Shelf Valley was initially formed by stable meltwater runoff followed by failure of the terminal moraine dam between Staten Island and Long Island, NY, which allowed for the catastrophic draining of glacial lakes occupying the Lake Ontario and Hudson river basins (Uchupi et al., 2001; Schwab et al., 2002; Donnelly et al., 2005; Thieler et al., 2007). Several lines of evidence led Uchupi et al. (2001) to propose catastrophic drainage of the glacial lakes behind the terminal moraine as well as subsequent flash floods. For example, the sediment lobe morphology of the continental shelf, the large erratics southwest of Hudson Shelf Valley, and the mastodon and mammoth teeth in the vicinity of Hudson Shelf Valley. Transport of the coarse debris and associated land vertebrate remains 10's of kilometers across the low relief shelf requires a high energy event (Uchupi et al., 2001). Once the lakes drained, their floors underwent fluvial erosion, which also contributed to the offshore sediment depocenters. High-resolution bathymetry and subbottom data imaged banks, levees, major sediment lobes, and an outer shelf wedge associated with Hudson Shelf Valley (Fig. 2a; Thieler et al., 2007). Similar to Block Island Valley, Hudson Shelf Valley has not been infilled by the recent transgression, unlike other previously incised valleys along the Atlantic margin.

Other lines of evidence that support our preferred interpretation of rapid draining of Lake Connecticut and Lake Block Island Sound is based on morpho-stratigraphic studies of Glacial Lake Missoula. It drained catastrophically multiple times creating the Channeled Scablands of eastern Washington State. These flows changed the Columbia Plateau from a dendritic drainage pattern to a barren, channelized landscape with loess islands, giant ripples, and major gravel bars (Bretz, 1969; Baker, 2009). Glacial Lake Missoula was located in Montana, much farther from the ocean than glacial Lake Connecticut and glacial Lake Block Island Sound (Fig. 1). After the meltwaters from Lake Missoula carved out the Channeled Scablands, they entered the Pacific Ocean via the Columbia River as hyperpycnal flows (Normark and Reid, 2003). The massive amount of sediment generated the Tufts fan and was transported offshore more than 800 km in the form of turbidites (Brunner et al., 1999; Zuffa et al., 2000; Normark and Reid, 2003).

In the regions where catastrophic glacial lake draining shaped the margin, these features still have a bathymetric expression (Figs. 1 and 2). Why these features have not been reworked and obscured by the recent transgression and wavebase erosion remains poorly understood. During a sea level transgression, wavebase energy erodes bathymetric highs and infills the lows diminishing relief (Klotsko et al., 2015); however, as mentioned above, the large depressions and regional erosional valleys in BIS were not reworked and infilled. In the gradual glacial lake draining model, the depressions near the Race are formed later by tidal currents after the most recent transgression, but this model does not account for Block Island Valley (Fig. 2). Bertoni et al. (1977) proposed a different explanation for the large depressions not being infilled during the transgression. The large depression, referred to as the “big hole” in their paper, is interpreted as a kettle hole; a large block of ice would have kept the depression free of sediment during the transgression and then it subsequently melted. There are many kettle lakes found onshore

at Block Island, which formed during the deglaciation (Sirkin and Veeger, 1998). Other offshore depressions have been observed just to the northeast of BIS near Woods Hole, MA (Poppe et al., 2008). These features were interpreted to be kettle holes that were eventually submerged during the transgression. Offshore kettle holes might explain the existence of the circular depressions and why they were not reworked and infilled during the most recent transgression; however, it does not explain why the large regional erosional valleys exposed in Block Island Sound (Figs. 1 and 11), or the Hudson Shelf Valley and Block Island Valley exposed on the shelf, were not reworked and obscured (Fig. 2). A potential explanation for the large regional features preserved on the shelf (i.e., HSV and BV) is that for these water depths on the shelf, the transgression was too rapid to significantly rework and obscure them.

The shoals that surround BIS and the small fetch may have limited the available wave base energy to rework and obscure the existing physiography (Fig. 1). Also, as inundation continued, attendant tidal currents would maintain and further erode portions of these features. Smaller paleochannels away from the large depression are infilled by localized deposits mantled by modern marine deposits (Figs. 3, 7, and 8). It is difficult to identify whether the infilling deposits are fluvial, estuarine, or transgressive lag deposits because the infill is acoustically transparent. For simplicity, they are labeled as lag deposits on the seismic profiles. Nevertheless, a marked high-amplitude reflector interpreted as the transgressive surface separates the localized infilling deposits below from the overlying regional modern marine deposits (e.g., Fig. 8).

Throughout the study region surrounding the large depression, modern sediments form thin veneers on the surrounding shoals (Fig. 5). Needell and Lewis (1984) mapped sediment deposits upwards of 40 m in the sand waves at the mouth of the Sound and other pockets of modern sediment up to 30 m thick in a few areas. Modern sediment is observed prograding down into the depression, where it is blocked by a high in the

acoustic bedrock and unable to infill the deepest point (Fig. 4). McMullen et al. (2014) suggests that obstacles such as drumlins divert fluid flow and cause eddies to form in the large depression, continuing the erosion. If this is correct, then eddies also need to explain the sediment patterns with prograding sediment from the southwest, moating and current-controlled deposits to the north, and a lack of sediment in the deepest part toward the east (Fig. 4). Sediment waves are present to the south and west of the large depression (Figs. 1A and 11) and indicate varying flow directions (Fig. 12; McMullen et al., 2014). Although the sediment is prograding east into the large depression, dominant flow direction in northern BIS is west into Long Island Sound. The dominant flow direction in southern BIS is to the east (Poppe et al., 2007). The depressions near the Race represent a constriction point between BIS and LIS and are subjected to swift tidal currents nearly 4 knots in speed (Poppe et al., 2007). This constricted flow likely prevents sediment deposition in these depressions with sediment settling occurring in lower velocity areas when the flow spreads out laterally, such as in the sand wave field at the southern boundary of BIS (Fig. 1A).

3.7 CONCLUSIONS

Analysis of new high-resolution CHIRP seismic and swath bathymetry data, as well as scanned 3.5 kHz seismic profiles, have provided important constraints on the factors controlling the development of complex morphology in Block Island Sound, RI. These new data have allowed us to update the model proposed by Lewis and Stone (1991) based on seismic profiles interpreted by Needell and Lewis (1984). The new CHIRP data images an unconformity separating modern sediment above from glaciolacustrine sediments below in the large depression (Fig. 5), suggesting the depression was eroded prior to modern times. Based on the morpho-stratigraphy in and around BIS, as well as other studies of nearby glacial lake draining (e.g., Uchupi et al.,

2001; Schwab et al., 2002; Donnelly et al., 2005; Thieler et al., 2007), our preferred model is that the depressions and Block Island Valley were formed by catastrophic glacial lake draining. The continuing existence of this morphology may be the result of a rapid transgression across these water depths on the shelf and limited wave energy for the preservation of the features within Block Island sound. The large depression has likely not been filled in during modern times due to lack of sediment in the vicinity. The modern sediment imaged prograding into the depression (Fig. 4) is only a thin layer that is prevented from infilling the deepest part of the depression by a high in the acoustic basement.

We propose that glacial Lake BIS drained catastrophically followed by the catastrophic drainage of glacial Lake Connecticut approximately 500 years later through BIS. These draining waters carved major depressions at the connection point between the sounds at the Race in addition to a large circular depression to the east (Fig. 11). The waters also carved the southeastward trending regional channels. After lakefloor exposure, fluvial and storm runoff drained through the sound creating channels of various scales (Fig. 8). As sea level rose, beaches and wetlands developed in BIS. These sediments were reworked into lag deposits that deposited in lows away from the large depression; these infilled channels are mantled by a thin veneer of modern sediments (Figs. 3 and 7). Swift tidal currents near the Race maintain and further erode portions of these features.

3.8 ACKNOWLEDGEMENTS

We would like to thank the Captain Sean Bercaw and the crew of the S/V Westward for sailing a great survey in Block Island Sound and the crew of the R/V Cape Henlopen for assistance collecting the 3.5 kHz profiles, side-scan data, and VanVeen cores. We thank Colby Nicholsen for his assistance with digitizing the paper seismic

records. This research was funded by the Office of Naval Research with a special thanks to Joseph Kravitz. Educational support for S. Klotsko was provided by the National Science foundation (GRFP).

Chapter 3 has been submitted for publication in: Klotsko, S. and Driscoll, N., Submitted. Geomorphological and stratigraphic evidence for rapid glacial lake draining in Block Island Sound, RI, Quaternary Research. The dissertation author was the primary researcher and author, and the co-author listed in this publication directed and supervised the research.

3.9 REFERENCES

Andrews, J.T., 1973. Maps of the maximum post glacial marine limit and rebound for the former Laurentide Ice Sheet. Arctic and Alpine Research 5, 41–48.

Andrews, B.D., Chaytor, J.D., ten Brink, U.S., Brothers, D.S., Gardner, J.V., Lobecker, E.A., and Calder, B.R., 2016. Bathymetric terrain model of the Atlantic margin for marine geological investigations (ver. 2.0, May 2016): U.S. Geological Survey Open-File Report 2012–1266, 12 p., 1 pl., http://dx.doi.org/10.3133/ofr20121266.

Balco, G., Stone, J. O., Porter, S. C., & Caffee, M. W., 2002. Cosmogenic-nuclide ages for New England coastal moraines, Martha's Vineyard and Cape Cod, Massachusetts, USA. Quaternary Science Reviews 21, 2127-2135.

Baker, V. R., 1973. Paleohydrology and sedimentology of Lake Missoula flooding in eastern Washington. Geological Society of America Special Papers, 144, 1-73.

Baker, V.R., 2009. The Channeled Scabland: A Retrospective. Annual Review of Earth and Planetary Sciences 37, 393-411.

Berger, W.H., and Eystein Jansen, 1994. Mid-Pleistocene Climate Shift: The Nansen Connection. The polar oceans and their role in shaping the global environment, 295-311.

Bertoni, R., Dowling, J., Frankel, L., 1977. Freshwater-lake sediments beneath Block Island Sound. Geology 5, 631-635.

Borns, H. W., 1973. Late Wisconsin fluctuations of the Laurentide ice sheet in southern and eastern New England. Geological Society of America Memoirs, 136, 37-45.

Boothroyd, J.C., Freedman, J.H., Brenner, H.B., and Stone, J.R., 1998. The glacial geology of southern Rhode Island. In: Guidebook to Field Trips in Rhode Island and Adjacent Regions of Connecticut and Massachusetts: New England Intercollegiate Geologic Conference, 90th Annual Meeting Kingston, Rhode Island.

Brennand, T.A., 2000. Deglacial meltwater drainage and glaciodynamics: inferences from Laurentide eskers, Canada. Geomorphology 32, 263-293.

Bretz, J.H., 1969. The Lake Missoula floods and the channeled scabland. The Journal of Geology, 505-543.

Brugger, K.A., 2007. Cosmogenic 10Be and 36Cl ages from Late Pleistocene terminal moraine complexes in the Taylor River drainage basin, central Colorado, USA. Quaternary Science Reviews 26, 494-499.

Brunner, C.A., Normark, W.R., Zuffa, G.G., Serra, F., 1999. Deep-sea sedimentary record of the late Wisconsin cataclysmic floods from the Columbia River. Geology 27, 463.

Cattaneo, A., Steel, R.J., 2003. Transgressive deposits: a review of their variability. Earth-Sci. Rev. 62, 187–228.

Catuneanu, O., Abreu, V., Bhattacharya, J.P., Blum, M.D., Dalrymple, R.W., Eriksson, P.G.,Winker, C., 2009. Towards the standardization of sequence stratigraphy. Earth Sci. Rev. 92, 1–33.

Clark, P.U., and Joseph S. Walder, 1994. Subglacial drainage, eskers, and deforming beds beneath the Laurentide and Eurasian ice sheets. Geological Society of America Bulletin 106, 304-314.

Colgan, P.M., Mickelson, D. M., & Cutler, P. M., 2003. Ice-marginal terrestrial landsystems: southern Laurentide Ice Sheet margin. Glacial landsystems. London: Arnold, 111-142.

Cutler, P.M., Colgan, P. M., & Mickelson, D. M., 2002. Sedimentologic evidence for outburst floods from the Laurentide Ice Sheet margin in Wisconsin, USA: implications for tunnel-channel formation. Quaternary International 90, 23-40.

Damman, A.W.H. and French, T.W., 1987. The ecology of peat bogs of the glaciated Northeastern United States: a community profile. U.S. Fish Wildl. Serv. Biol. Rep. 85(7.16) 100 pp.

Donnelly, J.P., Driscoll, N.W., Uchupi, E., Keigwin, L.D., Schwab, W.C., Thieler, E.R., Swift, S.A., 2005. Catastrophic meltwater discharge down the Hudson Valley: A

potential trigger for the Intra-Allerød cold period. Geology 33, 89.

Driscoll, N. W., Weissel, J. K., & Goff, J. A., 2000. Potential for large-scale submarine slope failure and tsunami generation along the US mid-Atlantic coast. Geology, 28, 407-410.

Dyke, A.S., Prest, V.K., 1987. Late Wisconsinan and Holocene History of the Laurentide Ice Sheet. Géographie physique et Quaternaire 41, 237-263.

Eakins, B.W., L.A. Taylor, K.S. Carignan, R.R. Warnken, T. Sazonova, and D.C. Schoolcraft, 2009. Digital Elevation Model of Montauk, New York: Procedures, Data Sources and Analysis, NOAA Technical Memorandum NESDIS NGDC-17, Dept. of Commerce, Boulder, CO, 23 pp.

Farran, M. 2008. IMAGE2SEGY: Una aplicación informática para la conversión de imágenes de perfiles sísmicos a ficheros en formato SEG Y. Geo-Temas 10, 2008 p. 1215 -1218. http://gma.icm.csic.es/node/67.

Gardner, J.V., Mayer, L.A., Armstrong, A.A., 2006. Mapping supports potential submission to U.N. Law of the Sea. EOS Trans., Am. Geophys. Union 87, 157–159.

Henkart, P., 2003. SIOSEIS, Software. Scripps Institution of Oceanography, La Jolla, CA (available at http://sioseis.ucsd.edu).

Ivy-Ochs, S., Schafer, J., Kubik, P.W., Synal, H.-A., Schluchter, C., 2004. Timing of deglaciation on the northern Alpine foreland (Switzerland). Eclogae Geologicae Helvetiae 97, 47-55.

Lewis, R. S., & Stone, J. R., 1991. Late Quaternary stratigraphy and depositional history of the Long Island Sound basin: Connecticut and New York. Journal of Coastal Research, 1-23.

Lewis, R.S., & DiGiacomo-Cohen, M., 2000. A review of the geologic framework of the Long Island Sound basin, with some observations relating to postglacial sedimentation. Journal of Coastal Research 16, 522-532.

Lisiecki, L. E., & Raymo, M. E., 2005. A Pliocene-Pleistocene stack of 57 globally distributed benthic $\delta^{18}O$ records. Paleoceanography, 20(1).

McMaster, R. L., Lachance, T. P., & Garrison, L. E. ,1968. Seismic-reflection studies in Block Island and Rhode Island Sounds. AAPG Bulletin, 52(3), 465-474.

McMaster, R.L., & Ashraf, A. S. A. F., 1973. Drowned and buried valleys on the southern New England continental shelf. Marine Geology 15, 249-268.

McMullen, K.Y., Poppe, L.J., Danforth, W.W., Blackwood, D.S., Clos, A.R., and Parker, C.E., 2014, Sea-floor morphology and sedimentary environments of western Block Island Sound, northeast of Gardiners Island, New York: U.S. Geological Survey Open-File Report 2014–1160, 1 DVD-ROM, http://dx.doi.org/10.3133/ofr20141160.

McMullen, K.Y., Poppe, L.J., Danforth, W.W., Blackwood, D.S., Winner, W.G., and Parker, C.E., 2015, Sea-floor morphology and sedimentary environments in western Block Island Sound, offshore of Fishers Island, New York: U.S. Geological Survey Open-File Report 2014–1224, 1 DVD-ROM, http://dx.doi.org/10.3133/ofr20141224.

National Geophysical Data Center, 1999. U.S. Coastal Relief Model - Northeast Atlantic. National Geophysical Data Center, NOAA. doi:10.7289/V5MS3QNZ [accessed 2015].

Needell SW, Lewis RS, 1984. Geology of Block Island Sound, Rhode Island and New York. US Geological Survey Miscellaneous Field Studies Map MF-1621, scale 1:125,000.

NOAA National Centers for Environmental Information, U.S. Coastal Relief Model, 10/12/13, http://www.ngdc.noaa.gov/mgg/coastal/crm.html

Nørgaard-Pedersen, N., Mikkelsen, N., Kristoffersen, Y., 2007. Arctic Ocean record of last two glacial-interglacial cycles off North Greenland/Ellesmere Island — Implications for glacial history. Marine Geology 244, 93-108.

Normark, W.R., & Reid, J. A., 2003. Extensive deposits on the Pacific Plate from late Pleistocene North American glacial lake outbursts. The Journal of Geology 111, 617-637.

Oakley, B.A., Boothroyd, J.C., 2012. Reconstructed topography of Southern New England prior to isostatic rebound with implications of total isostatic depression and relative sea level. Quaternary Research 78, 110-118.

Oldale, R.N., & O'Hara, C. J., 1980. New radiocarbon dates from the inner Continental Shelf off southeastern Massachusetts and a local sea-level–rise curve for the past 12,000 yr. Geology 8, 102-106.

Poppe, L.J., Paskevich, V.F., Lewis, R.S., and DiGiacomo-Cohen, M.L., 2002, Geological framework data from Long Island Sound, 1981–1990: A digital data release: U.S. Geological Survey Open-File Report 02–002 DVD-ROM. [Also available at http://woodshole.er.usgs.gov/openfile/of02-002/index.htm.]

Poppe, L.J., DiGiacomo-Cohen, M.L., Smith, S.M., Stewart, H.F., Forfinski, N.A., 2006.

Seafloor character and sedimentary processes in eastern Long Island Sound and western Block Island Sound. Geo-Marine Letters 26, 59-68.

Poppe, L.J., DiGiacomo-Cohen, M.L., Doran, E.F., Smith, S.M., Stewart, H.F., and Forfinski, N.A., 2007, Geological interpretation and multibeam bathymetry of the sea floor in the vicinity of The Race, eastern Long Island Sound: U.S. Geological Survey Open-File Report 2007–1012 DVD-ROM. [Also available at http://pubs.usgs.gov/of/2007/1012/.]

Poppe, L.J., McMullen, K.Y., Foster, D.S., Blackwood, D.S., Williams, S.J., Ackerman, S.D., Barnum, S.R., and Brennan, R.T., 2008. Sea-Floor Character and Sedimentary Processes in the Vicinity of Woods Hole, Massachusetts, U.S. Geological Survey Open-File Report 2008-1004, http://woodshole.er.usgs.gov/pubs/of2008-1004/index.

Poppe, L.J., Danforth, W.W., McMullen, K.Y., Blakenship, M.A., Glomb, K.A., Wright, D.B., and Smith, S.M., 2014a, Sea-floor character and sedimentary processes of Block Island Sound, offshore Rhode Island (ver.1.1, August 2014): U.S. Geological Survey Open-File Report 2012–1005, http://pubs.usgs.gov/of/2012/1005/.

Poppe, L.J., McMullen, K.Y., Danforth, W.W., Blankenship, M.A., Clos, A.R., Glomb, K.A., Lewit, P.G., Nadeau, M.A., Wood, D.A., and Parker, C.E., 2014b, Combined multibeam and bathymetry data from Rhode Island Sound and Block Island Sound – A regional perspective: U.S. Geological Survey Open-File Report 2014–1012, DVD-ROM, 9 p., http://dx.doi.org/10.3133/ofr20141012.

Ridge, J.C., Balco, G., Bayless, R.L., Beck, C.C., Carter, L.B., Dean, J.L., Voytek, E.B., Wei, J.H., 2012. The new North American Varve Chronology: A precise record of southeastern Laurentide Ice Sheet deglaciation and climate, 18.2-12.5 kyr BP, and correlations with Greenland ice core records. American Journal of Science 312, 685-722.

Robb, J.M., 1984. Spring sapping on the lower continental slope, offshore New Jersey. Geology 12, 278±282.

Ruddiman, W.F., Raymo, M., Martinson, D. G., Clement, B. M., & Backman, J., 1989. Pleistocene evolution: northern hemisphere ice sheets and North Atlantic Ocean. Paleoceanography 4, 353-412.

Russell, J.A., Knudsen, O., H. Fay, H., 1998. Controls on the sedimentology of the November 1996 Jokulhlaup deposits, Skeidorarsandur, Iceland. Abstracts 15 International Sedimentological Congress, Alicante, Spain, p. 683.

Schwab, W.C., Allison, M.A., Corso, W., Lotto, L.L., Butman, B., Buchholtz ten Brink,

M., Denny, J.F., Danforth, W.W., Foster, D.S., 1997. Initial results of high-resolution seafloor mapping offshore of the New York-New Jersey metropolitan area using sidescan sonar. Northeast. Environ. Sci. 9, 243-262.

Schwab, W.C., Denny, J.F., Foster, D.S., Lotto, L.L., Allison, M.A., Uchupi, E., Danforth, W.W., Swift, B.A.,Thieler, E.R., and Butman, B., 2002. High-Resolution Quaternary Seismic Stratigraphy of the New York Bight Continental Shelf. USGS Open-File Report 02-152.

SegyMAT(C) 2001-2012 Thomas Mejer Hansen. http://segymat.sourceforge.net/

Sejrup, H.P., Hjelstuen, B.O., Torbjørn Dahlgren, K.I., Haflidason, H., Kuijpers, A., Nygård, A., Praeg, D., Stoker, M.S., Vorren, T.O., 2005. Pleistocene glacial history of the NW European continental margin. Marine and Petroleum Geology 22, 1111-1129.

Shaw, J., Kvill, D., & Rains, B., 1989. Drumlins and catastrophic subglacial floods. Sedimentary Geology 62, 177-202.

Shaw, J., Munro-Stasiuk, M., Sawyer, B., Beaney, C., Lesemann, J. E., Musacchio, A., Rains, B. and Young, R. R. (1999). The channeled scabland: back to Bretz? Geology, 27(7), 605-608.

Sirkin, LA, 1982. Wisconsinan glaciation of Long Island, New York to Block Island, Rhode Island. In: Larson GJ, Stone BD (eds) Late Wisconsinan glaciation of New England. Kendall/Hunt, Dubuque, pp 35–60.

Sirkin, L., 1991. Stratigraphy of the Long Island platform. Journal of Coastal Research SPECIAL ISSUE NO. 11. Quaternary Geology of Long Island Sound and Adjacent Coastal Areas: Walter S. Newman Memorial Volume 217-227.

Sirkin, L. and Veeger, A., 1998. Geology and hydrogeology of Block Island, Rhode Island. In: Guidebook to Field Trips in Rhode Island and Adjacent Regions of Connecticut and Massachusetts: New England Intercollegiate Geologic Conference, 90th Annual Meeting Kingston, Rhode Island.

Smalley, I. J., & Unwin, D. J., 1968. The formation and shape of drumlins and their distribution and orientation in drumlin fields. Journal of Glaciology, 7, 51, 377-390.

Stone, B.D., and Borns, Harold W., 1986. Pleistocene glacial and interglacial stratigraphy of New England, Long Island, and adjacent Georges Bank and Gulf of Maine. Quaternary Science Reviews 5, 39-52.

Stone, J.R., DiGiacomo-Cohen, M., Lewis, R.S., and Goldsmith, R., 1998. Recessional

moraines and the associated degkacial record of southeastern Connecticut and Long Island Sound. In: Guidebook to Field Trips in Rhode Island and Adjacent Regions of Connecticut and Massachusetts: New England Intercollegiate Geologic Conference, 90th Annual Meeting Kingston, Rhode Island.

Stone, J.R., Shafer, J.P., London, E.H., DiGiacomo-Cohen, M., Lewis, R.S., and Thompson, W.B., 2005, Quaternary Geologic Map of Connecticut and Long Island Sound Basin, U.S. Geological Survey Geologic Investigations Series Map I-2784, scale 1:125,000, 2 sheets and pamphlet. p. 1–72.

Svendsen, J.I., Gataullin, V., Mangerud, J., & Polyak, L. , 2004. The glacial History of the Barents and Kara Sea Region. Developments in Quaternary Sciences 2, 369-378.

Thieler, E.R., Butman, B., Schwab, W.C., Allison, M.A., Driscoll, N.W., Donnelly, J.P., Uchupi, E., 2007. A catastrophic meltwater flood event and the formation of the Hudson Shelf Valley. Palaeogeography, Palaeoclimatology, Palaeoecology 246, 120-136.

Waitt, R.B., 1998. Cataclysmic flood along Jokulsa a Fjollum, north Iceland, compared to related colossal jokulhlaups of Washington's Channeled Scablands. Abstracts, 15th International Sedimentological Congress, Alicante, Spain, pp. 811-812.

Winkelmann, D., Jokat, W., Jensen, L., & Schenke, H. W., 2010. Submarine end moraines on the continental shelf off NE Greenland e Implications for Lateglacial dynamics. Quaternary Science Reviews 29, 1069-1077.

Woodworth, J.B., Wigglesworth, E., Berry, E.W., Bryan, K., Hollick, C.A., Stephenson, L.W., 1934. Geography and geology of the region including Cape Cod, the Elizabeth Islands, Nantucket, Martha's Vineyard, and Block Island. Harvard University, Museum of Comparative Zoology, Cambridge, MA.

Uchupi, E., Oldale, R.N., 1994. Spring sapping of the enigmatic valleys of Cape Cod and Martha's Vineyard and Nantucket Islands. Geomorphology 9, 83-95.

Uchupi, E., Driscoll, N., Ballard, R. D., & Bolmer, S. T., 2001. Drainage of late Wisconsin glacial lakes and the morphology and late quaternary stratigraphy of the New Jersey–southern New England continental shelf and slope. Marine Geology 172, 117-145.

Veillette, J.J., 1994. Evolution and paleohydrology of glacial lakes Barlow and Ojibway. Quaternary Science Reviews 13, 945-971.

Zuffa, G.G., Normark, W. R., Serra, F., & Brunner, C. A., 2000. Turbidite megabeds in an oceanic rift valley recording jökulhlaups of late Pleistocene glacial lakes of the western United States. The Journal of geology 108, 253-274.

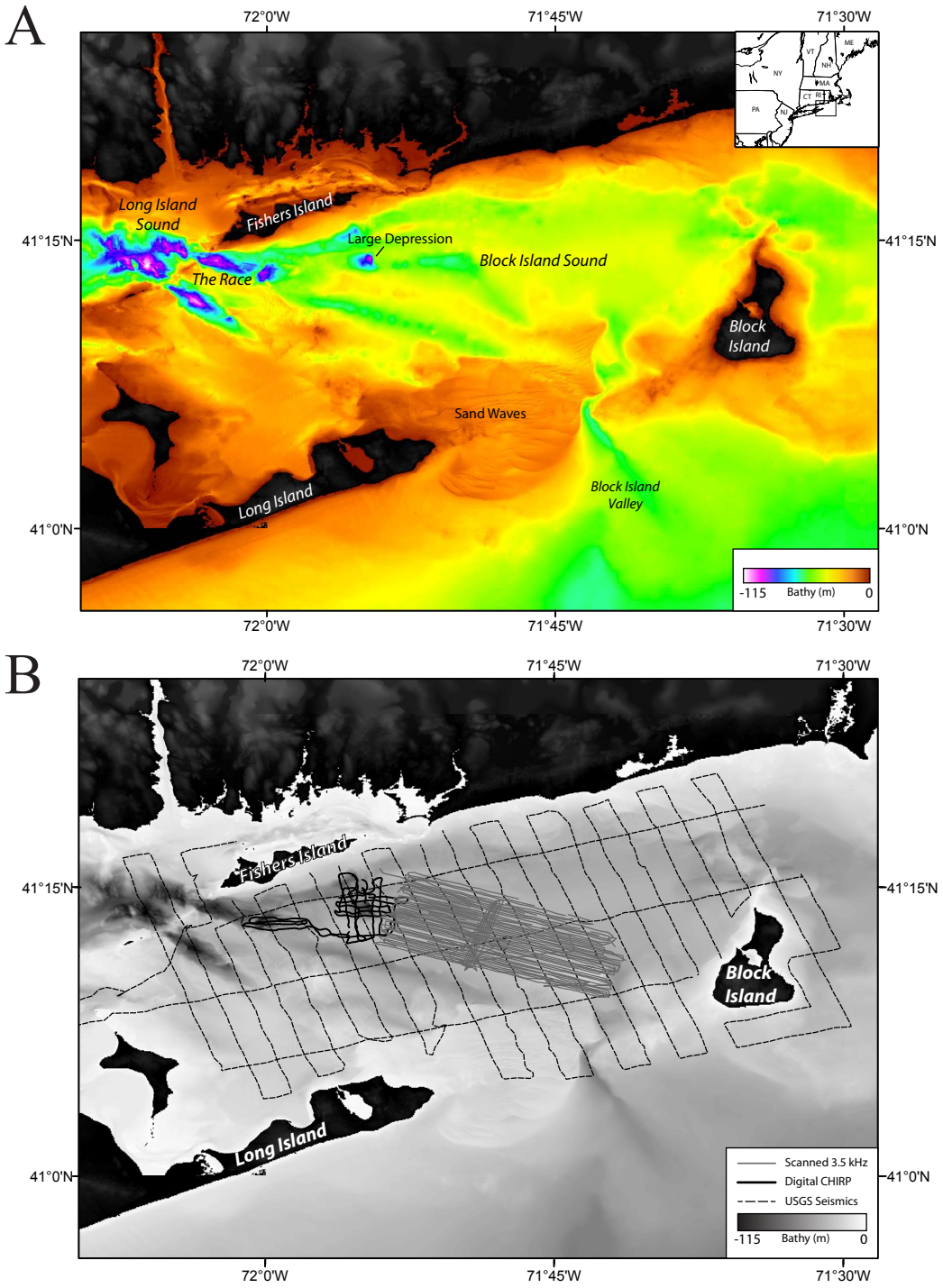

Figure 3.1. (A) Regional bathymetric map showing major features in study area. Bathymetry is from the coastal relief model (NGDC, 1999), the NOAA tsunami inundation Montauk zone (Eakins et al., 2009), and NOAA multibeam interpreted by the USGS (Poppe et al., 2007; Poppe et al., 2014). An inset shows the study area in New England. (B) Trackline map for seismic surveys. Scanned CHIRP profiles collected in 1995 on the R/V Henlopen are shown in grey, digital CHIRP collected in 1999 on the S/V Westward are in solid black, and USGS uniboom seismics are shown in black dashed lines (Needell and Lewis, 1984; Poppe et al., 2002).

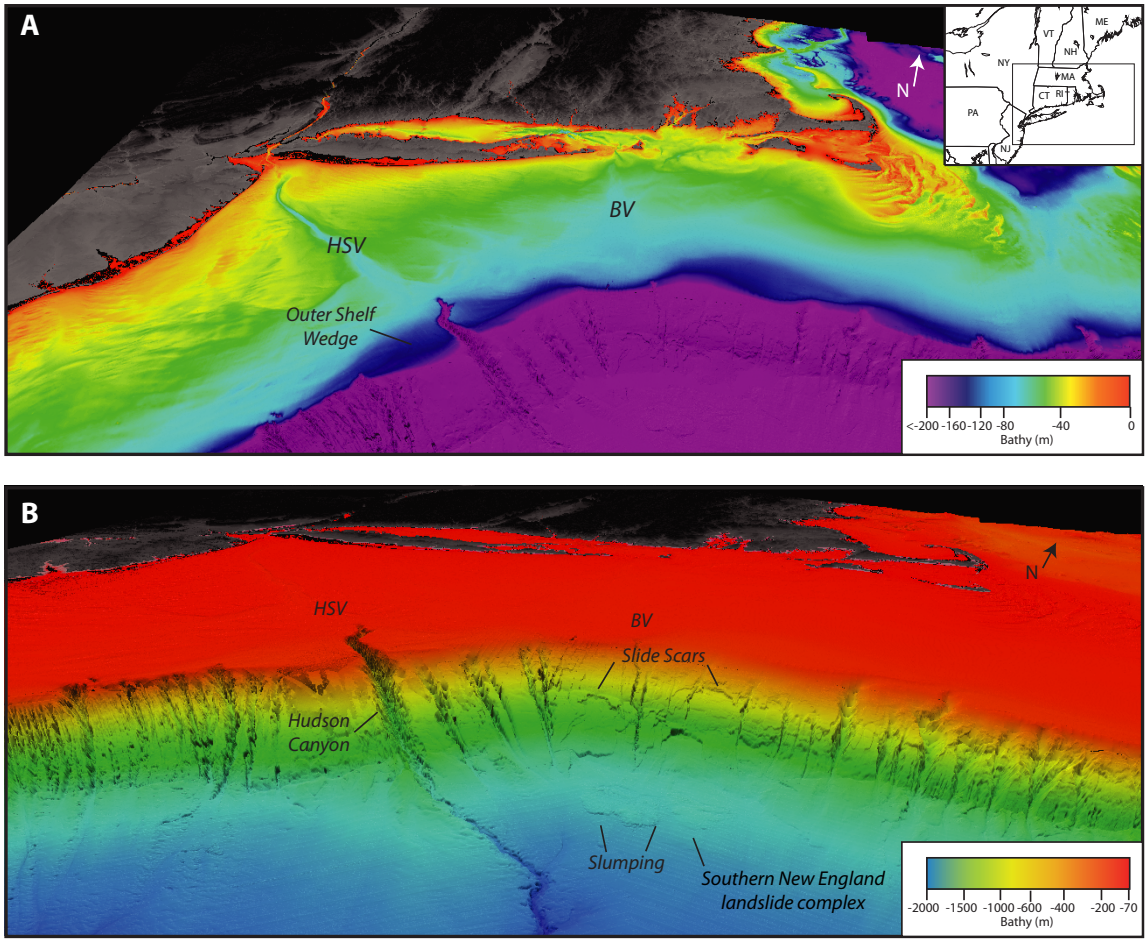

Figure 3.2. Regional perspective bathymetry maps of the study region (VE: 15). Inset in (A) shows the displayed region. (A) Perspective image shelf bathymetry highlighting the Hudson Shelf Valley, Block Island Valley, and the outer shelf wedge at the distal end of Hudson Shelf Valley. (B) The slope variability for the region is shown. Hudson Shelf Valley leads into a large canyon (Hudson Canyon) at the shelf edge that continues down slope into a channel on the rise. South of Block Island Valley on the slope are slide scars and slump complexes. Bathymetry data are from the coastal relief model (NGDC, 1999), University of New Hampshire collected for the Law of the Sea (Gardner et al., 2006), and from the USGS (Andrews et al., 2016). HSV = Hudson Shelf Valley and BV = Block Island Valley.

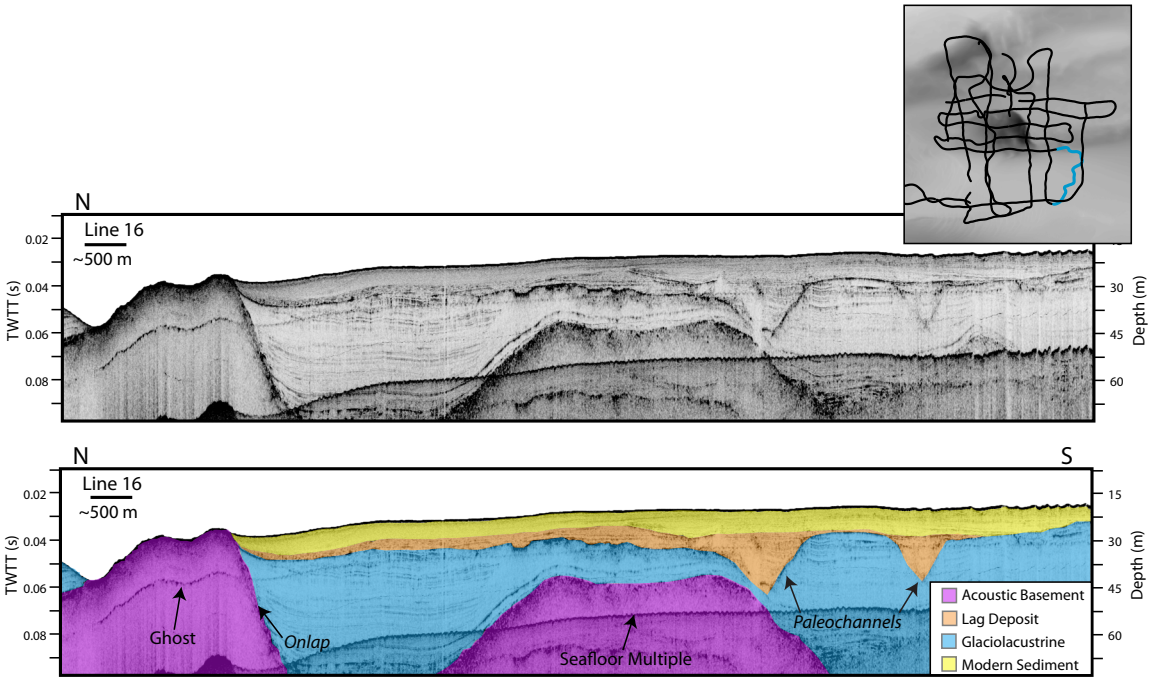

Figure 3.3. CHIRP line 16 uninterpreted (top) and interpreted (bottom). The trackline is highlighted in blue on the inset. Note the shiptrack deviations are the result of being under sail on the S/V Westward, strong currents, and avoiding fishing gear. Crystalline bedrock, coastal plain strata, and glacial moraine deposits are shown in purple and are referred to as acoustic basement, the glaciolacustrine sediments are in blue, the lag deposit that fills in channels is in orange, and the modern sediment is in yellow. There are major channels cut into the glaciolacustrine sediment that have been infilled. The modern sediment and lag deposit onlap onto an exposure of acoustic basement in the northern part of the profile.

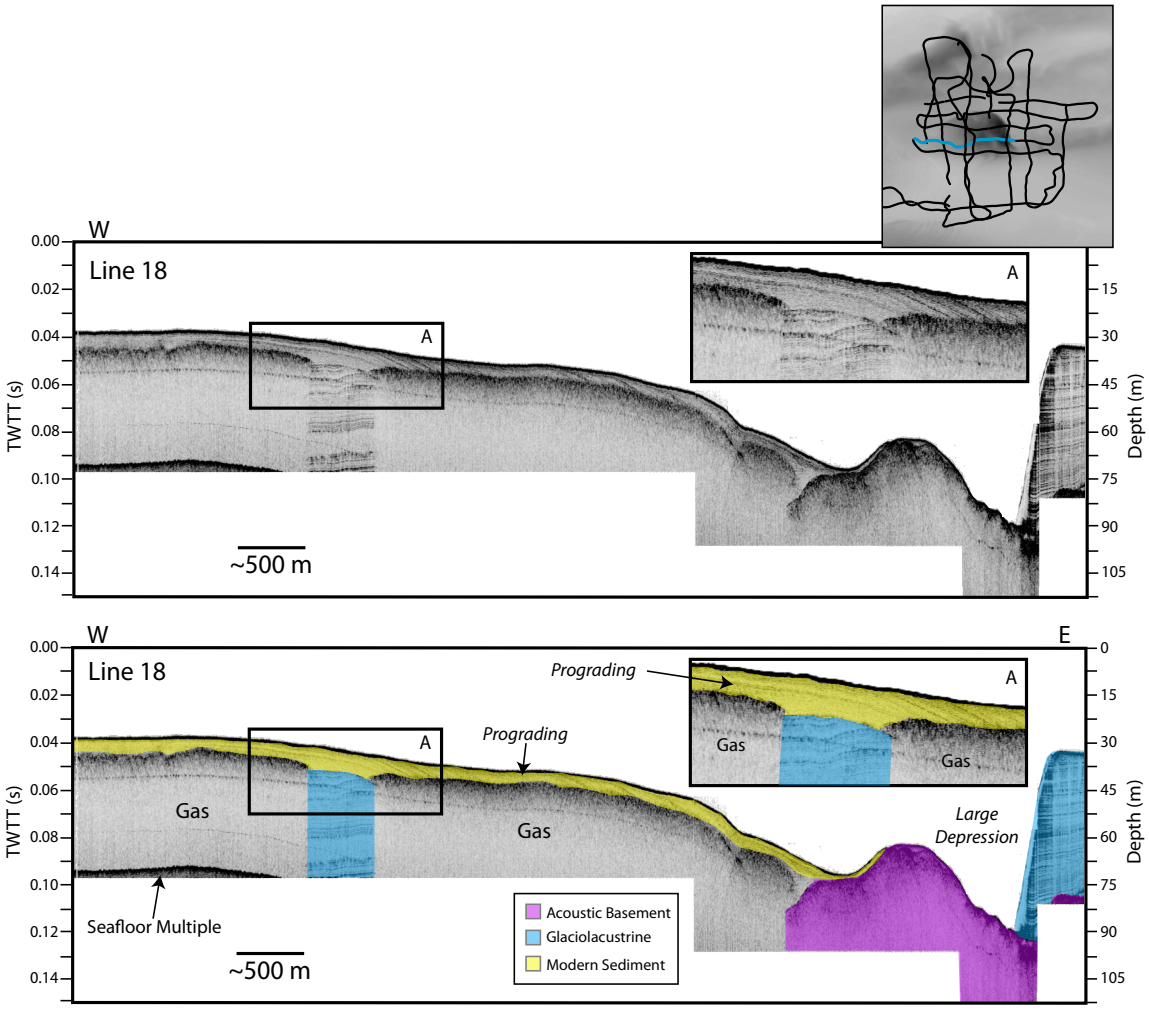

Figure 3.4. CHIRP line 18 with uninterpreted (top) and interpreted (bottom). The trackline is highlighted in blue on the inset. Acoustic basement is in purple, the glaciolacustrine sediments are in blue, and the modern sediment is in yellow. Seismic imaging and penetration is limited by gas in the sediments. Where the glaciolacustrine unit is visible, the boundary between this layer and the modern sediment above can be observed. The modern sediment is prograding downslope (inset A shows an enlargement) where it onlaps onto a high in the acoustic basement. This high is sufficient to block the sediment from infilling the large depression to the east.

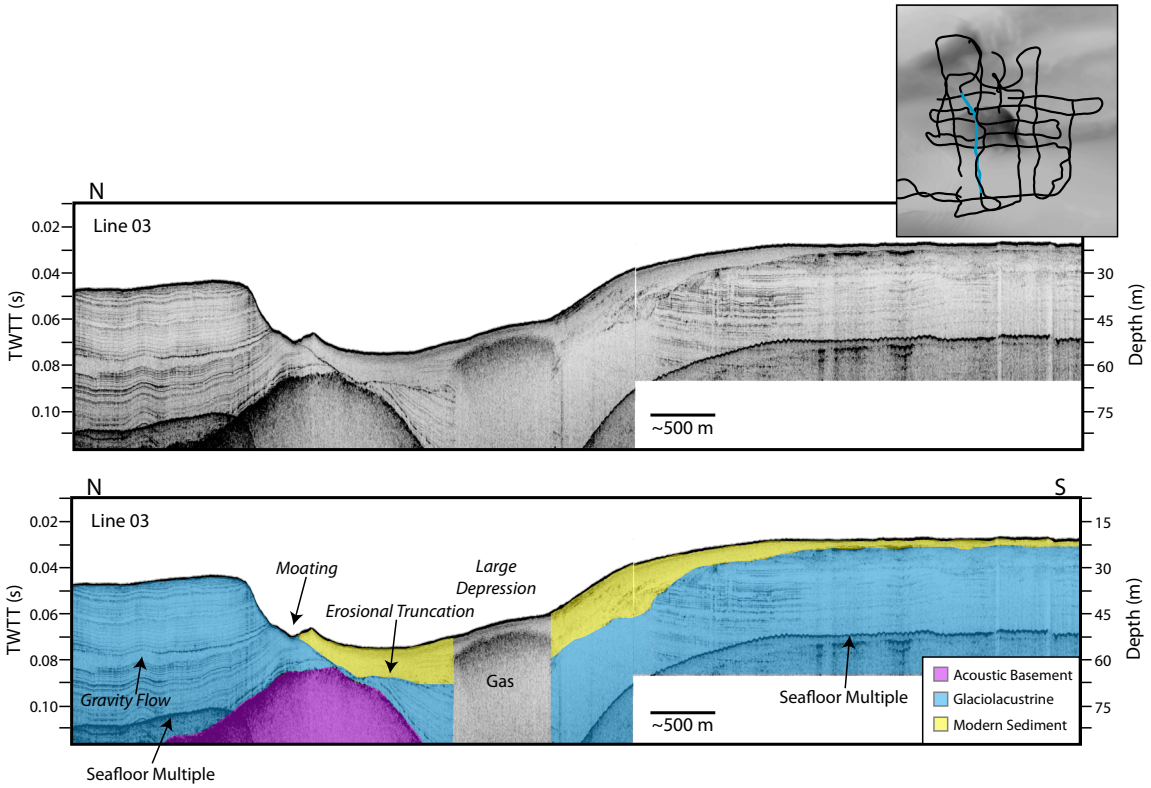

Figure 3.5. CHIRP Line 03 with uninterpreted (top) and interpreted (bottom) versions. The line is highlighted in blue on the inset. The acoustic basement is in purple, the glaciolacustrine sediments are in blue, and the modern sediment is in yellow. A gas wipeout in the data is labeled. There is a marked erosional unconformity in the glaciolacustrine layer that is covered by modern sediment. The modern sediment has also been shaped by currents.

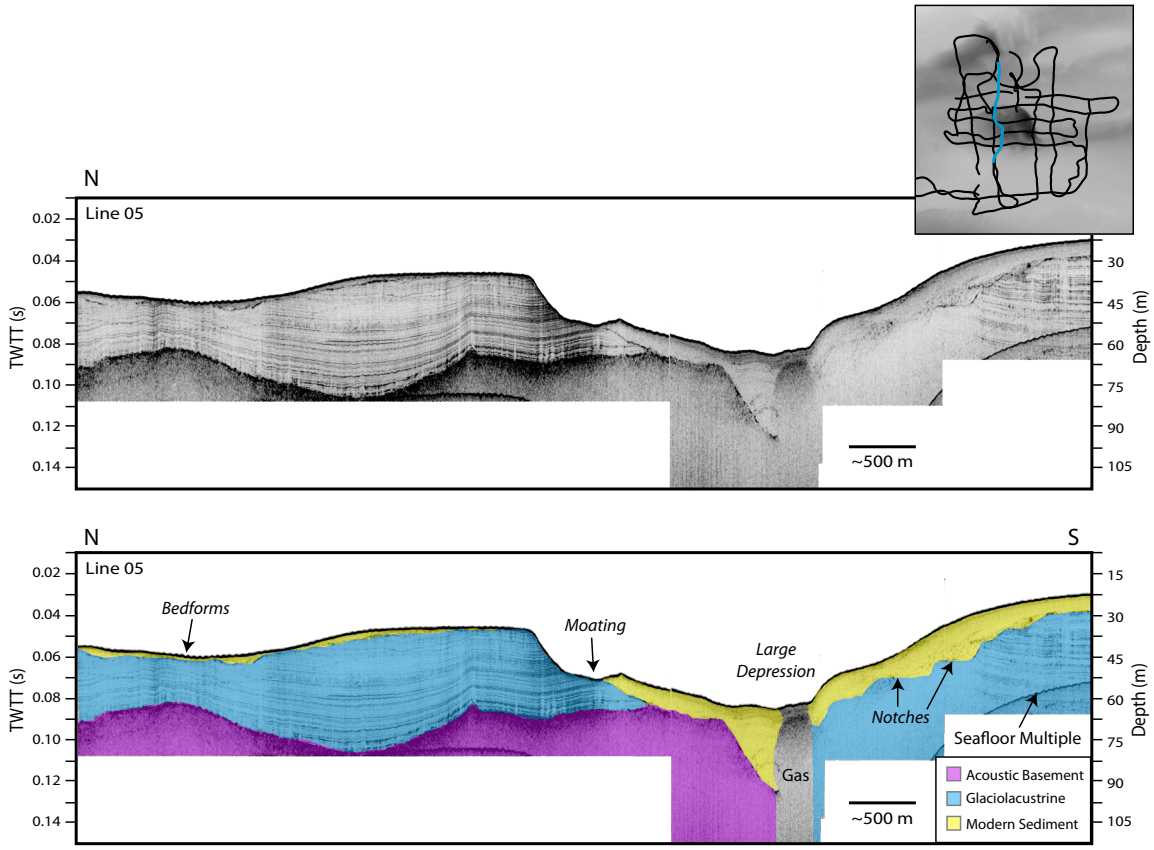

Figure 3.6. CHIRP line 05 with uninterpreted (top) and interpreted (bottom). The trackline is highlighted in blue on the inset. The acoustic basement is in purple, the glaciolacustrine sediments are in blue, and the modern sediment is in yellow. A gas wipeout in the data is marked. The glaciolacustrine sediments drape over the morainal material and mimics their morphology. This unit is also sequentially eroded on the southern end of the line. Bedforms at the northern end of the line show migration of modern sediment.

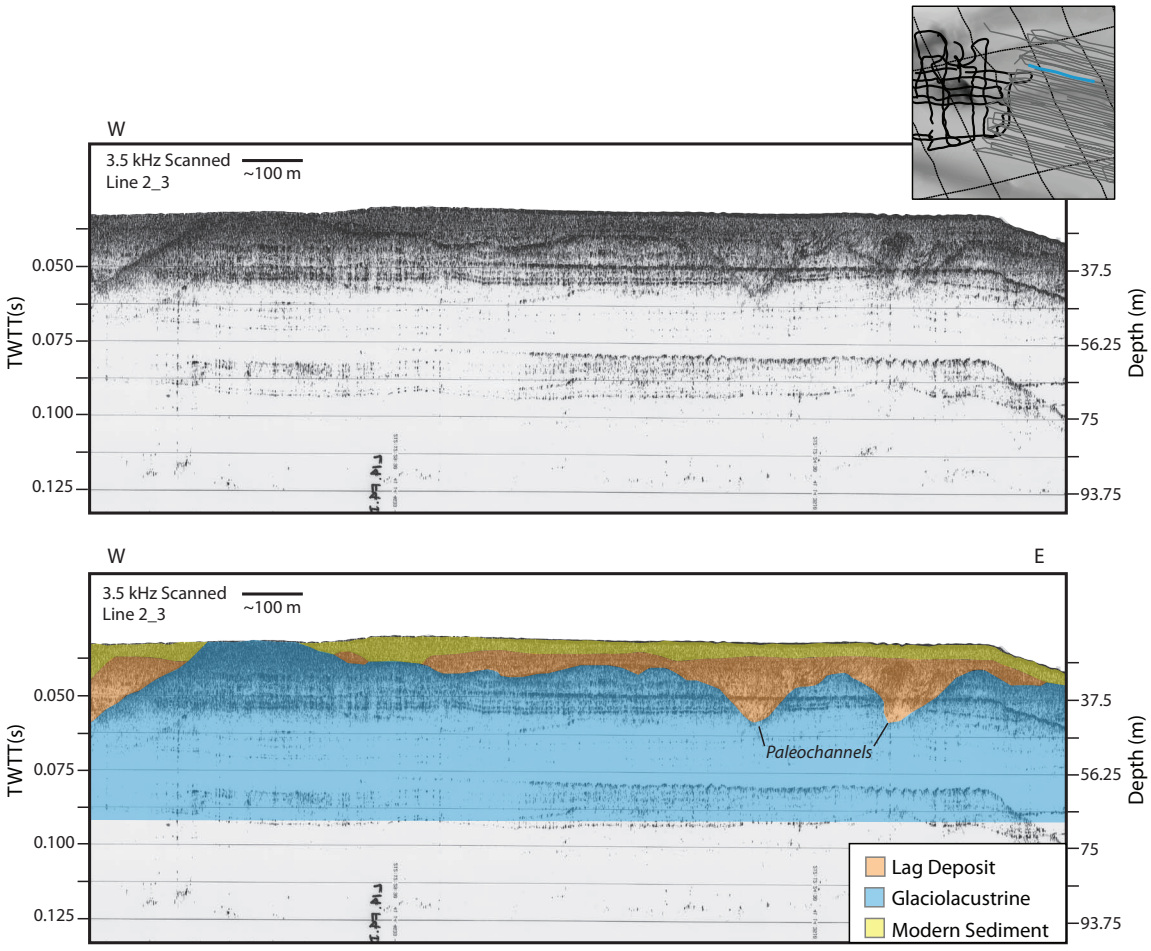

Figure 3.7. A section of scanned 3.5 kHz line 2_3 with uninterpreted (top) and interpreted (bottom) versions. The line is highlighted in blue on the inset. The glaciolacustrine sediments are in blue, the lag deposit that fills in channels is in orange, and the modern sediment is in yellow. Similar features to the digital CHIRP data can be observed in the scanned scrolls, including layering in the glaciolacustrine sediments, and paleochannels.

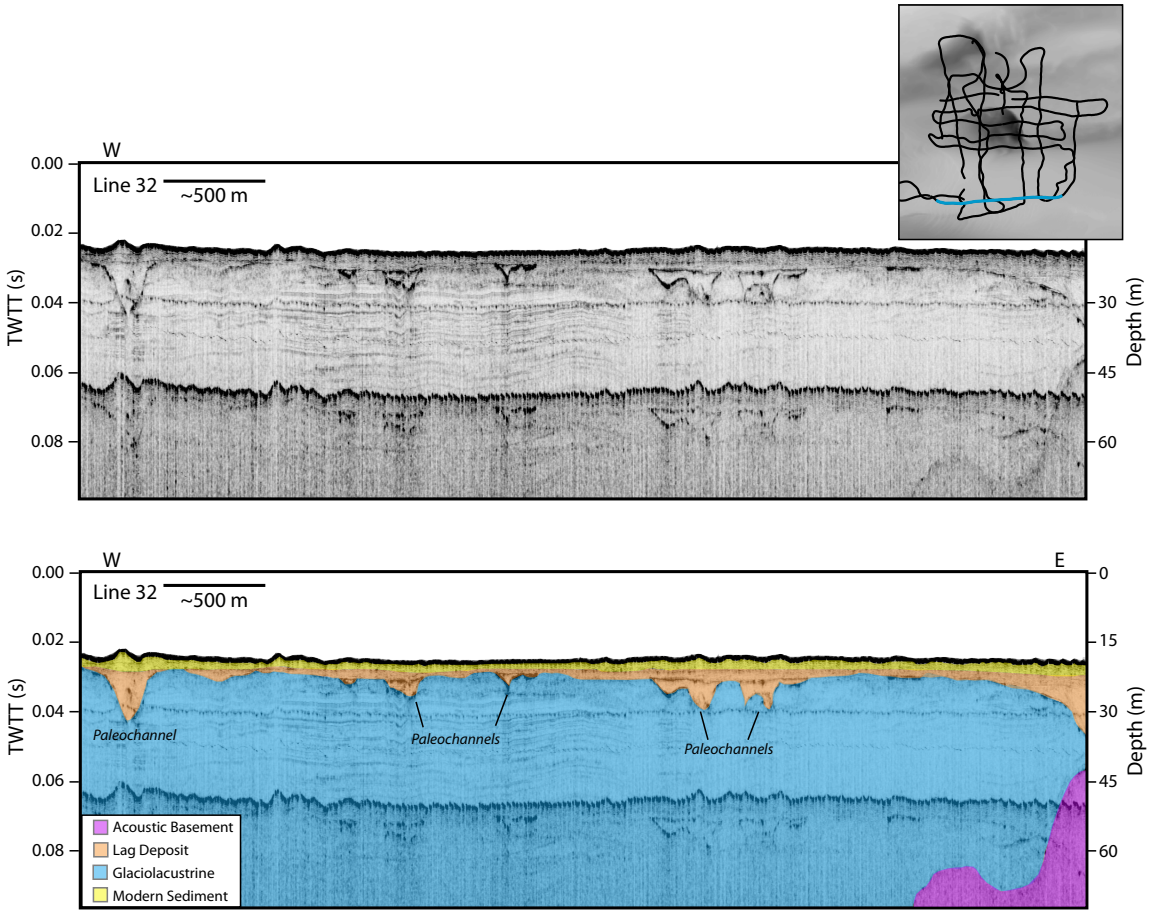

Figure 3.8. CHIRP line 32 with uninterpreted (top) and interpreted (bottom) versions. The line is highlighted in blue on the inset. The acoustic basement is in purple, the glaciolacustrine sediments are in blue, the lag deposit that fills in channels is in orange, and the modern sediment is in yellow. There are paleochannels cut into the glaciolacustrine sediments of varying sizes that were formed when the sound was subaerially exposed.

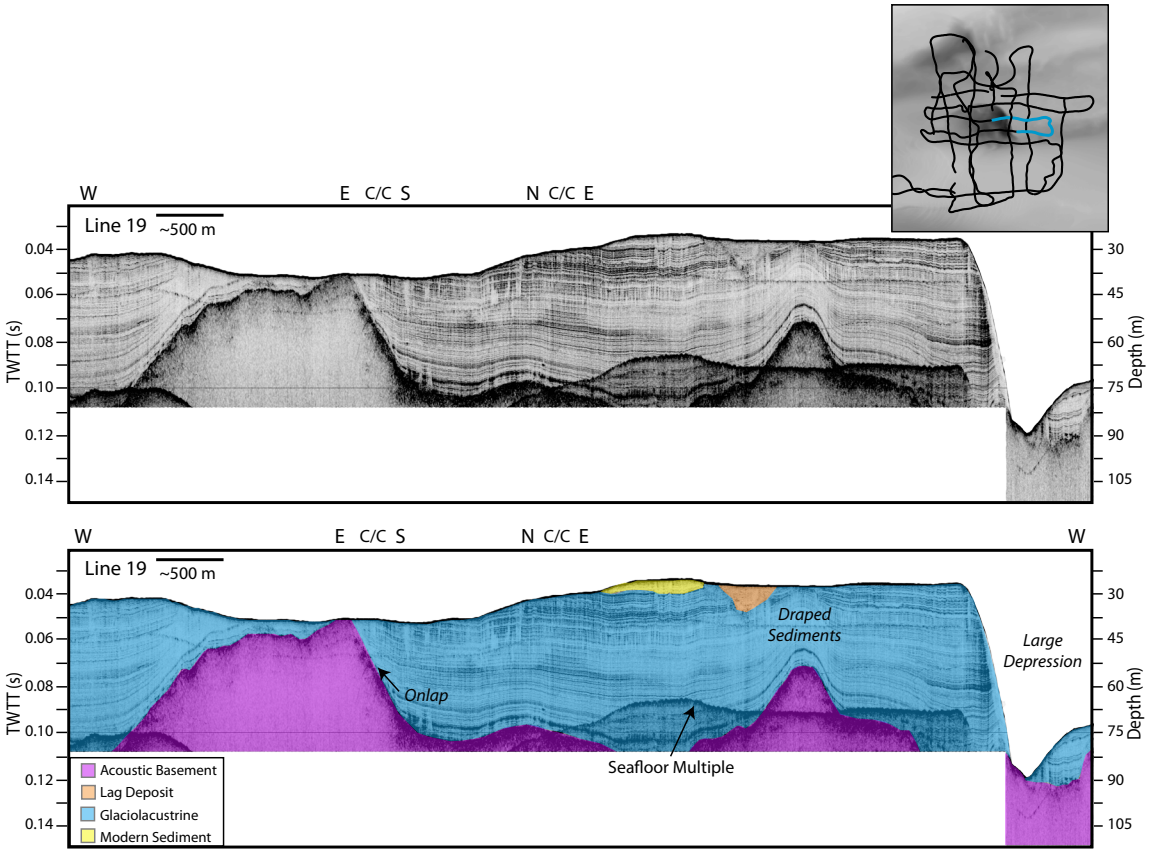

Figure 3.9. CHIRP line 19 with uninterpreted (top) and interpreted (bottom) versions. The line is highlighted in blue on the inset. The acoustic basement is in purple, the glaciolacustrine sediments are in blue, the lag deposit that fills in channels is in orange, and the modern sediment is in yellow. Course changes are marked on the profile. Draping and onlapping of the glaciolacustrine sediments on the acoustic basement are imaged.

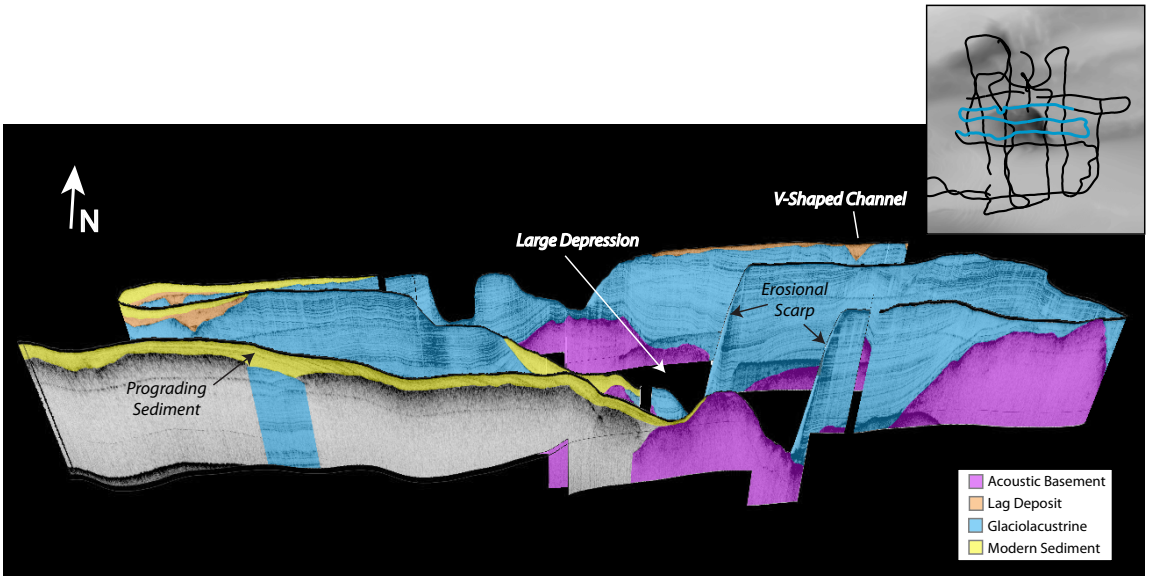

Figure 3.10. Perspective view looking north at the large depression. Profiles shown are highlighted in blue on the trackline map. Crystalline bedrock, coastal plain strata, and glacial moraine deposits are shown in purple and are referred to as acoustic basement is in purple, the glaciolacustrine sediments are in blue, the lag deposit that fills in channels is in orange, and the modern sediment is in yellow. Modern sediment is observed prograding down into the depression, but is blocked by a high in the acoustic basement.

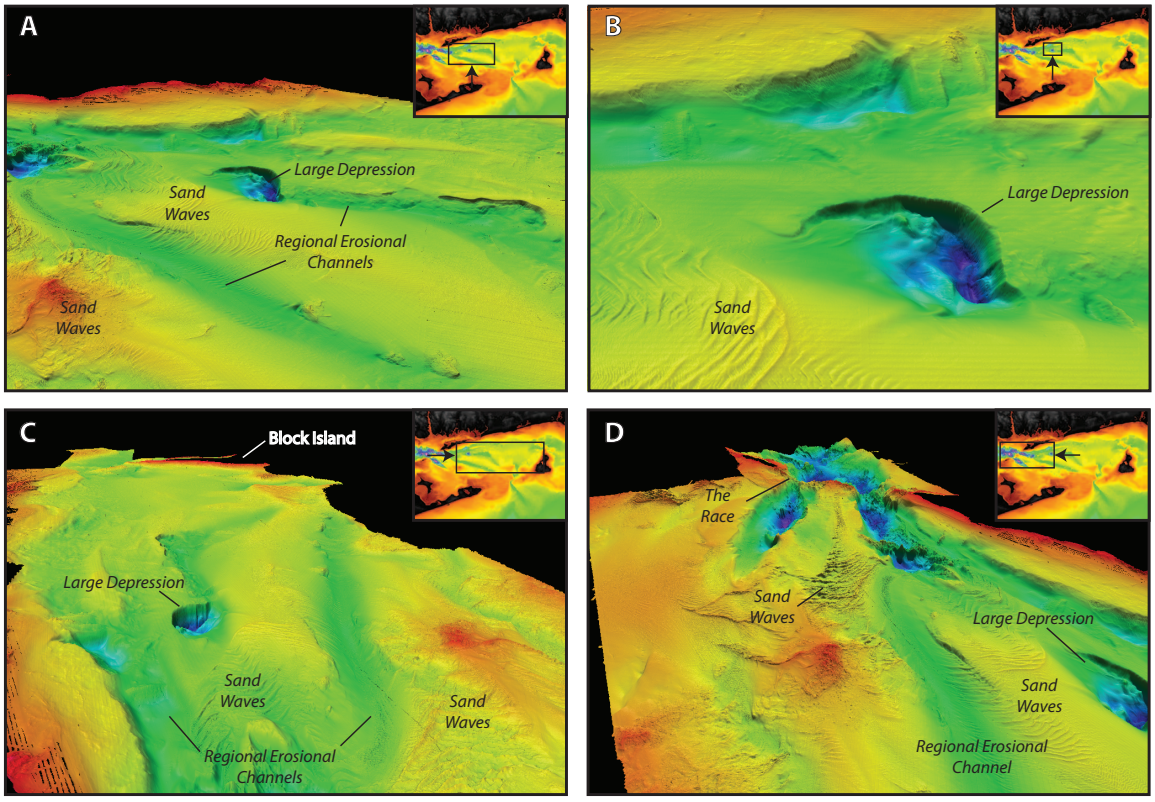

Figure 3.11. Perspective scenes of the high-resolution bathymetry in Block Island Sound collected by NOAA multibeam interpreted by the USGS (Poppe et al., 2007; Poppe et al., 2014). All data are 15x vertically exaggerated. Cooler colors are deeper and warmer colors are shallower. Each image has an inset of Block Island Sound, with a box and arrow showing the image extent and view direction. (A) Looking north towards the large depression. Regional erosional channels and sand waves are evident around the large depression. (B) A zoom in on the large depression. The gradual sloping western side and the steep eastern wall of the depression are imaged. (C) Looking east towards Block Island and view of the regional erosional channels going towards the entrance to Block Island Sound. (D) Looking west towards the connection to Long Island Sound at the Race. Highlights the deep elongate depressions at the connection between the two sounds. Transition from the Race to the regional erosional channels is imaged.

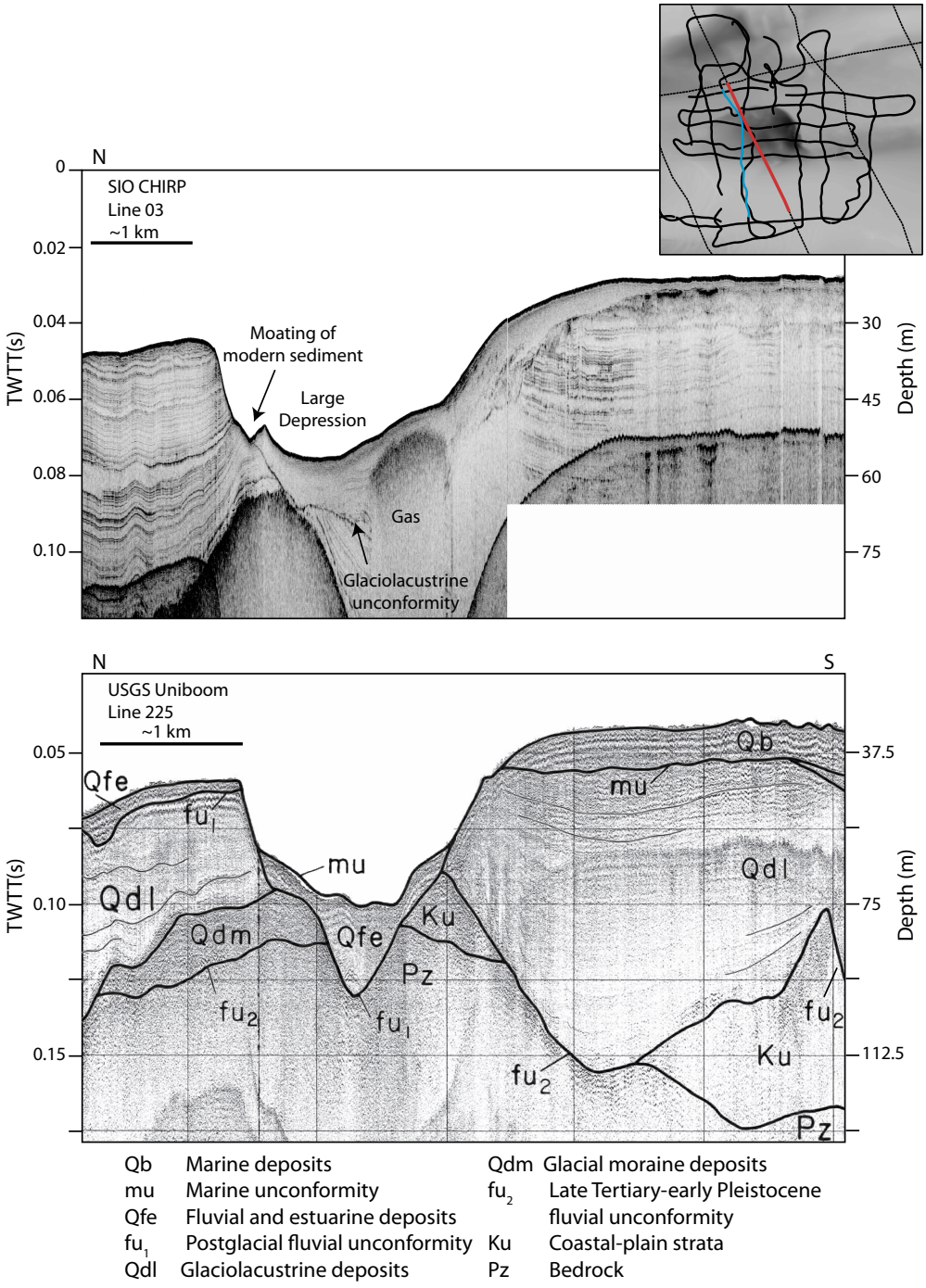

Qb	Marine deposits	Qdm	Glacial moraine deposits
mu	Marine unconformity	fu_2	Late Tertiary-early Pleistocene fluvial unconformity
Qfe	Fluvial and estuarine deposits		
fu_1	Postglacial fluvial unconformity	Ku	Coastal-plain strata
Qdl	Glaciolacustrine deposits	Pz	Bedrock

Figure 3.12. Comparison of digital CHIRP line 03 (top) and USGS uniboom line 225 (bottom; Needell and Lewis, 1984; Poppe et al., 2002). CHIRP line 03 is scaled differently than in Figure 5 for comparison to the uniboom line. The CHIRP line is highlighted blue on the inset and the uniboom line is highlighted in red. Interpretations for uniboom line 225 are from Needell and Lewis (1984). The legend for their interpretations is below the profile. The CHIRP profile is higher resolution, while the uniboom line has deeper penetration as a result of acquisition frequencies. An unconformity that truncates glaciolacustrine sediments in the large depression is imaged by the CHIRP profile. The glaciolacustrine sediments are not imaged below this unconformity in the uniboom line and was interpreted as basement (Pz) by Needell and Lewis (1984).

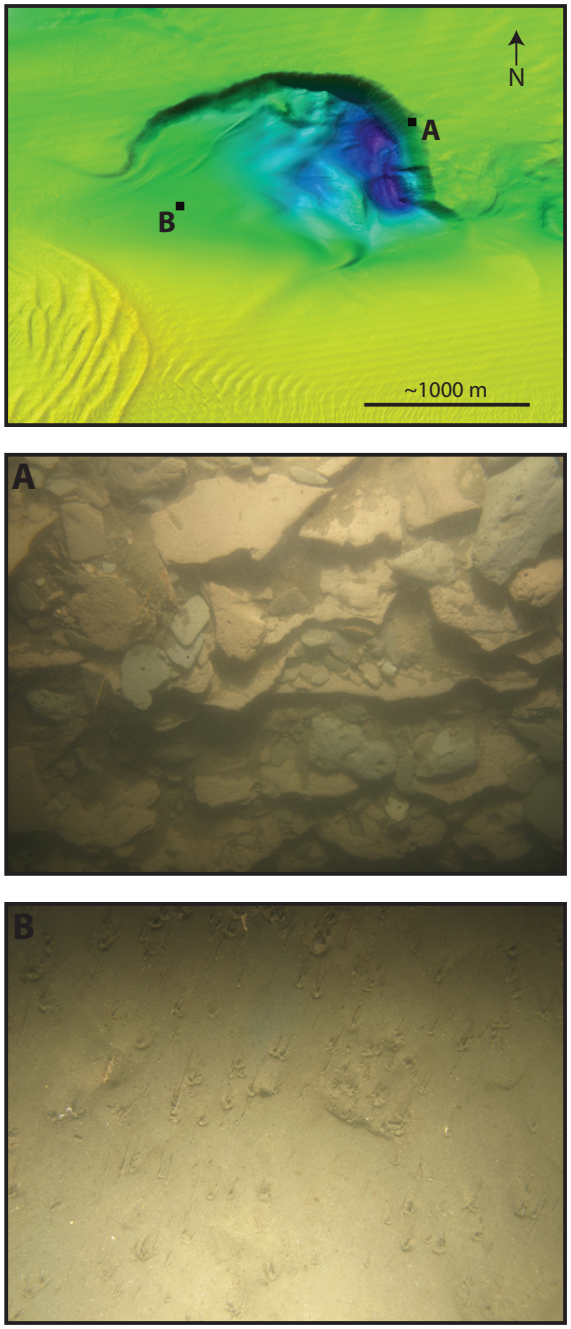

Figure 3.13. Photos of sedimentary deposits in the large depression (McMullen et al., 2014). The top image shows photo location. (A) Photograph 298_36d from the steep wall of the depression where the glaciolacustrine varve deposits crop out on the seafloor. The layers are composed of reddish-brown and gray silty clay, along with rip up clasts. Evidence of bioturbation in the clasts is present, along with hydrozoans. (B) Photograph 298_12a from the gradually sloping southwest entrance to the large depression. Based on a grain size sample (McMullen et al., 2014), the seafloor here is composed of fine sand and is heavily bioturbated. Scours have formed around objects, delineating the dominant flow direction.

3.10 SUPPLEMENTAL MATERIAL

3.10.1 Converting paper seismic records to seg-y

Paper seismic records were converted to digital images in tiff format using a large format printer at Imprints on UCSD main campus. In total, eight scrolls were scanned. Each scan was over a gigabyte in size, so the images were cropped into two or three individual images. The following is presented as a procedure to be used for anyone interested in converting paper seismic records to digital seg-y's.

Latitudes and longitudes printed on the seismic profile should be entered into an excel spreadsheet or another text file. These then need to be converted to UTM (ours were converted using Matlab). The conversion from image file to seg-y is done using the code image2segy.m (Farran, 2008, http://gma.icm.csic.es/node/67) in Matlab. The script needs the Matlab library "SegyMAT" (Thomas Mejer Hansen, http://segymat.sourceforge.net/) in the Matlab path to work. For each image conversion, an input text file is needed. To acquire much of this information, the file should be opened up in Adobe Photoshop or another software that can give x,y pixel information. The first line of the file must be specific input about the seismic image. The order of the first line is: trace length in pixels, line number in numerics only, marine (0) or land (1) profile, seg-y revision format (0 or 1, but 1 is recommended), seg-y numeric format (1 for 32 bits IBM floating point, 3 for 16 bits IBM floating point, which is recommended, or 5 for IEEE format), and the UTM zone for the header. An example file is in supplemental file 1. Following the first line is a line for each navigation point on the seismic profile. Each line will have the Px, Py, X1, Y1, TD, and TL. Px is the horizontal location of the navigation point in pixels and Py is the vertical location of the top of the data window in pixels. Since scanning is not perfect, the data window will typically meander up and down throughout the image—the Py will fix this and create a straight profile. X1 and Y1 are the UTM coordinates for the navigation point. TD is the time delay in milliseconds for when profiles start below 0

seconds. TL is the time range in milliseconds, based on the end of trace time minus the time delay.

To run the script in Matlab, the image2segy_253.m file should be in the same directory as the image files and the input text files for each image. The first box that pops up allows you to name the survey, the line, month, year, first trace offset, and institution name. The values that are the same throughout the scans being converted can be changed within the first line of the script. Next, a browser pops up to the select the input text file and then again to select the image file in .bmp, .jpg, or .tif. Then select if the image is grayscale or red, white, and blue. Finally, select the polarity as negative or positive. For the Block Island Sound scans, negative was selected. The process will start and a trackline location map will pop up. Exit out of this window when done viewing.

If UTM is needed for the digital seg-y's, then the process is finished, but to return to latitude/longitude from UTM, the navigation needs to be extracted from the seg-y file. This can be done using SeiSee (http://www.dmng.ru/en/freeware.html), a freeware for the Windows platform. In SeiSee, open the directory containing the seg-y files and the select the seg-y to be edited. Under the "trace headers" tab select bytes 73 and 77. Under "file", select export trace headers to ascii file. This exports a text file with a header, then columns of trace number and the UTM coordinates. Extract the UTM coordinates from the output file and use Matlab to convert back to longitude and latitude. Add these to a new file with the trace number, and the copied output file header. The resulting file can then be imported into SeiSee, replacing the UTM coordinates with the new longitudes and latitudes. To check everything in the process works, the seg-y's can be imported into Kingdom Suite and checked relative to other datasets.

```
2017,0104,0,1,3,19
548,135,2.5801e+05,4.5648e+06,0,125
1307,138,2.5739e+05,4.5651e+06,0,125
2063,135,2.568e+05,4.5653e+06,0,125
2813,135,2.5625e+05,4.5652e+06,0,125
3572,135,2.57e+05,4.565e+06,0,125
4328,138,2.5794e+05,4.5647e+06,0,125
5084,138,2.5873e+05,4.5644e+06,0,125
5837,138,2.5952e+05,4.5641e+06,0,125
6590,135,2.6031e+05,4.5638e+06,0,125
7346,132,2.6108e+05,4.5635e+06,0,125
8108,132,2.6183e+05,4.5633e+06,0,125
8852,132,2.6259e+05,4.563e+06,0,125
9600,132,2.6337e+05,4.5627e+06,0,125
10360,130,2.6372e+05,4.5623e+06,0,125
11115,126,2.6351e+05,4.5629e+06,0,125
11872,123,2.6377e+05,4.5637e+06,0,125
12626,120,2.6502e+05,4.5645e+06,0,125
13382,117,2.6438e+05,4.5653e+06,0,125
14138,117,2.6466e+05,4.5661e+06,0,125
14890,117,2.6496e+05,4.5669e+06,0,125
15650,114,2.6526e+05,4.5679e+06,0,125
16400,111,2.6554e+05,4.5685e+06,0,125
17160,105,2.6558e+05,4.5691e+06,0,125
```

Figure 3.S1. Example input file for paper seismic record conversion to digital seg-y. The first line is the header with specific input information described in the text. Each line after this corresponds to a navigation point on the line.

4

Deglacial floods in the Beaufort Sea

4.1 ABSTRACT

The origin of Younger Dryas (YD) cooling at ~13 ka, after 2 kyr of postglacial warming, is a century-old climate problem. The YD is thought to have resulted from a slow-down of the Atlantic meridional overturning circulation (AMOC) in response to a flood of Laurentide ice sheet meltwater from glacial Lake Agassiz in Canada. Although there is no oxygen isotopic (δ18O) evidence in the western North Atlantic for a local source of meltwater where it was predicted, we report here that the eastern Beaufort Sea contains the long-sought δ18O minimum at ~12.9 ka, suggesting that Lake Agassiz meltwater flowed down the Mackenzie River and into the Arctic Ocean. This fresh water would have traveled north along the Canadian Archipelago, and through Fram Strait to the Nordic Seas where surface freshening and freezing near sites of deep water formation would have suppressed convection, and caused the YD by reducing the AMOC.

4.2 INTRODUCTION

It is well known that conditions in the Arctic Ocean have a profound effect on the North Atlantic Ocean, for example the Great Salinity Anomaly (GSA) of the 1960s and 1970s (Dickson et al. 1988), and that export of excess fresh water and ice through Fram Strait was the origin of the GSA (Aagard and Carmack 1989; Hakkinen, 1993). During transit of the GSA around convective regions of the Nordic Seas, decreased sea surface salinities and increased sea ice cover reduced convective overturn and contributed to very harsh winters. There is reason to expect that similar and even larger climate events occurred in the past, especially during deglaciation when huge volumes of meltwater and ice entered the Arctic and Nordic Seas. For example, it was discovered several decades ago that an abrupt decrease in δ18O in surface-dwelling planktonic foraminifera midway through deglaciation in the Gulf of Mexico was a signal of fresher surface waters (Kennett and Shackleton, 1975). The source of this runoff must have been the decaying

Laurentide Ice Sheet (LIS) via the Mississippi River, but it ended abruptly at about 13 ka. Kennett and Shackleton (1975) proposed that, as the southern margin of the LIS retreated northward, an eastern outlet was opened to the Gulf of St. Lawrence, and the western North Atlantic. A low δ18O signal, however, has never been detected in high-quality sediment cores from the western North Atlantic (Keigwin and Jones 1995; de Vernal and Hillaire-Marcel 1996; Keigwin et al. 2005), yet it is widely believed that the fresh water diversion from the Gulf of Mexico interrupted deep ocean convection and caused the well-known Younger Dryas (YD) cold episode (13-11.7 ka) in the North Atlantic region (Broecker et al 1989). The YD was discovered around the beginning of the 20th Century as one of several appearances of the Arctic wildflower Dryas octopetala in postglacial deposits in Scandinavia (Andersson, 1896; Hartz and Milthers, 1901). It was later proposed that a massive freshwater flood to the North Atlantic caused the YD (Johnson and McClure, 1976; Rooth, 1982).

In the past decade, a glacial systems model showed that fresh water stored in glacial Lake Agassiz most likely traveled north to the Beaufort Sea via Mackenzie River at 13 ka (Tarasov and Peltier, 2005), and extensive field work on the Mackenzie Delta identified clear evidence of massive flood deposits that occurred about the same time (Murton et al., 2010). Although the Murton et al. (2010) conclusions have been questioned (Carlson and Clark, 2012), application of a high resolution ocean circulation model (Condron and Winsor, 2012) showed that, only when released to the Arctic Ocean (via Mackenzie River), could the Lake Agassiz flood have caused the Younger Dryas reduction of AMOC (McManus et al., 2004) and subsequent northern hemisphere cooling.

4.3 RESULTS AND DISCUSSION

Here we present data that show two events of substantial sea surface freshening

during deglaciation in newly acquired large diameter (jumbo) piston cores (JPCs) from 690 m on the continental slope ~100 km east of Mackenzie River (JPCs 15 and 27, Fig. 1). These and other new cores lie in the Atlantic water that enters the Arctic at Fram Strait and Barents Sea in the depth range ~100 to 800 m and circulates counter-clockwise along the continental slopes (Rudels et al. 1994). JPC-15 penetrated ~13 m of sediment and was probably stopped by a coarse layer that has high magnetic susceptibility, ice rafted debris (IRD), and Ca content (Fig. 2), and makes a prominent reflector in the acoustic stratigraphy across the region (Fig. 3). A second core at the same site (JPC-27) was longer and penetrated the coarse layer. As these cores have nearly identical stratigraphies, we spliced them together to make a composite JPC-15/27 (Fig. S1).

Compared to the lower layer, the upper coarse layer at this site is thicker, has multiple phases, and fewer IRD grains (Fig. 2), but each layer also has finer sand and silt (Fig. 3). These data indicate that each was a time of enhanced sediment transport to the upper slope of the Beaufort Sea. The two main events must be the same that Scott et al. (2009) noted earlier in Canadian core PC-750 (Fig. 1). X-ray fluorescence (XRF) counts of calcium (interpreted as detrital CaCO3 content) show that the two events have similar carbonate content, but also that lowest carbonate delivery to the region occurred before the oldest event and was only a little higher between the events (Fig. 2). Sediment deeper than ~5 m is faintly laminated at the cm scale, except for the massive appearance of the deeper event (13.0-13.5 m). Laminae are better developed between 6 and 12 m, where about 300 cycles are evident in the core X-radiography (Fig. S2).

As with the sediment and geophysical data, δ18O on the polar planktonic foraminifer Neogloboquadrina pachyderma (sinistral) (Nps) in JPC-15/27 is marked by two prominent events at the same depths in the core (Fig. 2). At those levels δ18O of Nps (δ18ONps) decreased at least 1.0 ‰ below the ~2.0 ‰ baseline that extends >4 m down the core. Above a pronounced maximum in δ18ONps at 2-3 m, values decrease by

~2.0 ‰ to the core top. Benthic (Cassidulina neoteretis) δ18O gives a stratigraphy more typical of the world ocean, with generally increasing values down the core, although they are consistently low at about 5 m in the same samples where δ18ONps is low.

4.3.1 Chronology

Chronology in Arctic sediments is uncertain because, although radiocarbon dating of foraminifera is the simplest method, at present there is no way to know accurately the near surface reservoir correction (ΔR) in the past. We made 10 accelerator mass spectrometer (AMS) 14C measurements on Nps from core 15 (Table S1). Those dates indicate maximum rates of sedimentation of at least 10 m per 1000 14C yrs between 6 and 12 m in the mid-deglacial interval of the core (Fig. 2F, S3). Before and after that mid-core extreme, rates are half that or less. Six of the Nps dates were paired with dates on C. neoteretis. On average, benthics are 120 ±220 yrs older than planktonics, in agreement with prior results from 1300 m in the Chukchi Sea (HLY0205 JPC-16, Fig. 1) (Keigwin et al. 2006). This suggests that the Atlantic layer may have had a structure and circulation similar to today (Ostlund et al. 1987) through deglaciation and the Holocene.

For a calendar (calibrated) 14C chronology, we chose a pre-bomb ΔR based on the analysis of 14C, tritium, and δ18O on samples collected decades ago when bomb produced nuclides were beginning to invade the deep Arctic (Ostlund et al. 1987). Ostlund et al. (1987) inferred the pre-bomb 14C activity of waters between 500 and 1500 m was about -55 ± 5 ‰ (Fig. 4). Although deep water 14C ventilation in the Arctic may have been very different in the past (Thornalley, 2015), we assume the ventilation of upper waters (<1500 m) in the Canada Basin in the past was similar to today. Because, on average, the age difference between C. neoteretis and Nps is equivalent to a ~15 ± 25 ‰ difference in Δ14C, it follows that Nps probably lived in the upper reaches of Atlantic water with Δ14C not significantly different from -55 ‰ (Fig. 4). Thus, before the bomb

effect, both planktonic and benthic foraminifera probably lived in water that had a reservoir age of ~440 14C yrs, and ΔR ~40 yrs.

This model gives interpolated calendar ages in JPC-15/27 of 12.85 ± 0.10 ka for the onset of the upper δ18O minimum and 14.5 ±0.23 ka for the lower one (Fig. 5). The age of the older event and its associated ice IRD is consistent with the ages (15.2-14.1 ka) reported for the initial withdrawal of ice tongues from Amundsen Gulf and M'Clure Strait (Stokes et al. 2009), suggesting the age model is reasonable. 14.5 cal ka is also similar to ~14 ka for the youngest event of Laurentide ice rafting around the Arctic (Darby et al. 2002). The interpolated age for the onset of the later freshening in the Beaufort Sea is the same as the beginning of the Younger Dryas at 12.85 ±0.14 ka in Greenland ice cores (Rasmussen et al. 2006), and close to the end of freshening in the Gulf of Mexico (12.94 ±0.17 ka) (Fig. 5).

4.3.2 Ocean and climate change in Beaufort Sea

Our composite sequence from the continental slope east of Mackenzie River began around 16 ka with modest ice rafting from local sources such as ice streams in M'Clure Strait and Amundsen Gulf. Icebergs would have travelled clockwise around Canada Basin via the Beaufort Gyre, and the counter clockwise shelfbreak current (Appen and Pickart 2012) would have been weakened with sea level below the depth of Bering Strait. Mackenzie River may not have supplied significant detrital carbonate because the extensive Devonian carbonate terrain south of Great Slave Lake and north of Ft. McMurray (Wheeler et al., 1996) was probably ice-covered, but it may have been a source of runoff and sediment at least since ~16 ka based on the background low δ18O (Fig. 5). This was a time when secular change in the ocean due to increased ice volume was about +0.8 ‰, indicating the sea surface was less saline than today by at least 1 psu, assuming the modern δ18O-salinity relationship (Cooper et al, 2005). This setting

prevailed until ~14.5 ka, when ice rafting dramatically increased from Amundsen Gulf and M'Clure Strait, and δ18ONps decreased by >1 ‰. The five samples defining this minimum were probably deposited within decades, and the flood is also coincident with meltwater pulse 1A in the North Atlantic region.

At the end of the 14.5 ka event, Amundsen Gulf probably remained a significant source of carbonate rich sediment to the continental slope in the eastern Beaufort Sea until the ice tongue was fully retreated. Mackenzie River may have always been a large source of sediment, but as more of its watershed north of Fort McMurray was deglaciated, the more important it must have become. The laminated lithology, high sedimentation rate, and general lack of coarse particle ice rafting suggest large sediment input from the Mackenzie River between 14.0 and ~13.7 ka (6-12 m in the core). The high sedimentation rates along the slope may be explained by discharge over bottom fast ice on the shelf, which could efficiently transport sediment farther seaward (e.g., Macdonald and Yu, 2006). Ongoing studies are examining the processes that led to the rapid sediment emplacement recorded during this time interval. Based on the diagnostic acoustic signature of the rapidly emplaced Bolling-Allerod section (Fig. 3), the western extent of the deposit pinches out between JPC-09 and JPC-06 (Fig. 1). Counts of ~300 layers within the ~300 year interval where sedimentation rates are highest show the layers are probably annual which is circumstantial support for the calendar chronology. The interval between the two δ18ONps minima represents the entire Bolling/Allerod climate warming, when the AMOC was thought to be almost as strong as today (McManus et al. 2004) but evidently the lowered salinity in the Beaufort Gyre had little direct influence on North Atlantic overturning.

Close to 13 ka the rapid increase in magnetic susceptibility and decreased δ18ONps in JPC-15/27 herald the beginning of the YD. Although the two δ18ONps minima in this core are similar in size, the YD event was more likely to have been a

flood of fresh water with high suspended load (Murton et al. 2010) because δ18O of C. neoteretis decreased in exactly the same samples as Nps. This, we propose, may record a hyperpycnal flow that would be more likely from a river flood, although there were also a few distinct ice rafting events (Fig. 2a-c). The major sediment depocenter in this model must be farther seaward because sedimentation rates drop during this time interval at 690 m water depth (Fig. 2). The YD flood can be traced to the west as far as core JPC-09 using δ18ONps (Fig. S5), but the signal is not clear west of that at JPC-06 (Fig. S6), and neither the δ18O minimum nor the maximum in magnetic susceptibility are evident as far west as JPC-02 near Barrow (Fig. S7).

About 200 yrs after the onset of the YD flood all four sediment and isotope proxies were briefly aligned in the first ("a") of several sub-events (Fig. 2 A-D). The low δ18ONps episode is mostly centered between the subpeaks "a" and "b" of the magnetic susceptibility (12.9 to 12.5 ka), but the last of the spikes in IRD and carbonate deposition ended with increased δ18ONps at the end of flooding. Maximum δ18ONps at about 12.4 ka (now also dated to <12.7 ka in JPC-06 (Fig. S6) probably marks an interval of relatively high salinity in the near surface Beaufort Sea (Schell et al. 2008), followed by more typical decreasing δ18O trends in benthic and planktonic foraminifera as ice volume decreased and climate warmed during the Holocene. The lingering high magnetic susceptibility late in the YD may indicate evolving sources of sediment from Mackenzie River, and it might also relate to the evidence of a second flood <13 ka (Murton et al. 2010).

Knowing the duration of the YD flood is important for calculating the fresh water transport and evaluating its affect on the AMOC. If we take the main flood interval of the YD as that part where δ18ONps was less than the 2‰ baseline, then it lasted ~400 years. If the lowest δ18ONps indicates peak discharge, then most of the fresh water transport could have occurred in less than a century (12.62-12.69 ka). However, it

must be kept in mind that if the Mackenzie River choke point at Fort McMurray was breached suddenly at the beginning of the YD, and this is contentious (Fisher et al. 2009), then initial salinities over our core site may have been too low for Nps to grow. Furthermore, estimates of very high fresh water transport during the flood are based on the assumption that it occurred on the timescale of a year (Leverington et al. 2000), yet if the main flood was so brief then it is unlikely enough planktonic foraminifera could have recorded the low δ18ONps to leave a signal in the geological record. Most likely the Mackenzie discharge at ~12.9 ka was first a flood with high but unknown transport, followed by decades or centuries of lower but sustained transport. This combination of both a routing change and a flood was probably effective in reducing the MOC (Meissner and Clark, 2006), especially considering it was an Arctic source (Condron and Winsor, 2012). However, even if the YD flood from Mackenzie River itself was too modest to trigger a collapse of the AMOC, many large rivers empty into the Arctic (Aagard and Carmack, 1989), and Lena River, one of the largest, also flooded about 13 ka (Spielhagen et al. 2005). Finally, it should be noted that in addition to fresh water floods in the Arctic around the beginning of the YD, it is also reported that enhanced sea ice export through Fram Strait had a Beaufort Sea source (Hillaire-Marcel et al., 2013).

By YD time, the AMOC may have already been close to a tipping point after 1500 years of low salinity export from the Beaufort Sea, especially in the nearshore convective regions of the Nordic seas (Mauritzen, 1996; Pedlosky and Spall 2005). Increased freshening has also been noted at other coastal locations including the proposed eastern outlet (St. Lawrence River system) using various proxies (Carlson et al. 2007; Cronin et al. 2012, Levac 2015), and off eastern Greenland where δ18ONps minima of YD age are thought to reflect local melting (Jennings et al. 2006) but could also be evidence of the Mackenzie flood. However, only in the eastern Beaufort Sea do the sediment and stable isotope data, and a pathway from Glacial Lake Agassiz, meet the standard set by Kennett

and Shackleton (1975). The coincidence of decreased δ18O in the Beaufort Sea and increased δ18O in the Gulf of Mexico at the beginning of the YD is a perfect fit to their diversion hypothesis (Fig. 5). In the context of all the other observations, and the lack of a large YD minimum in δ18O anywhere else in the North Atlantic Ocean, the ~12.9 ka flood from Mackenzie River was most likely the trigger for the Younger Dryas cooling and reduction of the AMOC.

4.4 ACKNOWLEDGEMENTS

The funding source is NSF grant ARC-1204045. All data will be archived at the NOAA paleoclimate site. We thank the officers and crew of USCGC Healy for their role in making this project a success. We are also indebted to M. Carman for help processing core samples; A. McNichol for helpful discussions of 14C in the Arctic; A. Gagnon for the stable isotope measurements; the NOSAMS staff for providing 14C data; M. McCarthy, C. Mosher, C. Griner, and C. Mayo for leading the coring effort.

Chapter 4 is being prepared for submission in: L.D. Keigwin, S. Klotsko, N. Zhao, B. Reily, L.Giosan, and N. W. Driscoll, In Prep. Deglacial Floods in the Beaufort Sea. The dissertation author was the involved in acquisition, processing, and interpretation of part of the data that forms the basis of this chapter. The dissertation author is secondary author on this publication.

4.5 REFERENCES

Aagard, K. and E. Carmack (1989). “The role of sea ice and other fresh water in the Arctic circulation.” Jour. Geophys. Res. 94: 14485-14498.

Andersson, G. (1897). Swedish vegetation history. Stockholm, P. A. Norstedt & Soners Forlag.

Appen, W. J. v. and R. Pickart (2012). “Two configurations of the western Arctic Shelfbreak Current in summer.” Jour. Phys. Oceanography 42: 329-351.

Broecker, W. S., Kennett, J. P., Flower, B. P., Teller, J. T., Trumbore, S., Bonani, G., & Wolfli, W. (1989). "The routing of meltwater from the Laurentide ice-sheet during the Younger Dryas cold episode." Nature 341: 318-321.

Carlson, A. and P. Clark (2012). "Ice sheet sources of sea level rise and freshwatrer discharge during the last deglaciation." Rev. Geophys, 50(2011RG000371).

Carlson, A. E., Oppo, D. W., Came, R. E., LeGrande, A. N., Keigwin, L. D., & Curry, W. B. (2008). "Subtropical Atlantic salinity variability and Atlantic meridional circulation during the last glaciation." Geology 36: 991-994.

Condron, A. and P. Winsor (2012). "Meltwater routing and the Younger Dryas." PNAS doi:10.1073/pnas.1207381109.

Cooper, Lee W., Ronald Benner, James W. McClelland, Bruce J. Peterson, Robert M. Holmes, Peter A. Raymond, Dennis A. Hansell, Jacqueline M. Grebmeier, and Louis A. Codispoti (2005). "Linkages among runoff, dissolved organic carbon, and the stable oxygen isotope composition of seawater and other water mass indicators in the Arctic Ocean." Jour. Geophys. Res. 110(doi:10.1029/2005JG000031).

Cronin, T. M., J. A. Rayburn, J-P. Guilbault, R. Thunell, and D. A. Franzi (2012). "Stable isotope evidence for glacial lake drainage through the St. Lawerence estaury, eastern Canada, ~13.1-12.9 Ka." Quat. International 260: 55-65.

Darby, Dennis A., Jens F. Bischof, Robert F. Spielhagen, Steven A. Marshall, and Stephen W. Herman (2002). "Arctic ice export events and their potential impact on global climate during the late Pleistocene." Paleoceanography 17(doi:10.1029/2001PA000639).

de Vernal, Anne, Claude Hillaire-Marcel, and Guy Bilodeau (1996). "Reduced meltwater outflow from the Laurentide ice margin during the Younger Dryas." Nature 381: 774-777.

Dickson, R.R., Meincke, J., Malmberg, S.A. and Lee, A.J. (1988). "The "Great Salinity Anomaly" in the Northern North Atlantic 1968-1982." Prog. Oceanog. 20: 103-151.

Fisher, T.G., Waterson, N., Lowell, T.V. and Hajdas, I. (2009). "Deglaciation ages and meltwater routing in the Fort McMurran region, northeastern Alberta and northwestern Saskatchewan, Canada." Quat. Sci. Rev. 28: 1608-1624.

Häkkinen, S. (1993). "An Arctic source for the great salinity anomaly: A simulation of the Arctic ice-ocean system for 1955-1975." Journal of geophysical Research 98: 16,397-316,410.

Hartz, N. and V. Milthers (1901). “The late glacial clay in the Allerod brickyard.” Meddelelser Dansk Geologisk Foreningen 8: 31-60.

Hillaire-Marcel, C., Maccali, J., Not, C. and Poirier, A. (2013). “Geochemical and isotopic tracers of Arctic sea ice sources and export with special attentiion to the Younger Dryas interval.” Quat. Sci. Rev. 79: 184-190.

Jennings, A.E., Hald, M., Smith, M. and Andrews, J.T. (2006). “Freshwater forcing from the Greenland Ice Sheet during the Younger Dryas: evidence from southeastern Greenland shelf cores.” Quat. Sci. Rev. 25: 282-298.

Johnson, R. G. and B. T. McClure (1976). “A model for northern hemisphere continental ice sheet variation.” Quaternary Research 6: 325-353.

Keigwin, L.D., Donnelly, J.P., Cook, M.S., Driscoll, N.W. and Brigham-Grette, J. (2006). “Flooding of Bering Strait and Holocene climate in the Chukchi Sea.” Geology 34: 861-864.

Keigwin, L. D. and G. A. Jones (1995). “The marine record of deglaciation from the continental margin off Nova Scotia.” Paleoceanography 10: 973-985.

Keigwin, L.D., Sachs, J.P., Rosenthal, Y. and Boyle, E.A. (2005). “The 8200 year B.P. event in the slope water system, western subpolar North Atlantic.” Paleoceanography 20: doi:10.1029/2004PA001074.

Kennett, J. P. and N. J. Shackleton (1975). “Laurentide ice sheet meltwater recorded in Gulf of Mexico deep-sea cores.” Science 188: 147-150.

Levac, E., Lewis, M., Stretch, V., Duchesne, K. and Neulieb, T. (2015). “Evidence for meltwater drainage via the St. Lawrence River valley in marine cores from the Laurentian Channel at the time of the Younger Dryas.” Global and Planetary Change 130: 47-65.

Leventer, A., Williams, D.F. and Kennett, J.P. (1982). “Dynamics of the Laurentide ice sheet during the last deglaciation: evidence from the Gulf of Mexico.” Earth and Planet. Sci. Letts. 59: 11-17.

Leverington, D.W., Mann, J.D. and Teller, J.T. (2000). “Changes in the bathymetry and volume of glacial Lake Agassiz between 11,000 and 9300 14C yr B.P.” Quater. Res. 54: 174-181.

Macdonald, R. and Y. Yu (2006). The Mackenzie estuary of the Arctic OCean. Handbook of Environmental Chemistry. Berlin, Springer-Verlag. 5: 91-120.

Mauritzen, C. (1996). “Production of dense overflow waters feeding the North Atlantic

across the Greenland-Scotland Ridge. Part 1: Evidence for a revised circulation scheme." Deep-Sea Res. 43: 769-806.

McManus, J.F., Francois, R., Gherardi, J.M., Keigwin, L.D. and Brown-Leger, S. (2004). "Collapse and rapid resumption of Atlantic meridional circulation linked to deglacial climate changes." Nature 428: 834-837.

Meissner, K. and P. Clark (2006). "Impact of floods versus routing events on the thermohaline circulation." Geophys. Res. Lett. 33(doi:10.1029/2006GL026705).

Murton, J.B., Bateman, M.D., Dallimore, S.R., Teller, J.T. and Yang, Z. (2010). "Identification of Younger Dryas outburst flood path from lake Agassiz to the Arctic Ocean." Nature 464: 740-743.

Östlund, H.G., Possnert, G. and Swift, J.H. (1987). "Ventilation rate of the deep Arctic Ocean from carbon 14 data." Jour. Geophys. Res. 92: 3769-3777.

Pedlosky, J. and M. Spall (2005). "Boundary intensification of vertical velocity in a beta-plane basin." Jour. Phys. Oceanography 35: 2487-2500.

Rasmussen, S.O., Andersen, K.K., Svensson, A.M., Steffensen, J.P., Vinther, B.M., Clausen, H.B., Siggaard-Andersen, M.L., Johnsen, S.J., Larsen, L.B., Dahl-Jensen, D. and Bigler, M. (2006). "A new Greenland ice core chronology for the last glacial termination." Jour. Geophys. Res. 111(doi:10.1029/2005JD006079).

Rooth, C. (1982). "Hydrology and ocean circulation." Prog. Oceanog. 11: 131-149.

Rudels, B., Jones, E.P., Anderson, L.G. and Kattner, G. (1994). "On the intermediate depth waters of the Arctic Ocean." Geophysical Monograph 85: 33-46.

Schell, T.M., Scott, D.B., Rochon, A. and Blasco, S. (2008). "Late Quaternary paleoceanography and paleo-sea ice conditions in the Mackenzie Trough and Canyon, Beaufort Sea." Can. J. Earth Sci. 45: 1399-1415.

Scott, D.B., Schell, T., St-Onge, G., Rochon, A. and Blasco, S. (2009). "Foraminiferal assemblage changes over the last 15,000 years on the Mackenzie-Beaufort Sea slope and Amundsen Gulf, Canada: Implications for past sea ice conditions." Paleoceanography 24 (doi:10.1029/2007PA001575).

Spielhagen, R.F., Erlenkeuser, H. and Siegert, C. (2005). "History of frewhwater runoff across the Laptev Sea (Arctic) during the last deglaciation." Global and Planetary Change 48: 187-207.

Stokes, C.R., Clark, C.D. and Storrar, R. (2009). "Major changes in ice stream dynamics during deglaciation of the north-western margin of the Laurentide ice sheet."

Quat. Sci. Rev. 28: 721-738.

Tarasov, L. and W. R. Peltier (2005). “Arctic freshwater forcing of the Younger Dryas cold reversal.” Nature 435: 662-665.

Thornalley, D.J., Bauch, H.A., Gebbie, G., Guo, W., Ziegler, M., Bernasconi, S.M., Barker, S., Skinner, L.C. and Yu, J. (2015). “A warm and poorly ventilated deep Arctic Mediterranean during the last glacial period.” Science 349(706-710).

Wheeler, J. O., Hoffman, P. F., Card, K. D., Davidson, A., Sanford, B. V., Okulitch, A. V., Roest, W. R. (1996). Geological Map of Canada. “A” Series Map 1860A; doi:10.4095/208175, Geological Survey of Canada.

Williams, Carlie, Benjamin P. Flower, and David W. Hastings (2012). “Seasonal Laurentide ice sheet melting during the “Mystery Interval” (17.5-14.5 ka).”

Geology 40: 955-958.

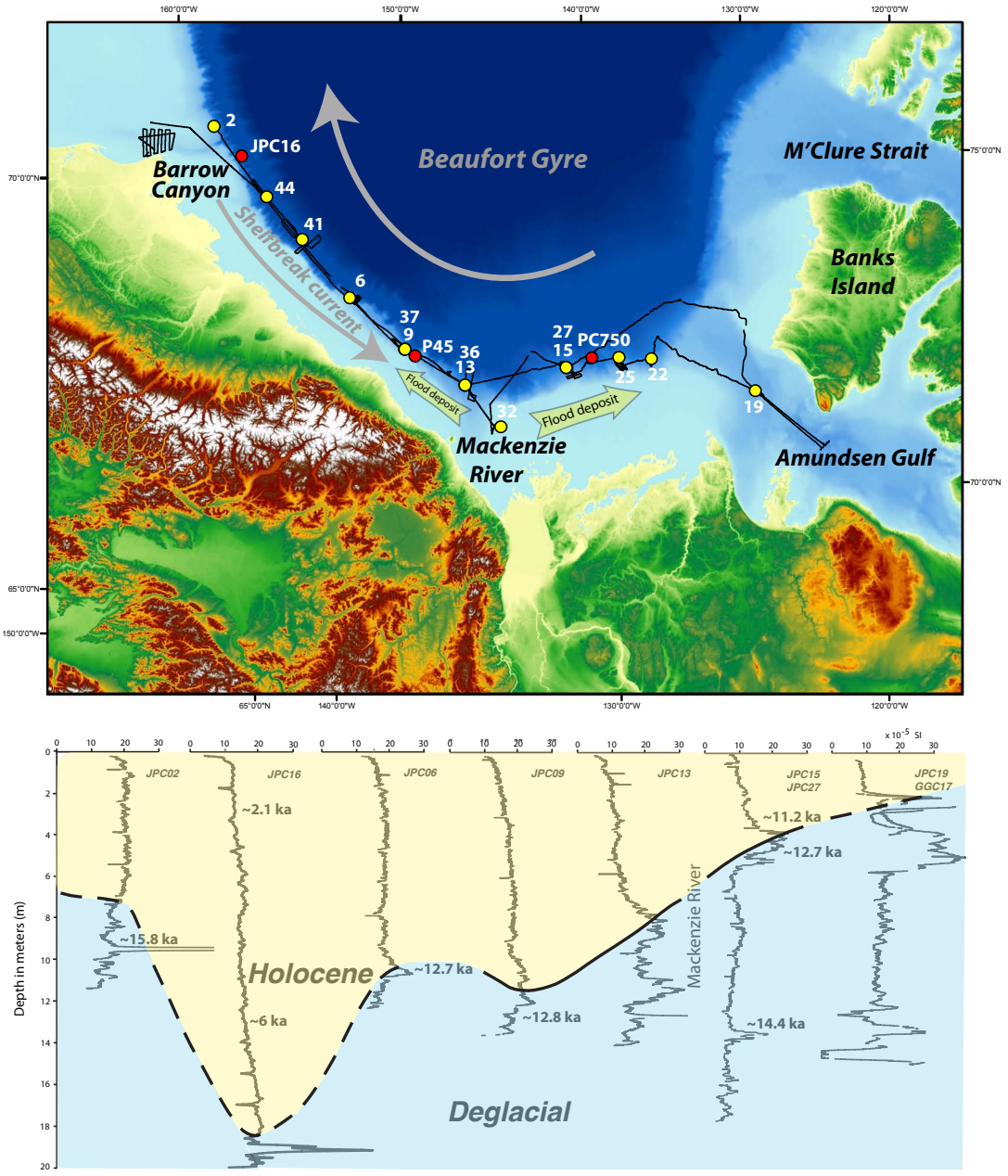

Figure 4.2. Overview of core locations and stratigraphy in the eastern Beaufort Sea. (Top) Healy 1302 ship's track and Jumbo Piston Core sites (yellow) from that cruise, and other cores (red) discussed in this study. Based on low δ18O in planktonic forams and acoustic evidence, the YD flood deposit is only observed as far west as JPC-09. Because of Coriolis force and lowered sea level, the flood would have travelled north and east beyond JPC-25 where the flood facies is last noted. (Bottom) Down core magnetic susceptibility is shown with selected dates (calendar ka) delineating the Holocene (yellow) - Deglacial (blue) boundary. Note the thicker Holocene section towards the west that probably reflects sediment derived from Bering Strait and Chukchi Shelf when the strait is flooded.

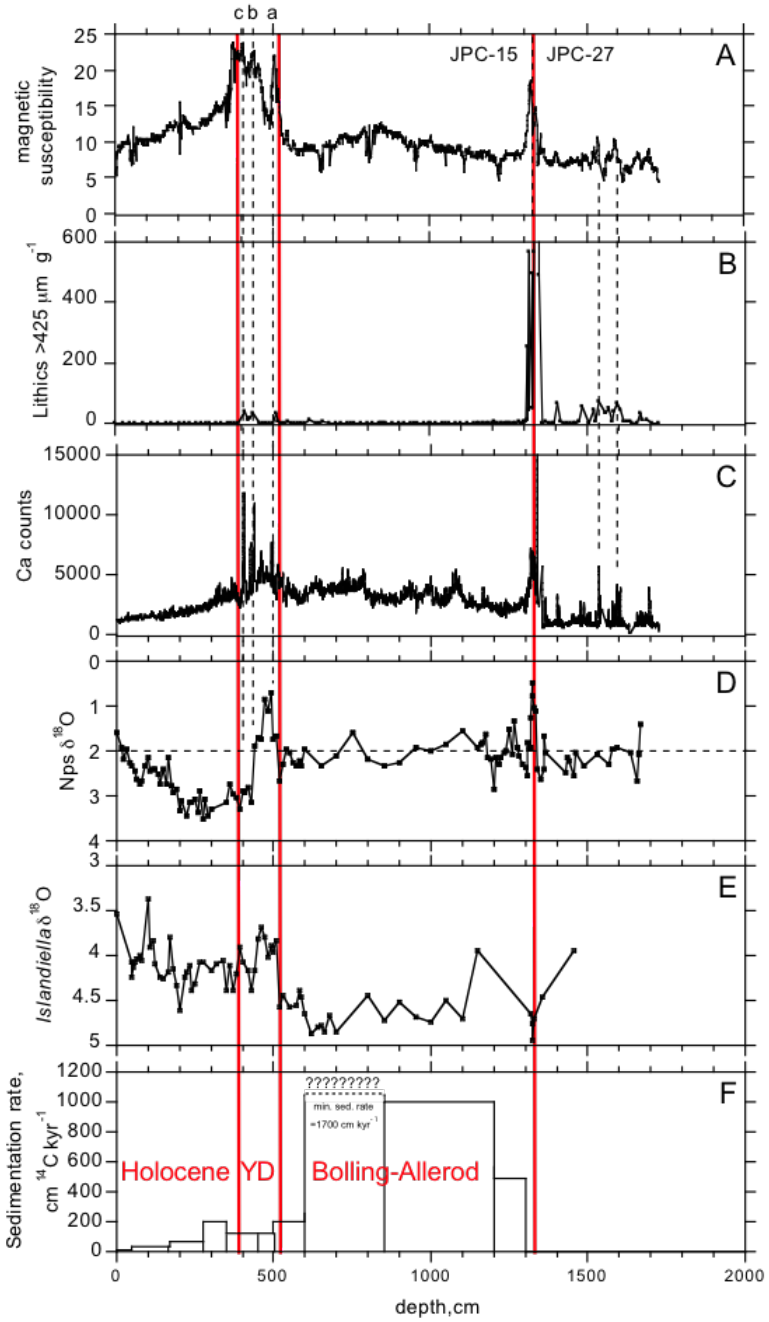

Figure 4.3. Various proxy data from HLY1302 JPC-15/27 in the eastern Beaufort Sea. Magnetic susceptibility (A), lithic particle abundance (B), Ca content (proxy for CaCO3) (C), and δ18ONps (D) all exhibit extreme values at the onset of the Bolling/Allerod warming at 14.5 ka (red line at 1320 cm) and during the YD (11.7-12.9 ka) (~380-520 cm). Dashed vertical lines correlate smaller features. Dashed horizontal line in (D) shows the ~2.0 ‰ baseline that extends >4 m down the core. A large dropstone at 1346-1355 cm was removed prior to XRF scanning the core, but another sharp Ca spike just above that suggests another carbonate dropstone may be buried in the scanned half of core. The C. neoteretis (benthic) δ18O (E) is unremarkable except that the clear minimum ~450-500 cm occurs in the same samples as the low δ18ONps. Sedimentation rates (F) are very high between 600-1200 cm where sediments are laminated and cycle counting of XRF data suggests the laminae are annual (Fig. S2).

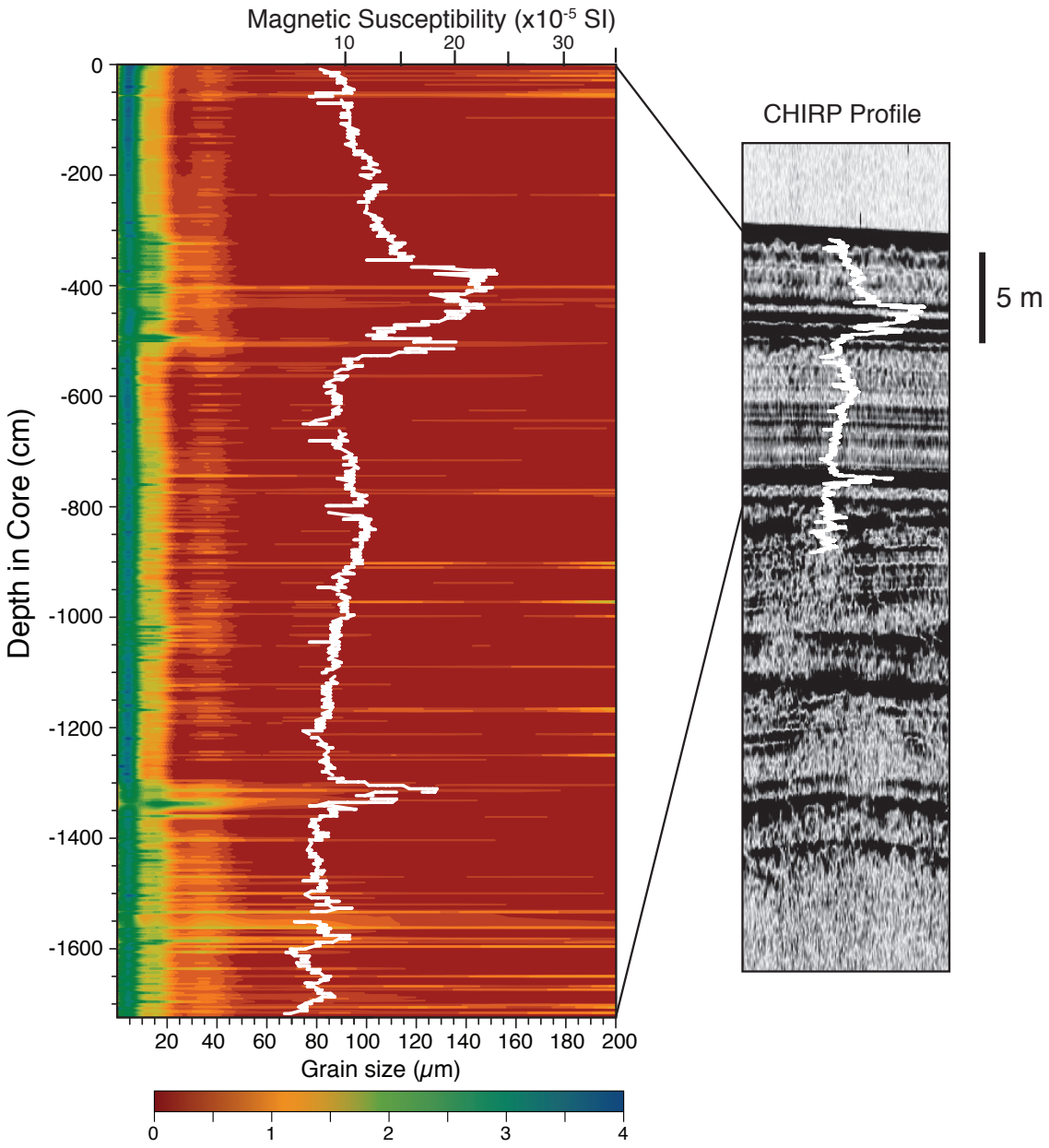

Figure 4.4. Downcore grain size variability in composite jumbo piston cores JPC15 and JPC27. Magnetic susceptibility data are superposed on the grain size and the seismic data, assuming the pressure wave velocity of the core measured using the multisensory track at sea. JPC 15/27 shows a strong correlation between coarse grain size, high magnetic susceptibility, and high amplitude acoustic character. The seismic data show a diagnostic reflector pattern with an upper (~380-520 cm) and lower high (~1320 cm) amplitude reflectors that bound a region of lower acoustic reflectivity. The zone of lower reflectivity correlates with high sediment accumulation rates, and low magnetic susceptibility, low ice rafted debris (IRD), and low Ca content (Fig. 2). This zone can be traced as far east as JPC-25, and as far west as JPC-09 (Fig.1).

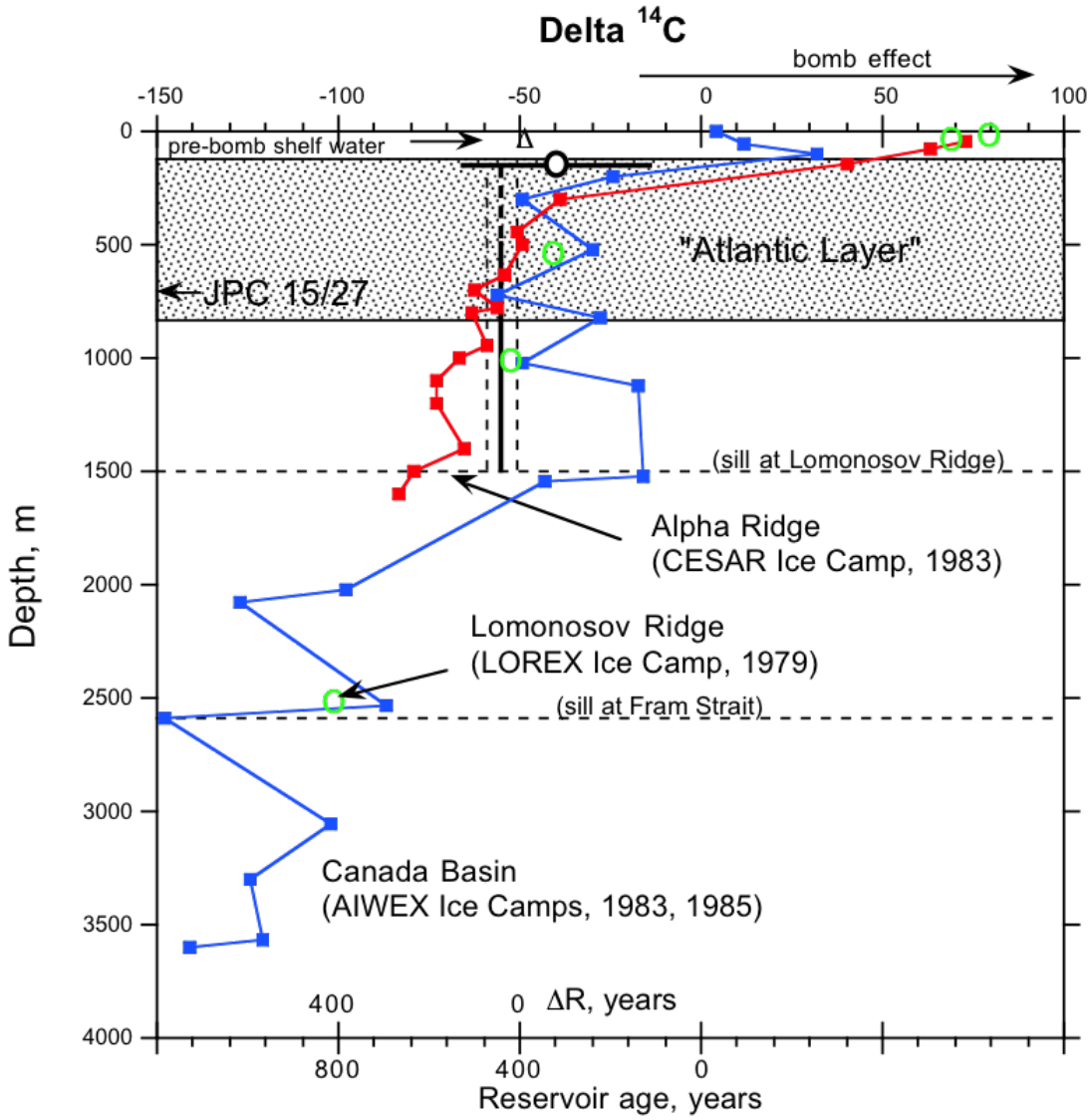

Figure 4.5. Radiocarbon basis for the age model in this paper. Ostlund et al. (1987) synthesized Δ14C, δ18O, and tritium data collected from several Arctic locations between 1977 and 1985 and concluded that the pre-bomb value of intermediate depth waters (500 or 600 to 1500 m) was -55 ±5 ‰ (vertical black line with dashed error bars), and pre-bomb shelf water was -48 ±3 ‰ (triangle). Depth profiles from ice camps were made in 1974 (LOREX, open green circles), 1983 (CESAR, small red squares), and during 1983 and 1985 in Canada Basin (AIWEX, blue squares), and all these are considered to be equivalent to Canada Basin water in that all are on the west side of Lomonosov Ridge. At ~690 m water depth, we assume benthic foraminifera from JPC-15/27 lived in the -55 ‰ water, however, the mean of our planktonic dates (open black circle) is younger than benthic dates by only 120 ±220 yrs (or 15 ±25 ‰ lower than the benthics), so they are within uncertainty of each other. Thus our age model is based on calibrated planktonic dates using a ΔR=40, reflecting the 5 ‰ difference from the standard -50 ‰ (400 year) assumption (see additional details in S2).

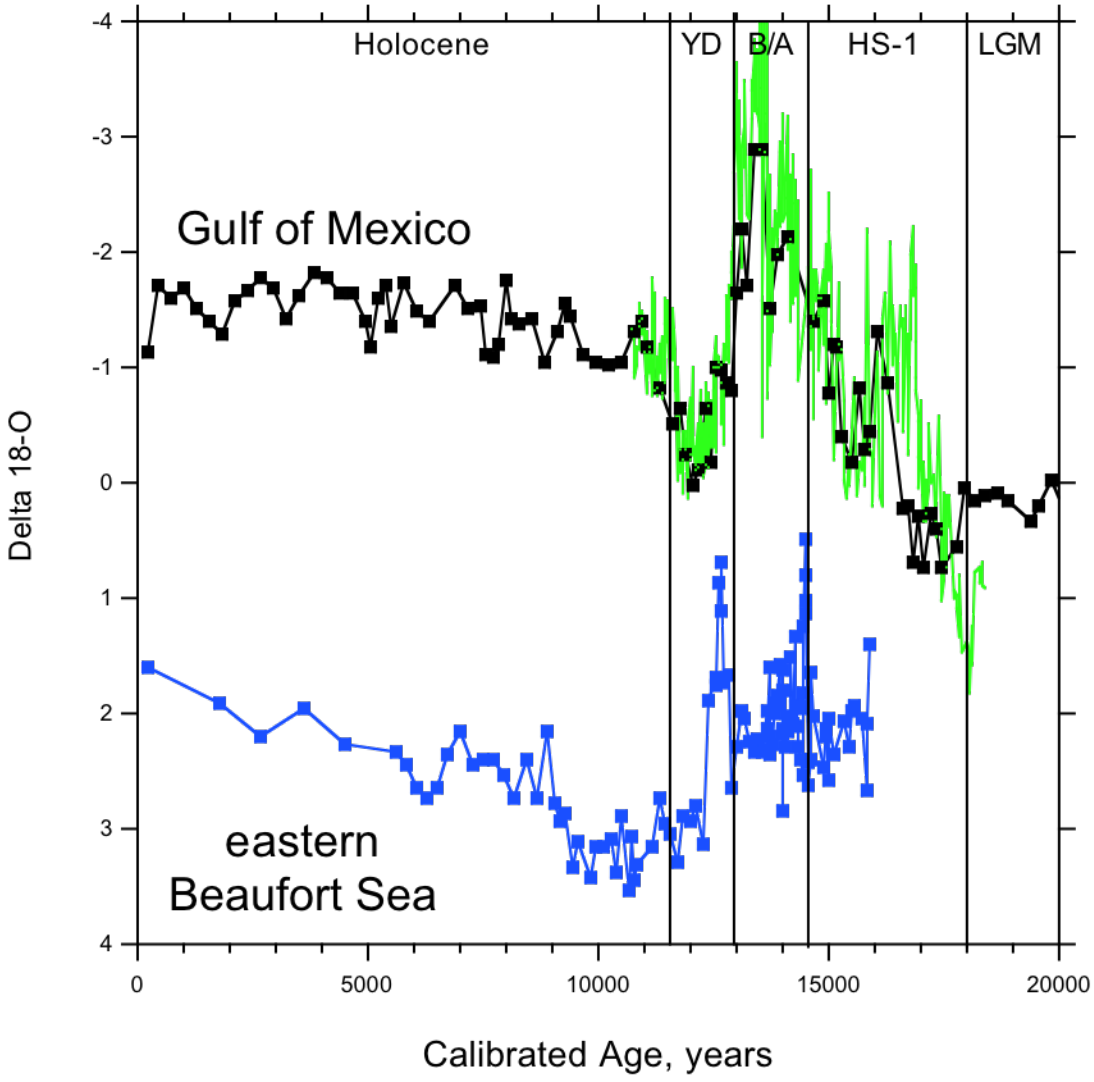

Figure 4.6. Comparison of deglacial δ18O between Orca Basin in the Gulf of Mexico and Beaufort Sea. The Arctic data are based on N. pachyderma s. (blue squares; this study) and the Orca Basin data are based on the planktonic foraminifer Globigerinoides ruber (green line, Leventer et al., 1982; black squares, Williams et al., 2012). The data show that the eastern Beaufort Sea freshened at about 12.9 ka coincident with the end of Gulf of Mexico freshening and consistent with the hypothesis that meltwater was diverted from the Gulf to a more northern outlet as deglaciation progressed (Kennett and Shackleton, 1975). YD= Younger Dryas, B/A = Bolling/Allerod, HS-1 = Heinrich Stadial 1, LGM = last glacial maximum. In the eastern Beaufort Sea the B/A minimum in δ18ONps at 14.4 ka is thought to reflect the retreat of the Amundsen and M'Clure Strait ice tongues and attendant iceberg melting, whereas the YD minimum is thought to be the flood of Glacial Lake Agassiz meltwater via Mackenzie River.

4.6 SUPPLEMENTAL MATERIAL

4.6.1 Stratigraphy

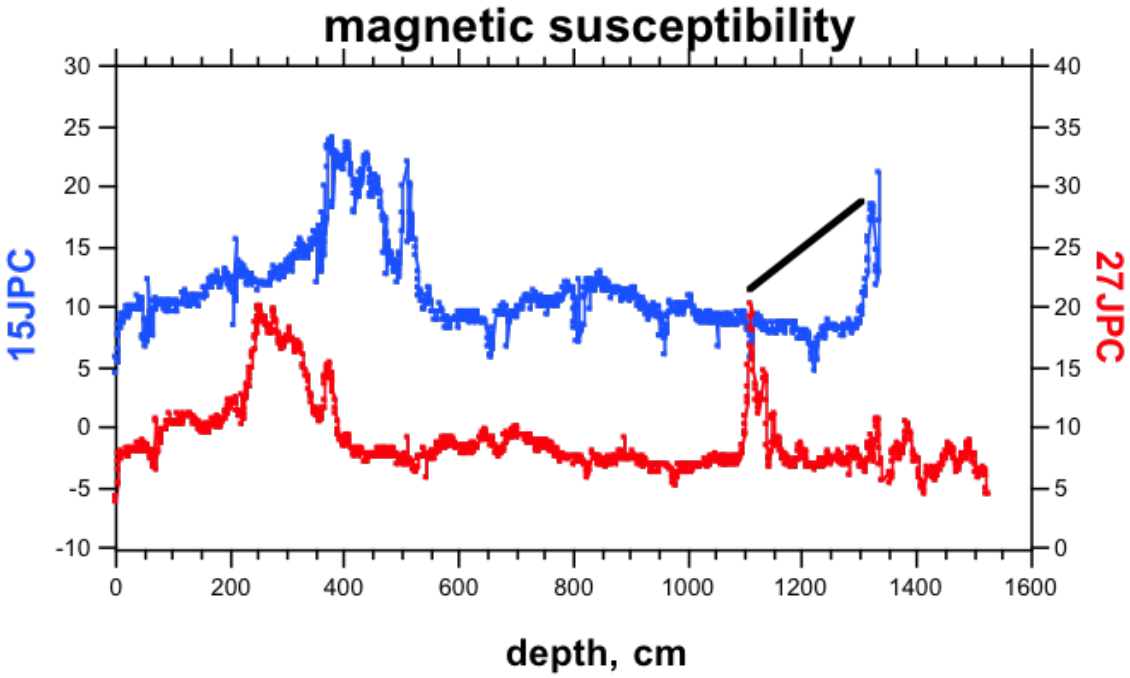

Figure 4.S1. Magnetic susceptibility records of HLY1302 cores JPC15/27 that were recovered from the same location at 690 m on the continental slope east of Mackenzie River. To make a 1729 cm composite section, we patched to JPC-15 at 1329 cm the data below 1125 cm in JPC-27 (with a +205 cm offset).

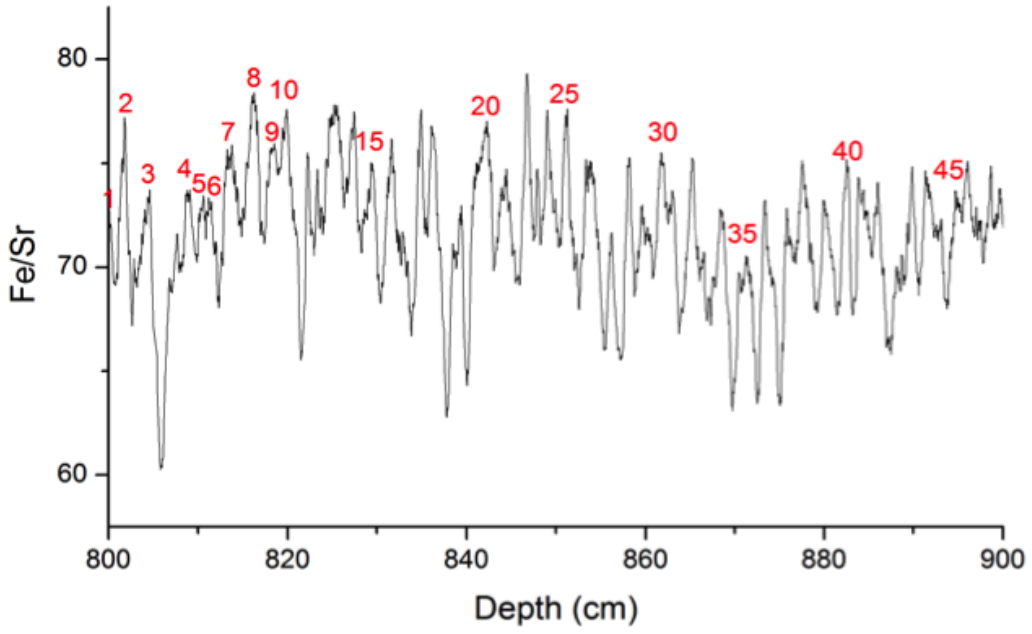

Figure 4.S2. Laminae counted using Fe/Sr variability of a one-meter section in HLY1302 JPC15. Many other elemental pairs show similar variability. High Fe/Sr suggests greater terrestrial content. The resolution of the data is 0.4 mm and the data are smoothed with a 19-point running mean. There are about 50 peaks in this section with 2cm/cycle on average, and the number of cycles varies little with counting method. We counted ~300 laminae between 600 cm (13655 ka) and 1201 cm (14001 ka) where the deposition rate is uniformly high, and those probably reflect ~300 annual oscillations in terrigenous input to the continental slope (300 laminae/345 years = 0.87 laminae/yr).

4.6.2 Chronology

Table 4.1. AMS radiocarbon results from this study.

Table S1. AMS radiocarbon results* of this study.

depth, cm	depth interval, cm	species	Accession number	conv 14C age yrs	uncertainty ± 1σ	median probability	uncertainty ± 1σ
HLY1302 JPC-15							
50	46-54	N. pachyderma	OS-110669	5,300	30	5618	32
167	163-171	N. pachyderma	OS-110857	8,340	40	8865	81
274	271-277	N. pachyderma	OS-110670	9,830	55	10651	73
350	348-352	N. pachyderma	OS-110671	10,200	45	11169	31
450	448-452	N. pachyderma	OS-110672	11,050	45	12551	39
500	498-502	N. pachyderma	OS-123914	11,300	35	12721	72
600	598-602	N. pachyderma	OS-110673	12,250	60	13654	94
850	846-854	N. pachyderma	OS-110674	12,250	55	13656	93
1201	1198-1204	N. pachyderma	OS-110675	12,600	60	14001	93
1300	1298-1302	N. pachyderma	OS-110676	12,800	65	14394	225
1340	several cm	Nps and BF	OS-106829	13,100	50	14992	146
50	46-54	C.neoteretis	OS-113087	5,020	20		
274	271-277	C.neoteretis	OS-113088	10,100	30		
350	348-352	C.neoteretis	OS-113089	10,200	30		
450	448-452	C.neoteretis	OS-113090	11,200	30		
1200	1198-1204	C.neoteretis	OS-113091	13,000	35		
1300	1298-1302	C.neoteretis	OS-113092	13,000	35		
HLY1302 JPC-02							
921.5	920-923	mixed benthics	OS-122350	13,500	70	15771	333
HLY1302 JPC-06							
1036		mixed benthics	OS-122351	11,250	65	12687	71
HLY1302 JPC-09							
1312		N. pachyderma	OS-127490	11350	45	12770	84

*all measurements were made at the National Ocean Sciences AMS (NOSAMS) facility.

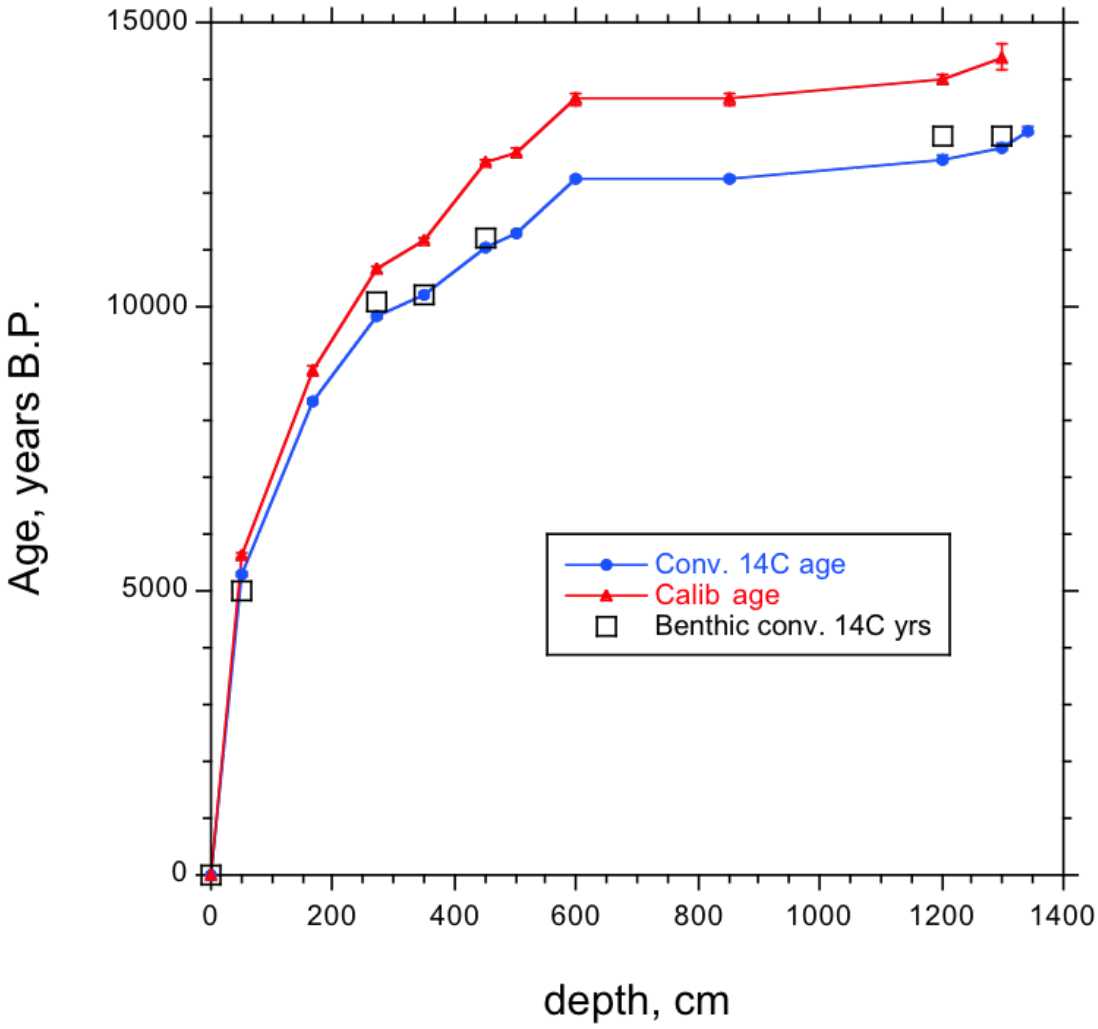

Figure 4.S3. Age-depth relationship of conventional AMS 14C dates on Nps (blue circles) and C. neoteretis (open black squares) from JPC-15, and calibrated (CALIB 6.1 with ΔR=40; Stuiver and Reimer, 1993) dates on Nps (red triangles). Uncertainty is generally smaller than the plot symbols, although for most of the record we assume it is about ±100 yrs. The calibrated age of the date at 850 cm was adjusted to 13750, near the upper limit of the 1σ error range, in order to have a finite rate of sedimentation between 600 and 1200 cm. The oldest date from this core comes from the core catcher sample of mixed Nps and C. neoteretis. We do not use this date in the age model for JPC15/27 because, first, it was not recorded how big a piece of mud was washed, nor its exact depth below the deepest mud in core section 1. Second, it is so close (~40 cm) to the date at 1300 cm that a little age uncertainty generates a big change in the extrapolated age model. JPC-27 contains too few foraminifera below 1100 cm to date, hence the extrapolation >14.5 ka.

4.6.2.1 Choice of ΔR

There are only two choices for the modern ΔR in Beaufort Sea, one based on study of radionuclides as tracers for Arctic processes (Ostlund and Hut, 1984; Ostlund et al. 1987), as described in the main text, and the other based on "pre-bomb" museum specimens of mollusks (especially bivalves (McNeely et al. 2006)). One notable thing about the Ostlund et al. (1987) analysis is the 14C measurement on surface waters in the east Greenland Current in 1959 that leads them to "safely assume" that shelf water had a pre-bomb Δ14C of -48 ± 3 ‰. Although east Greenland is about as far as you can get in the Arctic from the Beaufort Sea, Ostlund and Hut (1984) showed that the residence time of shelf and near surface waters in the Arctic is only ~10 years. However, they had no shelf water data from the west Arctic where there is low "preformed" Δ14C, based on the bivalves.

McNeely et al. (2006) compiled mollusk 14C data from all around Canada for the specific purpose of knowing ΔR at continental shelf depths for dating in paleo studies. In the Beaufort-Chukchi Seas they reported dates on 7 bivalve specimens collected from two stations (Fig. S4). Six bivalves were suspension feeders and one was a deposit feeder; that one is significantly older than the others (ΔR=610 yrs). Excluding that datum, the others have a mean ΔR of 440 ±101 yrs, or a mean Δ14C close to -100 ‰. That result is greatly different than the Δ14C of -48 ‰ directly measured in in East Greenland shelf waters (Ostlund et al. 1987).

The missing element in the Ostlund and Hut (1984) and Ostlund et al. (1987) analysis was a source of relatively old waters from the NE Pacific via the Alaska Coastal Current and, through Bering Strait, the shelf break current in the Beaufort Sea. The shelf break current can be traced as far east as Amundsen Gulf, by which point it is dissipated without evidence of entering the Gulf (von Appen and Pickart, 2012), but the McNeely et al. (2006) pre-bomb data can be used to trace transport to the Labrador Sea through

the Canadian archipelago in recent times. Forty Δ14C measurements of Pacific mollusks (Victoria, BC to Bering Strait), excluding deposit feeders, average ΔR=388 ±86 yrs, not significantly different from the Chukchi/Beaufort value cited above (440 ±101 yrs). By Amundsen Gulf, where McNeely et al. (2006) have 7 observations from 5 sites (Fig. S4), the result, ΔR=350±116, is essentially the same as the Bering Strait source waters. However, by Foxe Basin, ΔR=286 ±74 yrs (n=8), which is significantly lower than the Beaufort/Bering Strait data. We choose Foxe Basin because it represents a pathway that is least likely to encounter younger Atlantic shelf waters, and for the same reason we only use those data on the south side of the strait that connects Gulf of Boothia to Foxe Basin. Nevertheless, a trend of increasing Δ14C suggests there was mixing with a North Atlantic component. These data are substantially older than the East Greenland mollusks, where ΔR=92 ±67 years (n=12). The difference between the pre–bomb reservoir age of east Greenland shelf waters and those that have a Bering Strait origin is significant.

In fact, the east Greenland shelf is the only place where pre-bomb Δ14C has been measured in both shelf waters (-48±3 ‰) and in mollusks (-61±7 ‰), and with results in reasonable agreement. However, this does not mean that shelf ΔR should be used to calibrate 14C ages from foraminfera on the Beaufort continental slope for a few reasons. (1) The shelf break waters that carry the old signal from Bering Strait are well inshore of the surface water overlying our core sites (von Appen and Pickart, 2012). (2) Although we do not know the pre-bomb 14C age of Beaufort Sea surface waters (Fig. 4), the rather close agreement of paired benthic and planktonic 14C ages suggests the planktonics live in water influenced by the Atlantic layer even in the Holocene. During pre-Holocene time (>11 ka), before Bering Strait was flooded (Keigwin et al., 2006), the Atlantic layer might have shoaled in the absence of Pacific water, all else being equal (pers. comm. 2016 from R. Pickart and M. Spall). However, most importantly, (3) the pre-Holocene absence of old Pacific water in the Arctic means that shelf waters must have had more

of an Atlantic character. Thus, for the present study, it is appropriate to calibrate our 14C ages with a ΔR of 40 years based on the pre-bomb measurements in the Atlantic layer, the similarity of benthic and planktonic AMS dates, and the assumption that during deglaciation in Beaufort Sea there would have been no influence of Pacific water.

Figure 4.S4. Locations of pre-bomb bivalve data (Dyke 2004) from off Alaska on left, downstream in the Amundsen Gulf (middle), and far to the east in Foxe Basin. These sites were chosen because they define a flow path where Bering Strait water always hugs the coast and turns right. Today the shelfbreak current has been traced to the entrance to Amundsen Gulf (von Appen and Pickart, 2012), but the bivalve 14C data have a Pacific signature as far as northern Foxe Basin.

4.6.3 Regional summary of oxygen isotope data

4.6.3.1 New core data

It is important to determine the spatial extent of the YD flood within the Beaufort Sea because Coriolis forcing would drive a buoyant flow to the right from Mackenzie River, and northward along the Canadian Archipelago toward Fram Strait. Such a direct path to the North Atlantic might have the most climate impact because the surface waters would be freshest. On the other hand, wind forcing could counteract the Coriolis driven flow and perhaps allow more mixing with Beaufort Gyre. In that case, the freshening in the North Atlantic region might have been less and may have lasted longer.

West of Mackenzie River at JPC-09 we have identified a δ18ONps minimum at about 13 m below the seafloor (Fig. S5A). It reaches 1 ‰, close to the minimum at JPC15/27 but unlike that site it occurs a meter below a prominent maximum in magnetic susceptibility. If the δ18ONps records the same near-surface lowering of salinity, then the magnetic properties of the sediment must differ between the two sites near 13 ka. To the east the low δ18ONps is found between the large peaks labeled “a” and “b” in Figure 2, whereas at this western site the low δ18ONps lies between two much smaller peaks. At JPC-09 the deepest peak in magnetic susceptibility contains the highest IRD content, suggesting that we have properly correlated it to event “a”.

If we assign the ages from core 15/27 to the δ18ONps minimum and the post YD maximum at JPC-09, the time series are identical at the two cores (Fig. S5B). JPC-09 is very close to core P45 of Andrews and Dunhill (2004), so we recalibrated the age model for that core using ΔR=40 and plotted their δ18ONps data with the new data from this study. Again, the agreement among these cores is excellent, although the age model of P45 makes the deepest data too old.

Even farther west of Mackenzie River, the δ18ONps at JPC-06 records only a small minimum (Fig. S6). This suggests that the YD meltwater plume must have been

very localized to the region east of JPC-06. In the Chukchi Sea off Barrow, most of the δ18ONps data fall higher than the 2‰ reference level for the entire record <15.8 ka (Fig. S7), including the nearby Holocene results from Keigwin et al. (2006). Thus, taking into account the ice volume effect on δ18O, we conclude that the near sea surface off Barrow was fresher than today during most of the deglaciation, but there must also have been a salinity gradient from the Chukchi Sea to the eastern Beaufort Sea. This points to Mackenzie River as the source of the freshening, but the absence of evidence for the YD flood off Barrow suggests that the flood waters were not diluted much by mixing in the Beaufort Gyre. If supported by further data, this would mean that the YD flood was brief compared to the mixing time of the Beaufort Gyre and might have been especially potent in affecting the AMOC.

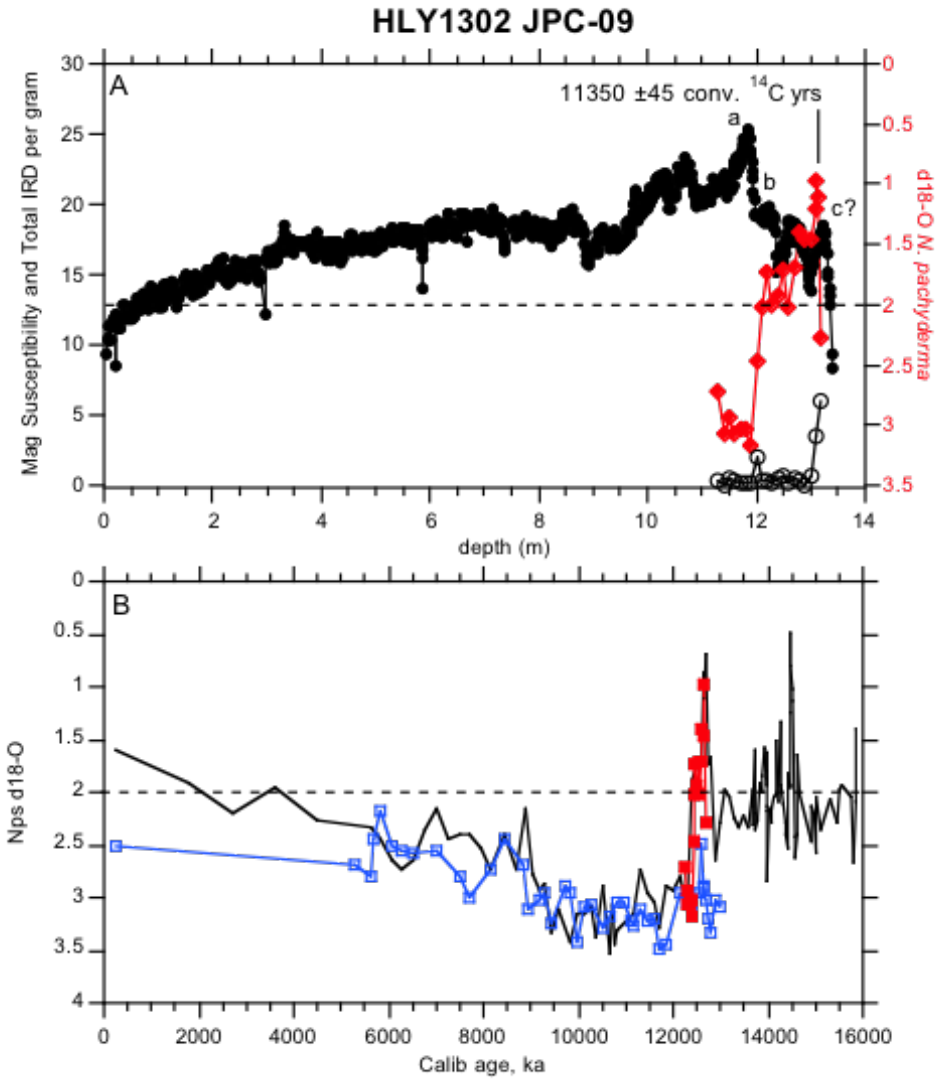

Figure 4.S5. Results at JPC-09 and comparison to other nearby sites. (A) δ18ONps (red diamonds) reached a minimum of ~1 ‰ at ~13 m between two small maxima in magnetic susceptibility (black data), and a maximum at ~12 m. The isotopic minimum is calibrated to 12.77 ka and is coincident with a small peak in IRD abundance (open circles). (B) When those δ18ONps results are combined with data from core P94 (Andrews and Dunhill, 2004) (open blue squares) after recalibration, and from core 15/27 (black line) it is seen that cores close to Mackenzie River record similar histories of low δ18ONps, and therefore salinity. Because the P94 AMS dates were on mixed benthics and planktonics, and only benthics in the deepest sample, the age model could be too old by one to three centuries. For the age model of JPC-09 we assume 12 m = 12.4 ka.

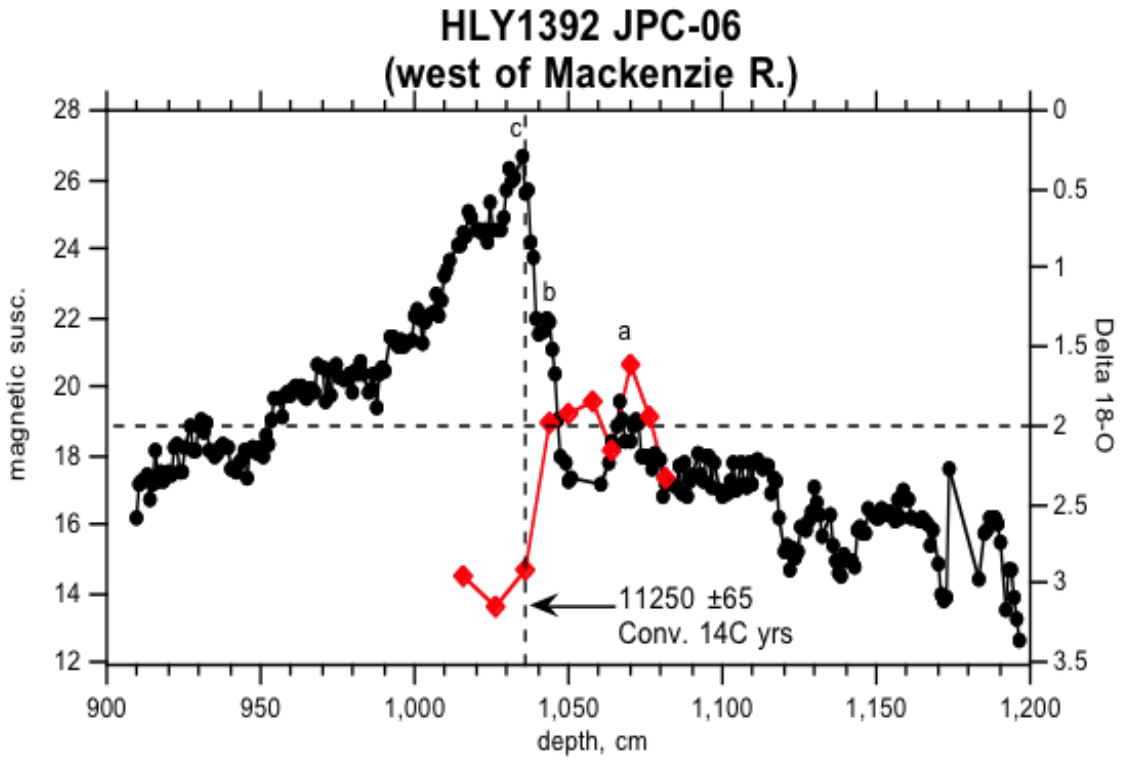

Figure 4.S6. Results at JPC-06. Consistent with JPC-09, the δ18ONps leads the magnetic susceptibility. We can use the maximum δ18ONps at 1020-1040 cm to correlate to JPC15/27, where it is dated to ~12.4 ka. In JPC-06 the maximum δ18ONps is younger than the 12.675 ±0.07 calibrated ka date at 1035 cm (dashed vertical line).

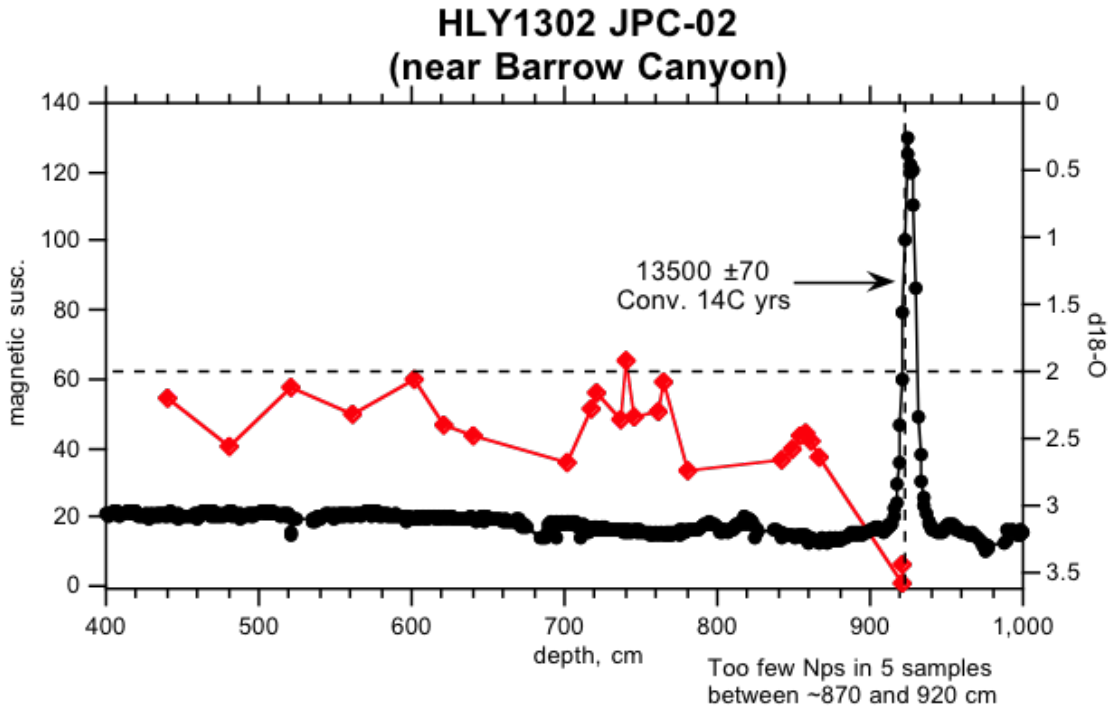

Figure 4.S7. Stratigraphic results at core JPC-02 near Barrow Canyon, far to the west of JPC 15/27. This core recovered an IRD and magnetic susceptibility peak at ~920 cm that dates to ~15.8 calibrated ka and includes a 6-cm dark non-carbonate dropstone. Because this event is not recorded at Core 15/27, and is >1000 years older than the 14.4 ka event, it gives a maximum age for the bottom of the composite section at 15/27, assuming the event came from the Canadian Archipelago and would probably have spread across the Beaufort Sea. Also of note is the maximum in δ18ONps coincident with this IRD layer; this is the opposite of what we see in the YD and 14.4 ka events closer to Mackenzie River and it is the heaviest we have measured in this study.

4.6.3.2 Other published core data

Several papers report stable isotope and radiocarbon data from the western Arctic (Mendeleyev Ridge) including, for example, Poore et al. (1999) and Polyak et al. (2004). We cannot directly correlate our results from the eastern Beaufort Sea with those because they have much lower rates of sedimentation and fewer 14C dates. Given that we also cannot correlate to our core off Barrow (Fig. S7), which does have high rates, it is possible that there was substantial spatial variability in near surface ocean conditions in the western Arctic during deglaciation. As an example of this, both Poore et al. (1999) and Polyak et al. (2004) found deglacial minima in δ18ONps that are 0 ‰ or even lower. These are probably not evidence of the YD flood from Mackenzie River because the δ18O is lower than we observe closer to the source.

Closer to the Beaufort Sea, on the Chukchi Borderlands, Polyak et al. (2007) do find a δ18ONps minimum of about 1‰ that could be related to one of those we see at core 15/27. However, using ΔR=0 they date the event to 13.8 ka which falls between the events we have found. This difference cannot result from the small difference between their ΔR and ours. Their event is associated with a small peak in ice rafting (but not magnetic susceptibility), and below that there is a much larger undated IRD event coincident with a large peak in magnetic susceptibility.

In addition to the comparisons discussed above, we can also correlate to results from Mackenzie Trough near our JPC-13 (Schell et al. 2008). They also sampled the high δ18ONps (3.11 ±0.28 ‰, n=9) interval ~10-12 ka. Their data fall mostly between 10,930 ± 219 and 10720 ± 50 yrs B.P. when recalibrated.

4.6.4 Supplemental References

Andrews, J. T. and G. Dunhill (2004). “Early to mid-Holocene Atlantic water influx and deglacial meltwater events, Beaufort Sea slope, Arctic Ocean.” Quaternary Res. 61: 14-21.

McNeely, R., Dyke, A.S. and Southon, J.R. (2006). “Canadian marine reservoir ages preliminary data assessment.” Geological Survey of Canada open file 5049: DOI: 10.13140/13142.13141.11461.16649.

Ostlund, H. G. and G. Hut (1984). “Arctic ocean water mass balance from isotope data.” Journal of Geophysical Research 89: 6373-6381.

Polyak, L., Curry, W.B., Darby, D.A., Bischof, J. and Cronin, T.M. (2004). “Contrasting glacial/interglacial regimes in the western Arctic Ocean as exemplified by a sedimentary record from the Mendeleev Ridge.” Palaeogeo., Palaeoclim., Palaeoeco. 203: 73-93.

Polyak, L., Darby, D.A., Bischof, J.F. and Jakobsson, M. (2007). “Stratigraphic contstraints on late Pleistocene glacial erosion and deglaciatiion of the Chukchi margin, Arctic Ocean.” Quat. Res. 67: 234-245.

Poore, R.Z., Osterman, L., Curry, W.B. and Phillips, R.L. (1999). “Late Pleistocene and Holocene meltwater events in the western Arctic Ocean.” Geology 27: 759-762.

5

Geologic and geophysical constraints on deglacial sediment dispersal along the Beaufort Margin, Arctic Ocean

5.1 ABSTRACT

New high-resolution CHIRP seismic reflection, multibeam bathymetry, and sediment core data acquired along the Beaufort Margin in the western Arctic Ocean provides important constraints on the deglacial sediment dispersal patterns for the region. The slope from Barrow Canyon to the Mackenzie Trough is characterized by thick Holocene sediments mostly sourced from Barrow Canyon and continental discharge. This acoustically transparent unit overlies coarse laminated sediments sourced from the Mackenzie and ice rafting. The margin from Mackenzie Trough to the Amundsen Gulf is characterized by many ice rafting and meltwater discharge events. Ice rafted debris layers were deposited around ~14.5 ka and ~13.8 ka and likely document enhanced ice discharge events from the Amundsen and M'Clure ice streams as they retreated. Stratigraphic patterns and XRF data suggest that all three meltwater discharge events were sourced from the Mackenzie region. The oldest discharge event occurred sometime between ~14.5 ka and ~12.9 ka and deposited finely laminated sediments more than 7 m thick sourced from proglacial lakes in the area. Following this was a major freshwater discharge event starting at ~12.8 ka, which generated high amplitude reflectors, deposited coarse debris, and caused a lightening in the $\delta^{18}O$ record. This is possibly a major outburst flood from glacial Lake Agassiz. After this was a third discharge event that occurred was initiated by ~11.1 ka, which deposited coarse laminated sediments focused in the Mackenzie Trough. Glaciogenic features on a bathymetric bench west of the Mackenzie Trough also record ice flow along the margin from east to west.

5.2 INTRODUCTION

Rapid climate change during the Arctic deglaciation is recorded in the offshore sedimentary layers. It is imperative to study sediments from the Arctic as it is presently experiencing rapid warming and sea ice loss (Stroeve et al., 2007; Screen and Simmonds,

2010) and any insight from the past could inform the future. Despite recent geophysical and geological surveys, large gaps in knowledge and spatial coverage remain. For example, sedimentary records from the western Arctic are mostly grouped along ridges in the central basin and in the Chukchi Borderland providing only a partial picture of the region's Quaternary history (e.g., Darby and Bischof, 1996; Polyak et al., 2001, 2007; 2009; Jakobsson et al., 2001, 2008; Backman et al., 2004; Spielhagen et al., 2004; Keigwin et al., 2006; Hill et al., 2007, 2008; Darby et al., 2005; 2009; Barletta et al., 2008; Hill and Driscoll, 2010). To establish further the Wisconsin deglaciation history for the western Arctic, a geologic and chronostratigraphic framework needs to be developed for the Beaufort margin. Here, we report on the first margin-wide geophysical and geological study of the Beaufort slope to understand deglacial processes, meltwater discharge, and sediment dispersal.

The Beaufort Margin (Figs. 1 and 2) is a critical area to study to better understand glacial processes, sediment dynamics, and meltwater discharge as it was the northwestern extent of the Laurentide Ice Sheet (LIS) during the last glacial maximum (LGM; Jakobsson et al., 2014). The margin encompasses the American and Western Canadian Arctic from Barrow, AK to the Amundsen Gulf (Figs. 1 and 2) and is bifurcated by the Mackenzie River Trough. Ice streams developed in both the Mackenzie and the Amundsen Gulf, which delivered ice and sediment to the margin (Blasco et al., 1990; Batchelor et al., 2013a). Since ice stream retreat, the Mackenzie has become the river with the highest water and sediment discharge in the western Arctic (Holmes et al., 2002). Investigation of the stratigraphy and paleoceanography of the Beaufort Margin was conducted by the Healy 13-02 cruise, which collected nearly 5000 km of multibeam bathymetry and seismic reflection data, 12 multicores, 13 gravity cores, and 14 jumbo piston cores (JPCs) along the continental slope. The geophysical data and core data (Fig. 2) were examined to define sedimentation patterns and develop a chronostratigraphic

framework for the Beaufort margin for the Wisconsin deglaciation.

5.3 BACKGROUND

5.3.1 Beaufort margin morphology and surrounding geology

The Beaufort margin extends over 1000 km from Barrow Canyon to the Amundsen Gulf (Figs. 1 and 2) and is separated by the American/Canadian border just west of the Mackenzie River. The margin has a wide shelf ranging between 70 and 120 km on the American side and between 65 and 180 km east of the Mackenzie (Johnson et al., 1990 and references therein). The shelf break occurs in ~100 m water depth (Blasco et al., 1990; Johnson et al., 1990) and gives way to a steep continental slope. The western slope is highly incised by submarine canyons, with sections that are also gullied. There are many large gravity driven slides and slump areas on the slope. Some failures are caused by weakening of sediments along deep listic normal faults (Grantz et al., 1990) and also by destabilization of sediments from gas hydrate disassociation (Kayen and Lee, 1991). Hydrate disassociation was driven by Pleistocene glacial-interglacial cycles, which caused repeated lowering of sea level (Kayen and Lee, 1991). The continental rise is wider in the eastern Beaufort versus the western side because of Mackenzie deposition (Johnson et al., 1990). The Beaufort shelf is cut by two geologically young, large paleo-valleys, the Mackenzie Trough and the Amundsen Gulf (Dixon and Dietrich, 1990). The Mackenzie Trough is 80 km wide, 150 km long (Schell et al., 2008), and ranges from about 100-500 m water depth (Dixon and Dietrich, 1990). The Amundsen Gulf is 200 km wide, 400 km long, and has an average water depth of ~300 m (Stokes et al., 2006).

The modern Mackenzie River has the fourth highest water discharge in the Arctic (behind Lena, Ob, and Yenisei in the eastern Arctic; Holmes et al., 2002; Wagner et al., 2011), but it has the largest sediment flux of any Arctic river (124-128 Mt/yr; Carson et al., 1998; Holmes et al., 2002). Most of the sediment input to the Beaufort Sea is

suspended silt and clay (Soloman et al., 2000) and forms a buoyant plume when entering the Arctic (Hill et al., 1991). A large amount of this sediment is deposited east of the Mackenzie, even reaching the southern Amundsen Gulf (Gamboa et al., 2017). The Mackenzie watershed is 1.78 x 106 km2, draining more than 20% of continental Canada (Holmes et al., 2012). The Mackenzie catchment is made of three main geologic units, North American Cordillera, the Interior Platform, and the Canadian Shield (Millot et al., 2003). The North American Cordillera is a tectonically active region containing the Mackenzie and Rocky Mountain belts, which are composed of a range of sedimentary rocks and some metamorphic rocks from the Proterozoic to the Mesozoic. The western reaches of this region contain some igneous rocks from Mesozoic batholiths, glacial till, and volcanic outcrops. The Interior platform region encompasses the Western plain of Alberta and British Columbia, which are mainly composed of marine-related Cambrian to Cretaceous sedimentary rocks. The Canadian Shield is comprised of Precambrian igneous and metamorphic basement rocks.

The Amundsen Gulf is bordered to the north by Banks and Victoria Islands (Fig. 1), part of the Canadian Arctic Archipelago (CAA). Banks Island is mainly comprised of sandstones and shales, carbonate rocks in the northeastern region, and extensive glacial deposits (Bischof and Darby, 1999; Lakeman and England, 2013). Victoria Island is of similar composition, but with larger regions of carbonates (Young and Long, 1977; Lakeman and England, 2013). Tills from these islands have high amounts of limestone and dolomite clasts, and consequently, many ice-rafted debris (IRD) layers found in the central Arctic have high carbonate content (Bischof et al., 1996). Sediments form the central Amundsen Gulf are composed of a mixture of Mackenzie and Banks Island material (Gamboa et al., 2017).

Barrow Canyon is a 250 km long, ~30 km wide depression that separates the Beaufort Margin from the Chukchi Sea (Fig. 1; Aagaard and Roach, 1990). The canyon

is maintained by the Alaska Coastal Current, which likely plays a role in erosional processes (Eittreim et al., 1982). Sediments recovered from Barrow Canyon are rich in chlorite and muscovite, which authors inferred were sourced from Alaskan rivers, such as the Yukon (mean annual discharge of 203 km3/yr and a sediment flux of 60 Mt/yr; Milliman and Meade, 1983; Holmes et al., 2002), and flowed into the Arctic via the Bering Strait (Ortiz et al., 2009). The Brooks Range (Fig. 1) in northern Alaska is notably less carbonate rich than the CAA. Some IRD layers found on the Chukchi Shelf and Borderland lack substantial carbonate (Polyak et al., 2007; Hill and Driscoll, 2010). Ice discharge from the Brooks Range, flowing across the Chukchi Shelf and funneling down Barrow Canyon could be the source of theses layers (Hill and Driscoll, 2010). The Colville River also drains northern Alaska into the Arctic Ocean. The Colville River has a much smaller sediment load than the Mackenzie and Yukon Rivers at 6 Mt/yr, but it has a higher sediment yield (120 t/km2/yr) than the Yukon (71 t/km2/yr; Milliman and Syvitski, 1992). Smaller Arctic rivers, such as the Colveille, are important contributors to the high amounts of Holocene sediment on the Alaskan shelf (Molnia et al., 1978; Milliman and Syvitski, 1992).

5.3.2 Glacial history

The northwestern Laurentide Ice Sheet reached its maximum extent during the late Wisconsin glaciation (Dyke et al., 2002). During this time, the LIS extended over Banks and Victoria Islands out onto the Beaufort shelf (Fig. 1; England et al., 2009; Lakeman and England, 2013, 2014). Due to the extensive nature of LGM ice, there is not much information on pre-Marine Isotope Stage (MIS) 2 glaciations (Kleman et al., 2010; Jakobsson et al., 2014). During the Late Wisconsin glaciation, the northwestern LIS discharged into the Arctic via three major ice streams: the Mackenzie, Amundsen Gulf, and M'Clure Strait (Figs. 1 and 2; Blasco et al., 1990; Stokes et al., 2005, 2006,

2009; Niessen et al., 2010; Batchelor et al., 2013a, 2013b, 2014; MacLean et al., 2015). Evidence for ice streams in the Amundsen Gulf and M'Clure Strait include mega-scale ridge and groove lineations and drumlin fields (Blasco et al., 2005; Stokes et al., 2006, 2009; MacLean et al., 2012, 2015), as well as prominent trough mouth fans (Stokes et al., 2005; Niessen et al., 2010; Batchelor et al., 2013, 2014). Even though a trough mouth fan did not develop offshore of the Mackenzie, other evidence for the ice stream are observed, such as glacial till sheets and trough-parallel ridges interpreted as lateral moraines (Blasco et al., 1990; Batchelor et al., 2013a, 2013b). Data from the Amundsen Gulf indicate at least 8 ice stream advances (Batchelor et al., 2014), while data from the Mackenzie indicates only 2 (Blasco et al., 1990; Batchelor et al., 2013a, 2013b). This suggests that the Amundsen Gulf ice stream was a more prominent discharge outlet, likely due to its more central location relative to the LIS (Batchelor et al., 2013a).

Evidence that material has been transported from ice streams in the eastern Beaufort to the western side has been observed since the early 20th century. Striated boulders and gravels in the Flaxman Member of the Gubik Formation observed on the Alaskan coastal plain were not sourced from the nearby Brooks Range, but from the Canadian Arctic Archipelago (Fig. 1; Leffingwell, 1919; Dinter et al., 1990). Engels et al. (2008) imaged glacial lineations on the western Beaufort outershelf in 400-700 m water depth. These were interpreted to be formed by a large floating ice mass sourced in the CAA. Glacial features of similar orientation have been found on the Chukchi Borderland (Polyak et al., 2001; Jakobsson et al., 2005), suggesting a similar CAA source. IRD layers in a core from the Chukchi margin (Hly0501-6JPC; Polyak et al., 2007, 2009) had high carbonate content primarily made up of dolomite, which is typical in the Canadian Arctic. IRD has also been found in cores from the eastern Beaufort slope and the outer Amundsen Gulf (PC124 and PC 750; Scott et al., 2009). Paleomagnetic properties for the IRD layers in the two cores indicate a similar source, which the authors infer is the

Amundsen Gulf ice stream. The timing of the layers, however, is very different between the cores, which could indicate multiple sources. The present study adds to evidence of along margin transport from the eastern Beaufort ice streams in the form of IRD deposits, glaciogenic bedforms, and sediment grain size.

5.4 METHODS

In 2013, a cruise was conducted along the Beaufort Margin on the USCGC Healy (designated Healy 13-02; Fig. 2). The cruise focused on the continental slope from Barrow, AK to the Amundsen Gulf and back. Towed CHIRP seismic reflection data, hull-mounted knudsen CHIRP seismic reflection data, and multibeam bathymetry were collected. Coring targets were based on the geophysical data. The towed CHIRP seismic profiles were acquired by Scripps Institution of Oceanography's EdgeTech X-Star CHIRP subbottom reflection sonar using a 1-6 kHz swept frequency acoustic source with a 50 ms sweep, which allowed for seafloor penetration up to 50 meters. The hull-mounted knudsen seismic profiles were collected using a Knudsen 320 B/R subbottom profiler. All seismic data were recorded in SEG-Y format with real-time GPS navigation recorded for each shot for location accuracy. The data were processed using SIOSEIS (Henkart, 2006) and plotted using seismic unix (Cohen and Stockwell, 1999) and then imported into the Kingdom software package (kingdom.ihs.com) for interpretation. A nominal value of 1500 m/s was applied to convert two-way travel time to depth; both are shown on seismic profiles. Hull-mounted knudsen data from many other cruises was used to supplement the data collected by Healy 13-02. These include Healy 08-06, Healy 09-05, Healy 10-02, Healy 11-02, and Healy 11-03 (NGDC). Towed CHIRP data was used from Healy 02-05 and parasound topaz data was used from Sikuliaq 2015-11S (Amy Waterhouse, personal communication).

12 multicores, 13 gravity cores, and 14 jumbo piston cores were collected during

Healy 13-02. For this paper, only the jumbo piston cores (JPCs) were examined. Two coincident JPCs (15 and 16) from the cruise Healy 02-05 were also used in this study. A list of the cores, and associated depths and lengths are in Table 1. Geotek Multi-Sensor Core Logger data were acquired for the JPCs onboard the Healy, which measured a suite of properties including magnetic susceptibility, P-wave velocity, and gamma ray attenuation. After the cruise, high-resolution grain size analysis was performed on many of the JPCs. For this, a small aliquot was taken every other centimeter throughout the length of core. Each sample was run on a Beckman Coulter LS 13 320 laser diffraction particle size analyzer, which outputs a grain size distribution for each sample and is plotted downcore.

Radiocarbon dates used in this paper are from Keigwin et al. (Chapter 4), where methods and reasons for calibration are described. X-radiograph (XRF) data from JPCs 15/27 are also from Keigwin et al. (Chapter 4). XRF data from JPC 25 and JPC 36 were acquired by the team at the National Marine Geoscience Collection, Geological Survey of Canada, Atlantic.

5.5 RESULTS

The results will be presented from west to east, with focus on locations where grain size analysis was performed. Grain size profiles are shown from 0 to 200 μm range because overall, the cores were extremely fine and we are interested in the fine scale variability. Layers with components coarser than 200 μm are reflected in the fine scale data.

5.5.1 Barrow Canyon Region

JPC 02 was collected just west of Barrow Canyon at a depth of 401 m (Fig. 2). Based on correlation with the trigger core and a gravity core from the same location, JPC

02 appears to have over penetrated by ~0.3 m. The magnetic susceptibility from the core (Fig. 2) has little variation with a slight negative trend for this first ~7 m, corresponding to an acoustically transparent unit. This unit is over 10 m thick in the down slope area and is interpreted as Holocene sedimentation (Fig. 3). There is one notable susceptibility peak at about ~9.5 m in the core associated with a thin high amplitude deposit (Fig. 3). This peak is dated at ~15.8 ka (Keigwin et al., Chapter 4; Fig. 2). The acoustic character and high magnetic susceptibility of this material suggests it is a coarse grained lag deposit filling in a low on the underlying erosive surface. This material was likely sourced from gravity flows funneled down Barrow Canyon.

Jumbo Piston Cores 15 and 16 from cruise Hly 02-05 were collected east of the Barrow Canyon (Fig 2). JPC 16 is over 20 m in length and composed almost entirely of Holocene material (Keigwin et al., 2006). Magnetic susceptibility from JPC 16 (Fig. 2) is fairly uniform throughout the Holocene, with a few lows. There is a large peak at the base of the core after it transitions to deglacial material. Grain size analysis was run on JPC 15 as JPC 16 had previously been sampled extensively. Grain size for Healy 02-05 JPC 15 (Fig. 4) is overall quite fine with the mean grain size generally between 10 and 30 μm. The coarser component, as evidenced by the green bands, appears to form a saw tooth pattern. The top of the core has a relatively higher coarse component that diminishes below 2.5 m before showing steady increases downcore. These coarse layers are in all likelihood event beds associated with across margin gravity flows funneling down Barrow Canyon. The magnetic susceptibility from JPCs 15 and 16 (Figs. 2 and 4) shows a steady increase with a fair amount of fluctuations throughout. This could indicate an increase in sediment input from Barrow Canyon and the Brooks Range during the Holocene. A series of high amplitude reflectors is imaged in the seismic data (Fig. 4) and could explain the cyclic nature of the coarse component in the grain size data. The outer shelf and slope area around Healy 02-05 JPCs 15 and 16 are incised by canyons, so most

of the seismic data does not image reflectors except for the pocket of laminated sediment that was cored.

5.5.2 Western Alaska Slope

JPC 41 was collected along the Western Beaufort Slope, a third of the way from Barrow Canyon towards the Mackenzie River at a water depth of 1439 m (Fig. 2). The sediments for the upper 6 m are fine grained with little variability (Fig. 5). This correlates with an acoustically transparent section ~6 m thick (Fig. 5); the acoustically transparent unit is interpreted to be Holocene deposition. Below this, there is an increase in the coarse component of the grain size data with various sand stringers (e.g., 840 cm and 1236 cm). This section in the seismic data exhibits more high amplitude reflectors, in response to the greater variability in grain size, and thus impedance (Fig. 5). These layers are likely a combination of material sourced from Barrow Canyon in the west and from the Mackenzie River in the east. The magnetic susceptibility data correlates well with the grain size and seismic acoustic character (Fig. 5).

5.5.3 Central Alaskan Region

JPC 06 was acquired approximately halfway between Barrow and the Mackenzie River at a water depth of 373.3 m (Fig. 2). Based on correlation with the trigger core and a gravity core from the same location, JPC 06 over penetrated by approximately 0.35 m. There is not much variation in the magnetic susceptibility from this core except a peak at ~10.5 m (Fig. 2). The downcore increase in magnetic susceptibility observed in JPC15 and 16 is not observed in JPC06. Sediments just below this peak are dated at ~12.8 ka (Keigwin et al., Chapter 4; Fig. 2). Seismic data from this area (Fig. 6) images a surficial acoustically transparent Holocene layer over 10 m thick. Beneath this is a series of higher amplitude reflectors (Fig. 6), with the onset of the layers corresponding to the

susceptibility peak at approximately 11 m (Fig. 2). The high amplitude acoustic character of the layered sediments indicates coarse grain sediment, which is consistent with being more proximal to the Mackenzie Trough.

5.5.4 Western Mackenzie Margin

JPCs 09 and 37 are spatially coincident cores acquired just west of the Mackenzie Trough at a water depth of 394.5 m (Fig. 2). Based on matching magnetic susceptibilities between the two JPCs, trigger cores, and a gravity core, JPC 37 over penetrated by more than 2 m. This allowed us to examine sediments over 16 m below the seafloor. There is almost no variability in magnetic susceptibility for the top 9 m of JPC 9 (Fig. 2). The same is true for the upper 7 m of JPC 37 (Fig. 7). There is a surficial acoustically transparent package that is ~6 m thick (Fig. 7), which is interpreted to be the homogenous Holocene deposition. The uniform magnetic susceptibilities extend below this unit into a series of laminated reflectors that exhibit a variety of acoustic amplitudes. The upper few meters of these reflectors do not appear to have much affect on grain size either (Fig. 7). The upper 7 m of JPC 37 are fairly fine, but with a small coarse component recorded by the green bands. Below this, the grain size is much less uniform, with larger variations in the amount of coarse versus fine sediment (Fig. 7). Note the peak in magnetic susceptibility correlates with a high amplitude reflector in the seismic profile, and appears to correlate with an increase in grain size below ~900 cm. A distinct coarse layer at ~1150 cm appears to correlate with a high amplitude reflector in the seismic data (Fig. 7), but does not have a corresponding signal in the magnetic susceptibility. These coarse layers may record a combination of ice-rafted debris from the retreating ice stream in the Amundsen Gulf and discharge down the Mackenzie River.

Glacial lineations are imaged in the multibeam data along the outer shelf/upper slope in the vicinity of JPCs 09 and 37 west of the Mackenzie trough (Fig. 2). They are

observed in water depths less than 400 m (Fig. 8). The lineations range from straight to curvilinear to wavy, and have lengths up to 5 km (Fig. 8). Despite curving pathways on- and offshore, the overall trend of the lineations is east-west along the margin.

In the northwest region, two mounds are observed extending across the upper slope (Figs. 8 and 9). These mound-like structures are acoustically transparent draped by acoustically laminated sediments (Fig. 9). The more seaward extent of these features overlies a series of flat reflectors that continue away from the features. The features are ~8 km across and cause a broad shallowing of the seafloor (Fig. 8). These features are much thinner in the landward seismic profile appearing less mound-like.

Just west of JPCs 09 and 37, in over 360 m of water, is a large circular mound with a collapsed central crater on the seafloor (Figs. 8 and 10). This pockmark is over 500 m across and the crater is over 200 m. The ship did not pass directly over the pockmark (Fig 10. upper left), but gas charged sediments are imaged in the seismic data at the closest approach to the pockmark. There are no other similar features imaged in the area. This could either because they do not exist, or that they are directly west or more inshore, areas we did not survey.

5.5.5 Mackenzie River Trough

JPCs 13 and 36 are coincident cores collected in the Mackenzie River trough at a water depth of 686 m. Based on magnetic susceptibility, JPC 36 is offset from JPC 13 by less than 0.5 m. There is only some minor variability in the magnetic susceptibility data for the top 5-6 m, which is consistent with the fine grain size for the upper part, ~600 cm of JPC 36 (Figs. 2 and 11). The upper acoustically transparent section with only faint reflectors is interpreted to be homogenous Holocene sedimentation that mantles the higher acoustic reflectors beneath. There are two broad peaks in the susceptibility and grain size, which appear to correlate with high amplitude reflectors in the seismic

reflection data. They are offset by about a meter or less (Fig. 11). In these coarsely laminated sediments are many sand stringers (e.g., 1034 cm), some of which are up to 2 cm thick (Fig. 11). These coarse sand layers are interpreted to be interglacial gravity deposits funneled down the Mackenzie Trough. This section is acoustically laminated with marked variation in acoustic amplitudes (Figs. 11 and 12). Below the extent of the core in the seismic data is another high amplitude reflector. This overlies a unit that is faintly laminated and over 5 m thick. X-rays of the layered deposits reveal homogenous material in the upper part of the core and occasional IRD within the lower, coarsely laminated sediments (Fig. 11). The upper-middle section of layered deposits is comprised of more high amplitude reflectors than the lower section (Figs. 11 and 12). XRF data from the core shows a distinct change at approximately 5 m (Figs.11, S1, and S2). The Holocene section (grey in Fig. 11) shows a gradual increase in the Ca/Ti ratio from the top of the core to ~5 m down (Fig. 11). K, Ca, Ti, Fe, Sr, Rb, and Zr also show a similar increase with depth to ~ 5m, while Mn shows a gradual decrease (Figs. S1 and S2). This indicates a slow transition in source material over time. The Ca/Ti XRF data for the coarse layered unit (blue in Fig. 11) is highly variable as a result of the Ca data (Fig. S1). A peak in Ca/Ti between 10 and 12 m in the core correlates with a zone of increased IRD (Fig. 11). The other element counts also exhibit large fluctuations in this unit (Figs. S1 and S2); however, the amplitudes are less than the Ca/Ti ratio.

5.5.6 Eastern Mackenzie Margin

Moving east, the width of the continental shelf increases (Figs. 1 and 2). JPCs 15 and 27 are located halfway between the Mackenzie River and the Amundsen Gulf (Fig. 2). JPCs 15 and 27 were acquired on the middle slope at water depths of 687 and 693 m, respectively. Based on their magnetic susceptibility, the cores were spliced together to yield a composite section 1730 cm in length (Figs. 2, 13, and 15). The magnetic

susceptibility data from the cores (Figs. 2 and 13) is relatively uniform with two sets of peaks, a series from ~3-5 m and an isolated peak at ~12 m. These susceptibility peaks correlate with coarser grain size and high amplitude reflectors in the seismic data (Fig. 13). These layers appear to correlate with increased IRD. Between the IRD layers is a unit more than 7 m thick that is very fine, with an average grain size of 5 μm. This section has faint sediment laminations in the core and is associated with low amplitude reflectors in the seismic data (Figs. 13 and 14). The acoustic reflectivity of this unit increases slightly below ~9 m in the core. Below the deeper IRD layer are many reflectors of differing amplitude and not all are flat lying. The reflector pattern imaged in the top 14 m here is imaged in seismic profiles throughout the area (Fig. 14) showing the extent of these acoustic packages.

Radiocarbon dates from these cores (Keigwin et al., Chapter 4; Figs. 2 and 15) provide an interpolated age of 14.5 ± 0.23 ka for the deposition of the basal IRD layer and 12.85 ± 0.10 ka for the onset of the upper IRD layer. The thick, faintly laminated unit was deposited between these dates. Sedimentation rates for this interval are anomalously high for the continental slope. Two 14C dates a meter and a half apart in this layer came back the same age. A minimum sedimentation rate for this interval of 1300 cm/ky is based on the maximum error ranges for the calibrated ages (Fig. 15). Rates earlier in this unit are 1000 cm/ky and 500 cm/ky. Prior to this, rates were ~133 cm/ky and after this layered unit, sedimentation rates were ~120 cm/ky or less. Both of the IRD layers are associated with a lowering in the $\delta^{18}O$ signal by ~1‰ (Fig. 15), indicating freshwater input.

XRF data from the combined JPCs 15/27 reflect four different sections, one from the top of the core to ~350 (Holocene unit), one from ~350-550 cm (upper IRD unit), one from ~550-1300 cm (fine-scale layered unit), and from ~1300 cm to the bottom of the composite cores (lower IRD unit; Figs. 13, S3, and S4). These sections are based on the

Ca/Ti plot (Fig. 13). Some sections of the XRF data were removed due to large carbonate rocks that caused a diminishing of the rest of the signals. A gradual lowering is recorded in Mn counts from the top of the core through the Holocene section (Fig. S3). There is a gradual increase during this interval for K, Ca, Ti, and Sr (Figs. S3 and S4). Within the upper IRD unit is a marked increase in Ca/Ti, Ca, and Sr. The XRF data for the fine-scale layered unit is fairly stable with only a few small inflections (Fig. 13). The lower IRD unit is associated with a large spike in the Ca/Ti XRF (Fig. 13). The rest of the section is also spiky, but to a lesser degree. The IRD event around 1300-1350 cm is also associated with lows in Fe, Rb, Sr, K, and Ti, and highs in Zr, Si, Ca, and Mn (Figs. S3 and S4). Note the major differences in elemental counts between the lower and upper IRD layers.

5.5.7 Western Amundsen Gulf Margin

JPC 25 was collected on the slope east of JPCs 15 and 27, towards the Amundsen Gulf, at a water depth of 746 m (Fig. 2). Magnetic susceptibility and acoustic character in the seismic data observed at JPC 25 are remarkably similar to that of JPCs 15 and 27. Spikes in grain size correlate with peaks in magnetic susceptibility and with high amplitude reflectors in the seismic data (Fig. 16). Based on correlation to the trigger core from JPC 25 and a gravity core collected in the same location, JPC 25 over penetrated by 1.3 m. Grain size data from the core shows that overall, the sediment is extremely fine, with grain size typically averaging around 5 μm (Fig. 16). The upper seismic unit here is acoustically transparent and less than 5 m thick, which is interpreted to be the homogenous Holocene package. There are several coarse spikes (e.g., 182, 470, 544, and 1282 cm) that break up the fineness of the core and correlate with IRD layers imaged in the X-ray data. Average grain size for some of these spikes is over 45 μm. These coarse layers are associated with high amplitude reflectors in the seismic data (Fig. 16). There is about 2 m of fine material of low magnetic susceptibility, with faint internal laminations

separating the upper and middle IRD layers ranging at ~1.5 and ~4 m in the core. The middle and lower IRD layers are separated by a ~6 m unit of low susceptibility, fine grain size, and faint internal laminations and reflectors. This has the same characteristics as the rapidly emplaced deposit observed at JPCs 15/27, which suggests this deposit has a large lateral extent along the Beaufort Margin.

X-rays from JPC 25 (Fig. 16) show the variation in sediment reflected by the grain size data, magnetic susceptibility, and seismic data. An X-ray from the shallowest IRD layer around 182 cm in the core, images a massive coarse grained layer. X-ray data from the fine grained unit images fine-scale laminations with a lack of any large IRD. The appearance of these laminations in the X-rays are much more faint than those imaged in JPC 36 (Fig. 11). An X-ray from the basal IRD layer at ~1282 cm in the core images fine-scale laminations with interspersed coarse IRD material.

XRF data from JPC 25 reflects five different sections, one from the top of the core to ~150 cm (Holocene unit), one from ~150-250 cm (upper IRD unit), one from ~250-1225 cm (fine-scale layered unit), which is separated by a middle IRD unit from ~400-600 cm, and from ~1225 cm to the bottom of the core (lower IRD unit). These sections are defined by the Ca/Ti plot (Fig. 16). There is a gradual increase from the top of the core to ~1.5 m in counts of K, Ca, Ti, Rb, Sr, and Zr (Figs. S5 and S6). This interval is associated with a decrease in Mn (Fig. S5). This could indicate a slow transition in source material during the Holocene. There is high variability in Ca/Ti for the upper IRD unit (Fig. 16). There are small increases in Rb and Sr, and larger increases in Ca and Mn within this unit at ~ 2 m in the core. Increases in Ca, Mn, and Zr, as well as a slight low in Rb occur for the middle IRD layer from 4-6 m depth (Figs. S5 and S6). The fine-scale layered unit has a very low Ca/Ti ratio, with some low amplitude spikes (Fig. 16). There is high variability in the Ca/Ti XRF for the basal IRD layer imaged in X-ray data (Fig. 16). This event coincides with spikes in Ca, Mn, and Zr, and lows in K, Ti, Fe, Rb, and Sr

(Figs. S5 and S6).

5.5.8 Amundsen Gulf

The Amundsen Gulf was the eastern extent of the Healy 13-02 survey (Fig. 2). JPC 19 was acquired in the Amundsen Gulf, south of Banks Island at a water depth of 442 m (Fig. 2). Based on correlation with the trigger core and a gravity core, JPC 19 over penetrated by 2 m. The magnetic susceptibility (Figs. 2 and 17) has a set of major peaks down to about 4 m, with a marked low at ~1 m. The first peak correlates with a high amplitude reflector, but the peak from ~2-4 m correlates with acoustically transparent sediment (Fig. 17). This is in contrast to the signals observed throughout much of the Beaufort Margin (Figs. 5, 11, 13, and 16). From ~4-10 m, the susceptibility is fairly uniform with only minor variations. Below ~10 m, the susceptibility varies greatly with a peak at approximately 11.25 m in the core. The grain size data is highly variable throughout the core (Fig. 17). The upper 4 m, where magnetic susceptibility is high, is composed of fine sediment with a small coarse grained layers up to ~40 μm. From ~4-10 m there is a coarse component that is episodic throughout the interval associated with laminated reflectors of varying amplitude (Fig. 17). In the upper two meters, many of these layers are coarse sand stringers. In the bottom few meters of the core, there is a ~50 cm broad spike in grain size and a small isolated one, likely another sand stringer. Seismic data from this area images many glacial related features (Fig. 18). There are glacially carved lows that have been filled in with acoustically transparent sediment. This is covered by a series of high amplitude reflectors that mimic the shape of underlying topography. There is a drumlinoid field that reflects a west-flowing direction from the Amundsen Gulf ice stream (Fig. 18). MacLean et al. (2015) previously mapped much of this area and attributed the drumlinoid field to fast flowing ice.

5.6 DISCUSSION

Sedimentation patterns along the Beaufort margin record the paleoceanographic history and depositional mechanisms of the margin. Clear signals in the magnetic susceptibility, seismic acoustic character, and grain size data are observed to the west versus east of the Mackenzie River. Here we discuss the different processes impacting margin sedimentation and how they vary spatially and temporally, with the aim to reconstruct the deglacial history of sediment dispersal for the Arctic region.

5.6.1 Western Margin

The continental slope between Barrow Canyon and the Mackenzie River is characterized by an acoustically transparent lens of Holocene sedimentation with uniform magnetic susceptibility (Figs. 2-7). Near Barrow Canyon, the acoustically transparent unit is over 10 m thick (Fig. 3), and systematically thins toward the east (Fig. 2). This sediment is mostly fine grained with an increase in coarse grained layers near Barrow Canyon as observed in Healy 02-05 JPC 15/16 (Figs. 2 and 4). The coarse grained layers are sometimes more than 50 cm thick and are cyclic in nature, which is consistent with gravity flows funneled down the canyon system. The change in thickness of the Holocene unit along the margin indicates that Barrow Canyon and discharge from the continent are significant sources of sediment during this time period. High sediment yields have been documented for small mountainous rivers in this region during modern times (Milliman and Syvitski, 1992). The thick Holocene deposits could indicate an increase in sediment discharge from these rivers as the Brooks Range (Fig. 1) was becoming less glaciated during Holocene warming.

The Holocene unit overlies layered sediments of varying amplitudes and thicknesses and correlates with a marked increase in the grain size, magnetic susceptibility, and acoustic reflectivity in the seismic data (Figs. 5-7, 9, 10). Radiocarbon

dating of the cores indicates that this change is associated with deglaciation along the Beaufort margin (Fig. 2). Within the laminated deposits, there are numerous coarse grained sand stringers with IRD. The sandy layers with IRD are best observed in the coarse layered unit at JPC36 in the Mackenzie Trough (Figs. 11 and 12). The coarse layered deposit is also observed by Schell et al. (2008) in their piston core (PC1) that was collected in the same location as JPCs 13 and 36. Radiocarbon dates for the coarse grained layered unit in PC1 yield 14C ages of ~9.8 ka and ~10.0 ka indicating that the layer was rapidly emplaced (1417 cm/ky; Schell et al., 2008). Using our age model (Keigwin et al., Chapter 4), these correspond to calendar ages of ~10.7 ka and ~10.9 ka, respectively. The authors infer that the discharge occurred under significant sea ice, generating the laminations. Schell et al. (2008) suggested the coarse grained sediments came from a hypothesized meltwater discharge event on the Russian shelf. Their basis for this was higher $\delta^{18}O$ values (~2.7-3.5‰) within the coarse laminated sediments compared to cores from farther west, closer to the Siberian shelf (Fig. 1). Core P45 from Andrews and Dunhill (2004) was acquired near JPCs 9/37 (Fig. 2) and exhibits a $\delta^{18}O$ low (~2.5 ‰) in laminated sediments dated slightly younger than the laminated deposits in PC1. The dates are within statistical error, and thus Schell et al. (2008) concluded they were the same event. Schell et al. (2008) also argues that cores from the Mendeleyev Ridge (Fig. 1) with a very light to slightly negative $\delta^{18}O$ are consistent with a Russian melt water source (Poore et al., 1999; Polyak et al., 2004). In summary, they infer that the increase in $\delta^{18}O$ from west to east indicates a meltwater event from Russia that transported sediments to the east along the Beaufort Margin to the Mackenzie Trough region.

In light of the new data acquired during Healy 13-02, we interpret the change from acoustically transparent to laminated sediments along the western Beaufort Margin as a change in source material and reworking of sediment transported offshelf by gravity flows, in addition to ice rafting during deglaciation. This change is also observed

in the magnetic susceptibility, XRF, and grain size data (Figs. 2, 4, 5, 7, 11). The acoustic amplitude of these layers and their occurrence increases toward the Mackenzie Trough, suggesting much of the sediment during the deglaciation was sourced from the Mackenzie River (Figs. 5-7, 9, 11, 12). The data imply that the observed variations in the coarse laminated unit reflect changes in more local conditions and not regional emplacement from the Siberian shelf. The rapid sedimentation rate for the coarse grained unit in the Mackenzie Trough (Schell et al., 2008), however, does record a large depositional event. Murton et al. (2010) documented major erosive surfaces and gravel deposits onshore that they attributed to two flood events that flowed down the Mackenzie drainage. The younger event is dated between ~11.7 and ~9.3 ka. This age estimate coincides with the timing of the coarse layered unit offshore, suggesting a discharge event from the Mackenzie. The extremely light $\delta^{18}O$ data from the more western sites could be recording a concomitant flood/discharge event from the Siberian continent.

The source of the observed IRD within the laminated unit appears to be from the Amundsen Gulf and possibly the M'Clure Strait ice streams. Engels et al. (2008) imaged iceberg scours and glacial lineations along the shelf and upper slope in this region and concluded they were from a large ice mass, possibly an ice shelf, and icebergs flowing from east to west. Hly13-02 multibeam swath bathymetry images glacial lineations (Fig. 8) with a similar character to those described by Engels et al. (2008). Based on the observations in the swath bathymetry data, Engels et al. (2008) concluded that the ice was sourced from the M'Clure Strait or Amundsen Gulf, and possibly the Mackenzie Trough because of the similar orientation of glacial features observed in the Chukchi Borderland (Fig.1; Polyak et al., 2001, 2007; Darby et al., 2005; Jakobsson et al., 2005).

The localized mounds (Fig. 9) are located on a bathymetric bench with an average slope between 1° and 6°, from 400 to 550 m water depth (Engels et al., 2008; Fig. 8). These mound features extend across the bench with the thicker accumulations farther

offshore giving the appearance of drumlins. This is in contrast with the inferred general along shelf flow of ice in this region (Fig. 8). If these mounds are in fact drumlins, the ice that formed them did not come from the continent because their tails are more shoreward than the thicker heads (Fig. 9). Rather, ice moved from the Beaufort Sea onshore and interacted with the seafloor at the bathymetric bench to form the drumlin-like features. Jakobsson et al. (2010) compiled evidence supporting an Arctic-wide ice shelf during MIS 6, but this ice shelf is hypothesized to have flowed away from the Beaufort margin and towards the Fram Strait.

Alternatively, the mound features may not be drumlins and could be part of glacial moraines. These features are much larger than other drumlins, which are typically less than 1000 m in length and 300 m in width (Clarke et al., 2009), and are extremely isolated compared to other drumlins fields found in the Arctic (MacLean et al., 2015). Engels et al. (2008) inferred that the large floating ice mass that created glacial bedforms in this area actually carved the bathymetric bench out of the preexisting slope. During or after this erosion, the large ice mass, or broken off sections of ice, could have piled up sediment into moraines. The formation of the bathymetric bench is hypothesized to have occurred between MIS 4 and MIS5d based on correlation to glacial features in the Chukchi Borderland (Engels et al., 2008). The shoreward extent of the mound features overlies a planar surface (Fig. 9). Reflectors are not well imaged below this surface, so it is difficult to determine if it is an erosive surface or not. However, the features were likely emplaced after the bathymetric shelf was created. The more seaward, larger side of the features overly some laminated sediments (Fig. 9). Age constraints in the area are sparse with only a date from nearby JPC 09, which is ~12.7 ka at ~13 m depth in the core (Fig. 2). Seismic reflector correlations reveal that the dated surface is ~5 m above these features in the acoustically laminated unit (star - Fig. 9). It is possible that the features were deposited after formation of the bathymetric bench during a later glacial period,

allowing for the deposition of the layered deposits below the seaward mounds. As ice pushed the mounds into place, laminated sediments beneath the shoreward extent of the mounds could have been eroded.

The singular gas pockmark is also located on the bathymetric bench, but on the far eastern side (Fig. 8). This feature falls into the "normal" pockmark category due to its large size and circular nature (Fig. 10; Hovland et al., 2002). This pockmark has a well-developed rim, which is quite rare because pockmark rims are typically eroded away quickly due to their fine sediment composition (Hovland et al., 2002). The presence of a rim could indicate that it is a relatively young feature. Pockmarks occur where there is focused fluid flow though fine grained sediments, which is often the case on the outer shelf/upper slope of continental margins (Hovland et al., 2002). On the upper slope, a common source of fluid is disassociation of gas hydrates (Giustiniani et al., 2013). In the Arctic, there is an extensive area of gas hydrate on the slope, which can migrate out of the hydrate stability zone due to changes in temperature and pressure (Kayen and Lee, 1991; Ruppel, 2011; Giustiniani et al., 2013; Phrampus et al., 2014). More studies are needed to investigate the recency of the isolated pockmark's formation. Continued research on gas pockmarks is warranted given methane is 84 times more effective than CO2 as a greenhouse gas in the first two decades after emission (www.EPA.gov) and the pockmark rim indicates that it is a young feature. Based on hydrate disassociation conditions, we would expect to see additional pockmarks in the area. The lack of other pockmarks could be due to the location of this feature on the edge of the bathymetric bench, which is flatter than the nearby slope and deeper than the shelf. We also may have not imaged other pockmarks due to the density of our survey.

5.6.2 Eastern Margin and Amundsen Gulf

The slope east of the Mackenzie Trough is dominated by sediments sourced from

the Mackenzie River for the past ~14.4 ky, which is reflected in the remarkably similar signals from JPCs 15/27 and JPC 25 (Figs. 13, 14, and 16). The tops of these cores are very fine grained and homogenous. This Holocene material has low sedimentation rates (Fig. 15), under 200 cm/ky, typical of Arctic slope sedimentation (Jakobsson et al., 2014). The upper IRD layer in JPCs 15/27 appears to have been deposited during the Younger Dryas cold period (Figs. 13, 15, and 16). The sudden influx of coarse material with fairly stable Fe, K, and Ti signals (Figs. S3-S6), elements typical of Mackenzie discharge (Gamboa et al., 2017), suggests these sediments are also sourced from the Mackenzie. Increases in Ca and Sr during this interval could reflect a shift in source for this event as the signals are only partially different compared to prior Mackenzie discharge (Figs. 13, 15, S3-S6). There is a lightening of the $\delta^{18}O$ signal by approximately 1‰ (Fig. 15; Keigwin et al., Chapter 4) in the upper IRD layer. Scott et al. (2009) also record IRD layers with a lightening in the $\delta^{18}O$ signal by about 1‰ in a core from the eastern Beaufort slope (PC750) located between JPCs 15/27 and JPC 25 (Fig. 2). The magnetic susceptibility data for PC750 also exhibits a similar signal to JPC 25, with two peaks separated by approximately 2 m of low susceptibility sediment. Scott et al. (2009) dated their upper IRD layer to end at ~10.8 14C ka, which calibrates to ~12.1 ka using our age model (Keigwin et al., Chapter 4). XRF data for this upper IRD layer in JPC 25 is consistent with that of JPCs 15/27 (Figs. 13, 15, 16, S3-S6). High acoustic amplitude and high magnetic susceptibility layers occur to at least ~11.1 ka in JPCs 15/27. This younger material was deposited after the light $\delta^{18}O$ event and could be recording a second discharge event. This timing is consistent with the rapid deposition of coarse grained layers in the Mackenzie Trough (Fig. 11) and could record the same event.

Andrews and Dunhill (2004) infer that the light $\delta^{18}O$ recorded in their core P45 from west of the Mackenzie indicated a meltwater flood. They suggest that it was waters draining from glacial Lake Agassiz down the Mackenzie River. An Agassiz flood into

the Arctic around this time has previously been suggested by other studies (Tarasov and Peltier, 2005; Murton et al., 2010; Condron and Windsor, 2012). The older discharge event recorded by Murton et al. (2010) is dated between ~13 and 11.7 ka. Based on our $\delta^{18}O$ data, grain size, XRF, and stratigraphic correlations, we infer that there was a meltwater discharge event down the Mackenzie at the onset of the Younger Dryas, which possibly was associated with meltwater from glacial Lake Agassiz. The sedimentary unit associated with this event is only ~2 m thick, but it is quite coarse. It is possible that a larger volume of fine sediment from this event was deposited farther offshore. The younger coarse layers imaged at JPCs 15/27 appear to correlate with the younger erosive flood that ranged from ~11.7 and ~9.3 ka (Murton et al. 2010), which has its depocenter in the Mackenzie Trough.

XRF, magnetic susceptibility, and grain size data from the faintly laminated sediment unit at JPCs 15/27 and 25 (Figs. 13 and 16, S3-S6) is extremely uniform. Sedimentation rates for this unit exceeded 1300 cm/ky, which is very high for the Arctic slope (Jakobsson et al., 2014). Two samples 2.5 m apart were both dated at 13.6 kya indicating the rapid emplacement of the younger part of this unit, which has less acoustic reflectivity than the older part of the unit. Deposition of the faintly laminated sediments was initiated by ~14.4 and ended prior to ~12.8 ka (Fig. 15). The unit is split in two sections at JPC 25 by an IRD layer, dated in PC750 as ending at ~12.45 14C ka (Scott et al., 2009). This yields a calendar age of ~13.8 ka using our age model (Keigwin et al., Chapter 4).

Given the distribution of the faintly laminated deposit along the margin (Fig. 2) and its thickness variations, it is likely sourced from glacial lakes that were more proximal to the Mackenzie River mouth than glacial Lake Agassiz (e.g., Lake Hughes; Lemmen et al., 1994). It is possible that there was seasonal drainage for a few hundred years, causing the very faint layers observed in the x-rays; however, there could have just

been drainage of multiple lakes through time. The middle IRD unit observed in JPC 25 was probably sourced from the Amundsen ice stream, as it is not observed in JPCs 15/27.

The change in Ca/Ti in XRF for the lower IRD layer in JPCs 15/27 and 25, in addition to lows in Fe, K, and Ti suggest an Amundsen Gulf/Banks Island source material (Gamboa et al., 2017). This is similar to the XRF data for the middle IRD layer at JPC 25 (Figs. 16, S5, and S6). The IRD layers also have a lightening in the $\delta^{18}O$ signal by approximately 1‰ (Fig. 15; Scott et al., 2009; Keigwin et al., Chapter 4). These events are likely from enhanced ice rafting as the Amundsen Gulf ice stream retreated, which was well underway by ~13 ka (Lakeman and England, 2012; MacLean et al., 2015). IRD events during several Quaternary glaciations are recorded in multiple other cores from the Arctic that indicate a Canadian Arctic Archipelago source (Darby et al., 2002; Polyak et al., 2001, 2002; Stokes et al., 2005; Stein et al., 2010). This demonstrates the pervasiveness of these ice streams as outlets for the LIS during glacial periods.

The Amundsen Gulf (Figs. 1 and 2) has been glacially shaped by the Amundsen ice stream. There have been many ice advances and retreats during the Quaternary as evidenced by layers of ice-contact sediments and interpreted drumlinoid fields (Fig. 18; Batchelor et al., 2014; MacLean et al., 2015). Thick glaciomarine sediments overlie the ice-contact sediments and the drumlinoid field (Fig. 18). The LGM retreat of the ice stream allowed for deposition of interbedded silts and sands (Fig. 17). A ~2 m thick unit that overlies these glaciomarine sediments is extremely fine, acoustically transparent, and has a substantially higher magnetic susceptibility than the sediments below, suggesting a different sediment source. This unit also thickens to the southwest (Fig. 18). Batchelor et al. (2014) mapped till sheets in the Amundsen Gulf and discovered that the youngest sheet was from the Anderson River, a river that enters the Beaufort margin just southwest of the Amundsen Gulf. A possible ephemeral ice stream developed in the Anderson River in response to changing ice dynamics (Batchelor et al., 2014). This ice stream likely

deposited the fine-grained unit with the high magnetic susceptibility. There is another layer with high magnetic susceptibility in the first few meters below the seafloor, but it has a high acoustic amplitude (Fig. 18). This layer also could possibly be from the Anderson River.

For both the hypothesized Agassiz flood and the ice rafting from the Amundsen Gulf, peaks in magnetic susceptibility are associated with an increase in grain size and high amplitude acoustic reflectors; as observed in JPCs 15/27 and JPC 25. This correlation has been noted before in regards to catastrophic meltwater discharge. Zuffa et al. (2000) observed these characteristics in turbidite deposits in the Escanaba Trough, far offshore the Columbia River. These deposits are thought to have been sourced from the many outburst floods of glacial Lake Missoula, a major meltwater lake located in the western United States.

5.7 CONCLUSIONS

Thick, acoustically transparent Holocene sedimentation imaged from Barrow Canyon to the Mackenzie Trough indicate that discharge down Barrow Canyon and sediment from the Alaskan continent were important sources during this time period possibly due to the Brooks Range becoming less glaciated. Laminated sediments with increased grain size and magnetic susceptibility underlie the Holocene unit. The acoustic reflectivity and thickness of this unit increases towards the Mackenzie Trough, suggesting that it is the source of many of the acoustically laminated sediment, in addition to ice rafting from the Amundsen and M'Clure ice streams.

There are many discharge and ice rafted debris events recorded in the deglacial sediments. The oldest is an IRD event that occurred ~14.5 ka and was sourced from the Amundsen Gulf and possibly M'Clure Strait ice streams. This was followed by the rapid emplacement of very uniform, finely laminated sediments with little to no IRD emplaced

between ~14.5 ka and ~12.9 ka that was likely sourced from proglacial lakes that flowed down the Mackenzie entering the Beaufort Margin. An additional IRD layer is observed closer to Amundsen Gulf and was deposited prior to ~13.8 ka. This layer is probably from the Amundsen Gulf ice stream. After deposition of the finely laminated section, a major freshwater discharge event occurred, starting at ~12.8 ka, that generated high amplitude reflectors, deposited coarse debris, and has a lightening in the $\delta^{18}O$ record. Timing of this flood coincides with the onset of the Younger Dryas cold period and this discharge event could be glacial Lake Agassiz outflow down the Mackenzie drainage. Subsequent to the inferred glacial lake draining, at or before ~11.1 ka, was a second flood event that transported large amounts of coarse material to the margin and generated coarse laminated sediments in the Mackenzie Trough.

5.8 ACKNOWLEDGEMENTS

Funding for this research was provided by the National Science Foundation (OCE0649410) and Southern California Edison.

Chapter 5 is being prepared for publication in: Klotsko, S., Driscoll, N., and Keigwin, L., In Prep, Geologic and geophysical constraints on deglacial sediment dispersal along the Beaufort Margin, Arctic Ocean. The dissertation author was the primary researcher and author, and the co-authors listed in this publication directed and supervised the research.

5.9 REFERENCES

Aagaard, K., & Roach, A. T., 1990. Arctic ocean-shelf exchange: Measurements in Barrow Canyon. Journal of Geophysical Research: Oceans, 95(C10), 18163-18175.

Andrews, J.T., Dunhill, G., 2004. Early to mid-Holocene Atlantic water influx and deglacial meltwater events, Beaufort Sea slope, Arctic Ocean. Quaternary Research 61, 14-21.

Backman, J., Jakobsson, M., Løvlie, R., Polyak, L., Febo, L.A., 2004. Is the central Arctic Ocean a sediment starved basin? Quaternary Science Reviews 23, 1435-1454.

Barletta, F., St-Onge, G., Channell, J.E.T., Polyak, L., Darby, D.A., 2008. High-resolution paleomagnetic secular variation and relative paleointensity records from the western Canadian Arctic: implication for Holocene stratigraphy and geomagnetic field behaviour. Can. J. Earth Sci. 45, 1265–1281.

Batchelor, C.L., Dowdeswell, J.A., Pietras, J.T., 2013a. Variable history of Quaternary ice-sheet advance across the Beaufort Sea margin, Arctic Ocean. Geology 41, 131-134.

Batchelor, C.L., Dowdeswell, J.A., Pietras, J.T., 2013b. Seismic stratigraphy, sedimentary architecture and palaeo-glaciology of the Mackenzie Trough: evidence for two Quaternary ice advances and limited fan development on the western Canadian Beaufort Sea margin. Quaternary Science Reviews 65, 73-87.

Batchelor, C., Dowdeswell, J., Pietras, J., 2014. Evidence for multiple Quaternary ice advances and fan development from the Amundsen Gulf cross-shelf trough and slope, Canadian Beaufort Sea margin. Marine and Petroleum Geology 52, 125-143.

Bischof, J., Clark, D.L., Vincent, J.S., 1996. Origin of ice-rafted debris: Pleistocene paleoceanography in the western Arctic Ocean. Paleoceanography 11, 743-756.

Blasco, S.M., Fortin, G., Hill, P.R., O'Connor, M.J., Brigham-Grette, J., 1990. The Late Neogene and Quaternary Stratigraphy of the Canadian Beaufort Continental Shelf. In The geology of north America, V.L., the Arctic Ocean Region. Grantz, A., Johnson, L., Sweeney, J.F. (Eds.), Geological Society of America, pp. 491-501.

Blasco, S.M., Bennett, R., Hughes-Clarke, J., MacLean, B., Mayer, L., Monahan, D., Mudie, P., Praeg, D., Rainey, W., Scott, D., Sonnichsen, G., 2005. Northwest Passage Marine Sediments: a Record of Quaternary History and Climate Change: Annual International Arctic Workshop, 35th. University of Alberta, Edmonton, Canada, Program and Abstracts. Canadian Circumpolar Institute, Edmonton, Canada.

Carson, M. A., J. N. Jasper, and F. M. Conly, 1998. Magnitude and sources of sediment input to the Mackenzie Delta, Northwest Territories, 1974 – 94, Arctic, 51, 116-124.

Clarke, G.K.C., Bush, A.B.G., Bush, J.W.M., 2009. Freshwater Discharge, Sediment Transport, and Modeled Climate Impacts of the Final Drainage of Glacial Lake Agassiz. Journal of Climate 22, 2161-2180.

Condron, A. and P. Winsor, 2012. Meltwater routing and the Younger Dryas. PNAS doi:10.1073/pnas.1207381109.

Cohen, J.K., Stockwell Jr., J.W., 1999. CWP/SU: Seismic Unix Release 33: a Free Package for Seismic Research and Processing. Center for Wave Phenomena, Colorado School of Mines.

Darby, D.A., Bischof, J.F., 1996. A statistical approach to source determination of lithic and Fe oxide grains: an example from the Alpha Ridge, Arctic Ocean. Journal of Sedimentary Research 66.

Darby, D.A., Bischof, J.F., 1999. Quaternary ice transport in the Canadian Arctic and extent of Late Wisconsinan Glaciation in the Queen Elizabeth Islands. Canadian Journal of Earth Sciences 36, 2007-2022.

Darby, D.A., Jakobsson, M., Polyak, L., 2005. Icebreaker expedition collects key Arctic seafloor and ice data. Eos, Transactions American Geophysical Union 86, 549-552.

Darby, D.A., Ortiz, J., Polyak, L., Lund, S., Jakobsson, M., Woodgate, R.A., 2009. The role of currents and sea ice in both slowly deposited central Arctic and rapidly deposited Chukchi–Alaskan margin sediments. Global and Planetary Change 68, 58-72.

Dinter, D.A., Carter, L.D., Brigham-Grette, J., 1990. Late Cenozoic geologic evolution of the Alaskan North Slope and adjacent continental shelves. In The geology of north America, V.L., the Arctic Ocean Region. Grantz, A., Johnson, L., Sweeney, J.F. (Eds.), Geological Society of America pp. 459-489.

Dixon, J. and Dietrich, J.R., 1990. Canadian Beaufort Sea and the adjacent land areas. In The Arctic Ocean Region, Geology of North America, Grantz A, Johnson GL, Sweeney JF (eds). Geological Society of America, pp. 237-256.

Dyke, A., Andrews, J., Clark, P., England, J., Miller, G., Shaw, J., Veillette, J., 2002. The Laurentide and Innuitian ice sheets during the last glacial maximum. Quaternary Science Reviews 21, 9-31.

Eittreim, S., Grantz, A., Greenberg, J., 1982. Active geologic processes in Barrow canyon, northeast Chukchi Sea. Marine Geology 50, 61-76.

Engels, J.L., Edwards, M.H., Polyak, L., Johnson, P.D., 2008. Seafloor evidence for ice shelf flow across the Alaska–Beaufort margin of the Arctic Ocean. Earth Surface Processes and Landforms 33, 1047-1063.

England, J.H., Furze, M.F., Doupé, J.P., 2009. Revision of the NW Laurentide Ice Sheet:

implications for paleoclimate, the northeast extremity of Beringia, and Arctic Ocean sedimentation. Quaternary Science Reviews 28, 1573-1596.

Gamboa, A., Montero-Serrano, J.C., St-Onge, G., Rochon, A., Desiage, P.A., 2017. Mineralogical, geochemical, and magnetic signatures of surface sediments from the Canadian Beaufort Shelf and Amundsen Gulf (Canadian Arctic). Geochemistry, Geophysics, Geosystems 18, 488-512.

Giustiniani, M., Tinivella, U., Jakobsson, M., Rebesco, M., 2013. Arctic ocean gas hydrate stability in a changing climate. Journal of Geological Research 2013.

Grantz A, May SD, Taylor PT, Lawver LA. 1990. Geology of the Arctic continental margin of Alaska. In The Arctic Ocean Region, Geology of North America, Grantz A, Johnson GL, Sweeney JF (eds). Geological Society of America, pp. 257–288.

Greenhouse gas emissions: Understanding Global Warming Potentials. https://www.epa.gov/ghgemissions/understanding-global-warming-potentials

Henkart, P., 2006. SIOSEIS. http://sioseis.ucsd.edu.

Hill, P.R., Blasco, S.M., Harper, J.R., Fissel, D.B., 1991. Sedimentation on the Canadian Beaufort Shelf. Cont. Shelf Res. 11, 821–842.

Hill, J.C., Driscoll, N.W., Brigham-Grette, J., Donnelly, J.P., Gayes, P.T., Keigwin, L., 2007. New evidence for high discharge to the Chukchi shelf since the Last Glacial Maximum. Quaternary Research 68, 271-279.

Hill, J.C., Driscoll, N.W., 2008. Paleodrainage on the Chukchi shelf reveals sea level history and meltwater discharge. Marine Geology 254, 129-151.

Hill, J.C., Driscoll, N.W., 2010. Iceberg discharge to the Chukchi shelf during the Younger Dryas. Quaternary Research 74, 57-62.

Holmes, R.M., McClelland, J.W., Peterson, B.J., Shiklomanov, I.A., Shiklomanov, A.I., Zhulidov, A.V., Gordeev, V.V., Bobrovitskaya, N.N., 2002. A circumpolar perspective on fluvial sediment flux to the Arctic Ocean. Global Biogeochemical Cycles 16.

Holmes, R.M., McClelland, J.W., Peterson, B.J., Tank, S.E., Bulygina, E., Eglinton, T.I., Gordeev, V.V., Gurtovaya, T.Y., Raymond, P.A., Repeta, D.J., 2012. Seasonal and annual fluxes of nutrients and organic matter from large rivers to the Arctic Ocean and surrounding seas. Estuaries and Coasts 35, 369-382.

Hovland, M., Gardner, J., Judd, A., 2002. The significance of pockmarks to understanding

fluid flow processes and geohazards. Geofluids 2, 127-136.

Jakobsson, M., Løvlie, R., Arnold, E.M., Backman, J., Polyak, L., Knutsen, J.O., Musatov, E., 2001. Pleistocene stratigraphy and paleoenvironmental variation from Lomonosov Ridge sediments, central Arctic Ocean. Global Planet. Change 31, 1-22.

Jakobsson, M., Gardner, J.V., Vogt, P.R., Mayer, L.A., Armstrong, A., Backman, J., Brennan, R., Calder, B., Hall, J.K., Kraft, B., 2005. Multibeam bathymetric and sediment profiler evidence for ice grounding on the Chukchi Borderland, Arctic Ocean. Quaternary Research 63, 150-160.

Jakobsson, M., Polyak, L., Edwards, M., Kleman, J., Coakley, B., 2008. Glacial geomorphology of the Central Arctic Ocean: the Chukchi Borderland and the Lomonosov Ridge. Earth Surf. Process. Landf. 33, 526-545.

Jakobsson, M., Nilsson, J., O'Regan, M., Backman, J., Löwemark, L., Dowdeswell, J.A., Mayer, L., Polyak, L., Colleoni, F., Anderson, L.G., Björk, G., Darby, D., Eriksson, B., Hanslik, D., Hell, B., Marcussen, C., Sellén, E., Wallin, Å., 2010. An Arctic Ocean ice shelf during MIS 6 constrained by new geophysical and geological data. Quaternary Science Reviews 29, 3505-3517.

Jakobsson, M., Mayer, L., Coakley, B., Dowdeswell, J.A., Forbes, S., Fridman, B., Hodnesdal, H., Noormets, R., Pedersen, R., Rebesco, M., Schenke, H.W., Zarayskaya, Y., Accettella, D., Armstrong, A., Anderson, R.M., Bienhoff, P., Camerlenghi, A., Church, I., Edwards, M., Gardner, J.V., Hall, J.K., Hell, B., Hestvik, O., Kristoffersen, Y., Marcussen, C., Mohammad, R., Mosher, D., Nghiem, S.V., Pedrosa, M.T., Travaglini, P.G., Weatherall, P., 2012. The international bathymetric Chart of the Arctic Ocean (IBCAO) Version 3.0. Geophys. Res. Lett. 39, L12609.

Jakobsson, M., Andreassen, K., Bjarnadóttir, L.R., Dove, D., Dowdeswell, J.A., England, J.H., Funder, S., Hogan, K., Ingólfsson, Ó., Jennings, A., 2014. Arctic Ocean glacial history. Quaternary Science Reviews 92, 40-67.

Johnson, G., Grantz, A., Weber, J., 1990. Bathymetry and physiography . In the geology of north America, V.L., the Arctic Ocean Region: Geological Society of America. In: Grantz, A., Johnson, L., Sweeney, J.F. (Eds.), Geological Society of America, pp 63-77.

Lakeman, T.R., England, J.H., 2012. Paleoglaciological insights from the age and morphology of the Jesse moraine belt, western Canadian Arctic. Quaternary Science Reviews 47, 82-100.

Lakeman, T.R., England, J.H., 2013. Late Wisconsinan glaciation and postglacial

relative sea-level change on western Banks Island, Canadian Arctic Archipelago. Quaternary Research 80, 99-112.

Leffingwell E de K. 1919. The Canning River region, northern Alaska. U.S. Geological Survey Professional Paper 109.

Robert E. Kayen & Homa J. Lee, 1991. Pleistocene slope instability of gas hydrate-laden sediment on the Beaufort sea margin, Marine Geotechnology, 10:1-2, 125-141, DOI: 10.1080/10641199109379886

Keigwin, L.D., Donnelly, J.P., Cook, M.S., Driscoll, N.W., Brigham-Grette, J., 2006. Rapid sea-level rise and Holocene climate in the Chukchi Sea. Geology 34, 861.

L.D. Keigwin, S. Klotsko, N. Zhao, B. Reily, L.Giosan, and N. W. Driscoll, In Prep. Deglacial Floods in the Beaufort Sea. Chapter 4.

Kleman, J., Jansson, K., De Angelis, H., Stroeven, A.P., Hättestrand, C., Alm, G., Glasser, N., 2010. North American Ice Sheet build-up during the last glacial cycle, 115-21 kyr. Quat. Sci. Rev. 29, 2036-2051.

MacLean, B., Blasco, S., Bennett, R., Lakeman, T., Hughes-Clark, J., Kuus, P., Patton, E., 2012. Marine evidence for a glacial ice stream in Amundsen Gulf, Canadian Arctic Archipelago: International Arctic Workshop, 42nd, Winter Park, Colorado, Abstract.

MacLean, B., Blasco, S., Bennett, R., Lakeman, T., Hughes-Clarke, J., Kuus, P., Patton, E., 2015. New marine evidence for a Late Wisconsinan ice stream in Amundsen Gulf, Arctic Canada. Quaternary Science Reviews 114, 149-166.

Milliman, J. D., and Meade, R. H., 1983, World-wide delivery of river sediment to the oceans: Jour. Geology: v. 91, p. 1-21.

Milliman, J. D., and J. P. M. Syvitski, 1992. Geomorphic/tectonic control of sediment discharge to the ocean: The importance of small mountainous rivers, J. Geol., 100, 524–544.

Millot R., Gaillardet J., Dupré, B. and Allègre C. J., 2003. Northern latitude chemical weathering rates: clues from the Mackenzie River Basin, Canada. Geochim. Cosmochim. Acta 67, 1305–1329.

Molnia, B. F.; Carlson, P. R.; and Levy, W. P., 1978, Holo- cene sediment volume and modern sediment yield, northeast Gulf of Alaska (abs): Am. Assoc. Petrol. Geol. Bull., v. 62, p. 545.

Murton, J.B., Bateman, M.D., Dallimore, S.R., Teller, J.T., Yang, Z., 2010. Identification

of Younger Dryas outburst flood path from Lake Agassiz to the Arctic Ocean. Nature 464, 740-743.

National geophysical data center, NOAA. https://ngdc.noaa.gov/

Niessen, F., Matthiessen, J., Stein, R., 2010. Sedimentary environment and glacial history of the Northwest Passage (Canadian Arctic Archipelago) reconstructed from high-resolution acoustic data. Polarforschung 79, 65-80.

Ortiz, J.D., Polyak, L., Grebmeier, J.M., Darby, D., Eberl, D.D., Naidu, S., Nof, D., 2009. Provenance of Holocene sediment on the Chukchi-Alaskan margin based on combined diffuse spectral reflectance and quantitative X-Ray Diffraction analysis. Global and Planetary Change 68, 73-84.

Polyak, L., Edwards, M.H., Coakley, B.J., Jakobsson, M., 2001. Ice shelves in the Pleistocene Arctic Ocean inferred from glaciogenic deep-sea bedforms. Nature 410, 453-459.

Polyak, L., Korsun, S., Febo, L.A., Stanovoy, V., Khusid, T., Hald, M., Paulsen, B.E., Lubinski, D.J., 2002. Benthic foraminiferal assemblages from the southern Kara Sea, a river-influenced Arctic marine environment. Journal of Foraminiferal Research 32, 252-273.

Polyak, L., Darby, D., Bischof, J., Jakobsson, M., 2007. Stratigraphic constraints on late Pleistocene glacial erosion and deglaciation of the Chukchi margin, Arctic Ocean. Quat. Res. 67, 234-245.

Polyak, L., Curry, W.B., Darby, D.A., Bischof, J., Cronin, T.M., 2004. Contrasting glacial/interglacial regimes in the western Arctic Ocean as exemplified by a sedimentary record from the Mendeleev Ridge. Palaeogeography, Palaeoclimatology, Palaeoecology 203, 73-93.

Polyak, L., Bischof, J., Ortiz, J., Darby, D., Channell, J., Xuan, C., Kaufman, D., Lovlie, R., Schneider, D., Adler, R., 2009. Late Quaternary stratigraphy and sedimentation patterns in the western Arctic Ocean. Global Planet. Change 68, 5-17.

Poore, R. Z., L. E. Osterman, W. B. Curry, and R. L. Philips, 1999. Later Pleistocene and Holocene meltwater events in the western Arctic Ocean, Geology, 27, 759 – 762, doi:10.1130/0091-7613

Phrampus, B.J., Hornbach, M.J., Ruppel, C.D., Hart, P.E., 2014. Widespread gas hydrate instability on the upper US Beaufort margin. Journal of Geophysical Research: Solid Earth 119, 8594-8609.

Ruppel, C. D., 2011. Methane hydrates and contemporary climate change, Nature

Education Knowledge, vol. 3, no. 10, article 29.

Schell, T.M., Scott, D.B., Rochon, A., Blasco, S., 2008. Late Quaternary paleoceanography and paleo-sea ice conditions in the Mackenzie Trough and Canyon, Beaufort Sea This article is one of a series of papers published in this Special Issue on the theme Polar Climate Stability Network. Canadian Journal of Earth Sciences 45, 1399-1415.

Scott, D.B., Schell, T., St-Onge, G., Rochon, A., Blasco, S., 2009. Foraminiferal assemblage changes over the last 15,000 years on the Mackenzie-Beaufort Sea Slope and Amundsen Gulf, Canada: Implications for past sea ice conditions. Paleoceanography 24.

Screen, J. A., & Simmonds, I., 2010. The central role of diminishing sea ice in recent Arctic temperature amplification. Nature, 464(7293), 1334-1337.

Solomon, S., Mudie, P., Cranston, R., Hamilton, T., Thibaudeau, S., Collins, E., 2000. Characterisation of marine and lacustrine sediments in a drowned thermokarst embayment, Richards Island, Beaufort Sea, Canada. International Journal of Earth Sciences 89, 503-521.

Spielhagen, R.F., Baumann, K.-H., Erlenkeuser, H., Nowaczyk, N.R., Nørgaard-Pedersen, N., Vogt, C., Weiel, D., 2004. Arctic Ocean deep-sea record of northern Eurasian ice sheet history. Quaternary Science Reviews 23, 1455-1483.

Stein, R., Matthiessen, J., Niessen, F., Krylov, R., Nam, S., and Bazhenova, E., 2010. Towards a better (litho-) stratigraphy and reconstruction of Quaternary paleoenvironment in the Amerasian Basin (Arctic Ocean): Polarforschung, v. 79, p. 97–121.

Stroeve, J., M. M. Holland, W. Meier, T. Scambos, and M. Serreze, 2007. Arctic sea ice decline: Faster than forecast, Geophys. Res. Lett., 34, L09501, doi:10.1029/2007GL029703.

Stokes, C.R., Clark, C.D., Darby, D.A., Hodgson, D.A., 2005. Late Pleistocene ice export events into the Arctic Ocean from the M'Clure Strait ice stream, Canadian Arctic Archipelago. Global and Planetary Change 49, 139-162.

Stokes, C., Clark, C., Winsborrow, M., 2006. Subglacial bedform evidence for a major palaeo-ice stream and its retreat phases in Amundsen Gulf, Canadian Arctic Archipelago. Journal of Quaternary Science 21, 399-412.

Stokes, C.R., Clark, C.D., Storrar, R., 2009. Major changes in ice stream dynamics during deglaciation of the north-western margin of the Laurentide Ice Sheet. Quaternary Science Reviews 28, 721-738.

Tarasov, L., Peltier, W.R., 2005. Arctic freshwater forcing of the Younger Dryas cold reversal. Nature 435, 662-665.

Wagner, A., Lohmann, G., Prange, M., 2011. Arctic river discharge trends since 7ka BP. Global and Planetary Change 79, 48-60.

Waterhouse, Amy, 2015. Personal communication and data transfer of Sikuliaq 2015-11S data.

Young, G. M., & Long, D. G. F., 1977. Carbonate sedimentation in a late Precambrian shelf sea, Victoria island, Canadian Arctic Archipelago. Journal of Sedimentary Research, 47(3).

Zuffa, G.G., Normark, W. R., Serra, F., & Brunner, C. A. , 2000. Turbidite megabeds in an oceanic rift valley recording jökulhlaups of late Pleistocene glacial lakes of the western United States. The Journal of geology 108, 253-274.

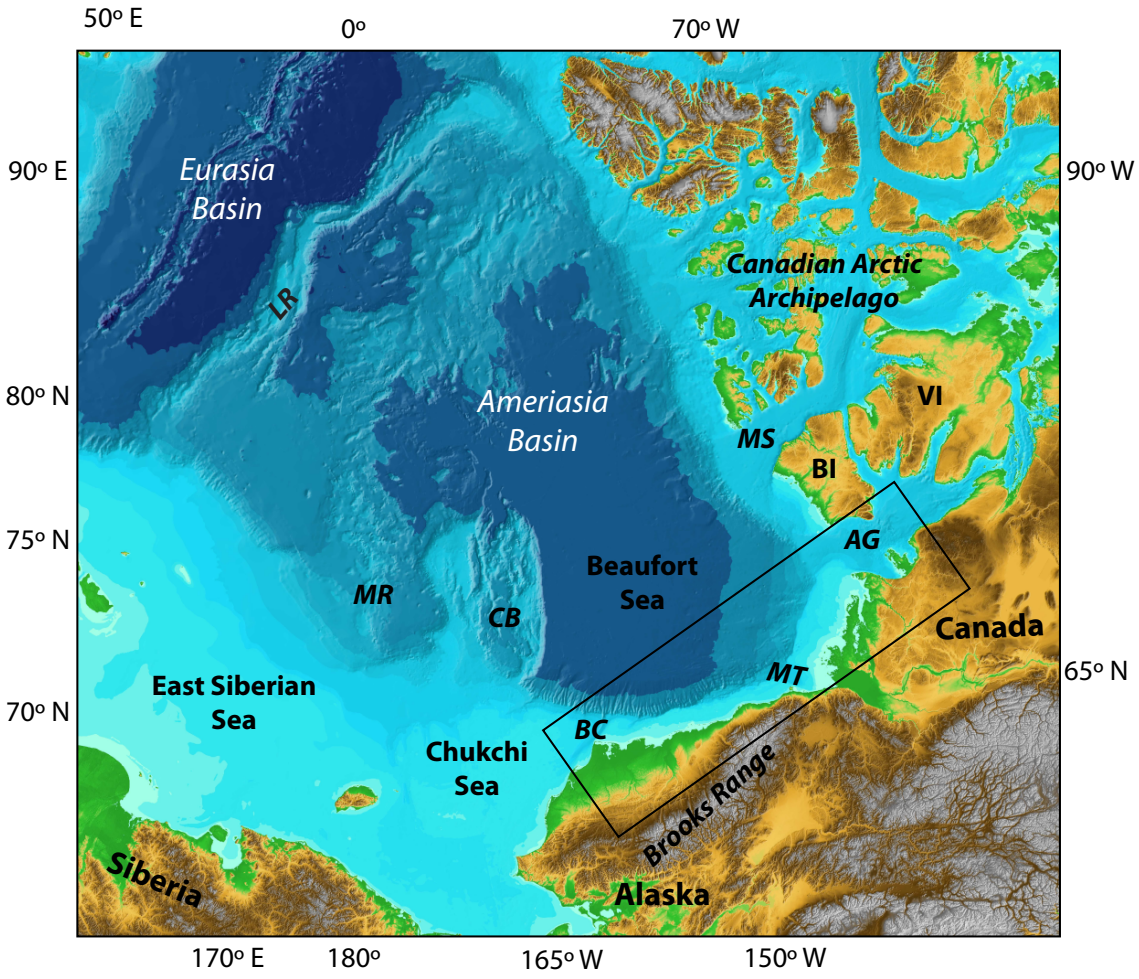

Figure 5.1. Regional map of the western Arctic with notable features and places labeled. The box outlines the study area, the Beaufort Margin. LR = Lomonosov Ridge, MR = Mendeleev Ridge, CB = Chukchi Borderland, BC = Barrow Canyon, MT = Mackenzie Trough, AG = Amundsen Gulf, MS = M'Clure Strait, BI = Banks Island, VI = Victoria Island. Topography and bathymetry is from the International Bathymetric Chart of Arctic Ocean (IBCAO) Version 3.0 (Jakobsson et al., 2012).

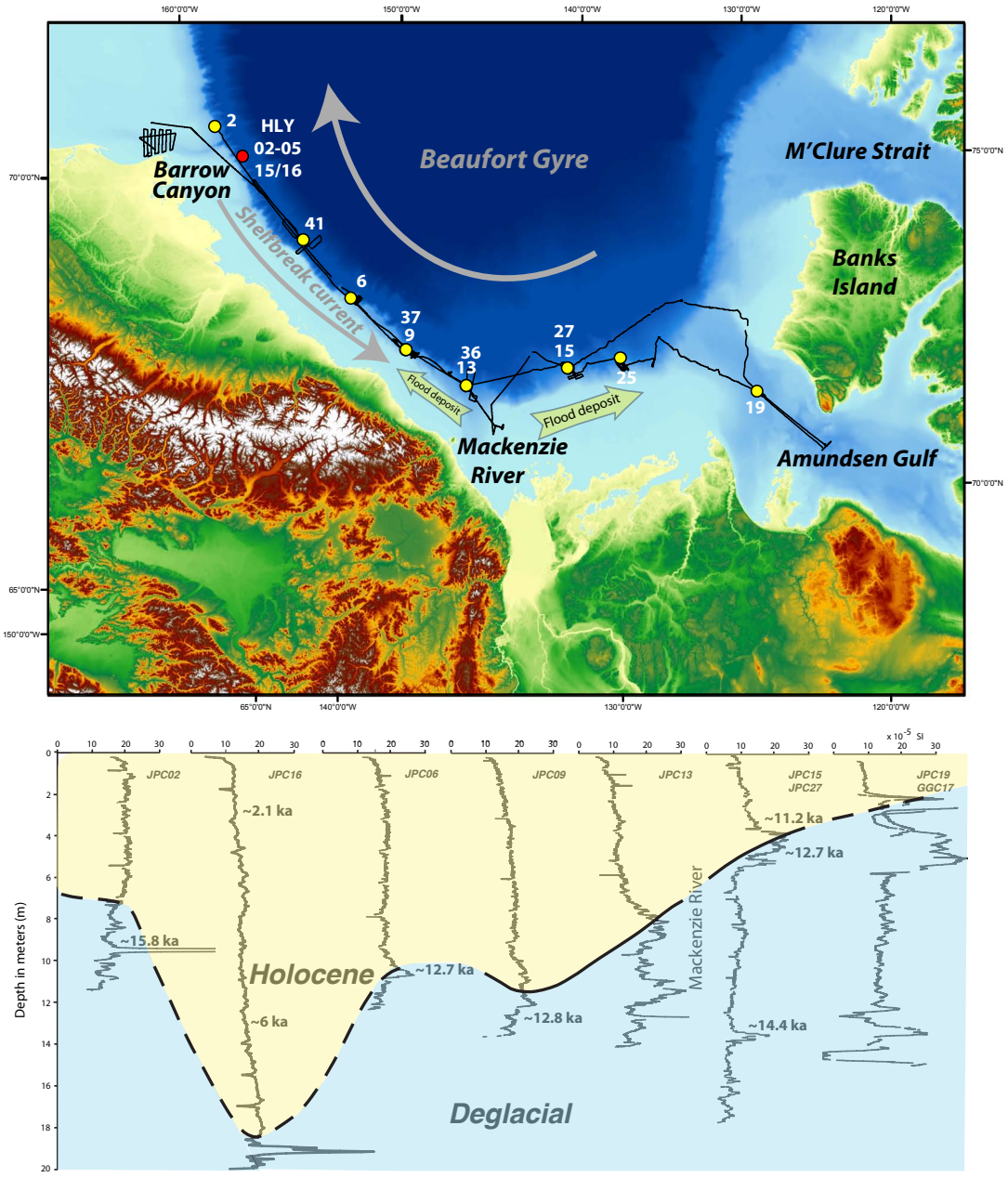

Figure 5.2. (Top) Survey map of the Beaufort Margin from Hly-1302. Ship tracklines are shown in black, jumbo piston cores collected during this cruise are in yellow, and jumbo piston cores collected during Hly 02-05 are in red. Major geographic features and currents are labeled. Green arrows show direction and relative magnitude of flood drainage along the Beaufort Margin. (Bottom) Magnetic Susceptibility profiles for multiple cores along the margin showing variability in Holocene and deglacial sediment thickness. The black line separating the timing of sedimentation is solid where radiocarbon dates have been acquired and dashed where the boundary is estimated based on magnetic susceptibility and acoustic character. Dates along the boundary are shown. Topography and bathymetry is from IBCAO Version 3.0 (Jakobsson et al., 2012).

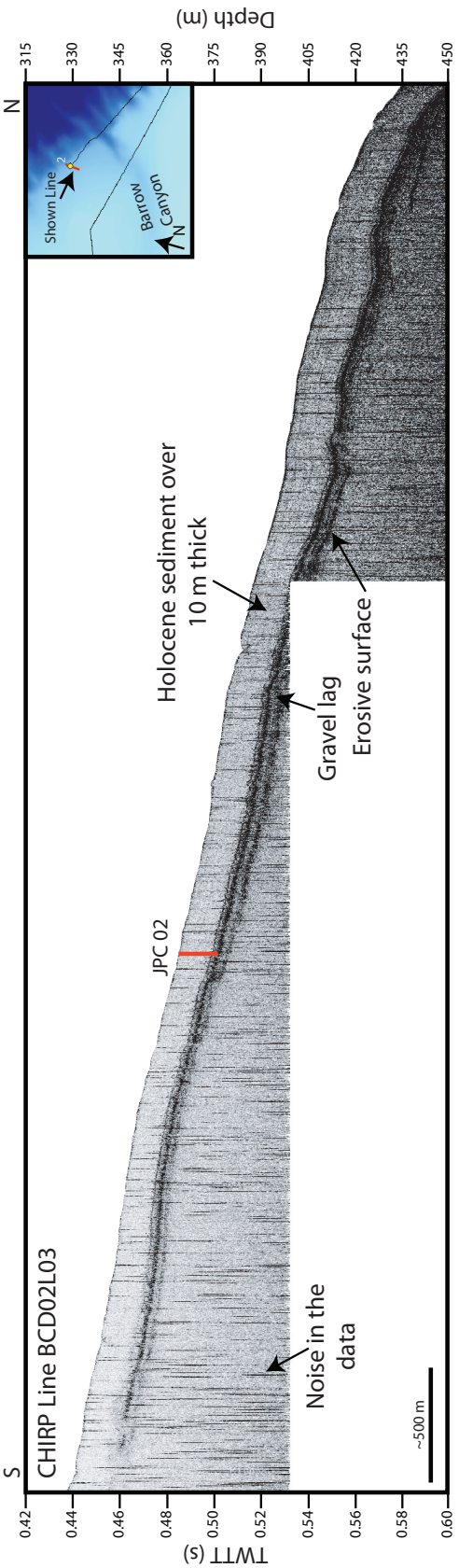

Figure 5.3. CHIRP Line BCD02L03 crossing the location of JPC 02 at the edge of Barrow Canyon. An inset shows the location of the profile. Here, at the far western Beaufort margin, there is thick, acoustically transparent Holocene sediment, which in places exceeds 10 m in thickness. Below this layer is a scour surface with irregular morphology. The rough morphology and high amplitude character of this reflector limits/prevents deeper acoustic imagining. Vertical lines are caused by noise in the water column during data collection.

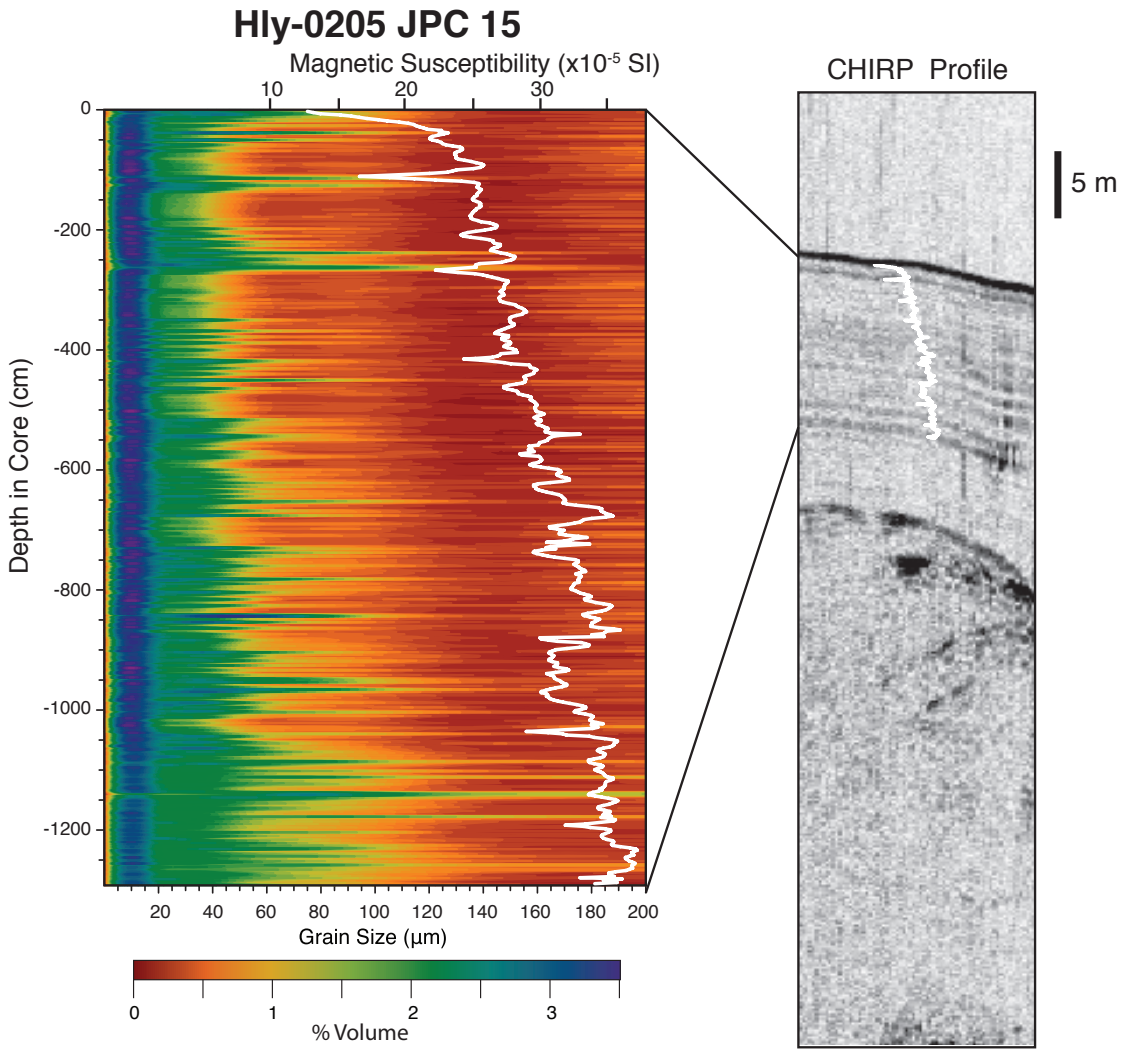

Figure 5.4. Grain size data and seismic section from Healy 0205-JPC 15 with magnetic susceptibility projected on both. Grain size is overall quite fine, but a number of coarser layers are shown by the green bands and reflectors in the seismic section.

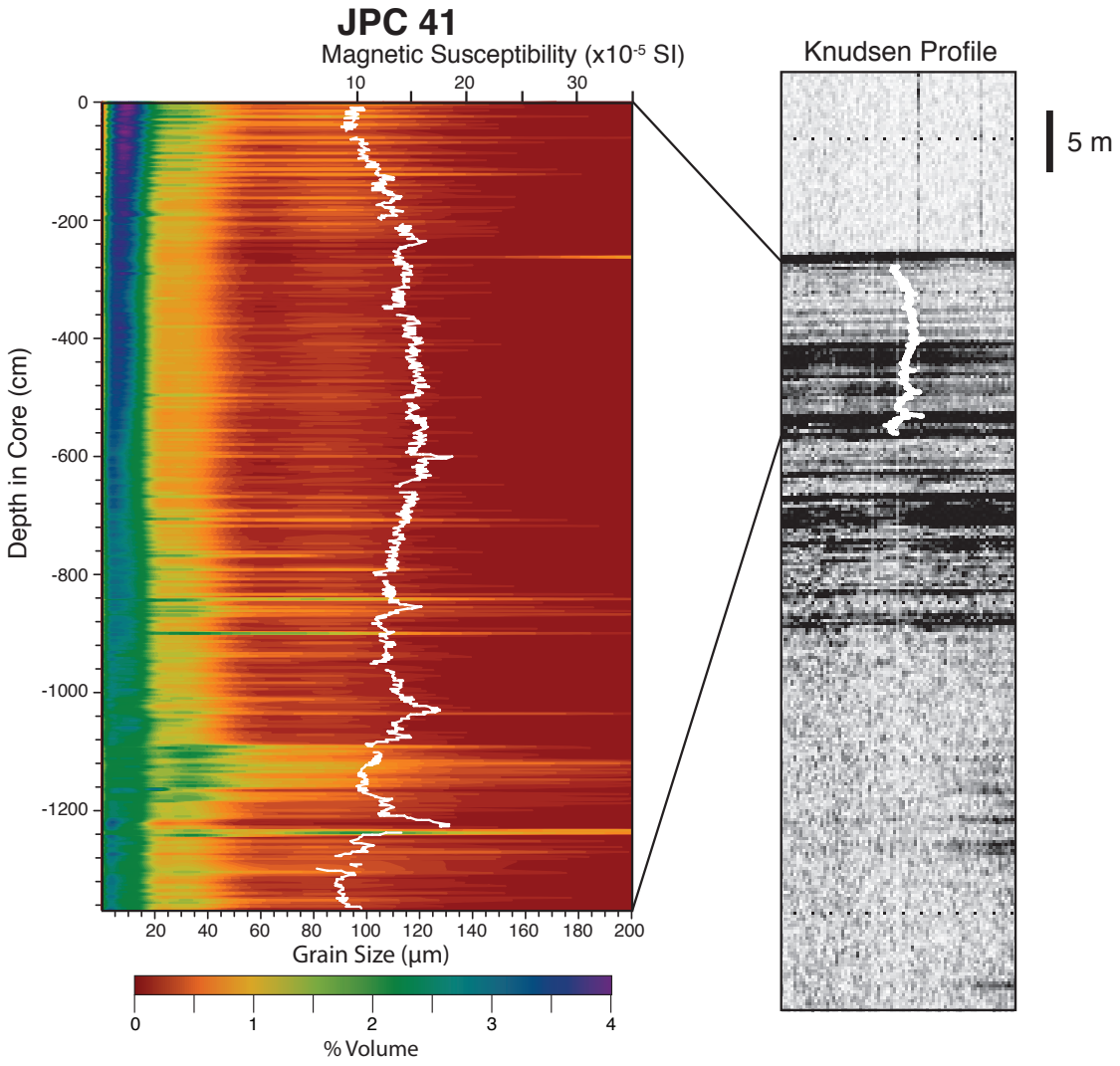

Figure 5.5. Grain size data and seismic section from Healy JPC 41 with magnetic susceptibility projected on both. Overall, there is little grain size variability, but it does exhibit a slight increase down core. The observed decrease in grain size and variability in JPC 41 is consistent with being farther away from Barrow Canyon.

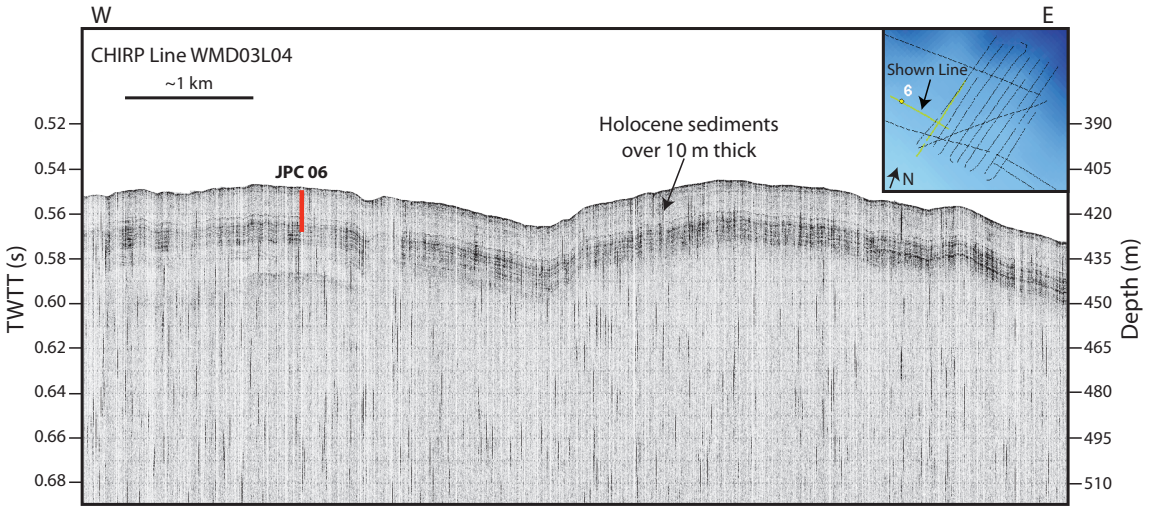

Figure 5.6. CHIRP Line WMD03L04 crossing the location of JPC 06. Holocene sediments are over 10 m thick in this region and overly laminated deposits that are more than 5 m thick. A radiocarbon date below the boundary between these layers (12.8 ka) indicates these are deglacial sediments (see Figure 2).

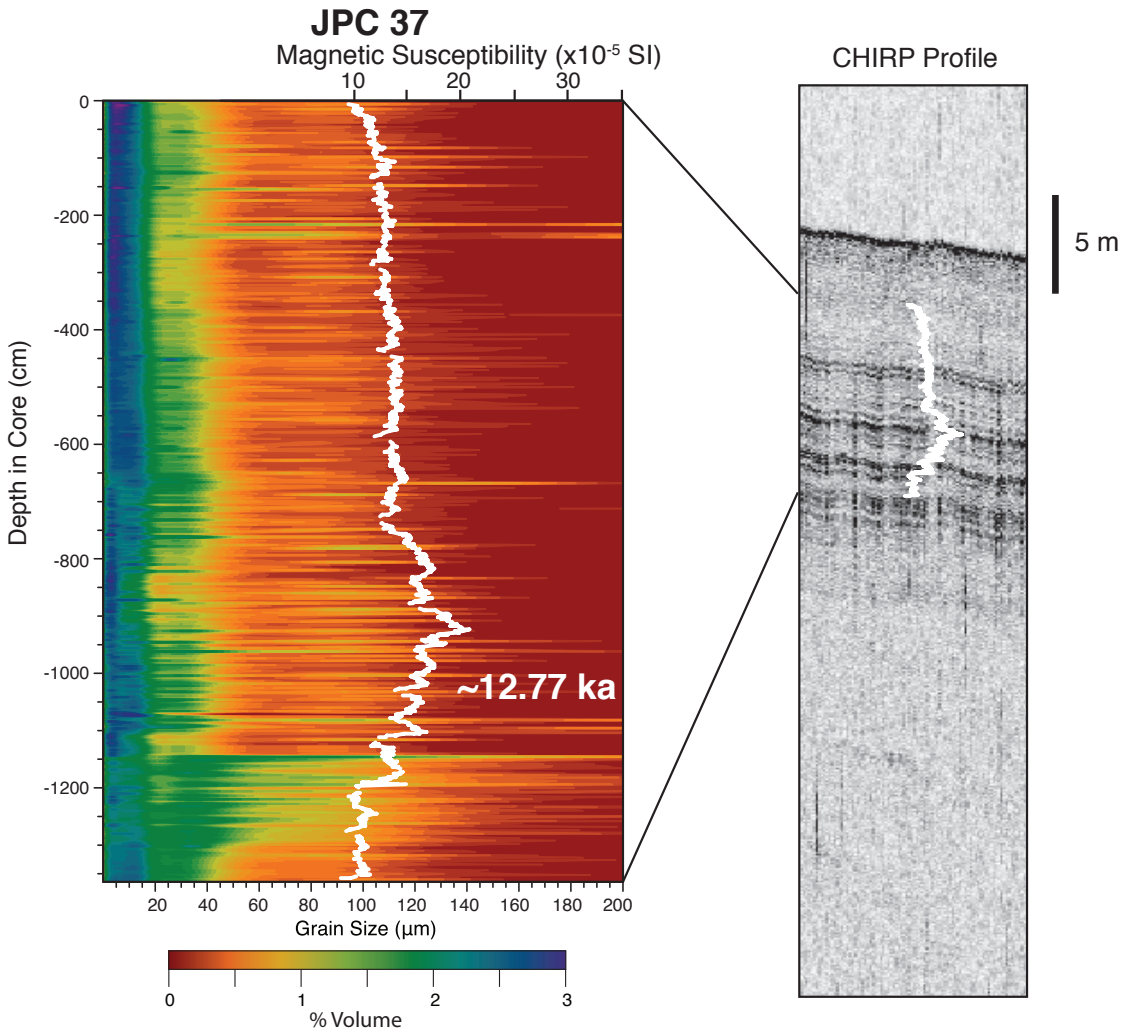

Figure 5.7. Grain size data and seismic section from JPC 37 with magnetic susceptibility projected on both. JPC 37 is located west of the Mackenzie Trough (coincident with JPC 09). There is minor variation in grain size and magnetic susceptibility for the upper ~7 m, which correlates with the acoustically transparent surficial layer in the seismic section. Beneath the acoustically transparent layers, there is more variation in the grain size data and the boundary appears to correlate with the onset of reflectors in the seismic section. The basal high amplitude reflectors are interpreted to be recording deglacial sediments. Date on the grain size is from JPC 09 with depth variation accounted for.

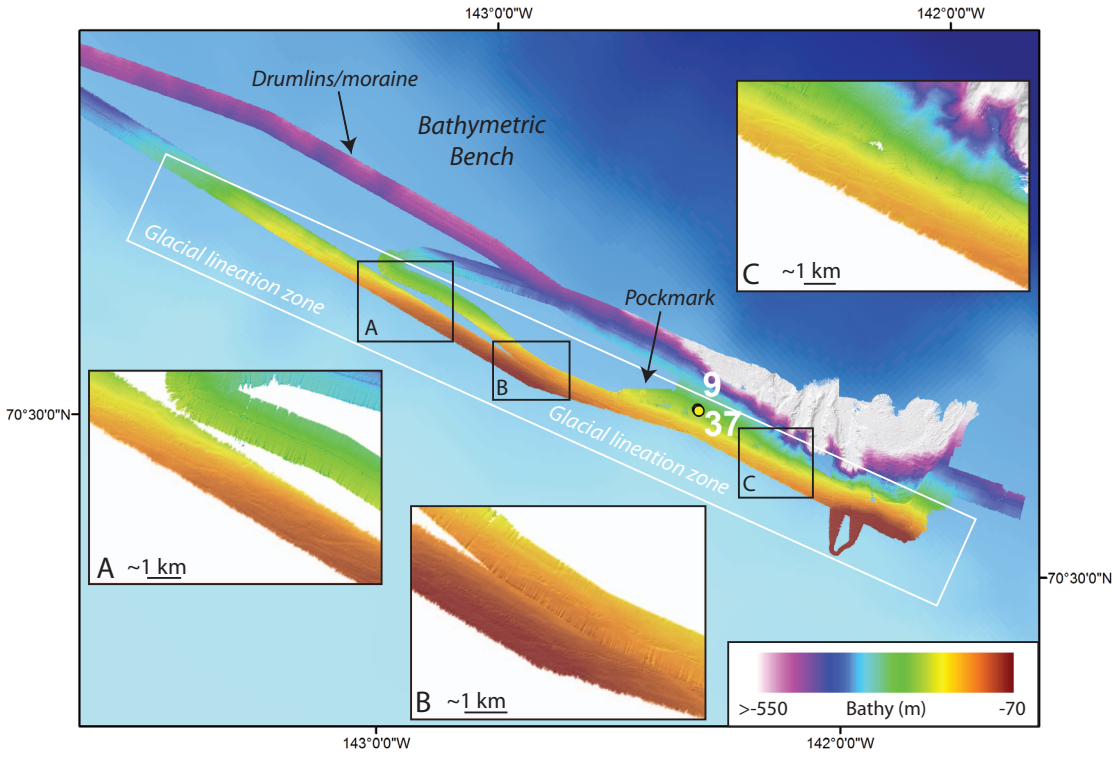

Figure 5.8. Glacial lineations along the margin. Multibeam data from Hly-1302 are shown in rainbow and overlies IBCAO Version 3.0 (Jakobsson et al., 2012) in blue. The general extent of glacial lineations (<400 m water depth) is outlined by the white box. (A) shows lineations that follow a more wavy pattern. (B) shows lineations that are shorter, more straight, and do not scour very deep. (C) shows a mixture or wavy, curvilinear, and more linear glacial lineations. Other notable features discussed in the paper are labeled.

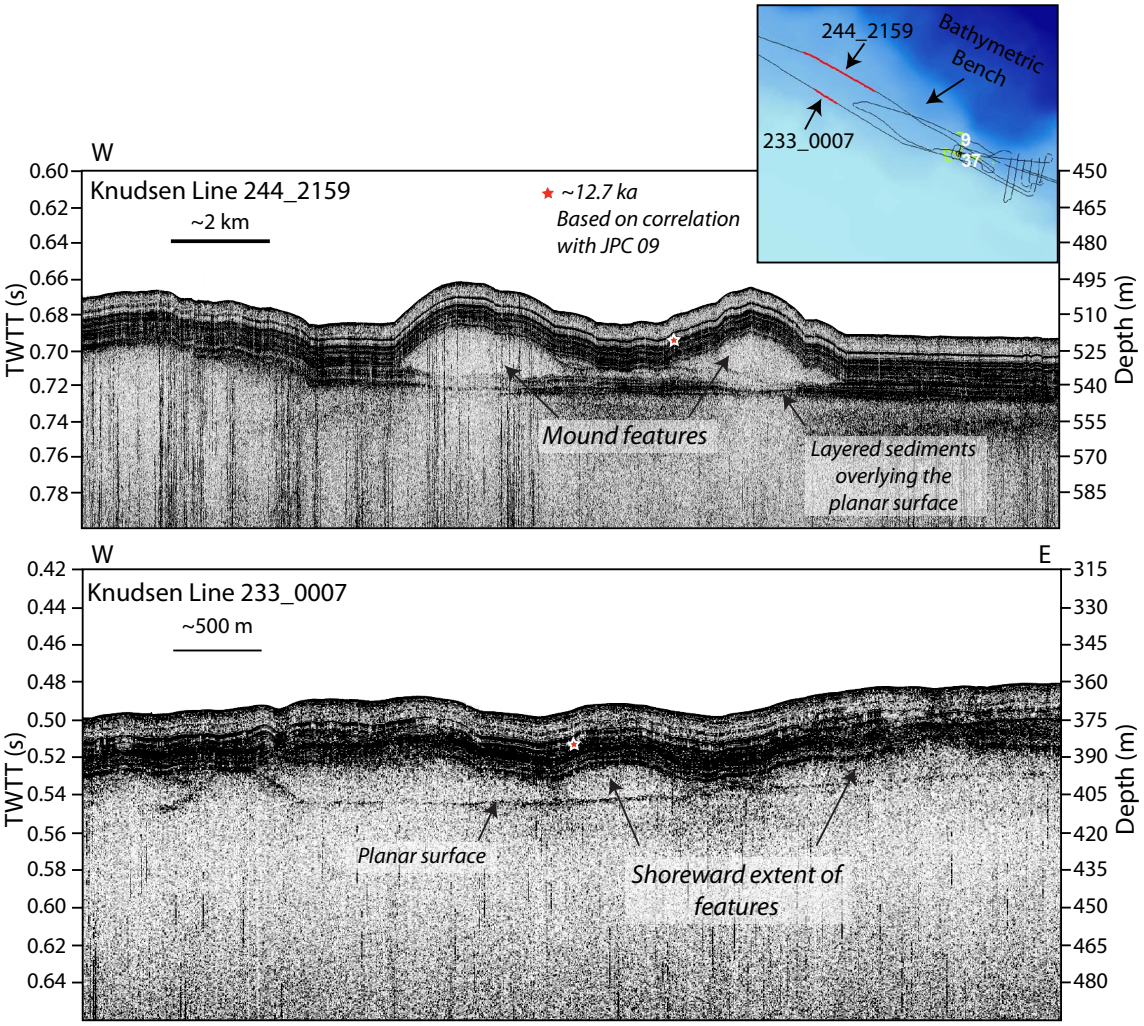

Figure 5.9. Mound features on the bathymetric bench. Knudsen Line 244_2159 shows the seaward extent of the mound features and Knudsen Line 233_0007 shows the more landward extent. The two mound-like features are large and well-defined in Knudsen Line 244_2159 and much thinner in Knudsen Line 233_0007. The red star indicates the reflector that correlates to a ~12.7 ka age date from nearby JPC 09. Inset shows seismic profiles highlighted in red.

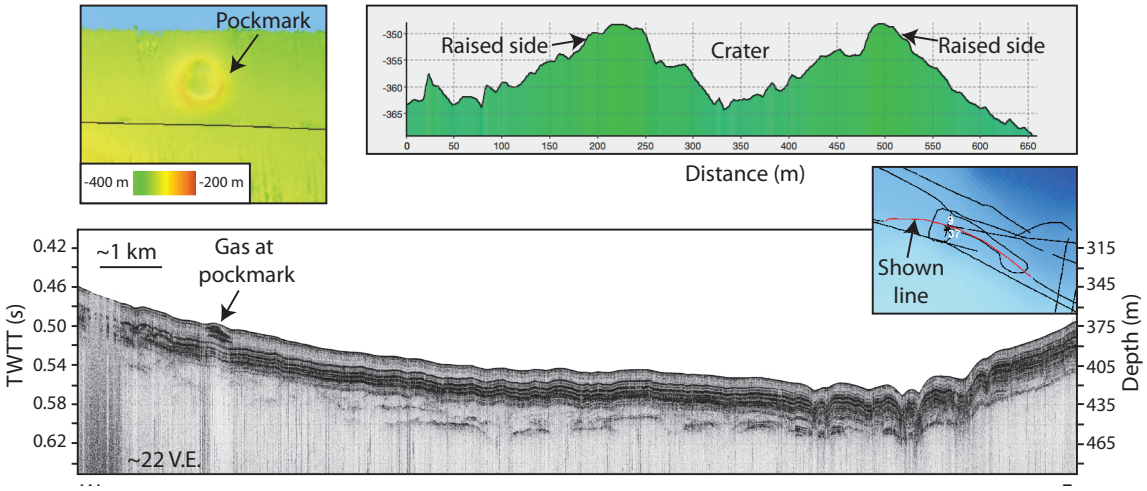

Figure 5.10. Gas pockmark on the outer shelf/upper slope just west of the Mackenzie Trough, near JPCs 9 and 37. The pockmark is a mounded shape with a circular crater in the middle. This can be observed in the multibeam data (top left) and in a profile across the feature (top right). The crater is over 200 m across and the entire pockmark is more than 500 m in width. The sediments beneath the pockmark are characterized by high acoustic reflectivity imaged in the seismic data (bottom). This acoustic reflectivity pattern is interpreted to be caused by gas. No other pockmarks are imaged in this region, but more could exist to the northwest of the pockmark as that region was not surveyed.

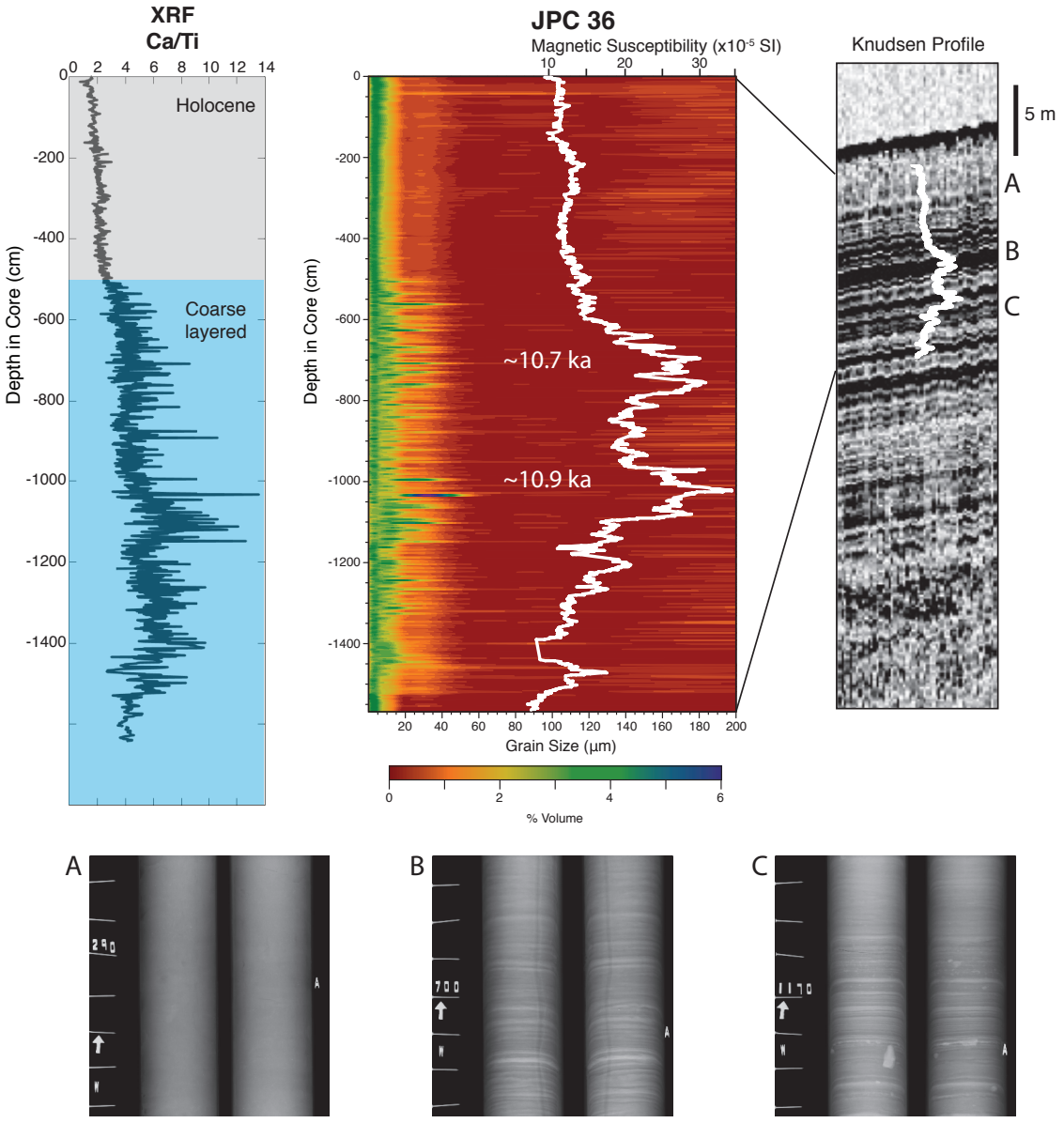

Figure 5.11. Grain size data and seismic section from JPC 36 with magnetic susceptibility projected on both. JPC36 is from the Mackenzie Trough (coincident with JPC13). The upper 5 m of the core is characterized by fine-grained homogenous sediment. Below this are multiple coarse sand stringers that are approximately 2 cm thick. X-rays show the difference between homogenous material, layered sediments, and layered sediments with IRD. Note the two large peaks in magnetic susceptibility appear to correlate with a high amplitude acoustic reflector in the seismic data The Ca/Ti ratio from XRF data shows two distinct sections, colored in gray and blue. Dates on the grain size are from PC1 (Schell et al., 2008) collected at the same location as JPCs 09 and 36 with depth correlation based on stratigraphy. The dates have been recalibrated using our age model (Keigwin et al., Chapter 4).

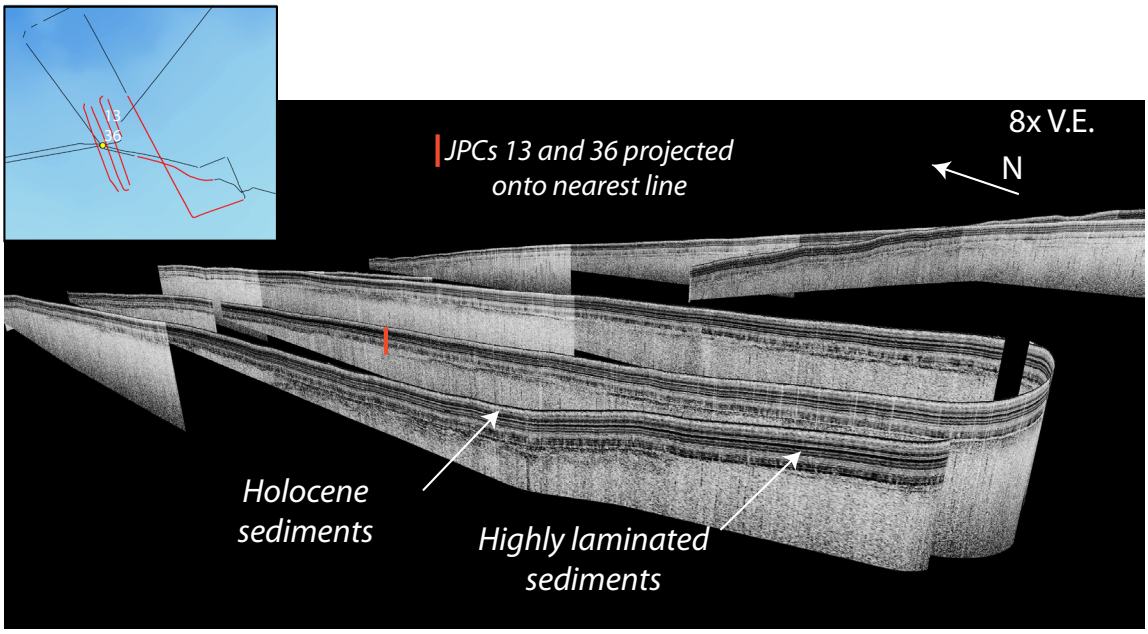

Figure 5.12. Seismic fence diagram around JPCs 09 and 36. That lateral continuity of the layered reflectors is well imaged. Inset shows seismic profiles highlighted in red.

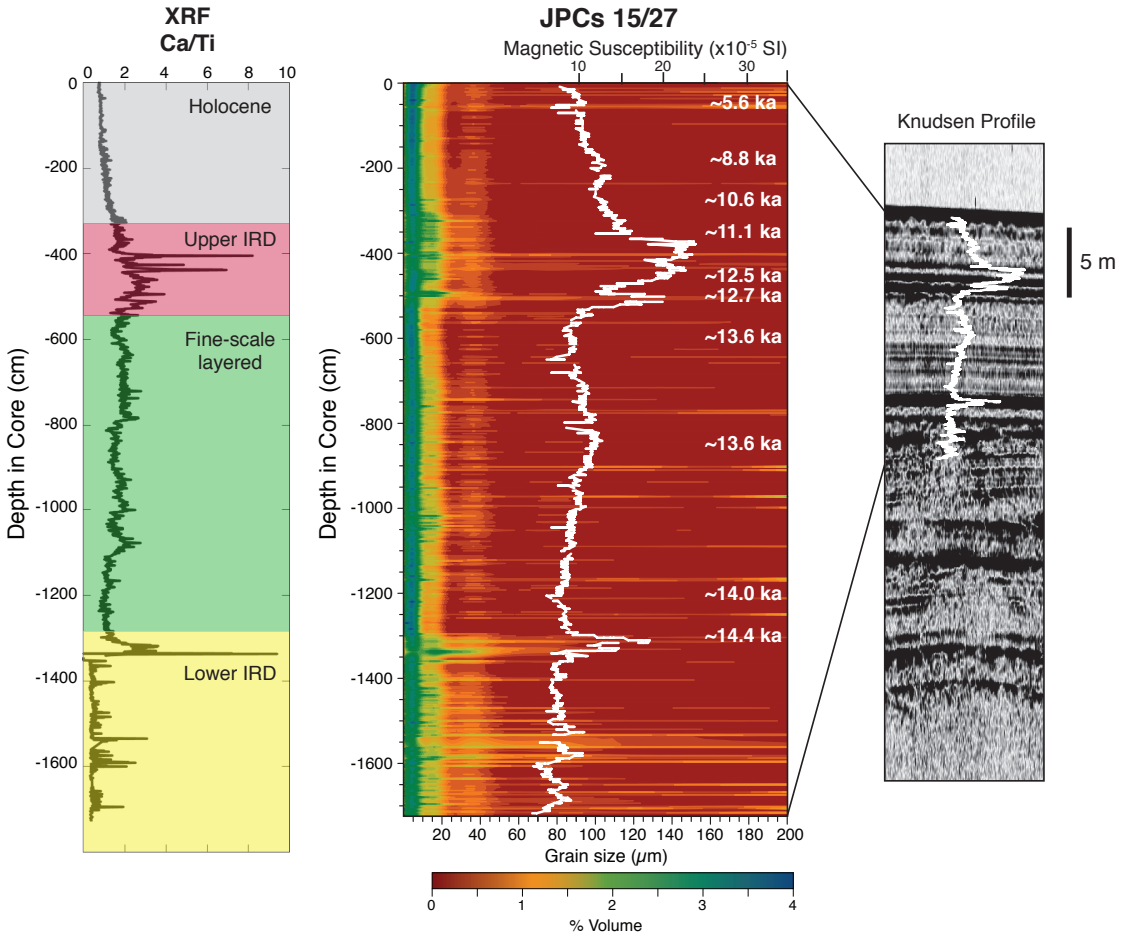

Figure 5.13. Grain size data and seismic section from composite cores JPCs 15/27 with magnetic susceptibility projected on both. There is a strong correlation between peaks in grain size, highs in magnetic susceptibility, and high amplitude reflectors in the seismic section. The Ca/Ti ratio from XRF data shows four distinct sections colored in gray, red, green, and yellow.

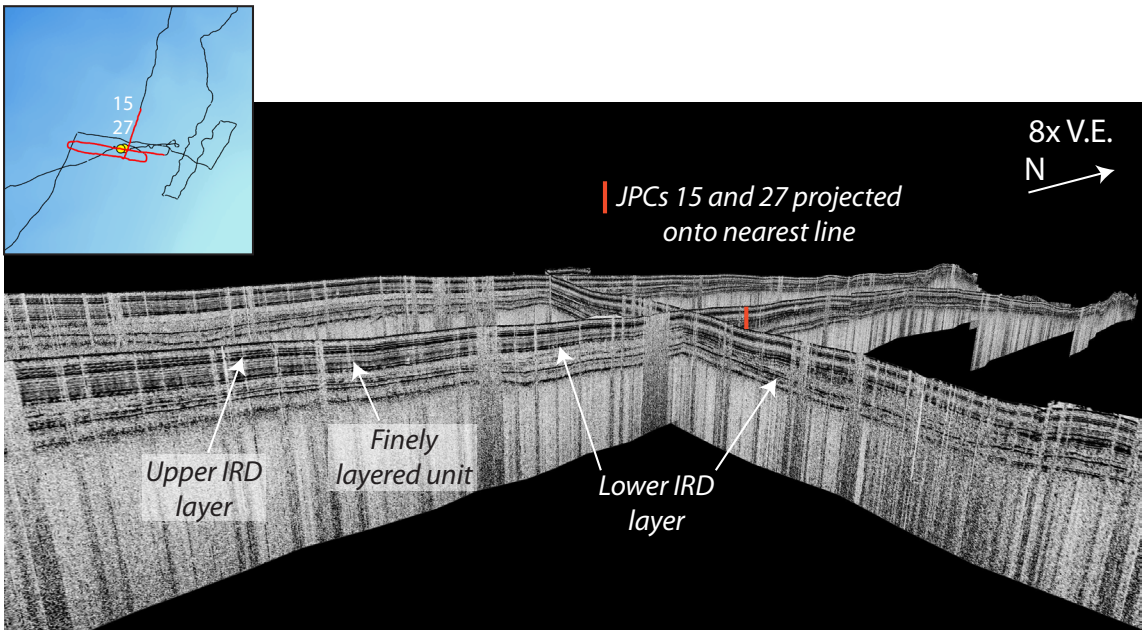

Figure 5.14. Seismic fence diagram around JPCs 15/27. The extensive nature of both sets of IRD and the faintly laminated deposit is imaged. Inset shows seismic profiles highlighted in red.

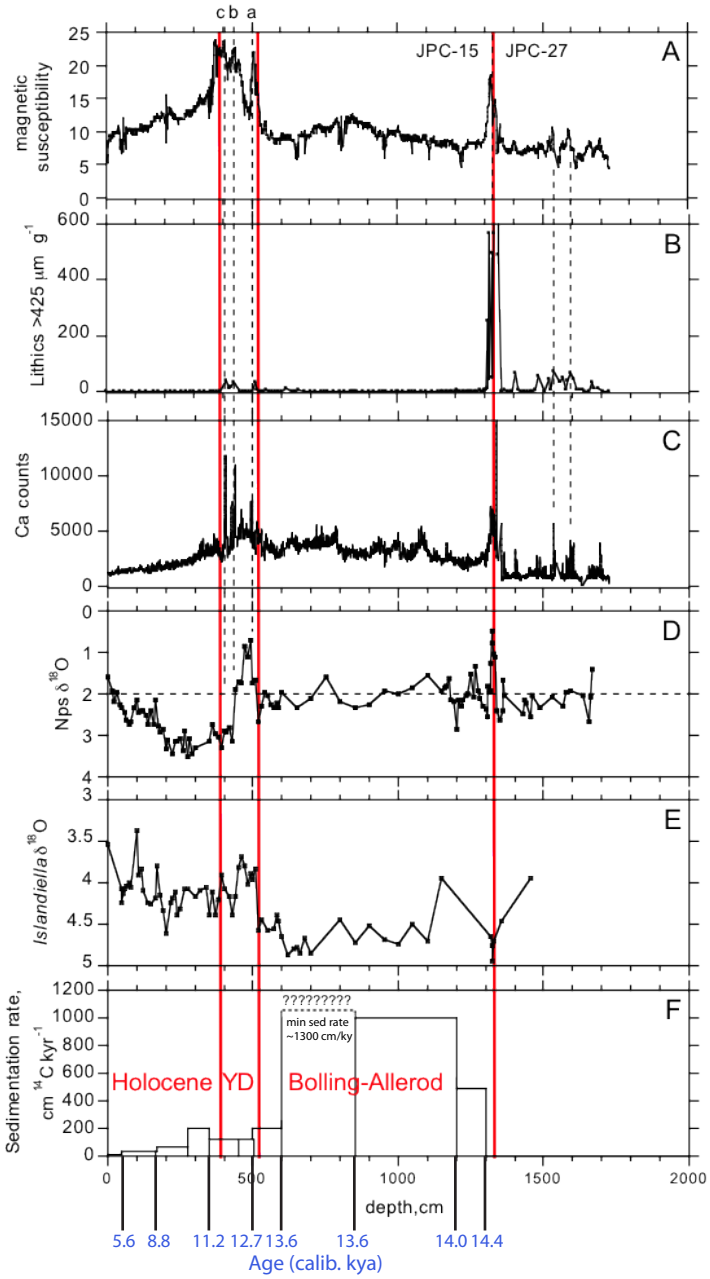

Figure 5.15. Various proxy data from JPCs 15/27. Magnetic susceptibility (A), lithic particle abundance (B), Ca content (proxy for CaCO3) (C), and d^{18}ONps (D), all exhibit extreme values at the onset of the Bolling/Allerod warming at 14.5 ka (red line at 1320 cm) and during the YD (11.7-12.9 ka) (~380-520 cm). Dashed vertical lines correlate smaller features. Dashed horizontal line in (D) shows the ~2.0 ‰ baseline that extends >4 m down the core. A large dropstone at 1346-1350 cm was removed prior to XRF scanning the core, but another sharp Ca spike just above that suggests another carbonate dropstone may be buried in the scanned half of core. The C. neoteretis (benthic) d^{18}O (E) is unremarkable except that the clear minimum ~450-500 cm occurs in the same samples as the low d^{18}ONps. Sedimentation rates (F) are very high between 600-1200 cm where sediments are laminated and cycle counting of XRF data suggests the laminae are annual. Calibrated age dates are listed below the sedimentation rates.

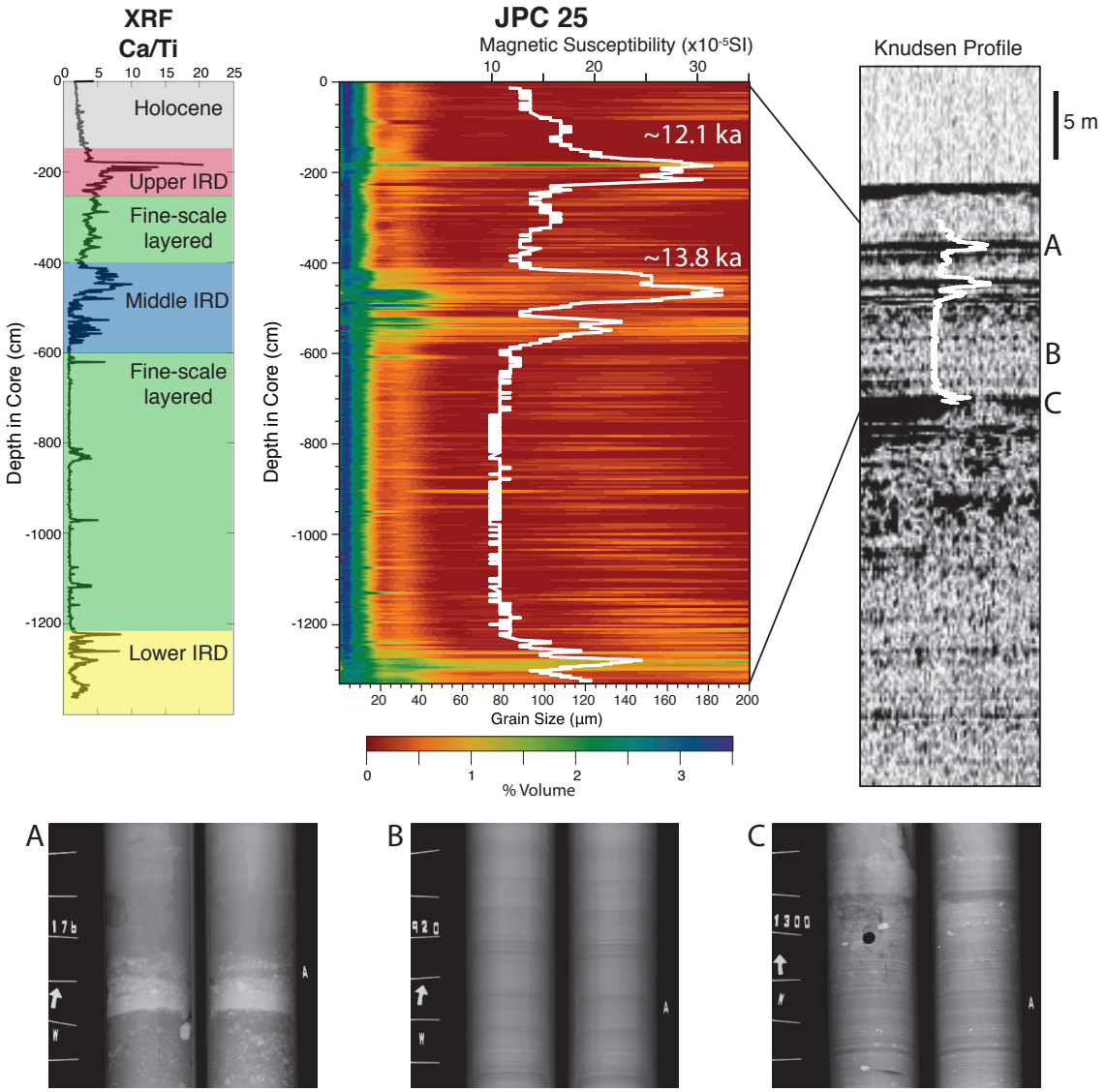

Figure 5.16. Grain size data and seismic section from JPC 25 with magnetic susceptibility projected on both. There is a strong correlation between peaks in grain size, highs in magnetic susceptibility, and high amplitude reflectors in the seismic section. The correlations observed at JPC 25 are very similar to those at JPCs 15/27. X-rays show the difference between a large IRD interval surrounded by homogenous material, finely layered sediments, and layered sediments with IRD. The Ca/Ti ratio from XRF data shows five distinct sections colored in gray, red, green, blue, and yellow, which are similar to core JPC 15/27. Dates on the grain size are from PC750 (Scott et al., 2009) collected in between JPCs 15/27 and JPC 25 with depth correlation based on stratigraphy. The dates have been recalibrated using our age model (Keigwin et al., Chapter 4).

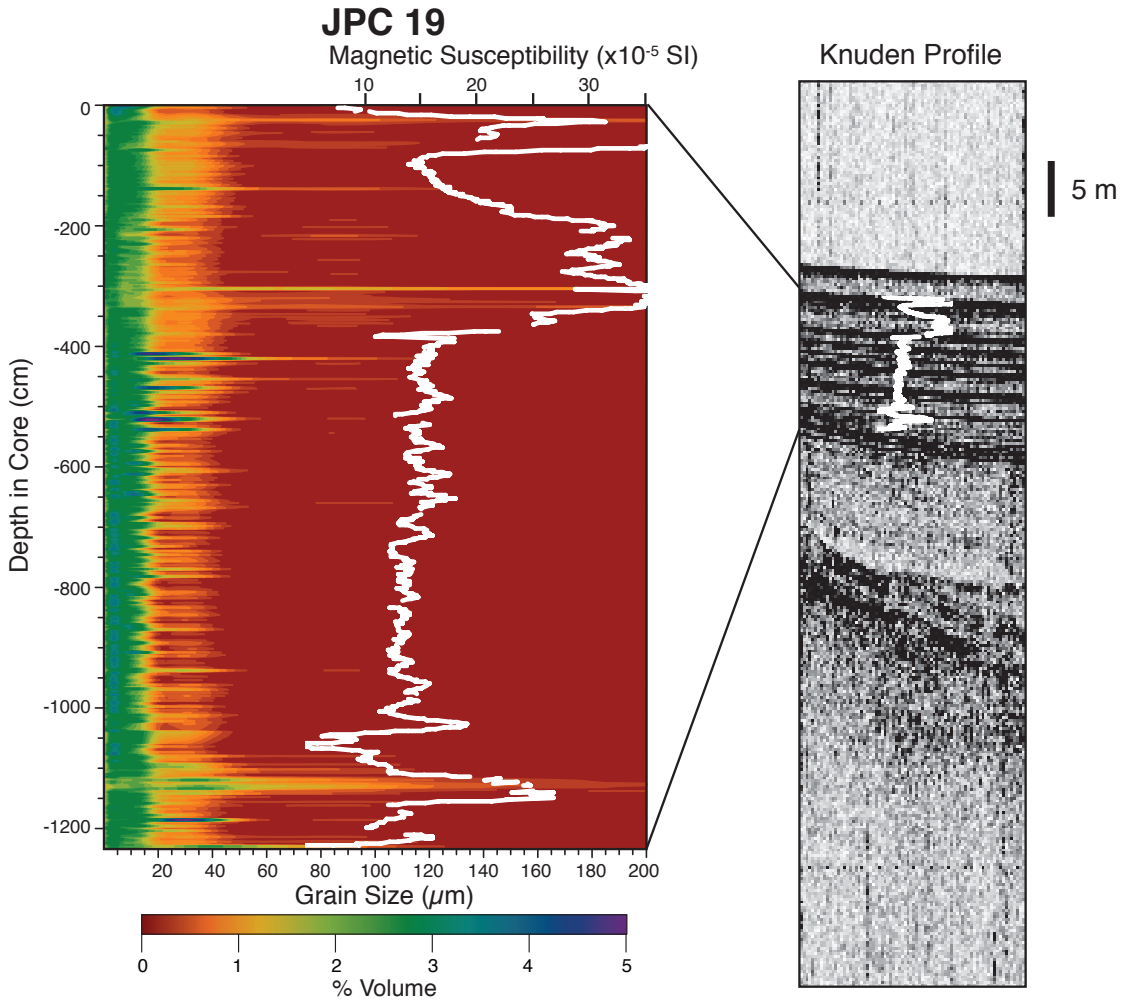

Figure 5.17. Grain size data and seismic section from JPC 19 with magnetic susceptibility projected on both. There is high variability in all of these datasets, which is likely associated with the deglacial history of Amundsen Gulf.

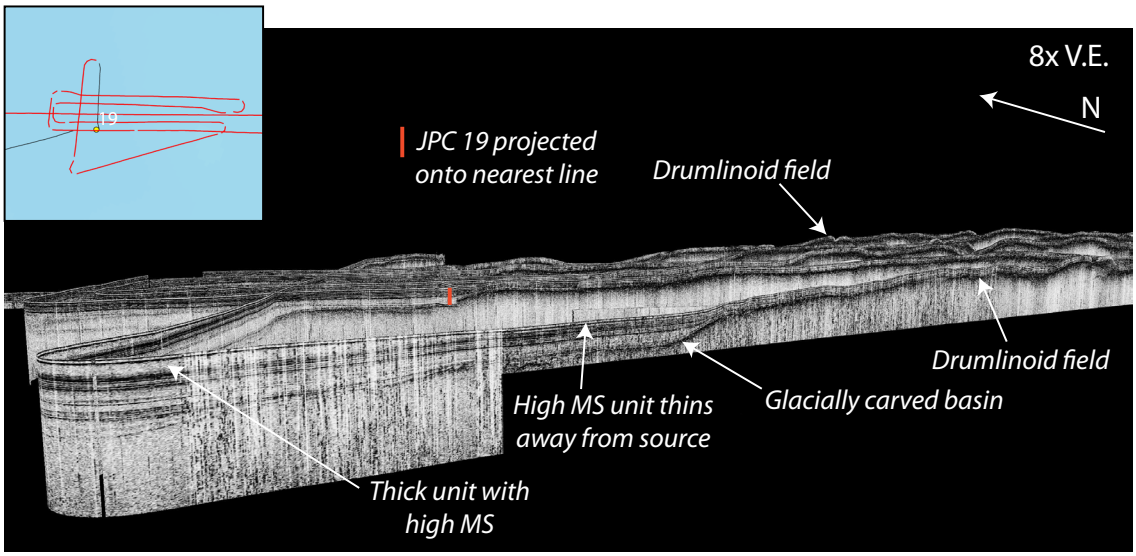

Figure 5.18. Seismic fence diagram around JPC 19. The acoustically transparent unit with high magnetic susceptibility (MS) is imaged thickening to the southwest. The large extent of the drumlinoid field is also imaged. Inset shows seismic profiles highlighted in red.

Table 5.1. Table of Jumbo Piston Cores used in this study.

Jumbo Piston Core	Latitude	Longitude	Water Depth (m)	Core Length (cm)	Sampled Length (cm)
2	72.14425	-155.3689	401	1123	
6	70.9531	-145.65675	415	1201	
9	70.583	-142.4213333	395	1341	
13	70.40213333	-139.3119333	685	1413	
15*	71.1037	-135.1354833	687	1335	1331
19	71.28933333	-126.2791667	442	1288	1235
25	71.44121667	-132.87015	746	1368	1331
27*	71.106	-135.1606667	693	1524	1523
36	70.40223333	-139.30975	665	1708	1569
37	70.58233333	-142.4184333	385	1366	1365
41	71.4036	-148.8757167	1623	1526	1369
HLY 02-05 JPC 15	72.0091	-153.4164	1250	1297	1293
HLY 02-05 JPC 16	72.0091	-153.4164	1250	2019	

*Composite JPC 15/27 length is 1730 cm

5.10 SUPPLEMENTAL MATERIAL

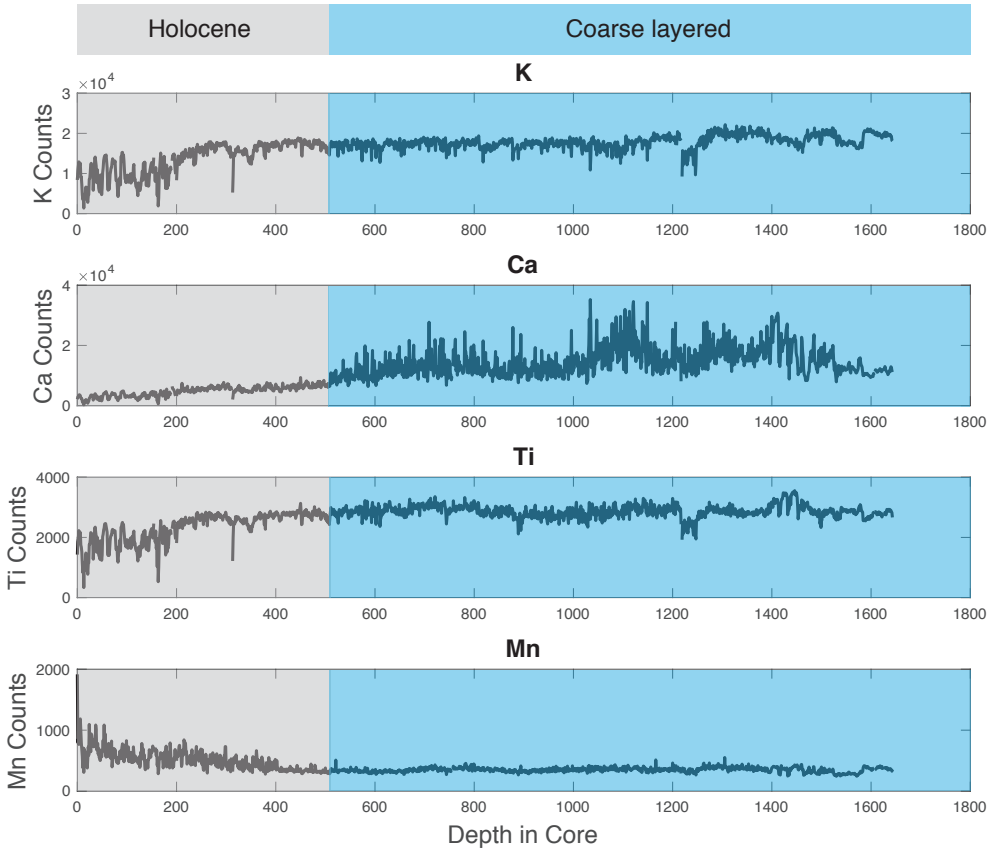

Figure 5.S1. XRF data from JPC 36 - set 1.

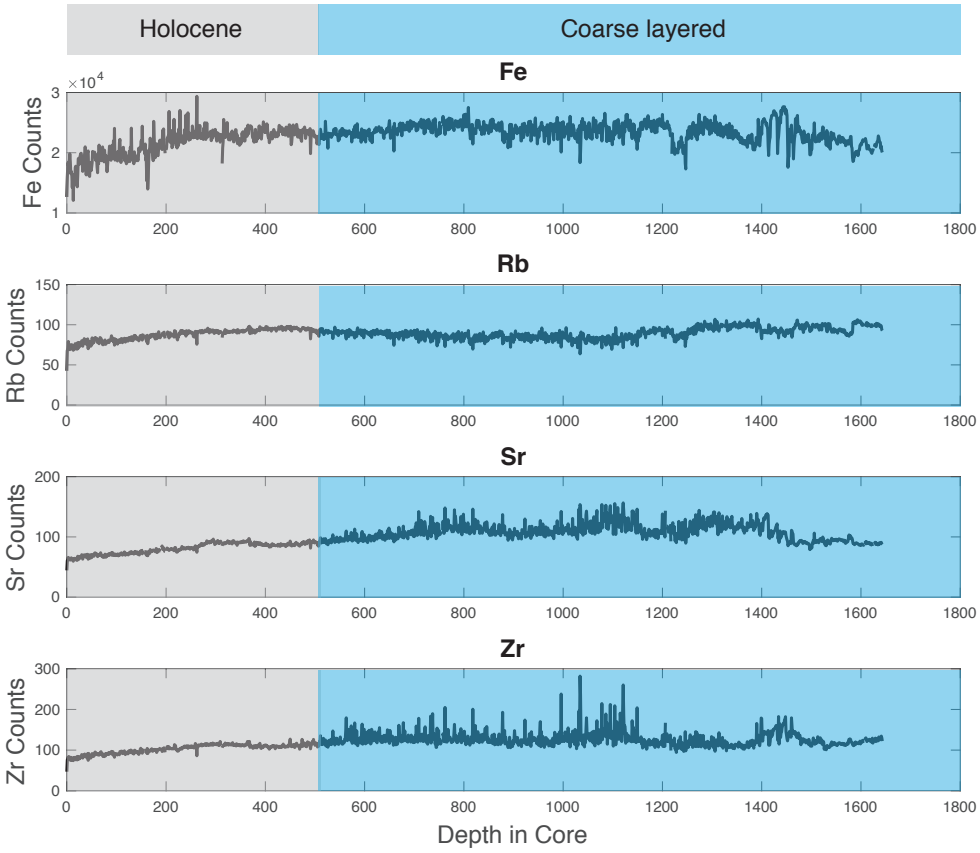

Figure 5.S2. XRF data from JPC 36 - set 2.

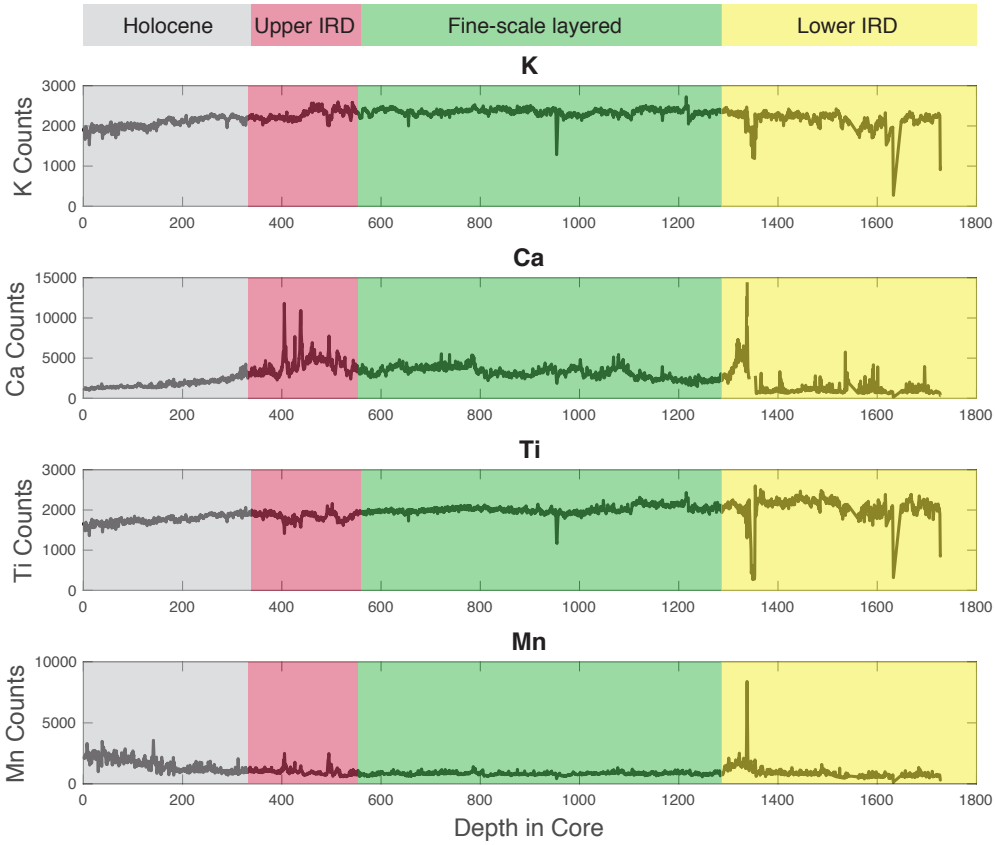

Figure 5.S3. XRF data from JPCs 15/27 - set 1.

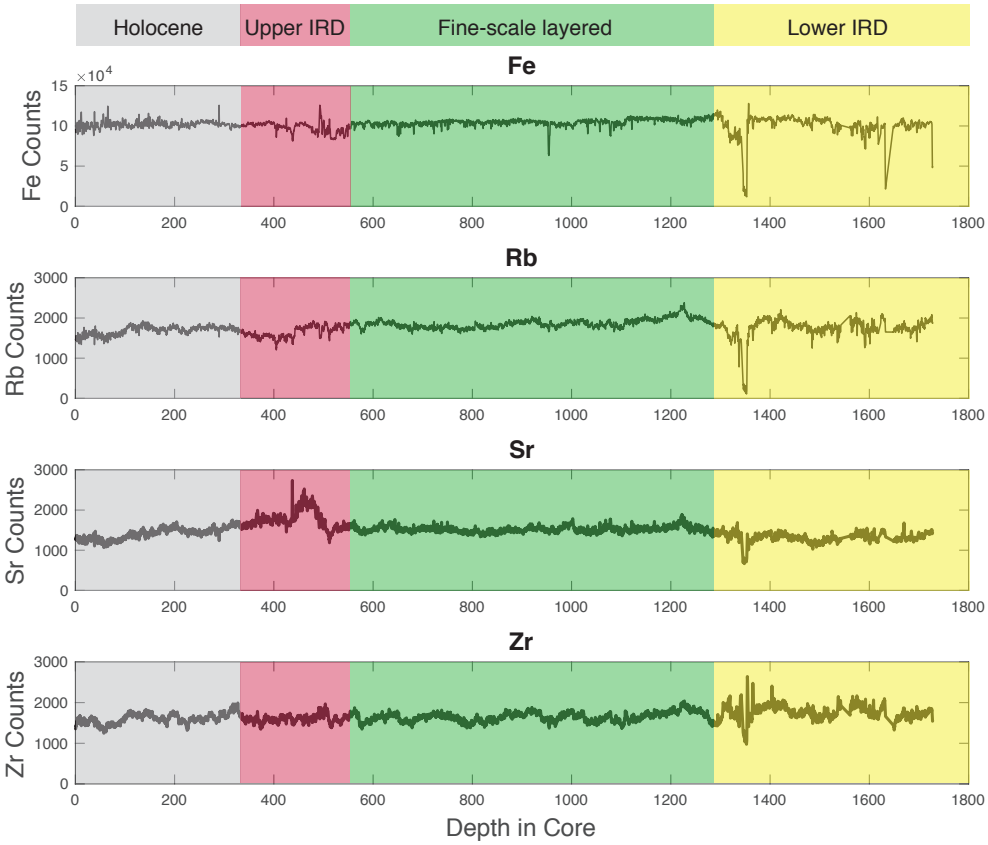

Figure 5.S4. XRF data from JPCs 15/27 - set 2.

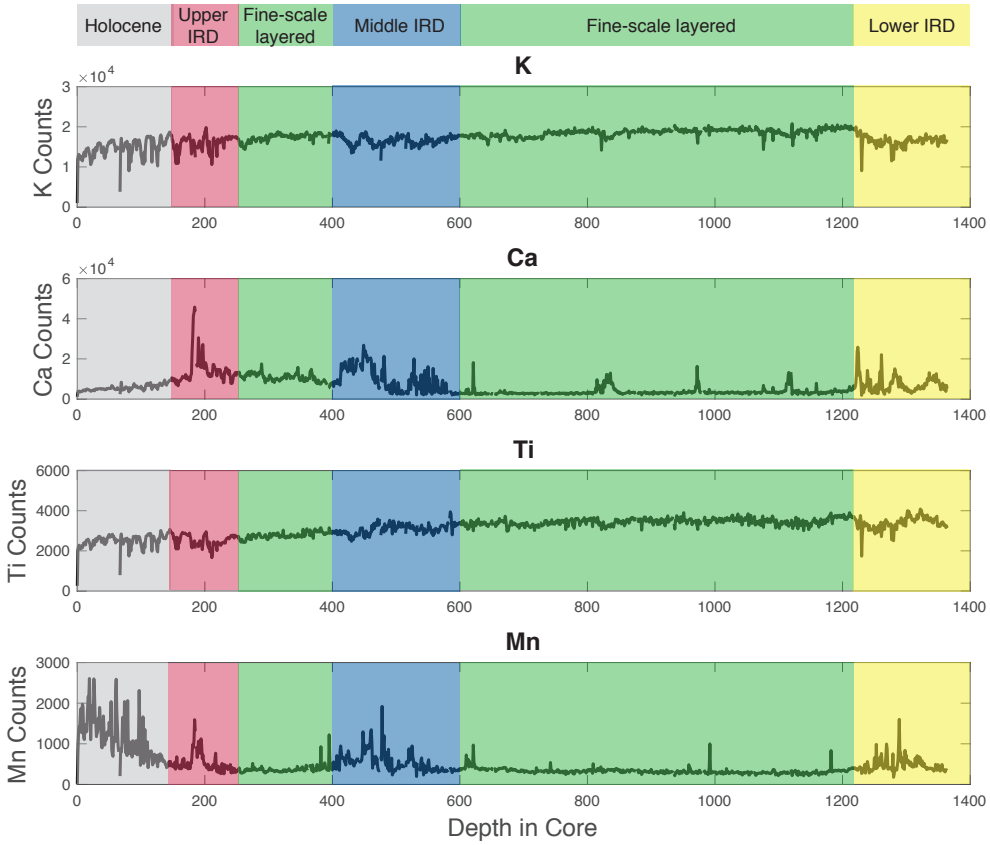

Figure 5.S5. XRF data from JPC 25 - set 1.

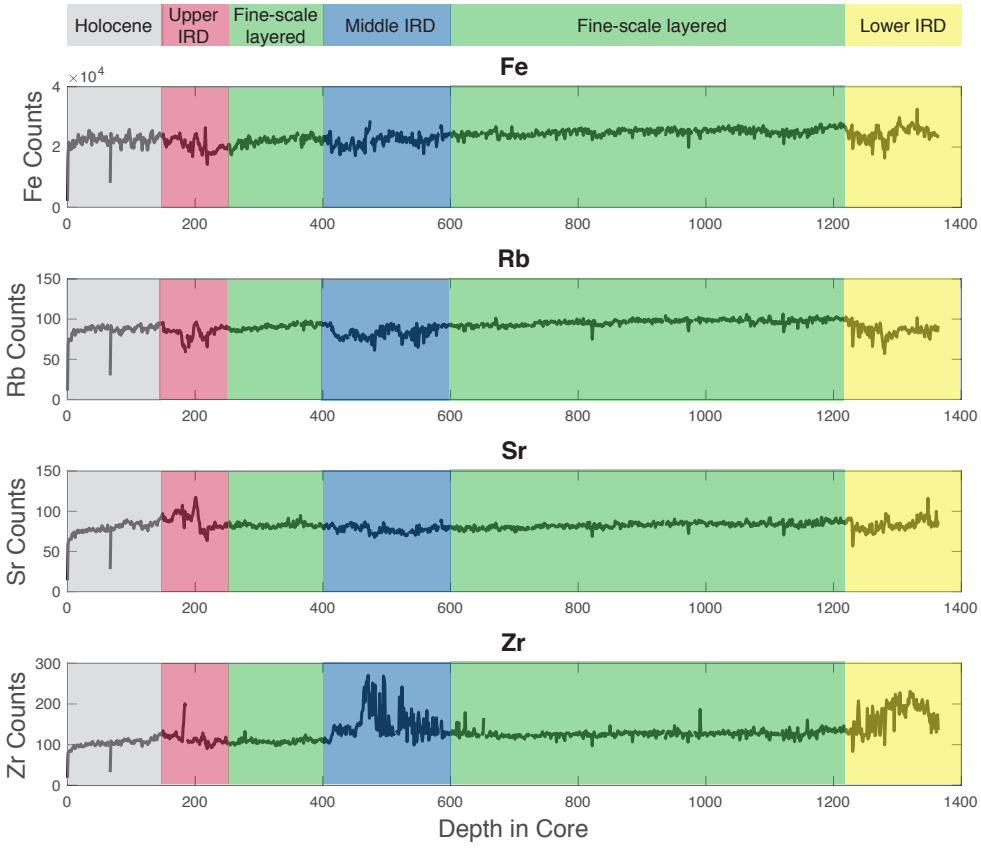

Figure 5.S6. XRF data from JPC 25 - set 2.

6

Conclusions

New geological and geophysical data presented in this dissertation provide important constraints on the processes that shape continental margins. Primary focus was on climatic variability and sea level fluctuations, but tectonic deformation was also examined. Three distinct case studies were presented to assess how these processes affect sediment distribution, glacial drainage patterns, erosion, and the influence of preexisting morphology in different margin environments. These studies were conducted using standard and repeatable methods to best examine each area. High-resolution CHIRP data provided detailed images of the shallow sub-surface that allowed us to assess margin processes over the last ~20 ky. These data were supplemented with lower frequency seismic reflection data, when available, to provide a nested view of the deeper structure and its influence on shallow sediments and morphology. Sediment cores were used in the Arctic to document the climatic events that took place during the deglaciation, as well as establish a chronostratigraphic framework for the region.

Chapter 2 focused on processes affecting sediment dispersal on the continental shelf offshore of San Onofre in southern California. New CHIRP sub-bottom and USGS mini sparker data indicate that the major controls on transgressive sediment distribution and facies variation are eustatic sea level rise and sediment supply with effects from preexisting morphology and tectonic deformation. Variation in rates of sea level rise generated a low in the transgressive surface interpreted to be an old shoreline cutoff. This low created accommodation allowing for deposition of thick sediments. Offshore of San Mateo and San Onofre Creeks, there is a significant amount of sediment in both lag deposit units compared to the surrounding area; suggesting the creeks were important sources of sediment during deglaction. This reduction in sediment supply likely reflects the overall trend toward a drier climate in southern California during the Holocene. The Newport-Inglewood/Rose Canyon Fault does not appear to offset the transgressive surface in this area, providing an important constraint on the timing of most recent event.

This is in contrast to north and south of this area where the Newport-Inglewood/Rose Canyon Fault has ruptured in the past 10,000 years. Folding and faulting imaged in the CHIRP data along the Cristianitos Fault suggests the fault is more likely a strike-slip fault with a down-to-the-northwest dip-slip component than a down-to-the-northwest normal fault, as previously defined. The findings from this project provide a great case study for regions of tectonic inactivity along active margins.

Chapter 3 focused on Block Island Sound, RI. The overarching goal of this project was to understand the formation process of the erosional morphology in the sound, which was formerly covered by the Laurentide ice sheet and then subsequently occupied by a glacial lake. We used new CHIRP data, 3.5 kHz seismic profiles, and high-resolution bathymetry to update the preexisting model for the lake drainage and morphology development. Stratigraphic correlation of sediment units indicated that large depressions on the sound floor developed prior to modern times. This, as well as the morphology of Block Island Valley and offshore slumping, led to the conclusion that Lake Block Island Sound drained rapidly. This was likely followed by the catastrophic draining of glacial Lake Connecticut in neighboring Long Island Sound through Block Island Sound. We infer that the draining of these lakes created much of the morphology in Block Island Sound. A rapid transgression and lack of modern sediment are probably the reasons for the preservation of this morphology. This research gives important insight into the morphology that develops along a glaciated margin. The results from this study can be used to understand better other formerly glaciated regions or areas that have experienced outburst floods.

Chapters 4 and 5 focus on the Beaufort Margin in the Arctic Ocean. The goal of this work was to investigate the deglacial history of the margin and determine if there had been any glacial meltwater floods into the region. With a regional and focused seismic survey of the Beaufort slope, multibeam bathymetry, and sediment cores we were able

to create a baseline for the sedimentation patterns in the region. From Barrow Canyon to the Mackenzie Trough, there is a greater thickness of Holocene sediment compared to the margin east of the trough. This suggests that Barrow Canyon and continental sedimentation are large sources of sediment during this time period. Large amounts of high amplitude reflectors below this layer indicate possible ice rafting events or coarser debris from Mackenzie discharge being distributed west along the margin. This reciprocal relation in sediment thickness places important constraints on sediment dispersal along the Arctic Beaufort margin through the deglaciation and Holocene time.

Three well-defined event layers characterize the margin east of the Mackenzie Trough to the Amundsen Gulf. The deepest unit is an ice rafted debris layer, dated at ~14.1 ka. This event is most likely an enhanced ice rafting event during the retreat of the Amundsen Gulf ice stream and possibly the M'Clure Strait ice stream as well. Glacial lineations just west of the Mackenzie Trough also document ice flow around the margin. This result complements other work that indicate icebergs from the ice streams flowed west along the Beaufort Margin, with some even making it all the way to the Chukchi Borderlands. The second event unit is ~7-8 m of fine-scale layered sediments deposited during the Bolling-Allerod time period. We infer that these sediments were sourced from proximal glacial lakes that flowed down the Mackenzie drainage. The third event unit started at ~12.8 ka and we infer that this was a major meltwater event that entered the Arctic via the Mackenzie. The freshwater signal and timing suggests that this is drainage from glacial Lake Agassiz and it could be the freshwater discharge event that caused the Younger Dyras cold period. The search for the flood that caused the Younger Dryas has been a longstanding paleoclimate question. The many lines of evidence we presented lead us to conclude that discharge down the Mackenzie may have solved this mystery. We have also demonstrated that the massive discharge from the Mackenzie, be it normal river drainage or major flood waters, mostly flows east when it enters the Arctic. Mackenzie

sediments do make it west, but not as far or in the amounts that they do to the east.